THE MINISTRY of EDUCATION and SCIENCE of RUSSIA FEDERATION
SAMARA STATE AEROSPACE UNIVERSITY

V. M. Zhuravlev

Physics of the near Earth space

Electronic Lecture Notes

SAMARA
2011

УДК 523.2
ББК 22.31

Author: **Zhuravlev Victor Mikhailovitch**

Editorial processing: V. M. Zhuravlev
Computer imposition: V. M. Zhuravlev

Zhuravlev, V. M. Physics of the near Earth space = Физика околоземного космического пространства [Electronic resource]: Electronic Lecture Notes / V. M. Zhuravlev; The Ministry of Education and Science of Russia Federation, Samara State Aerospace University. - Electronic text and graphic data (5,4 Mb). - Samara, 2011. - 1 CD-ROM.

Interuniversity Space Research Department, Master Program Educational Content "Space Information Systems and Nanosatellites. Navigation and Remote Sensing" for education direction 010900.68 «Applied Mathematics and Physics»

V.M. Zhuravlev

Physics of the near Earth space

Lectures

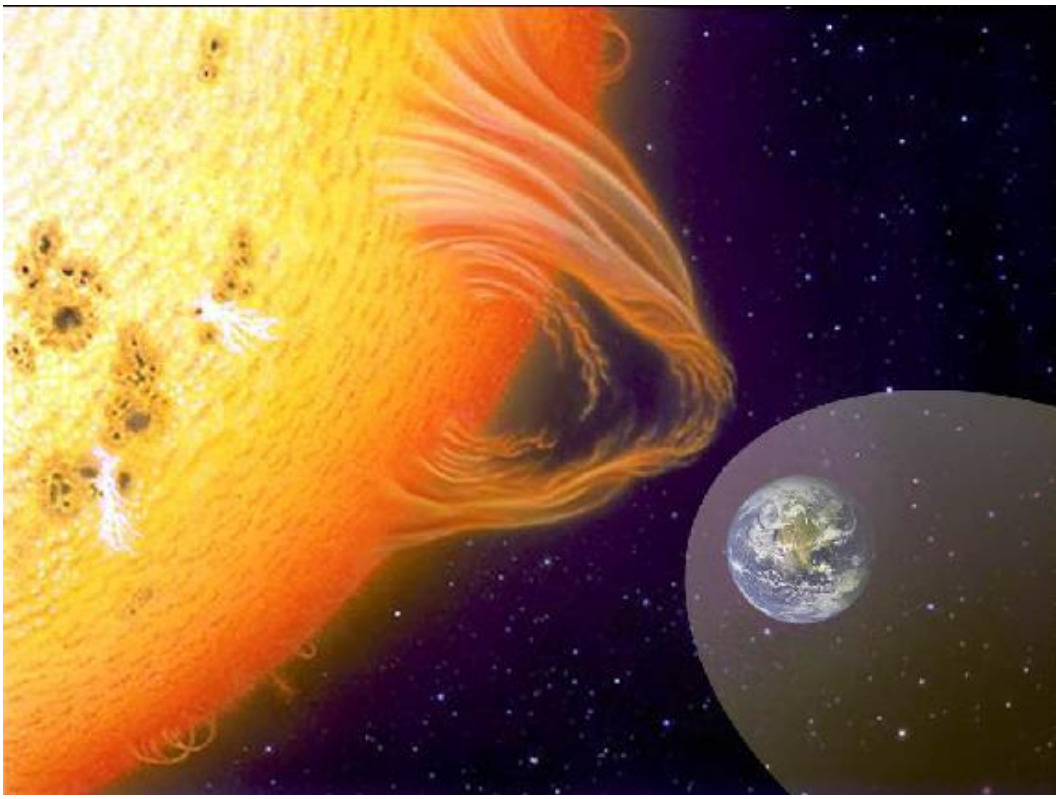

R.Descartes ``Explain the meaning of words - and you will save the world from half of its delusions"

Chapter 1. The Universe

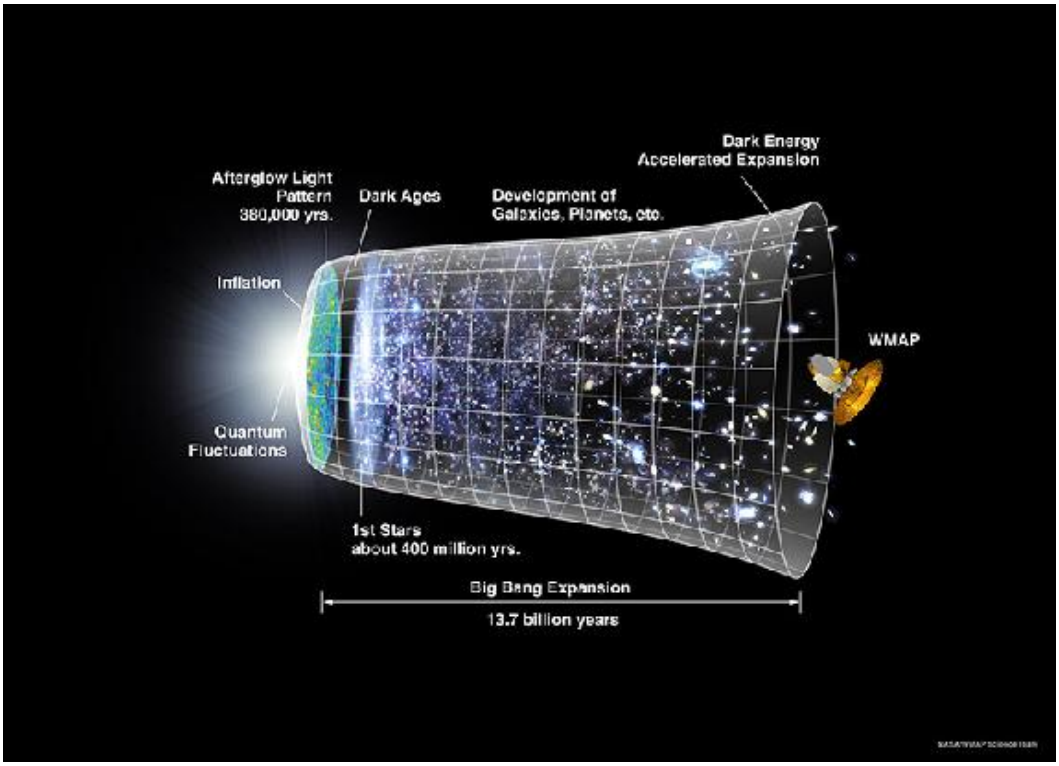

1.1 Lecture 1.

What is the reason to study the near-Earth space, the Sun, the Solar System planets, stars, the Milky Way, the other galaxies, and finally the whole Universe - visible and invisible? Maybe you have heard famous sayings of physicists like academician Lev Andreevich Artsimovich's saying - "The science is the best way to satisfy one's curiosity at the expense of State". Though scientists' activity sometimes looks alike, especially for those who deal with mathematics and study of remote galaxies and stars, this statement does not correspond to the real state of things. We have to study the whole surrounding world - visible and invisible permanently, as it is the guarantee of our survival as species. The world is enormously large and casual. That's why it is unknown where danger is to come from.

There are a lot of examples to this. Especially in the Space. We live thanks to the Sun, which has been warming the Earth by its warmth for about 4,5 billion years. It has created the background for the beginnings and the maintenance of the life on the Earth. But the Sun is a small star - a dwarf. The energy of processes going on inside the Sun and on its surface is so high, that it can easily destroy the life on our planet or put into very difficult conditions. Bursts on the Sun generate strong flows of radiation - ultraviolet, X-rays, gamma radiation, and flows of charged particles of different origin - they are mostly protons and electrons. Having reached the Earth these flows are able to kill everything alive. Magnetosphere and atmosphere of the Earth prevent from this. We are going to discuss these

objects in our lectures. But this is not the whole variety of threats for the Earth and everything alive.

The Earth appeared not alone in the Solar system but together with the other planets and small planets asteroids and minor planets and other objects, for example comets. There is a lot of debris left after the great construction in the Solar system, which are scattered across the Solar system irregularly and casually. They are asteroids and comets and meteorites of different size and what is not less important all these object have different speed with the respect to the Earth. The most dangerous are comets which move with a great speed due to big ellipticity of their orbits. Falling of even relatively small comet or its debris on the Earth can lead to a horrible disaster. For example there was a global extinction of species at the end of Cretaceous period about 65 billion years ago, and the extinction of dinosaurs was the part of it. One of the most widespread hypothesizes of this extinction is the hypothesis of a big asteroid or a comet drop in the vicinity of the present Yucatan peninsula in the north of the South America.

But although these threats are enough, in the XX century with the development of astronomy and astrophysics and later with the development of cosmology it became clear that there are much more threats than the Earth inhabitants could imagine in the XIX century. In the XX century using new discoveries in physics astronomers received new powerful instruments for the observation of stars and later galaxies. As a result new very important discoveries were made. One of them was that the stars which seem to be bright sparks in the star sky, unchanging and eternal, have its own changing destiny. They born, live undergoing a number of phases and transformations and then they die, sometimes relatively silently, sometimes in a form of great explosions warning the Universe about the star's death by a giant emission of energy and matter. These are so-called supernova explosions. The bigger the mass of the star the shorter its life and the higher the amount of energy, matter and substance to be emitted at the moment of the star's death.

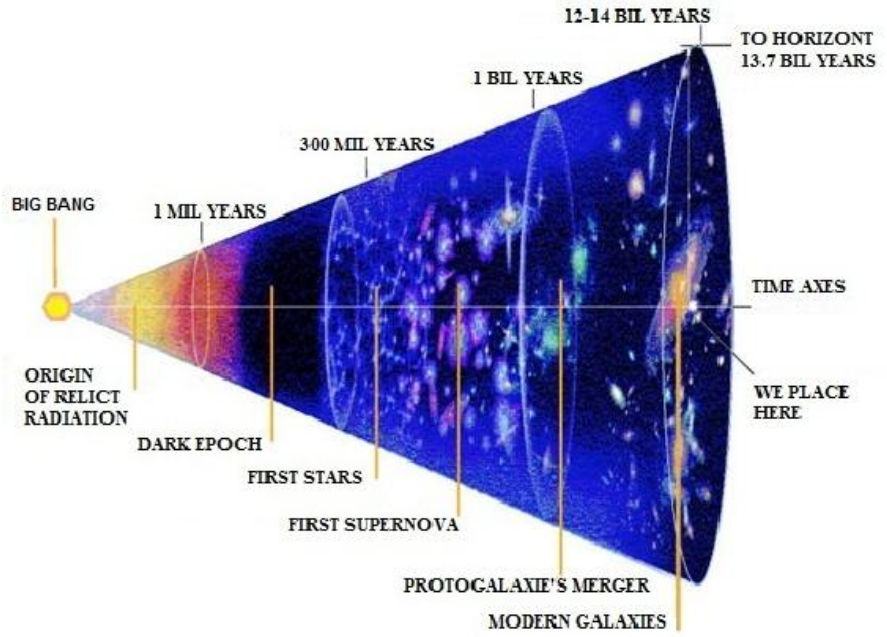

Fig. I-1-1. Schematic image of The Universe development. [1]

It is possible to ask a question - how could the life appear on the Earth if the Sun consists of 74% of hydrogen, 24% of helium and only 2% of the other elements? In reality, the world surrounding us consists mostly not of hydrogen and helium. We ourselves consist of water and carbohydrates and some heavy elements like iron play a very important role in maintenance of our life. Where did it

[1] L.Ksanfomaliti. Dark Univers. Surprises to 100-years Eienstein discovery.Nauka I zhizn', N5, 2005

appear from? If there were not enough oxygen (water!), carbon (amino-acids!), iron and chrome (hemoglobine and chlorophyll!) the life in its present appearance could not arise. This question was set in the XX century and in the same century the answer was found. Heavy elements are born in the stars during their "calm" evolution. But very heavy elements, heavier than iron are born in supernova explosions. It is the death of heavy stars that enriches the space with heavy elements which become breaks of life including our planet. That's why before the life could arise in the vicinity of the Sun, our star dancing around the center of our galaxy - The Milky way - should collect a lot of substance for the life passing through clouds appeared after supernova explosions for billions years. Of course, one circumstance favored that - our Sun is the third generation star.

It means that in accordance to the present concept the observable Universe appeared about 3.7 billion years ago.

The Universe was born during the Big Bang. It broadened fast to the size that one cannot even imagine. In several minutes after that explosion the usual matter started to form - the neutral atoms, mostly hydrogen, some deuterium, helium and other light elements. After several million years the substance concentrated into primary galaxies and the formation of massive hydrogen stars started there. These initial giants existed not long - just about several tens or hundreds years - and started to explode emitting heavy elements into the space - the construction material for new not born stars. After several billion years the second generation stars started to form of this material and after several billion years the third generation stars appeared. So 4.5 billion years ago just in about 9 billion years after the Big Bang our Sun appeared. And next 3 more billion years the first signs of life appeared on the Earth and maybe on the Mars.

This wonderful history of our Sun birth and us later, looks like a kind of fairy tale. Life in reality is not such a bright and pleasant process. Supernova explosions create so powerful flows of radiation and charged particles that the other nearby stars and their star systems experience horrible strokes. These flows of radiation can partially deprive the planet of its upper atmosphere if the planet is just several light years from the supernova. For more distant planets rays will pierce the atmosphere and destroy complicated organic molecules. Consequently the life can end suddenly. That's why supernovas creating conditions for a new life can easily destroy it. Is it connected with our place in the galaxy? Is seems to be connected and very directly!

1.1.1 The Universe, The Milky way, The Solar system, Planet N3

The observable Universe is enormous. Conditions are very different there. Therefore to understand how lucky we are with our placement here we have to determine it. On the Universal level our address can look like this:

The Universe, The Virgo galactic cluster, The Milky Way galaxy, star system of The Sun, planet Earth etc.

Basic structure components of the Universe - its houses - are galaxies. Galaxies form streets, squares, communities and wastelands - so-called voids ("emptiness"). Communities filled dense enough with galaxies are called galactic clusters. They can be very dense and quite rarefied. Our home - The Milky Way - belongs to a very big cluster, the center of which is in the Virgo constellation. Unlike houses on the Earth galaxies are moving constantly. Gravity makes them to move - the force moving the worlds. This force makes galaxies to approach and collide. The way of our galaxy is directed to the center of the Virgo cluster. After many billion years our Galaxy or the object it will transform into will arrive at the destination point in this cluster. But at the same time we are not the only to move in the same direction so do our neighbors in a local bystreet (local galactic cluster). One of our neighbors is a galaxy in Andromeda constellation - The Andromeda Galaxy. This galaxy is several times more massive than our galaxy the Milky Way. And therefore it attracts us. Our homes

will join long before we come together to the central areas of the Virgo cluster.

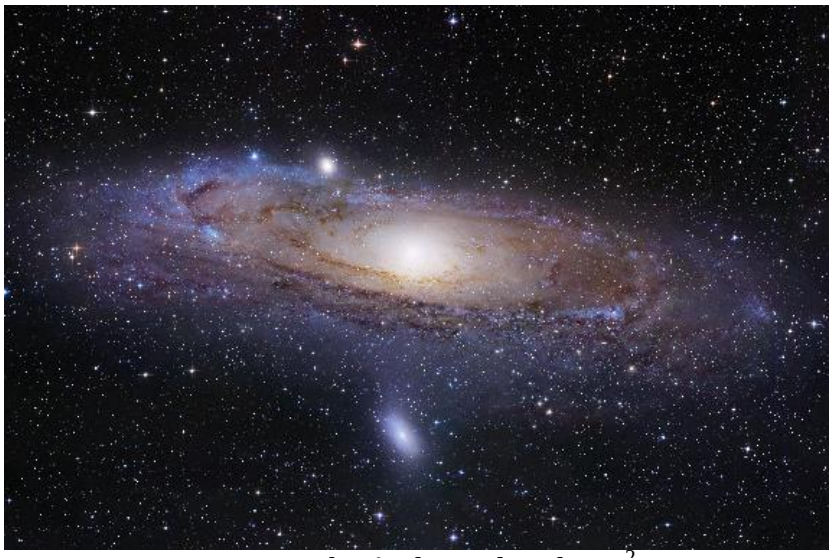

Fig. I-1-2. The Andromeda galaxy [2]

Our placement in the surrounding space of streets, squares and wastelands one can imagine with the help of fig I-1-3, where the image received from NASA "WIMAP" satellite shows the glow of matter in a big scale.

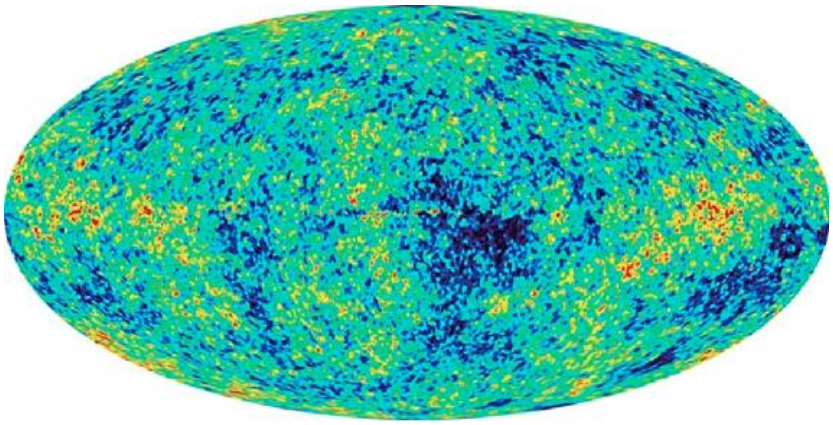

Fig. I-1-3. Data of WIMAP (Wilkinson Microwave Anisotropy Probe). [3]

Galaxies

Houses themselves - galaxies can be organized in different ways. Their structure can also create conditions for life or on the contrary prevent from it. In the fig. I-4 the classification of galaxies given by Edwin Hubble is shown. In this classification galaxies are divided into two major classes.

Elliptic galaxies are marked with letter E: (E0, E3, E5, E7) and spiral are marked with letter S. In turn spiral galaxies are also divided into two classes - galaxies with a bar - they are SBa, SBb, SBc and galaxies without a bar - they are S0, Sa, Sb, Sc. Nowadays one more class is singled out - irregular

[2] http://www.astronet.ru/db/msg/1210528/m31_gendler_Nmosaic1.jpg.html
[3] map.gsfc.nasa.gov

or peculiar galaxies. As it is considered nowadays, elliptic galaxies are the younger formations which appear at the present time during the collisions of galaxies. Spiral galaxies are the product of the elliptic galaxies evolution. Irregular galaxies are the direct product of collisions or interaction of separate galaxies or their groups or they appear as a result of active processes going on in nucleus of these galaxies. Elliptic galaxies and a fortiori irregular galaxies contain many active objects, heated gas and dust, what creates substantial radiation flows from newborn stars and supernova explosions which appear at the end of fast evolution of a number of massive stars born by shock waves in gas and dust. Therefore in the vicinity of stars similar to our Sun where the origin of live is possible powerful flows of charged particles and radiation exist more often preventing from the appearance of stable conditions which could let the life to develop into complicated forms.

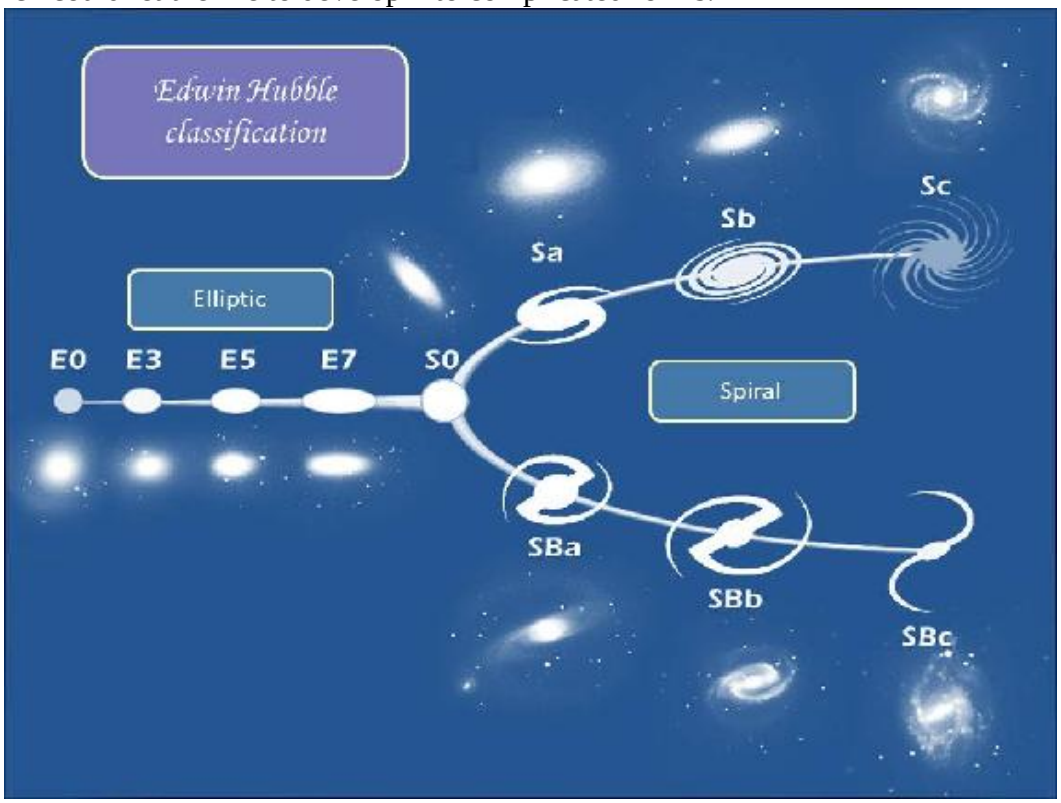

Fig. I-1-4. The Galaxy classification by E. Hubble.

Even greater danger for the life in the Universe is such objects as active galaxies, their nucleuses and objects to be called nowadays Black holes. For some unknown yet reasons these objects sometimes eject jets into space - powerful flows of charged particles and gamma radiation. These outbursts, so called gamma ray burst, were discovered by an accident in the 60s of the previous century and they are studied intensively nowadays. In short time these gamma ray bursts can destroy the life in a great part of galaxy which gets into the jet at a short distance from the source. All these sources together create the general background of cosmic rays which reaches the vicinity of the Sun, the Earth and even its surface. This background of cosmic rays is called galactic cosmic rays with shortening GCR. These rays together with the solar cosmic rays (SCR) create all the major processes in the space surrounding the Earth. That is why it is very important to know the general information about the organization of our Universe - "the city where our house - The Milky Way galaxy - is". On the basis of this analysis it is possible to suppose the most favorable conditions for the origin of life to be in calm spiral galaxies with not big bars. The Milky Way belongs exactly to this class.

The Milky Way structure

Our home - The Milky Way is organized like a great number of spiral galaxies. It is a flat disk with the diameter of about 100000 light years. In the center of spiral galaxies including The Milky Way there is a spherical bulge. Bulge diameter is about 3000 light years. This part of the galaxy turns almost like a solid body. The arms of the spiral structure move faster than stars. They represent a compression wave in the disk. The period of rotation for this wave is about 50 million years, while the Sun performs the complete revolution around the center of the galaxy in 220-250 million years.

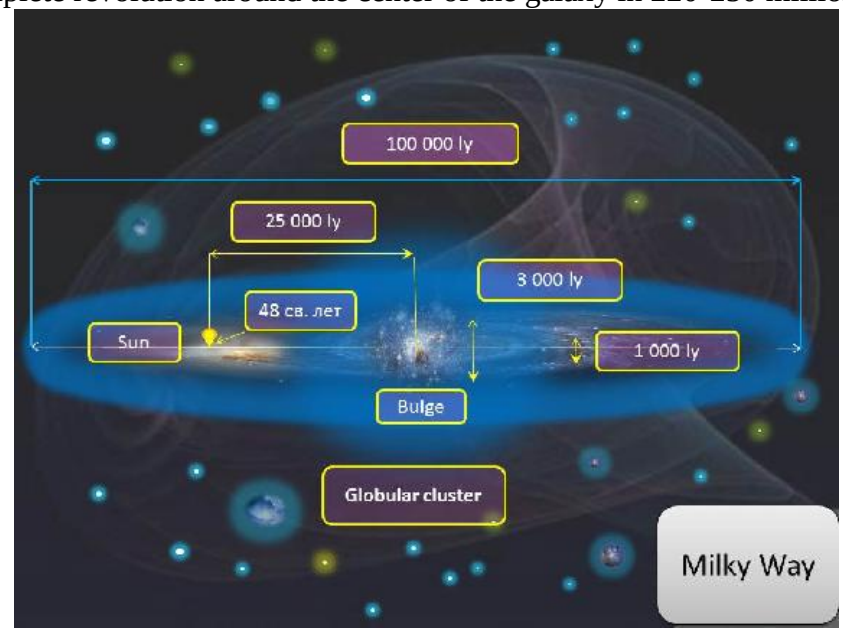

Fig. I-1-5. The Milky Way structure. Edge view.

Placement of the Sun in the Milky Way

Placement of the Earth in the space defines properties of its nearest surrounding - the near-Earth space environment. The Sun is one of the stars of the Milky Way galaxy. We observe the Milky Way as a glowing stripe of stars going across the sky in the night. In fig I-1-5 and Fig. I-1-6 the approximate position of the Sun in the Milky Way is shown. More exact data is given in table I-1-1.

Average distance from the Earth	1.496 10^{11} (8.31 light minutes)
Apparent magnitude (m)	-26.74
Absolute magnitude	4.83
Spectral class	G_2
Distance from the galaxy center	App. 2.5 10^{20} m (26000 light years)
Distance from galactic plane	4.6 10^{17} m (48 light years)
Galactic revolution period	2.25-2.50 10^{8} years
Speed	2.2 10^{5} m/s (on the orbit around the center of galaxy) 2 10^{4} [m/s] (in relation to nearest stars)

Tab. I-1-1. Placement of the Sun in the Galaxy.

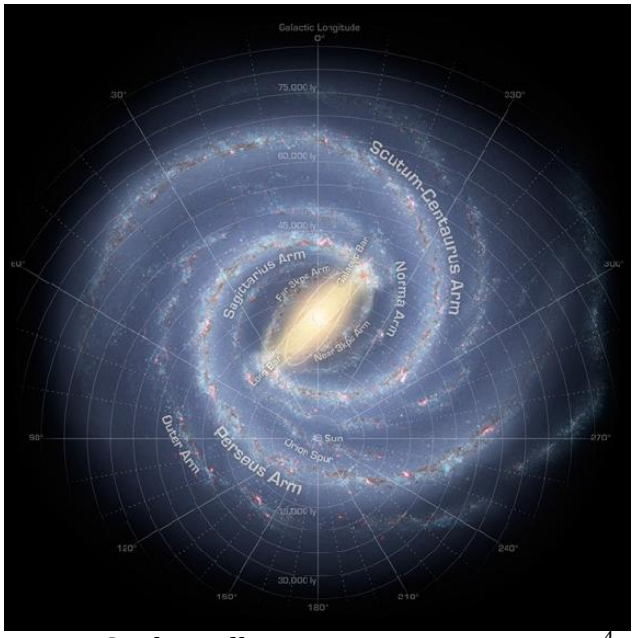

Fig. I-1-6. The Milky way structure. Top view [4]

The Earth is far enough from the Milky Way center and from active areas where the process of stars formation goes. The nearest alike area is the Orion nebula. It is situated in 6500 light years distance from us. It makes our existence relatively safe because powerful flows of radiation and hard electromagnetic radiation from it reach us being weakened. At once it does not save us from dangerous neighbors - massive stars the explosion of which can destroy us. The example of such star is Betelgeuse, the star situated at 650 light years distance from us. It is a massive star at the end of its evolution. The star's -a red giant - diameter is equal to the diameter of the Jupiter. The explosion of this star can cause a very strong radiation flow in the vicinity of the Sun which can lead to the loss of ozone layer and it can increase the ultraviolet radiation flow from the Sun on the Earth's surface up to the mortal level.

1.2 Lecture 2. What the stars are?

1.2.1 Observable characteristics of stars

Photometric characteristics of stars

Stars are so far away from us that the distances to the stars many times exceed their own dimensions and even the dimensions of their planet systems if the latter exist. Therefore being observed from the Earth they look like glowing dots and all accessible direct information about them can be received only from the analysis of electromagnetic radiation characteristics in different spectral range starting from millimeter SHF radiation to X-rays and γ-radiation. Major electromagnetic radiation characteristics helping to receive useful information about physical nature of stars, their structure and dynamics are the following:

- apparent and absolute stellar magnitude;
- radiant flux from the star;

[4] http://en.wikipedia.org/wiki/File:236084main_MilkyWay-full-annotated.jpg

- luminosity;
- spectral class (color);
- spectrum;

For binary stars (multicomponent) and variable stars two more characteristics play an important role. They are the light curve and the radial velocity curve. Consider each characteristic separately

Apparent stellar magnitude

This characteristic historically appeared as the first way for astronomers to distinguish stars by apparent brightness with naked eye. Apparent stellar magnitude values appeared as descriptive adjectives to compare the apparent brightness with the full Moon. A positive value of the apparent stellar magnitude m corresponds to the number of times the Moon shines brighter than the star. A negative value shows how many times the object shines brighter than the Moon.

When it became possible (the beginning of the XX century) to measure the direct radiant flux from the star at the Earth the relation between the apparent stellar magnitude and the flux at the Earth was established. This relation is expressed by the Pogson ratio:

$$\frac{F}{F_{\odot}} = 2.512^{m-m_{\odot}}. \qquad (1.1)$$

Here F is the radiant flux measured in $erg \cdot cm^{-2} \cdot s$, $F_{\odot} = 1.37 \cdot 10^{6}$ $erg \cdot cm^{-2} \cdot s^{-1}$ - the radiant flux from the Sun, m - apparent stellar magnitude, $m_{\odot} = -26.73$ - apparent stellar magnitude of the Sun. For example the Sirius - the brightest star in the sky, visible in the southern hemisphere - has apparent stellar magnitude m=-1.6. The dimmest stars the human eye can see have apparent stellar magnitude $m = +5-6$. With the best telescope on the Earth one can see stars with $m = +24$ [5]

Maximum apparent stellar magnitude	Approximate quantity of this magnitude stars	Observation way
1.0	10	Visible with naked eye
2.0	41	
3.0	138	
4.0	357	
5.0	1030	
6.0	3500	Visible only with a telescope
7.0	14 300	
8.0	41 000	
10.0	324 000	
15.0	32 000 000	
20.0	1 000 000 000	
21.0	2 000 000 000	Visible only after a long exposure
25.0	32 000 000 000	

[5] Let's note, formula (1.1) confirms Weber-Fechner law known from the beginning of the XX century. This law associates different sense organs sensation intensity and external action intensity. The law says: sensation intensity is proportional to the external action logarithm. In our case the sensation is the apparent stellar magnitude m and the external action intensity is radiant flux: $m \sim logF$.

Tab.1 . Quantity of stars having the given apparent stellar magnitude [6]

Absolute stellar magnitude and luminosity

It is clear from a simple physic that the apparent stellar magnitude contains information about two more physical quantities which cannot be distinguished having only the data about apparent stellar magnitude. Indeed, proposing energy F_0 being radiated from the unit of area per one second and the star has radius R and is at the distance r from us we have a radiant flux at the receiver on the Earth equal to

$$F = \frac{F_0 4\pi R^2}{4\pi r^2}. \qquad (1.2)$$

Quantity $L = F_0 4\pi R^2$ is called star luminosity and represents the whole quantity of energy radiated into the space by the star per one second. The Sun's luminosity $L_\odot = 3.8 \cdot 10^{33}$ erg/s.

Except the luminosity L formula (1.2) contains the distance r from the star to the Earth. Both characteristics are very important for the star physics but unfortunately the distance is unknown for the majority of stars in the Galaxy. But absolute stellar magnitude M is introduced to use this quantity similar to apparent stellar magnitude making a use of indirect data. Absolute stellar magnitude is defined as apparent stellar magnitude if only the star were at 10 pc from the Earth. If the distance from the Earth to the star is measured in parsecs (pc) the formula connecting absolute and apparent stellar magnitude looks like:

$$M = m + 5 - 5\log r + A.$$

Name of star	Abs. magnitude	Mass of star per $M_\odot$ (mass od Earth)
Capella	-0.2	4.2
Capella's satellite	+0.1	3.3
Sirius	+1.3	2.5
α -Centauri	+4.7	1.1
η Ursae Majoris' satellite	+5.7	0.7
η Bootes' satellite	+7.8	0.5
β 416's satellite	+9.2	0.3
σ Eridanus' satellite	+12.9	0.2
η Scorpio's satellite	+13.4	0.18

Tab. 2. .Absolute stellar magnitude dependence on star mass. [7]

Star's color

To describe physical processes taking place inside the star and in surface layers it is necessary to have an of the temperature on the star's surface and about how the temperature changes with the distance from the surface to the center in layers. This information can be obtained from the analysis of the star emission spectrum.

The most important physical law allowing to establish relation between the star's spectrum and

[6] Data is taken from [2]

[7] Data is taken from Tomilin A.N. The Earth's sky. M.: "Detskaya literatura" 1974 [2]

the temperature of the star's surface is the blackbody radiation law discovered by Plank in 1900. This event marked the beginning of a new epoch in physics - the quant laws epoch. The idea of Plank's law is that if the radiation is in thermodynamic equilibrium with matter on conditions that both the radiation and the matter are placed into a thermostat (this system is historically called a blackbody) with the temperature T the radiation has a frequency spectrum with the shape described by Plank's formula :

$$\rho(\omega) = \frac{8\pi\hbar\omega^3}{c^3} \cdot \frac{1}{e^{\hbar\omega/kT} - 1}. \qquad (1.3)$$

According to Plank's formula the maximum of radiation of a blackbody having the temperature T can be found from the equation

$$\left(1 - \frac{\hbar\omega}{3kT}\right) e^{\hbar\omega/kT} = 1.$$

As it follows from this ratio, one of frequencies corresponding to different temperature will prevail in this radiation and it will be perceived by our eyesight as the color of the object. Comparing it to what we see in the sky when we look at the stars of different colors it is possible to say that this difference in color is begot by the difference in temperature of these stars.

Usage of relations (1.3) for the stars is based on the fact that stars in a manner can be considered as blackbodies. Indeed, as it was said above, a blackbody is a system consisting of radiation and matter in thermodynamic equilibrium. If we count the time needed for photon emitted in the center of the Sun as the result of thermonuclear reactions to get Sun's surface and if we take into account all its absorptions and reemissions this time will turn out paradoxically big - about 30000 years. It is related to the fact that hot matter is not transparent for electromagnetic radiation and the higher the temperature the higher non-transparency. Therefore the radiation in each layer of the star is in equilibrium with the matter even on the condition that the temperature changes from layer to layer. A remote observer sees radiation emitted from near-surface layers of the star (photosphere), but the radiation is generated in deeper layers.

Therefore the real spectrum deviates from the equilibrium one, corresponding to the equilibrium radiation of the star. As far as photosphere contains much colder matter than the inner layers the absorption lines corresponding to chemical elements contained in photosphere appear in spectrum. For the Sun a wavelength corresponding to the maximum of radiation in visible optical range is 555 nm (see fig. II-3-1). This is the frequency of visible green light [8].

Therefore, with the help of described methods stars can be distinguished by their color and the "average" temperature of the star can be matched to its color. Historically a special color scale for stars formed. It is called the spectral class of the star. Spectral classes are marked with Latin letters. Letter O matches the hottest stars. Then go classes B, A, F, G, K, M. Later classes R and N were added to those ones. This consequence can be easily memorized as "O, Be A Nice Girl. Kiss Me Right Now". The Sun belongs to the G spectral class. Nowadays a division into 9 groups by the color seems to be very rough. Therefore each class is subdivided into 10 subclasses. A number from 0 to 9 fits each subclass. The Sun belongs to G2 class according to this improvement

At the beginning of the XX century there had already existed a possibility to estimate the distance from the Earth to some nearest stars using the indirect data and therefore to calculate their luminosity and at the same time to measure their color - the frequency of maximum spectral density. As a result, it became possible to make diagram having the name of its first creators, The

[8] Let's notice that the basic spectral range of energy supply from the Sun is connected with color of terrestrial plant's leaves. Leaves have green color in order to reflect the most energetic component of the solar light

Hertzsprung-Russell diagram - color-luminosity diagram. This was one of the first attempts to correlate different stars to each other on the basis of the objective data.

1.2.2 The Hertzsprung-Russell diagram

One of the most important achievements for astronomy at the beginning of the XX century was the discovery of presence of regular dependence of the color or spectral class of the star on its absolute stellar magnitude (or luminosity). This dependence was discovered by Herzsprung (Danish astronomer) and Russell (American astronomer) with the help of a simple method of integration of data from a great number of stars in one general diagram. Absolute stellar magnitude is on the ordinate axis and spectral class of the star is on the abscissa axis. The difficulty of its creation at the beginning of the XX century concluded in the difficulty to define the distance to a sufficient number of stars which was necessary to calculate absolute stellar magnitude. Both scientists were able to cope with this problem independently and they created the diagram. Russell reported his discovery on the 13th of June 1913 [9]. Nowadays this diagram is one of the most important tools for star's characteristics definition from its evolution prognostication point of view.

The diagram is present in fig.I-2-1 with the indication of the most important elements in the contemporary appearance

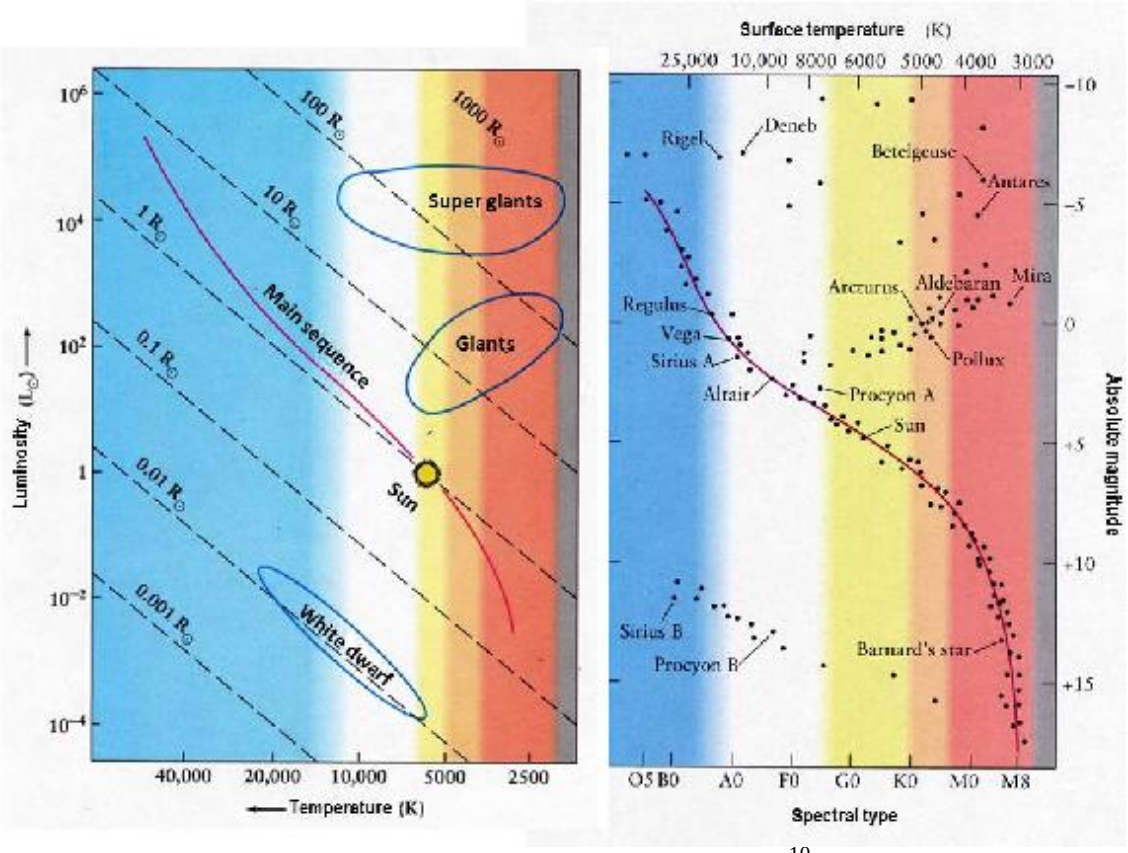

Fig I-2-1 Herzsprung-Russel diagram. [10]

Except the spectral class the color index V-B related to the intensity of star radiation through the given light filters, absolute stellar magnitude, a surface (effective) temperature of the star is

[9] see [2]

[10] http://astro.wsu.edu/worthey/astro/html/lec-hr.html

estimated by radiation in certain spectral range.

As it is seen from the picture, Herzsprung-Russel diagram contains three major objects: the main sequence, the crossing diagonal, going from the upper-left to the lower-right corner, a group of stars closer to lower left corner - white dwarfs and a group closer to upper-right corner - red giants, giants and supergiants. The area of the main sequence corresponds to the stars being in the prolonged (from hundreds million to tens billion years) stable evolution phase. In the upper part of the main sequence massive blue giants are concentrated, their evolution goes very fast. The lower the star is on the main sequence the less massive it is. And a period of its stable evolution increases. Stars in the white dwarf area are remnants of stars which had not enough mass to pass into the final stage of evolution - a supernova explosion. Additionally in this area there are stars thrown away from multicompoment stellar systems after the explosion of a more massive companion which has scratched off the shell from its partner leaving a helium core. These are so-called Wolf-Rayet stars. Stars in the red giants area are initial areas of stars formation and the stars massive enough being at final stages of their stable evolution accompanied with outer shell inflation to a giant size. For example Betelgeuse goes with those stars; it is a red giant visible with naked eye in the upper-left corner of the Orion constellation.

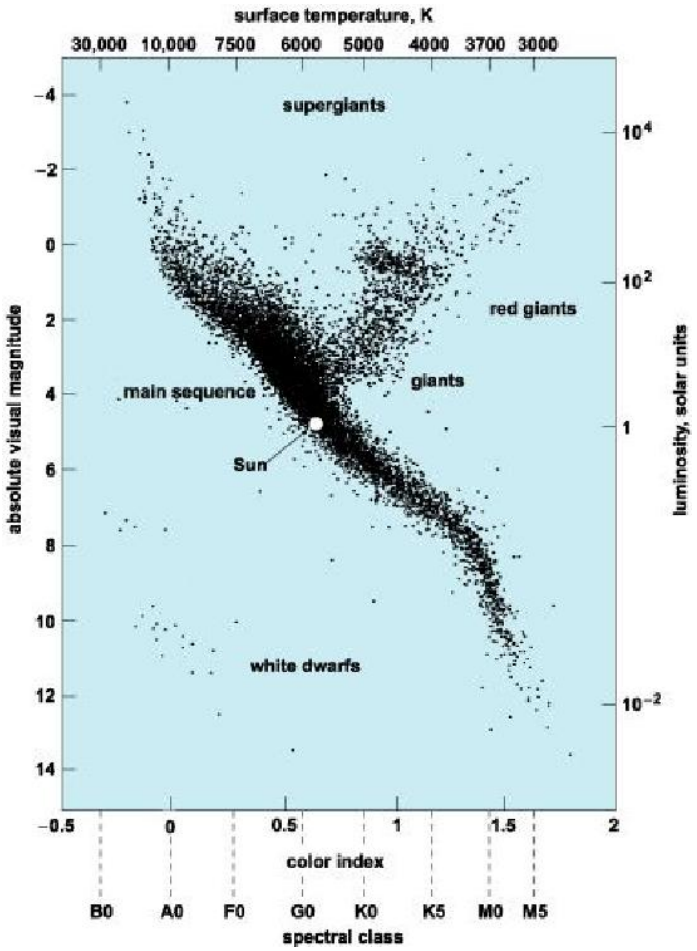

Fig. I-2-2. Herzsprung-Russell diagram of 1500 stars in 1000 parsec radius (got with the help of Hipparcose catalogue) [11]

Disclosure of a regular structure on the Herzsprung-Russell diagram rose a problem for the

[11] http://www.answers.com/topic/hertzsprung-russell-diagram

scientists how to explain this dependence basing on physical representation of stars' structure and evolution. This problem appeared to be very difficult and the answer was found only after the general models of stars' evolution at different stages were created with the help of ideas about thermonuclear sources of stars' energy which were unknown by the moment of the Herzsprung-Russel diagram appearance.

1.2.3 Evolutionary star classes

The general conception of the evolution of a star

The time and character of stars' evolution depends on the fact whether they are accompanied with other stars or they are single stars. As it is established nowadays, a number of stars being a component of multicomponent stellar systems equals to approximately the half of all the stars in the Galaxy. Approximately one third among all these stars has three or more companions. Among these three and more multiple stars approximately has 4 and more components. Et cetera. As shown by the qualitative analysis of star movement in complicated multiple systems some of them have one common peculiarity. After the formation of a multiple star system two the most massive stars appear in the center of the system and other less massive stars are pushed to the periphery of the system and do not influence the movement of the two massive components. Therefore in the majority of cases multiple star systems are represented by close binary systems. Star evolution in such systems is very various and complicated in comparison to a single stars evolution. That is why we are going to start with single stars.

For single stars their evolution is basically determined by the initial mass and chemical composition. The majority of newborn single stars are hydrogen stars with insignificant quantity of other elements. In this case the evolution of a star is determined by its mass assumed after the birth. In fig. I-2-3 a brief star classification of different evolution types depending on the initial mass is shown. Two mass limits play an important role in the analysis of the further evolution of a single star. The first one is called Chandrasekhar limit and the second one is Oppenheimer-Volkoff limit. Mass values determined by Chandrasekhar limit and Oppenheimer-Volkoff limit are related to the ability of the star matter to resist the gravitational contraction. The star is in equilibrium when the heated plasma pressure equalizes the gravity in all layers of the star. This condition can be written with the help of the following simple formula:

$$\frac{P}{R} = \frac{GM\bar{\rho}}{R^2}, \tag{1.4}$$

which represents the equality between the pressure gradient and the gravity force applied to a unit volume. Here P - is an average pressure within the star, R - the radius of the star, $\bar{\rho}$ - average substance density, M - mass of the star, G - gravitation constant. In the dependence on chemical composition of a star and its density the matter can undergo structural changes when the pressure grows. It changes the equilibrium conditions. For a regular star consisting mostly of hydrogen the pressure is described by a common formula for ideal gas pressure:

$$P = \frac{\bar{\rho}}{\mu} AT, \tag{1.5}$$

where μ - molar mass of star matter, A - universal gas constant, and T - is an average temperature of the star. In this case the equilibrium equation gives the following equilibrium condition (1.4) :

$$T = \frac{GM\mu}{AR}, \tag{1.6}$$

which shows the relation between the temperature, mass and radius of the star in order to put the star into equilibrium. To calculate the temperature and the radius of the equilibrious star with given mass it is necessary to specify how the heat is generated in the star core at the expense of thermonuclear reaction and how the heat is emitted in surrounding space. The condition of the heat balance can be stated with the help of the following formula:

$$\gamma(T_{core}, \rho_{core}) M_{core} = \sigma T_s^4 4\pi R^2. \tag{1.7}$$

Here T_s - surface temperature, σ - Stefan-Boltzmann constant, $\gamma(T_{core}, \rho_{core})$ - coefficient characterizing the quantity of energy emanated per unit time in unit mass of the star core having mass M_{core}. The parameter depends considerably on temperature in the core and substance density in the core. The average temperature is related to the surface temperature in the following manner:

$$T_s = \frac{T}{3R\bar{\rho}\kappa}. \tag{1.8}$$

Here $\kappa(T, \bar{\rho})$ - coefficient of opacity of the star. All these relations let estimate roughly conditions when the star having given mass and chemical composition stabilizes. Particularly these relations explain qualitatively the form of Herzsprung-Russell diagram. Stars on the main sequence are mostly hydrogen stars being equilibrious and having given mass. In equilibrium the star spends the most part of its life the duration of which is determined by its mass. The more massive star the shorter is its evolution. Single stars having solar mass live approximately for 10 billion years ending their lives with its shell dump and passing to a white dwarf which gradually cools down and turns firstly into a brown dwarf and then into a black dwarf - a very dense chilled object. In fig. I-2-3 and I-2-4 these processes are shown by the corresponding evolution lines.

More massive stars having about two to three solar masses live less and can end their lives not as a white dwarf but as a supernova explosion and turn into a neutron star. More massive stars with masses more than 5 solar masses can turn into an object called nowadays as a black hole. These evolution elements are represented in fig. I-2-3 and I-2-4.

During its evolution from the initial hydrogen star all the stars of different masses except the most massive stars of O and B classes pass through the stage of a red giant or a super giant what is shown in the figures. At the end of the evolution the radius of the star increases by an order or even more due to convection area extension. The Betelgeuse the brightest star in the Orion constellation can serve as the example. This star having more than 20 solar masses is at the end of its evolution and has the diameter equal to Jupiter's orbit diameter. This is a red supergiant.

Although this star is at more than 600 light years distance from us it is possible to see contrast spots on its giant surface with the help modern telescopes. The evolutionary stage of the star as a red giant or a supergiant ends with a catastrophic compression of the star usually called a collapse of the star.

Chandresekhar limit points at the maximum value of star's mass at the end of its evolution. The value defines whether the star can become a white dwarf during its compression or matter structure must change to let the star become just a neutron star or, in case of bigger mass, a black hole. Chandresekhar limit can be calculated with the same formulae of star equilibrium as for hydrogen star if formula for pressure of **ultrarelativistic degenerate electron gas** is substituted into the equilibrium condition. Equation of state for this gas has the following form:

$$P = K_e \bar{\rho}^{4/3}. \tag{1.9}$$

Here constant K is expressed in terms of fundamental constants $\hbar$ - Plank constant and c - speed

of light. The word ultrarelativistic means that gas density and electrons movement speed in the matter is so high that the special theory of relativity effects influence their movement. Electron gas turns to be degenerate because its pressure does not depend on temperature in case of that density corresponding to equation of state (1.9) . This specific state is effect of quantum laws playing an important role in case of great density in the depth of white dwarfs. Electron gas is degenerated in metals in case of indoor temperature. Substituting the relation (1.9) into the equilibrium equation (1.4) we obtain the following expression:

$$K\bar{\rho}^{4/3} = \frac{GM\bar{\rho}}{R}. \qquad (1.10)$$

Average density, mass and radius of the star are connected by density definition:

$$\bar{\rho} = \frac{M}{\frac{4}{3}\pi R^3}.$$

Hence:

$$R = \left[\frac{3M}{4\pi\bar{\rho}}\right]^{1/3}.$$

substituting this relation into (1.10) we obtain:

$$M_{Ch} = \left[\frac{3}{4\pi}\right]^2\left[\frac{K}{G}\right]^{2/3} \simeq 1.44M_{\odot}. \qquad (1.11)$$

It is clear from this relation that the ultimate mass of a white dwarf is determined by fundamental constants only. For the first time this mass value was found by an outstanding Indian astronomer Subrahmanyan Chandrasekhar (1910-1995) in the 30s of the XX century.

If by the end of star's evolution the mass of a star turns out to be bigger than Chandrasekhar mass then in the time of its collapse the mattaer cannot hold the compression on the level of degenerate electron gas pressure and the compression continues until more powerful forces start to act - forces of nuclear interaction. It appeared that nuclear forces are not able, as it is considered nowadays, to equalize gravity forces if the mass of the star exceeds some ultimate value by the end of the star's evolution. In rough approximation this ultimate value was calculated by Oppenheimer and Volkoff with the help of formula close to Chandrasekhar formula (1.11) , but for degenerate neutron gas not for electron one. Oppenheimer and Volkoff supposed "neutronization" of substance to take place which means that electrons are "pressed" into protons and substance turns into neutron gas. So far as neutron gas obeys the same static laws as electron gas, formula will have the form equal to Chandrasekhar formula, but with substitute of electron mass by neutron mass which is 1840 times bigger. Obtained result turns out approximately two times bigger than Chandrasekhar limit i.e. equal to $M_{OV} \simeq 2.8M_{\odot}$. But in calculation of this limit specific properties of neutron interaction determined by strong interaction were not taken into account. The reason for this is the fact that these specific forces have not been studied enough yet. So Oppenheimer-Volkoff limit is supposed not to be exactly known. It can be bigger than it is calculated with the help of simple relations for a degenerate neutron gas. But the most important conclusion from this theory is the assumption that this limit exists. What will happen if the mass of the star appears to be more than Oppenheimer-Volkoff limit?

As it is considered nowadays if the mass of the star is more than the ultimate Oppengeimer-Volkoff mass even nuclear forces will not be able to resist the gravitational compression. In this case only a strong curvature of the space can lead to equilibrium. As of today the only theory able to give the method of approximate calculation of arising object structure is the general theory of relativity. According to this theory such object will stop to emit electromagnetic waves under the condition that the radius of the area containing all the mass of the object will be less

than so-called gravitational radius. And it will happen not because electromagnetic wave will not be emitted by the star matter but because the waves will not be able to leave such an object, since the escape velocity will exceed the speed of light. A "black hole" will appear in the sky instead of a shining star. Objects appearing at the end of evolution of star with mass more than Oppenheimer-Volkoff limit are called like this. With some certainty it is possible to say that such objects will appear with mass $M > 5M_{\odot}$.

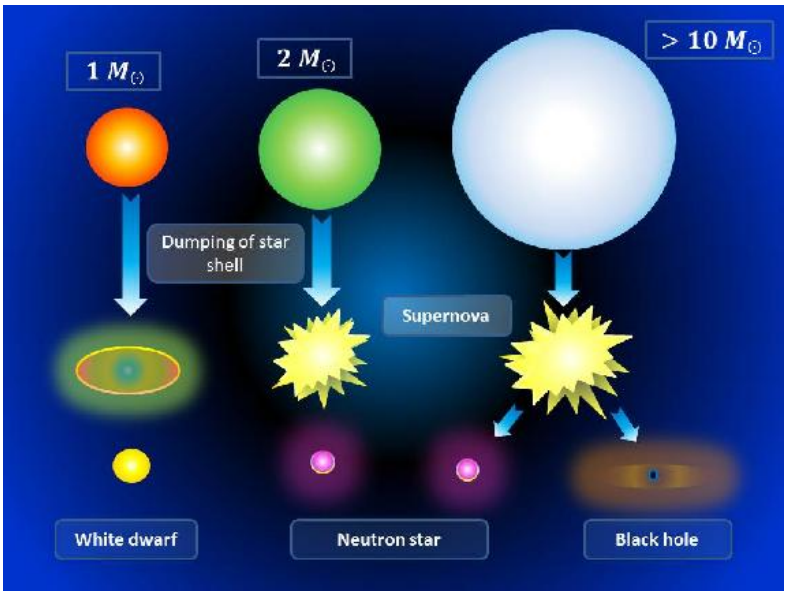

Fig. I-2-3 Evolution of stars with different masses.

In fig. I-2-3 and I-2-4 there is a stage shown as a powerful explosion and called supernova. This is very a short period of the star's existence when a red giant or a supergiant loses stability and explodes within several hours or even seconds. On the basis of the general considerations it is possible to estimate roughly the energy of this explosion. Depending on processes going on during the explosion this energy is estimated approximately as $10^{41}-10^{42}$ erg. This colossal energy is discharged into the space within split seconds and the star flashes for several hours or even days so bright that its brightness is compared to the whole Galaxy brightness. During the explosion in that area where density is still high enough, nuclear processes take place which are impossible under conditions of stable equilibrium of the star. As a result all heavy elements with atomic number more than iron are born. As for today we do not know any other ways for the formation of such heavy elements. With that enough elements are born to saturate shells of planets like the Earth with radioactive elements like uranium, thorium etc.

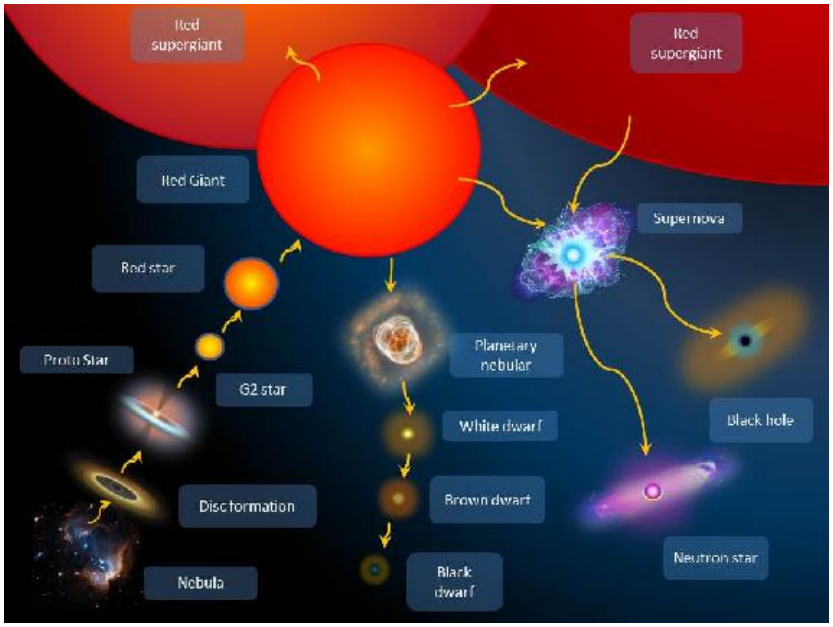

Fig I-2-4 The general overview of star evolution.

What is the main reason for the loss of stability by red giants, supergiants and other massive stars? The main reason is that under the conditions of fixed mass and chemical composition only such nuclear reactions of heavier elements synthesis can take place when enough energy for equilibrium maintenance is given off. The first nuclear reaction of such type is the reaction of transformation of hydrogen into helium. If hydrogen burns down the star shrinks and it is accompanied with a shell dump and a growth of temperature in its core. This stage is shown in fig. I-2-4 as appearance of planetary nebula around the star having dumped the shell. If mass of the star is big enough the temperature increases so much that possibility for a new thermonuclear reaction of carbon synthesis from helium appears inside the core. After helium burnup passing much faster than hydrogen burning the turn for carbon to burn comes. Carbon turns into magnesium etc. The end of this nuclear reaction chain is the reaction of iron formation inside the star. Iron nucleuses different in that way that the absorption of energy from outer source is necessary for heavier elements synthesis. Therefore the reactions of heavier elements synthesis from iron cannot be self-maintained and stop quickly. With that energy emission stops and balance between pressure and gravity cannot exist. The star compresses catastrophically and turns either into a neutron star or into an object called nowadays a black hole.

Regular stars

Under the term "regular star" a star is understood which has the equation of state with no considerable differences from equation of state for ideal gas. Such stars are young stars with not very big mass and they mostly consist of hydrogen. Except regular matter (mostly hydrogen) the radiation pressure (of photon gas) makes a contribution into the internal pressure of young massive stars. The general structure of such stars does not differ seemingly from the Sun's structure shown in fig. II-3-1. These stars have a core - an area where the thermonuclear reaction goes on, an area of radiative energy transport where thermonuclear reaction does not go on but the temperature is high enough for the energy transport from inner layers to outer layers to be realized exclusively with the help of radiation. Then closer to the star's surface area of convective energy transport can be placed like it is on the Sun. then follows the area of rapid drop of temperature to some certain minimum. This area is called

photosphere. After the photosphere there is a thin area of growth of temperature and then there is corona. The structure of such stars will be examined in further lectures by example of the Sun - the typical example of such stars.

Red giants and supergiants

The last but one stage of all regular stars with not too big mass life is their form - red giant or supergiant. This stage precedes the final hydrogen, helium and carbon burning down in the star's core. During the evolution process of hydrogen star hydrogen gradually turns into helium. This heavier element almost does not undergo a reaction of carbon and nitrogen synthesis under temperatures of hydrogen burning. The higher temperature is necessary for that. Being a heavier element helium is accumulated in the star's core and extrudes hydrogen closer to the surface. That means that if helium concentration becomes high enough helium synthesis reaction stops in the core but continues closer to its surface. In this case they say about layerwise burning of hydrogen, keeping in mind that the reaction goes on in some spheric layer close to the core. So the core temperature becomes equal at all points. In case of layerwise source appearance the area of convective energy transport broadens and with it the star grows. This is the stage of a red giant or a supergiant. Some stars reach giant sizes. Sizes of Betelgeuse and Aldebaran are shown in fig. I-2-5 to compare with blue giants Rigel, Bellatrix and Solar system orbits.

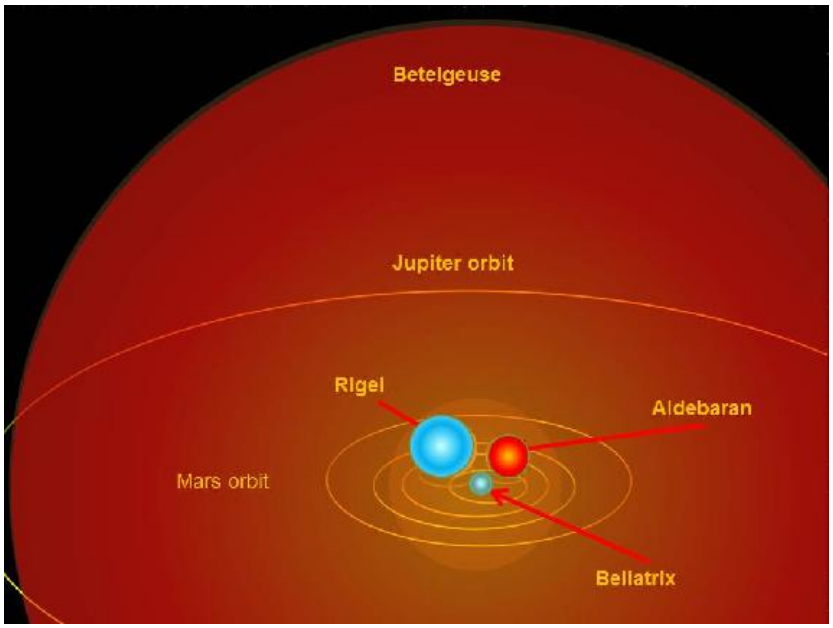

Fig. I-2-5 Comparison of red giants Betelgeuse, Aldebaran sizes with blue giants Rigel, Bellatrix and Solar system orbits sizes.

Red giants structure can be imagined by the following reconstruction, represented in fig I-2-6. In the core there are elements - products of thermonuclear reaction - continuing in layerwise energy sources. Two layerwise sources are shown in fig. I-2-6. In one of them closer to the surface where the temperature is enough only for hydrogen burning the reaction of helium synthesis goes on. In the deeper area where the temperature is higher the reaction of carbon and nitrogen synthesis can take place. In all probability reactions for even heavier - carbon for example - elements burning can take place simultaneously in very massive supergiants. Products of this reactions sink deeper inside the star where an isothermal core forms and synthesis does not take place there. Such star structure is able to

maintain stability just for tens million years. Finally relatively light elements burn down and a collapse of the star takes place. For the stars with the mass less than the Chandrasekhar mass it leads to the shell dump which can be seen in a form planetary nebula and white dwarf formation.

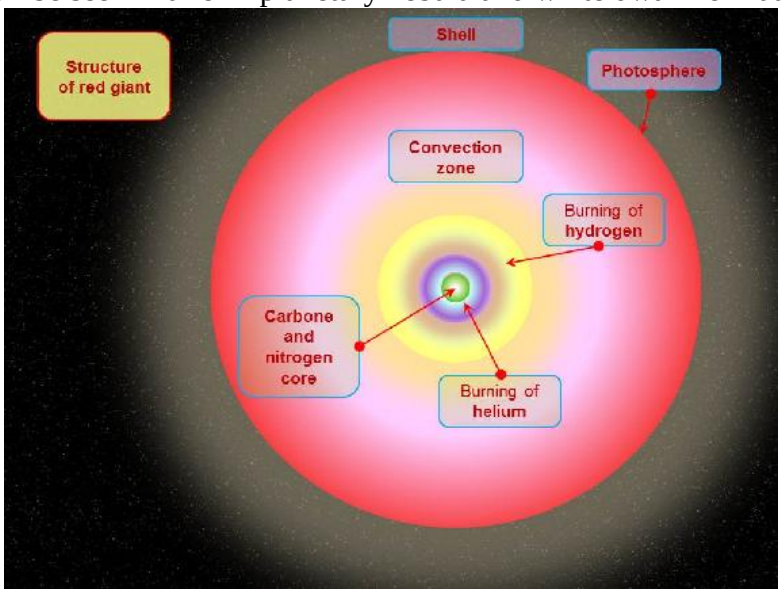

Fig. I-2-6 Inner structure of red giants.

For more massive stars a collapse is usually accompanied by the supernova explosion and a neutron star formation or a black hole formation if the mass is more than Oppenheimer-Volkoff limit [12]

White dwarfs

White dwarfs are the product of low mass, less than Chandrasekhar limit, stars evolution. Thermonuclear reaction cannot continue in these stars due to lack of temperature in the core of stars. So such stars are doomed to a slow cooling-down for millions of years and to the transformation first into a brown dwarf and then into a black one. These are very dense stars. They are so dense that matter inside purchases new properties. The pressure inside the star is mostly determined not by nucleuses of elements but by the surrounding electron gas. This gas is called degenerate. The white dwarf structure can be represented schematically as it is shown in fig. I-2-7. It consists of the inner part containing oxygen, carbon, nitrogen and helium in some proportions depending on the dwarf's mass surrounded by degenerate electron gas and of the outer shell consisting mostly of hydrogen. In the insert of this figure the photo Chandrasekhar is shown:

Neutron stars. Pulsars

Neutron stars are very small in size. For example, Neutron star with the mass of the Sun must have radius of about 10-12 km. So even with the enormous temperature of the star's surface it is impossible to observe it directly. It was considered so until 1968 when a pulsar was discovered in the remainder area of the supernova flashed in the Earth sky and called the Crab nebula.

[12] G. M. Rudnitckiy. Fate of planet systems.

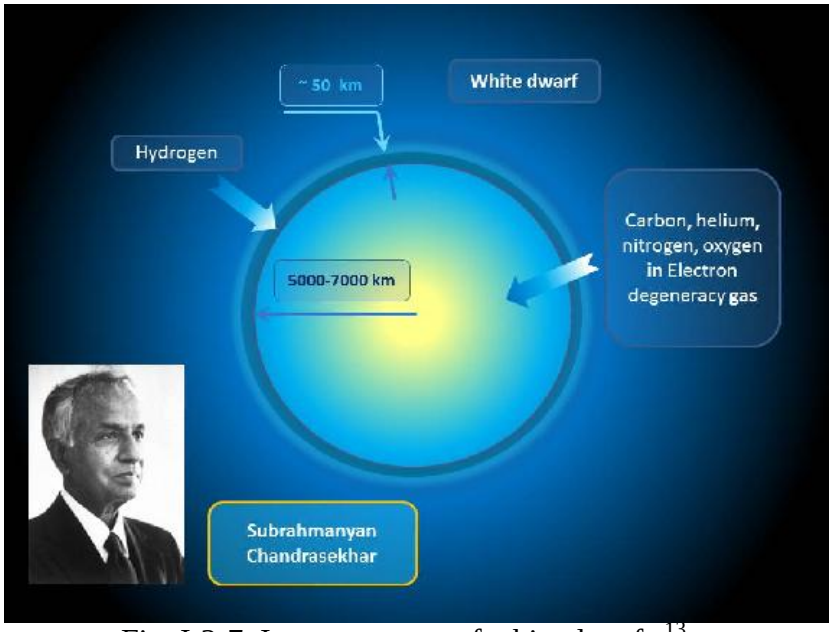

Fig. I-2-7. Inner structure of white dwarf. [13]

Pulsar is a fast turning neutron star having a great magnetic field. Due to the great magnetic field the radiation is not emitted in all directions from the surface but only in two narrow beams as it is shown in fig. I-2-7. Therefore if such beam or ray falls on the Earth a burst of radiation is observed in telescopes and especially in radio telescopes. Burst of radiation is fixed with each turn of the star. as far as such stars in spite of their great mass turn with the angular velocity of several turns per second the bursts appear several times per second. Radiation of this star pulsates in the radio range. According to that such objects are called pulsars. The first pulsar PSR B0531+21discovered in the Crab nebula makes about 30 turns per second and has the radius of about 10 km. It was considered to be the fastest for a long time. But later much faster turning pulsars were discovered. Until recently the time record of rotation velocity among neutron stars belonged to pulsar PSR B1937+21 which maks 642 turns per second. Historically it was the first millisecond pulsar discovered. If was found in 1982 and more than 20 years it was the leader. Recently a new pulsar was discovered with even higher velocity. Rate of rotation is so high that it involves some theoretical difficulties. Specifically the rotation must lead to a very fast loss of energy for gravitational waves radiation. So before it was considered that the pulsars making more than 700 rotations per second cannot exist. Considerations of stability also constrain neutron star size - its radius cannot be more than 16 km. By the way with this its equator movement speed will be about quarter of speed of light. [14].

[13] http://elementy.ru/lib/430511
http://cse.ssl.berkeley.edu/bmendez/ay10/2000/cycle/whitedwarf.html

[14] http://elementy.ru/news/430053

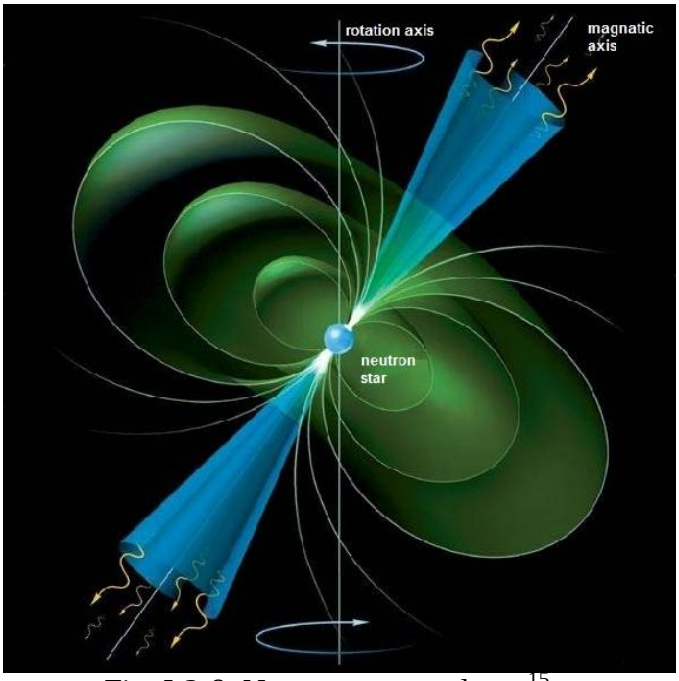

Fig. I-2-8. Neutron star - pulsar. [15]

Black holes

As it was said, black holes are the products of massive stars evolution if by the end of evolution their mass is more than Oppenheimer-Volkoff limit. If following the conventional concept we explain structure of these objects with the help of the General theory of relativity, a black hole must be considered to be the bounded area inside of which the escape velocity equals to the speed of light. Radius of this spherical surface can be calculated basing on some classical considerations. The escape velocity for a body with the mass M and radius R can be calculated with the relation:

$$V_{II} = \sqrt{\frac{2GM}{R}}.$$

Substituting the speed of light c instead of V_{II} into this formula we receive:

$$R_G = \frac{2GM}{c^2}.$$

This value is called the gravitational radius. This formula was obtained in the XVIII century by J. Mitchell and Pierre-Simon Laplace. The formula can be obtained and in the General Theory of Relativity (GTR). From the point of view of GTR any observer having got inside the gravitational radius cannot return back or send any information about himself. A conception of a black hole appearance for outer observer is given in fig. I-2-9. As it follows from the black hole sense its discovery is a problem for astronomers. But as it became clear nowadays black holes can be observed due to the process of falling of surrounding matter on it. This fall is called **accretion**. With this substance warms up and starts to shine intensively. This phenomenon can be detected at long distances from black hole.

The most important peculiarity of the objects called black holes is a strong curvature of spacetime. This leads particularly to a strong time dilation nearby this object. Therefore for the outer observer fall of bodies will take a long time (for point objects - infinite). Due to the same effect GTR

[15] http://www.vokrugsveta.ru/vs/article/2725/

black hole formation for the outer observer must take almost infinite time. So there are definite doubts that objects forming beyond Oppenheimer-Volkoff limit are GTR black holes. But in all likelihood the fact of curvature of space takes place. Some indirect data of objects related to black holes study points at this.

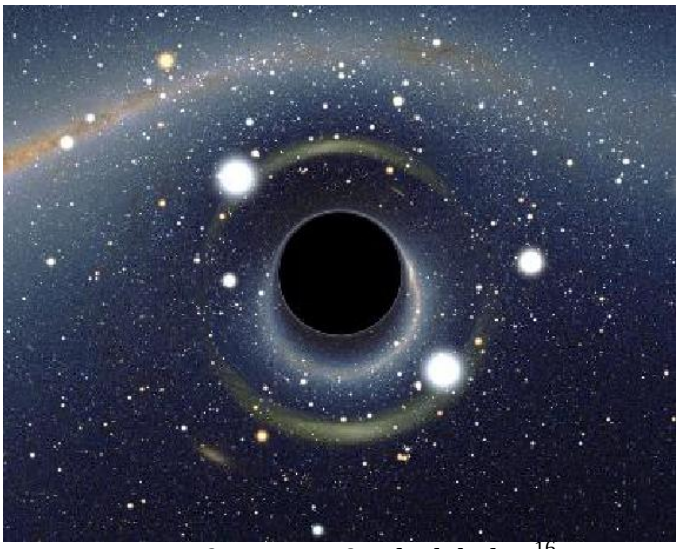

Fig. I-2-9. Fig. I-2-9. Black hole. [16]

One more important element of modern knowledge about black holes is Stephen Howking quantum theory of the evaporation of black holes. This effect is related to the fact that according to the quantum theory objects with such a great energy density must born virtual particle-antiparticle pairs, which must emit the light when they annihilate and this light takes away the energy of the black hole. This radiation spectrum must be described by Plank formula with the temperature calculated from the black hole parameters. This process is so important that if it is realized in reality there are no low mass black holes left since the moment of the Universe birth. It follows that black holes can remain only in the centers of galaxies. Black holes in galaxy centers can have masses equal to million times the mass of the Sun and therefore having not vaporized yet.

[16] http://www.at-universe.ru/chernye-dyry-mogut-proizvodit-vybrosy/\#more-115

Chapter 2. The Sun

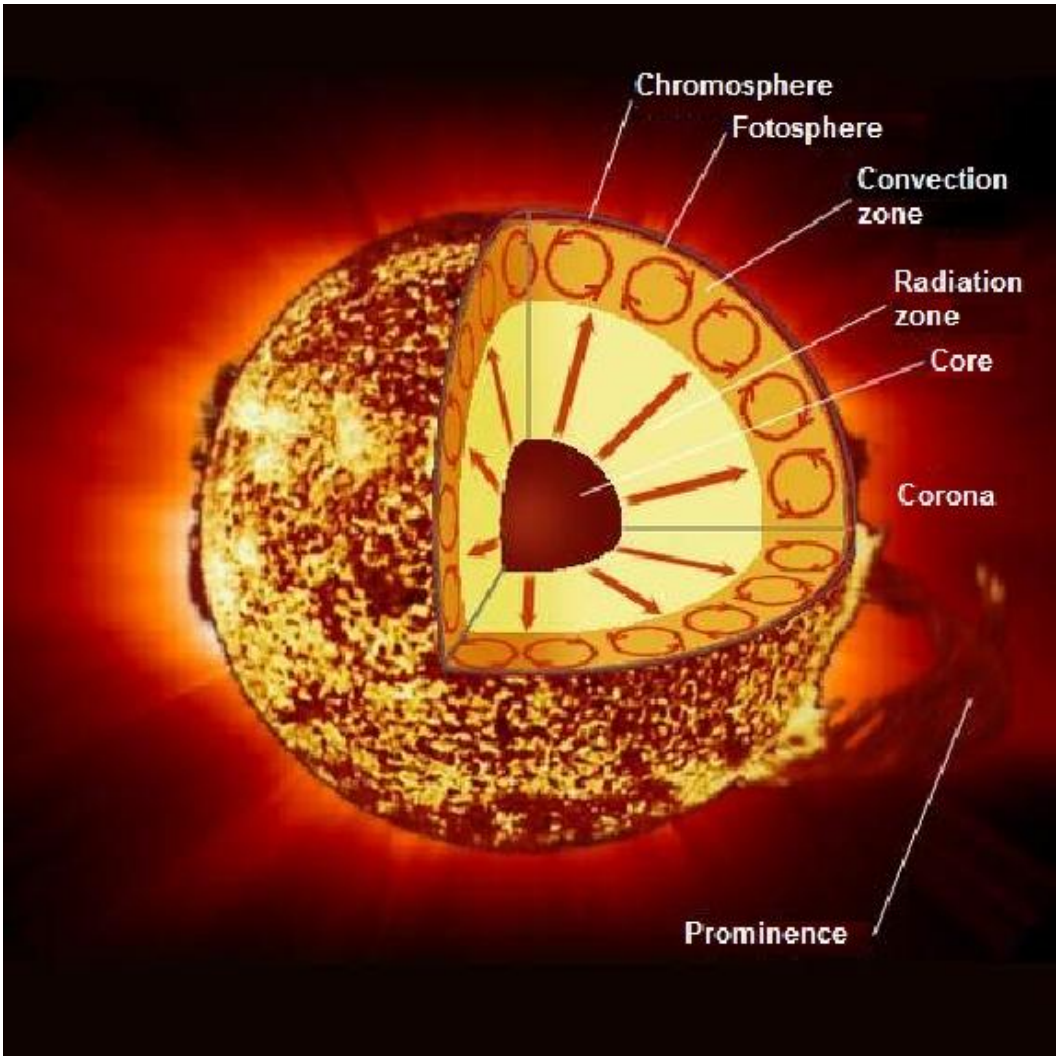

2.1 Lectures 3. The Sun - the daytime star

In previous lectures we have discussed the general conditions in the great scale space. We have cleared that the Space is full of objects either constantly or on the contrary very seldom eject flows of radiation and charged particles in the space. These flows fill the space and finally reach the vicinity of the solar system and the Earth - our apartment in the building called The Milky Way galaxy. These particles and radiation play an important role in the formation of conditions in the near-Earth space. So the exploration of these flows is important to understand the processes in this section of modern science and technique. But our own star - The Sun plays even more important role in the formation of conditions near the Earth. This is the only star visible in daytime while the other stars are visible only at night. So for the further studying of the questions devoted to the physics of processes taking place near the Earth - in its magnetosphere and atmosphere - it is necessary to clarify the major features of

this object - the daytime star.

2.1.1 Parameters of the Sun

The Sun is a yellow dwarf, it belongs to G2 spectral class. Judging by the major parameters the Sun is an ordinary star like many other in our Galaxy. The major parameters of the Sun are shown in the tables II-1,2,3

Average diameter	$1{,}392 \cdot 10^9$ m (1 392 000 km) (109 Earth's diameter)
Equatorial radius	$6{,}955 \cdot 10^8$ m (695 500 km)
Equator circumference	$4{,}379 \cdot 10^9$ m
Flatness	$9 \cdot 10^{-6}$
Surface area	$6{,}088 \cdot 10^{18}$ m^2 (11 900 Earth's square)
Volume	$1{,}4122 \cdot 10^{27}$ m^3 (1 300 000 Earth's volume)
Mass	$1{,}9891 \cdot 10^{30}$ kg (332 946 Earth's mass)
Average density	1409 kg/m^3
Equatorial acceleration	274,0 m/s^2 (27,94 g)
Escape velocity (for the surface)	617,7 km/s (55 Earth's V_{II})
Effective temperature on the surface	5788 K (5515 °C)
Corona temperature	1 500 000 K (1 500 000 °C)
Core temperature	13 500 000 K (13 500 000°C)
Luminosity	$3{,}846 \cdot 10^{26}$ W $3{,}75 \cdot 10^{28}$ Lm
Brightness	$2{,}009 \cdot 10^7$ W/m^2 /sr

Tab. II-1. Parameters of the Sun. The basic characteristics.

Slope of plane of rotation	7,25° (relative to plane of ecliptic)
	67,23° (relative to plane of the Galaxy)
Right ascension	286,13° (19 h 4 min 30 s)
Declination of the northern pole	+ 63,87°
sidereal period of outer visible layers (at latitude of 16°)	25,38 day (25 day 9 hour 7 min 13 s)
(at equator)	25,05 day (7284 km/hour or near 2 km/s)
(at poles)	34,3 day

Tab. II-2. Parameters of the Sun. The physical characteristics
Slope of plane of rotation

Inclination of rotation plane	7,25° (relative to plane of ecliptic)
Hydrogen	73,46
Helium	24,85
Oxygen	0,77
Carbon	0,29
Iron	0,16
Sulfur	0,12
Neon	0,12
Nitrogen	0,09
Silicon	0,07
Magnesium	0,05

Tab. II-3. Parameters of the Sun. Photosphere composition

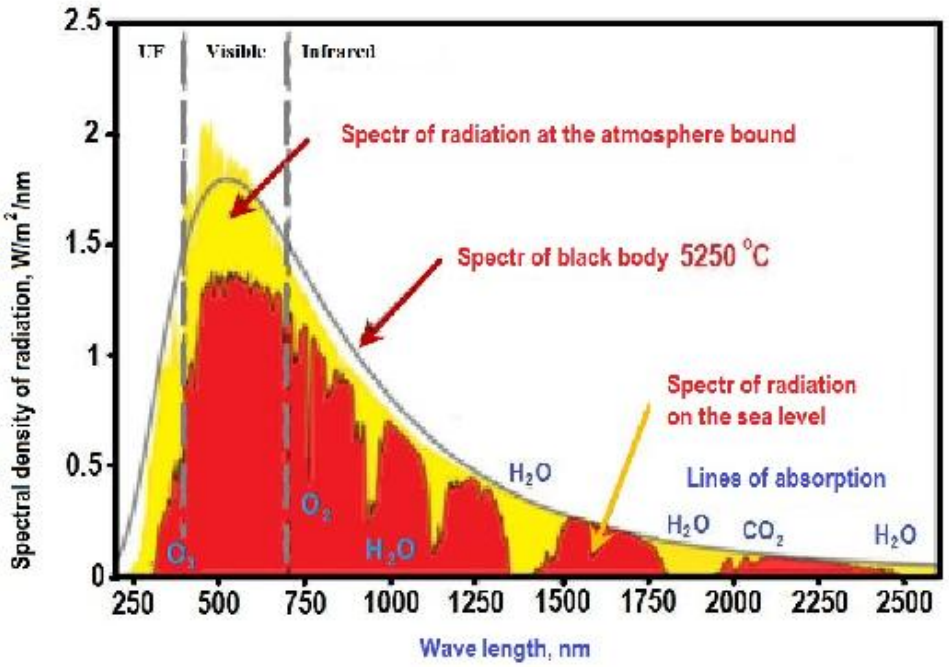

Fig. II-3-1. The Sun radiation spectrum

2.1.2 The standard model of the Sun

In 1920s English astrophysicist Arthur Eddington made an attempt to "peep" into the star to know its general structure, composition and interior parameters. A separate area appeared in

astrophysics - the star modeling. Making a start from observed characteristics - mass, luminosity, temperature of the surface, it is possible to make and solve system of equations conditioning stability of a star: equations of state of matter and energy transport, hydrostatic and thermal stability of each unit volume. It was supposed that the star is a slow rotating spherically symmetrical body without a strong magnetic field emitting energy in the central, the hottest part. Now we know that the energy properties of stars are based on the thermonuclear fusion reactions which depend strongly on the temperature and therefore the center of the star is its power reactor. Not knowing about this Eddington placed the source of the energy in the central area by intuition and it was not a fault. Models developed on the basis of astrophysical knowledge accumulation and what is not less important on the improvement of calculation techniques when computers provided a dramatic progress of it. At present good models of stars of all classes are made - from the young stars living at the expense of hydrogen "burning" like the Sun to the old ones having changed to helium, carbon or heavier nuclear fuel (red giants) and even to having exhausted all fuel resources (white dwarfs, neutron stars).

According to the standard model, the Sun consists of three areas deferent in temperature, density and process of energy transport. The central area (the core in bounds of 0.2 of radius) - is the densest and the hottest part of the star ($\rho_{core} = 150$ g/cm^3, $T_{center} = 15 \cdot 10^6$ K). Transport of energy to the boundary of this area goes on due to a weak convection. This is solar thermonuclear reactor where during the fusion reactions when four nucleuses of hydrogen fuse into helium nucleus the energy is liberated. This energy is million times greater (per mass unit) than that of chemical reaction of oil and gas burning. Then liberated heat goes through the whole star and is emitted as a flow of light. The temperature gradually decreases along the radius so in the result the temperature drops to 10^6 K, in the next static area of radiation. This temperature is not enough for nuclear "burning". The heat is transmitted by multiple absorption and reemission of x-ray quanta by atoms. Slow diffusion of heat flow takes place until the flow cooling-down within million years reaches the boundary of the radiation area at the depth of about 0.75 of the Sun radius. Here the mechanism of transmission changes into more effective convective transmission. The outer convective area is filled with boiling hot plasma gushing into photosphere ($\rho_{foto} \simeq 10^{-8}$ g/cm^3, Ò = $6 \cdot 10^3$ K).

Despite of accepted simplification the standard model represents the inner structure of the Sun with a high accuracy. With its help radial profiles of density, temperature and composition of matter were received. They let understand the outer effects of the celestial body in general. Besides the general energetic designated by the thermonuclear core these effects are determined by convective zone with its complicated magnetic hydrodynamics of high-temperature plasma. Due to heavy turbulence of plasma flows and the process of the magnetic fields generation the processes going on in the convective area are the most tangled and less clear. We explore their effects in the photosphere, in the atmosphere and in the corona of the Sun - the most rarefied upper layer of the atmosphere ($\rho \simeq 10^{-14}$ g/cm^3, Ò$\simeq 10^6$ K), but hidden under the photosphere the laws relevant to them are still things in itself.

In general the appearance of sunspots is clear. Their temperature is less than that of hot and bright photosphere. Sunspots form on magnetic flux tubes as the magnetic field prevents from the heat exchange with surroundings. The corona of the Sun appearing in all its splendor during eclipses is the initial stage of solar wind - the flow of hydrogen-helium plasma breaking through the photospheric granulation pores and accelerating going away from the star. It was a very distressful enigma why corona's temperature is hundred times higher than the temperature of the photosphere. It was solved just recently thanks to orbital observations. Solar chromospheric bursts with the liberation of energy equal to million atomic bombs explosion are explained only qualitatively. The detailed model allowing to predict the moment and energy of each burst is a dreamboat. And observed in x-ray radiation coronal holes and coronal ejections -great clouds of plasma breaking out into the space -

seem the most mysterious. All listed peculiarities of our star - its not unkind but strict enough character - got the name of solar activity (SA).

r/R_o	T,K	P, Pa	ρ , g/cm^3
Energy release area (the core)			
0	15 500 00	$2.3\cdot10^{16}$	149
0.1	13 100 00	$1.3\cdot10^{16}$	87.4
0.2	9 420 000	$4.4\cdot10^{15}$	35.3
Area of radiation energy transport			
0.3	6 180 000	$1.1\cdot10^{15}$	12.1
0.4	5 140 000	$2.7\cdot10^{14}$	3.94
0.5	3 980 000	$7.0\cdot10^{13}$	1.32
0.6	3 130 000	$2.1\cdot10^{13}$	0.50
Area of convection			
0.7	2 340 000	$6.4\cdot10^{12}$	0.20
0.8	1 380 000	$1.6\cdot10^{12}$	0.09
0.9	602 000	$2.0\cdot10^{11}$	0.02
0.98	99 600	$1.7\cdot10^{9}$	0.001
Photosphere			
1.0	4 560	$1.2\cdot10^{4}$	$0.74\cdot10^{-7}$

Table II-3 The Sun structure data taken from multi-media course [17]

The Core

The core - is the central part of the Sun where thermonuclear reactions go on spontaneously and where the energy is liberated in a form of powerful electromagnetic radiation and high energy neutrino. The mass of the core is about 10% Sun's mass, and radius about 1/3 of Sun radius. The temperature of core about $15\cdot10^6$ K, density is about 160 g/cm^3

Energy release almost completely is provided by pp-reaction. Only in the very center the role of carbon cycle reaches 8%. The hottest stars shine thanks to fusion of three nucleuses of helium into ne nucleus of carbon.

As it is show in fig. II-3-3 fusion reaction undergoes three stages

I. $^1H+^1H\rightarrow^2H+e^+ +\nu+0.42$ MeV

II. $^1H+^2H\rightarrow^3He+\gamma+5.5$ MeV

III. $^3He+^3He\rightarrow^4He+2^1H+12.8$ MeV

[17] Ed. Kanonovich V.K. Earth life in the Sun atmosphere. M.: NRI of MSU, 2007

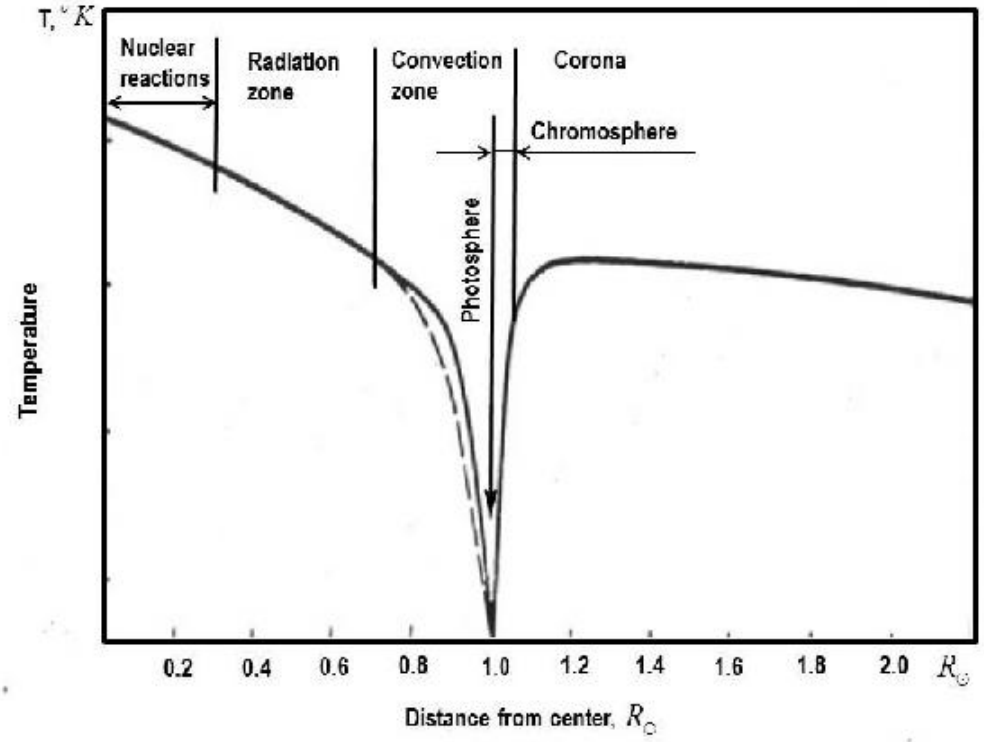

Fig. II-3-2 Diagram of temperature changing with the distance from the center of the Sun with the main elements of the Sun's structure designation.

At first two protons collide and one of them turns into neutron. With this positron and neutrino are born. So a very high temperature is needed in the core to provide heat energy of colliding protons higher than electrostatic repulsion energy between the two protons. As the result nucleus of deuterium appears - deuteron ^2H . Collisions of protons are very rare but due to their great quantity in the core the reaction goes on continuously. A very high density of matter in the core is needed for that. At the second stage deuterium nucleus collides with one more proton. This reaction is more frequent. For a randomly chosen deuteron the time of its collision with any other proton will be just than 1 second. As the result helium isotope ^3He appears. At the last stage two colliding nucleuses ^3He yield one helium nucleus ^4He. Time of this reaction is also great and equals to 10^6 years. Helium nucleus do not react practically. A higher temperature than the Sun core has is needed for that. Helium ^4He accumulates in the Sun core what in the course of time will lead to the termination of the nuclear reaction of helium fusion and the Sun will turns into a white dwarf.

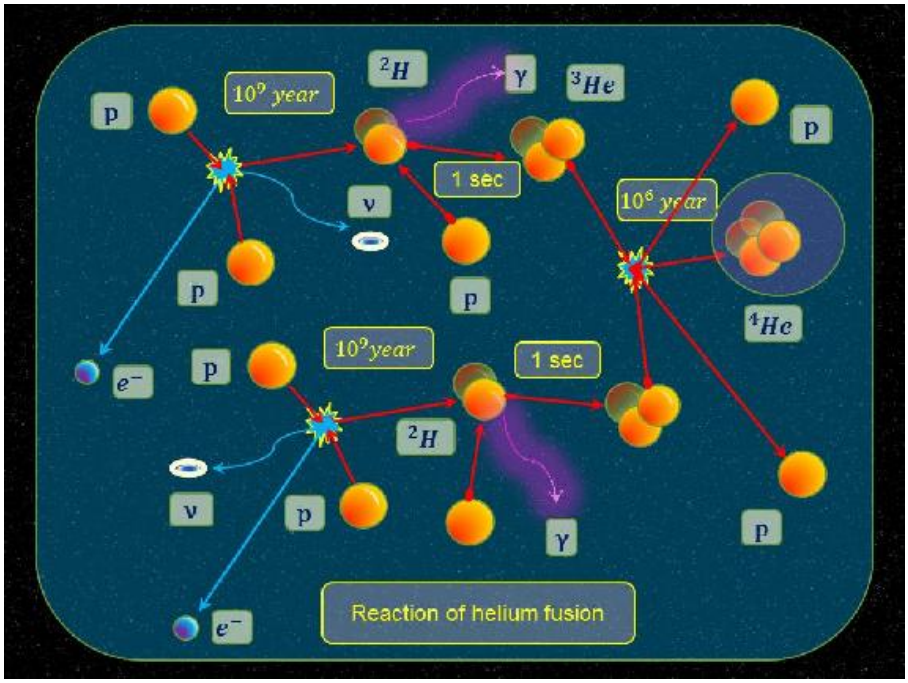

Fig. II-3-3 Reaction of helium fusion from protons - pp reaction

SNU = solar neutrino unit is determined as neutrino flow when in detector containing 10^{36} nucleuses of chlorine ^{37}Cl appear one nucleus of argon ^{37}Ar at 1 s. One can find more details about methods and discoveries in solar neutrino astronomy in R. Davis Jr.'s Nobel lecture [34] and article [35].

In neutrino detector "Super-K" within 500 days of accumulation a unique very diffuse image of the Sun "in neutrino rays" was obtained. The whole size of the sky segment is 90×90 degrees on a (right ascension) and d (declination). A black dot in the center is the real Sun size. Brightness of the image is proportional to neutrino flow.

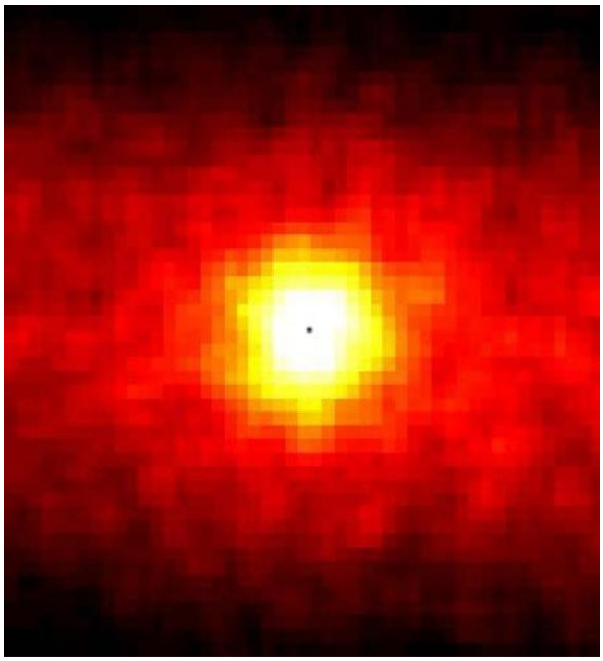

Fig II-3-4 Image of the Sun in neutrino telescope

Area of radiative energy transport

Energy transport as the result of multiple absorption and reemission of quanta by atoms (diffusion of radiation) is the main for the most stars being in radiative equilibrium and the only mechanism of transport in their radiative areas. With the temperatures below 10^7 thermonuclear reactions inside the Sun decay very fast and the luminosity of the core reaches the value of the luminosity of the whole Sun. So the layers enclosing the core from 0.3 to 0.7 of the Sun radius (radiative area) having no own sources of energy just reemit it. The flow of radiative energy formed in the core and passing through the surface of sphere with radius r remains in radiative area equal to the luminosity of the Sun $L_\odot$:

$$4\pi r^2 \sigma T^4 = const = L_\odot.$$

According to Stefan-Boltzmann law radiation flow density is proportional to the fourth power of temperature. Therefore in the radiative area the temperature is usually inversely proportional to quadratic root of radius r:

$$T \sim r^{-1/2}$$

Radiation is transported from layer to layer only as the result of radiative diffusion along the whole length of radiative area.

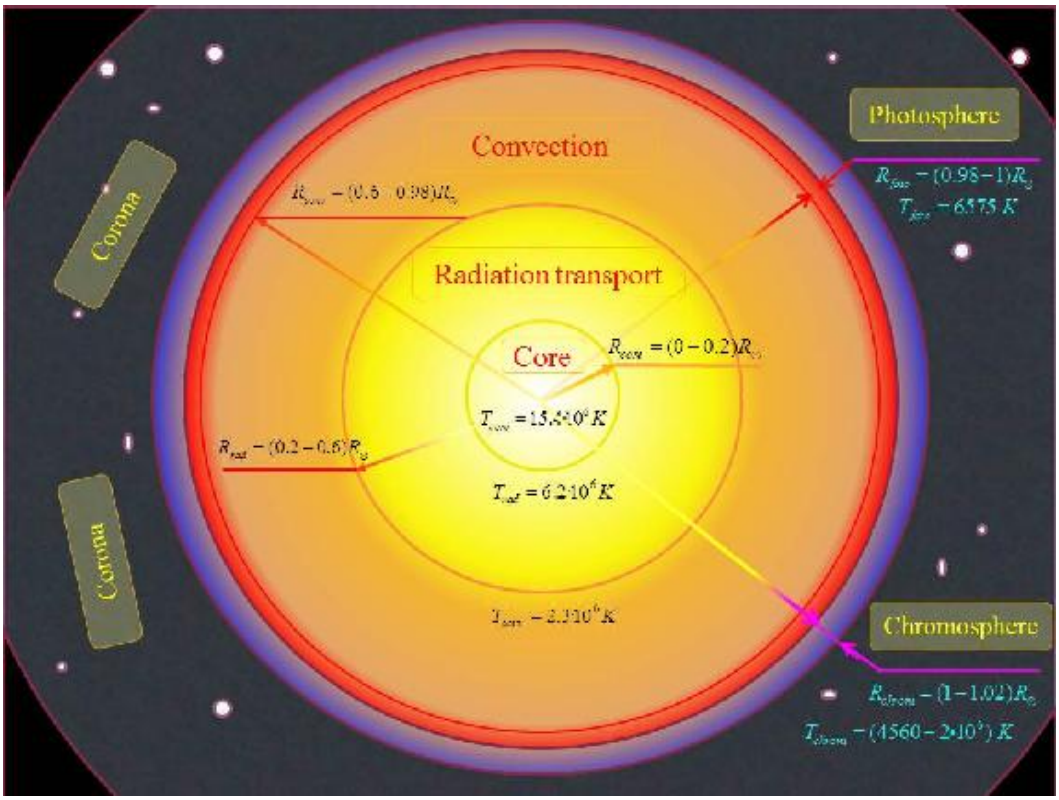

Fig II-3-5 Structure of the Sun

Convection area

In the convection area separate overheat elements rise, illuminate and cool-down (the white arrows). Their tops are visible in photosphere as bright granules and they form the general image of granulation. Colder streams going down start in dark intergranular areas, then they flow together in a flow going down and finish this cyclic process (the black arrows).

Photosphere

Photosphere is the deepest part of the Sun atmosphere. It represents a very thin layer of about 10000 km where the temperature reaches its minimum. First it decreases to about 4560K and then it sharply increases (see fig. II-1 and II-2). In its lower layers the temperature exceeds 6000 K but in the outer layers of the photosphere the temperature reaches its minimal value for the whole Sun - about 4560K. It is this area with the minimum temperature that can be considered as the surface of the Sun. With this temperature only one of 10000 atoms of hydrogen is ionized. And with it the same number of times the number of atoms of elements which easily ionize giving at least one electron (mostly metals) is less. So photosphere substance is still in a form of heavily ionized hot plasma even in the area of the temperature minimum. Irregularity of luminescence of photosphere is conditioned by unevenly heated convection cells touching the photosphere directly. Convective cells in the photosphere are observed in a form of granulation of a great number of areas changing fast in the course of time. These areas have the increased temperature in the center and decreased at the edge. But under certain conditions on the photosphere surface relatively dark and cold spots form - ***sunspots*** which have noticeably greater magnetic field than surrounding areas. -

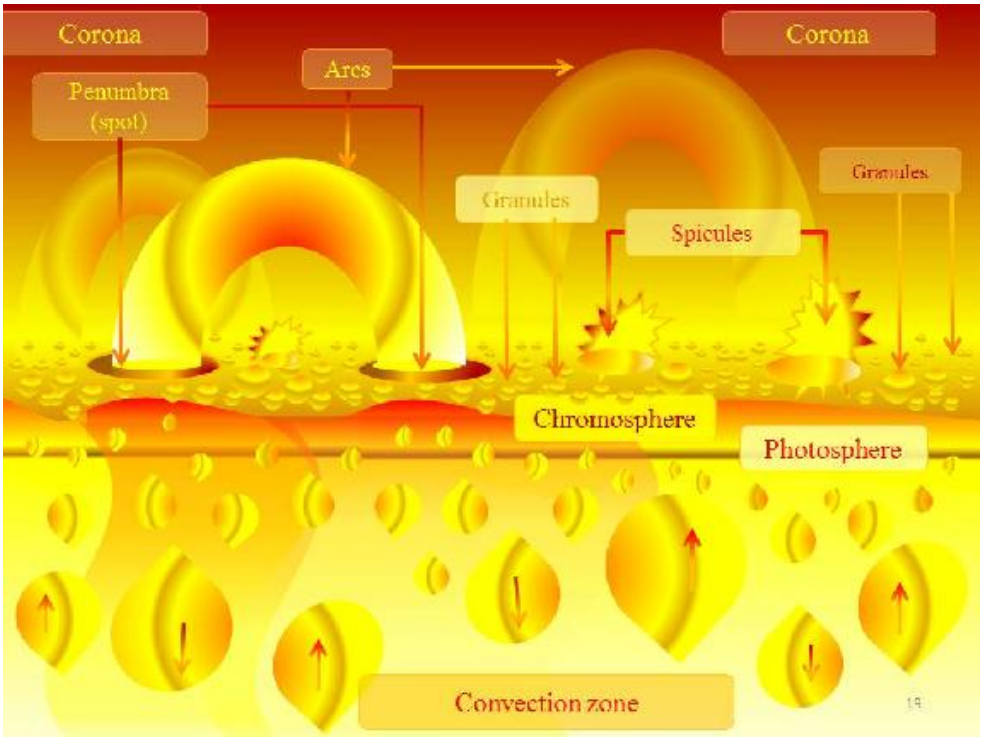

Fig. II-3-6. Photosphere. Illustration of interaction with convective cells

Chromosphere

The chromosphere is a layer of the Sun atmosphere inhomogeneous in structure, placed directly above the photosphere. The chromosphere is called so thanks to its red-purple color. It can be seen during full solar eclipses as a shaggy bright ring around the black disk of the Moon covered the Sun.

The chromosphere is inhomogeneous enough and it consists mostly of ***elongated extended languets - spicules***, making it to look like a burning grass. The temperature of these chromosphere jets

is two to three times higher than in the photosphere and the density is hundreds times less.

The total length of chromosphere is 10-15 thousand kilometers. The chromosphere temperature rises with the altitude from 6000 K to about 20000 K. With this temperature intensive radiation in hydrogen atom lines forms in the chromosphere, specifically in H-alpha line.

One of the most interesting details to be seen in chromosphere in H-alpha line images is ***prominences***. They are areas of cold dense plasma, penetrating high into the corona and therefore they are visible over the solar limb. Radiation of the solar chromosphere in H-alpha line lies in the visible area of spectrum and has a bright red color.

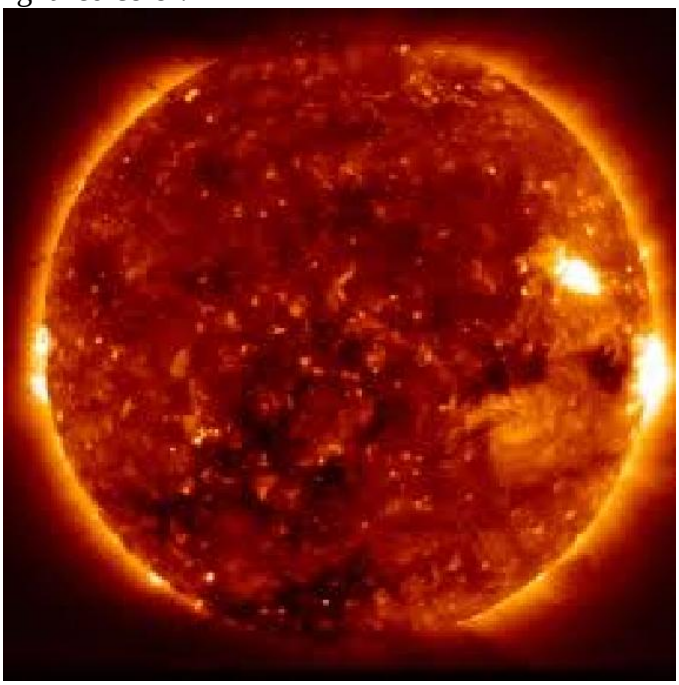

Fig. II-3-7 Chromosphere. Bright rim around the limb of the Sun.

The growth of temperature in chromosphere is explained by the propagation of waves and magnetic fields penetrating here from the convective area. Matter warms-up as it would be in a giant microwave oven. Thermal velocities of particles increase, collisions of them become more frequent and atoms lose their outer electrons: the matter becomes hot ionized plasma. The same physical processes also maintain enormously high temperature in the outer layers of the solar atmosphere placed above the chromosphere.

Corona

The temperature rises fast in the chromosphere, ionization of hydrogen and other elements increases and in the palace where the temperature reaches million of Kelvin degrees the chromosphere passes into hot highly rarefied plasma - the corona, expanding into the space forming the solar wind - the flow of charged particles (plasma) carrying along the magnetic field lines and washing the Earth magnetosphere. A high resolution image of corona made from the Earth is shown in fig. II-3-5. The area near the solar limb having purple color is the chromosphere.

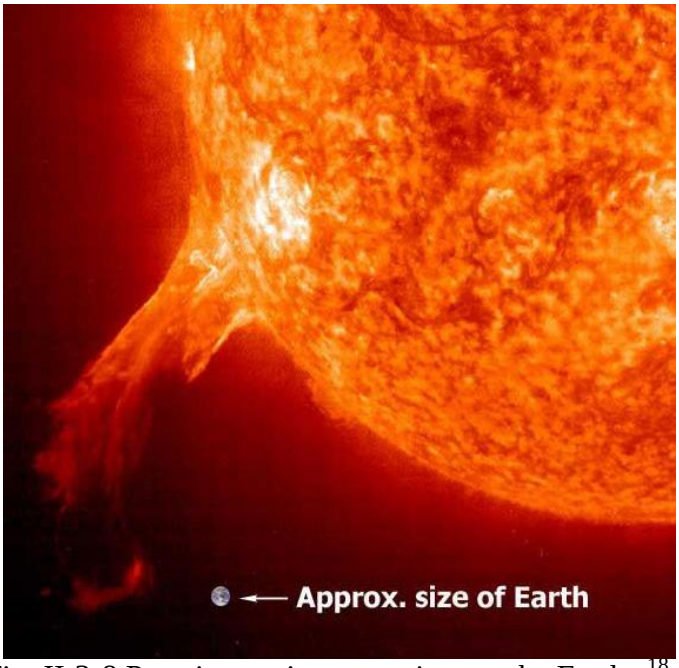

Fig. II-3-8 Prominence in comparison to the Earth. [18]

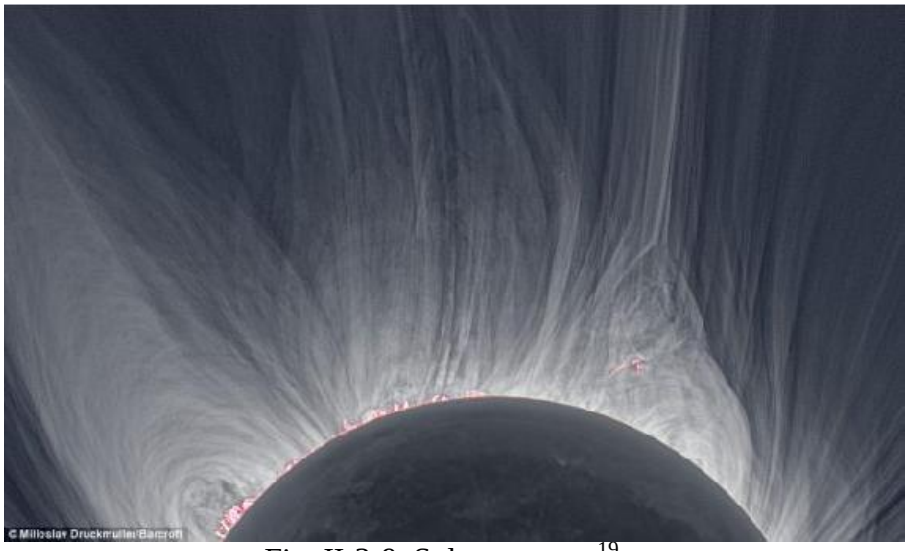

Fig. II-3-9. Solar corona. [19]

Corona changes depending on solar activity. Aleksey P. Ganskiy created the first classification of corona types. This classification is shown in fig. II-3-6 [20]

The average temperature of rarefied gas in the solar corona is about $(1-2)\cdot 10^6$ K. Gas is almost fully ionized and consists of electrically charged particles. This ionized gas is called plasma. Gravitation is not able to hold it in the Sun. It was established in 1950s based both on observation and on physical considerations. Primary explanation is based on the assumption that due to great

[18] http://tvsh2004.narod.ru/astr_sun/ss_sun5.html

[19] Shooting by Miroslav Drakmiller http://www.infuture.ru/article/3126

[20] Earth life in Solar atmosphere. Ed. E.V.Kanonovich. MSU, 2007;http://www.astronet.ru/db/msg/1212879

temperature of gas the corona must expand from the Sun with the supersonic speed. Nowadays this statement is doubted. As it was

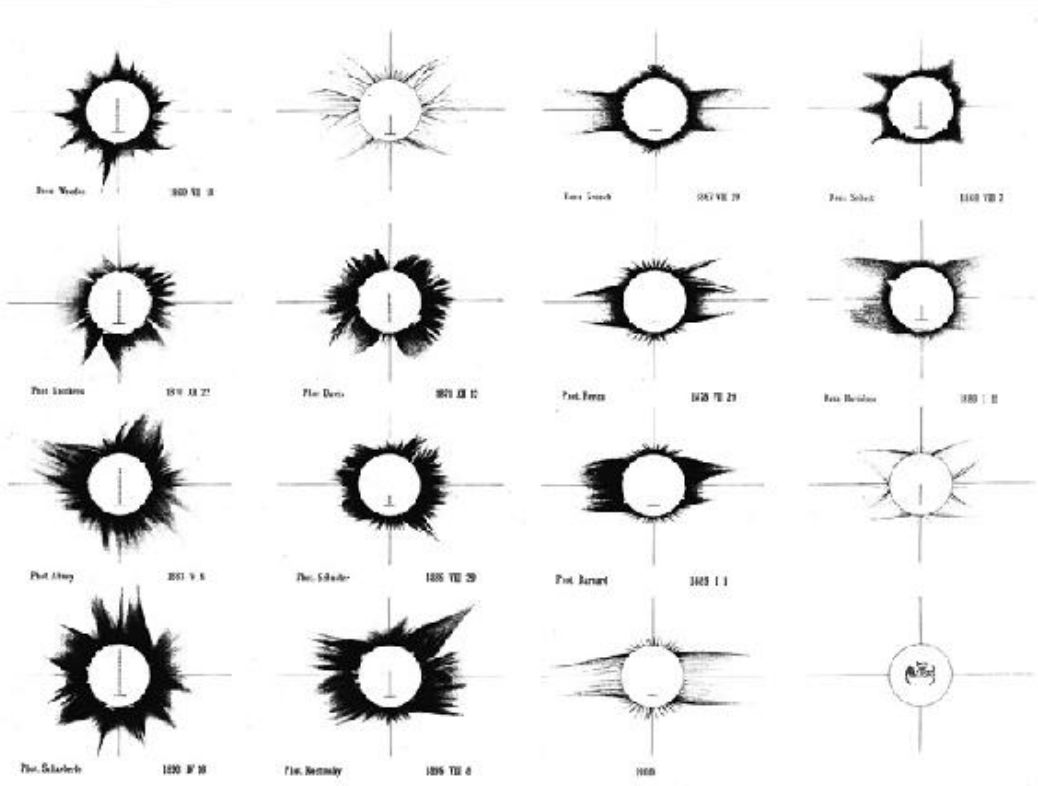

Fig. II-3-10. Classification of corona types according to A.P. Ganskiy. [21]

established with the help of Ulysses satellite placed on the orbit over the solar poles the fast solar wind blows from ***coronal holes***. Therefore there is a hypothesis (Veselovskiy I.S.) that the solar wind is generated by electromagnetic processes in plasma in areas of coronal holes where the magnitude of magnetic field is higher.

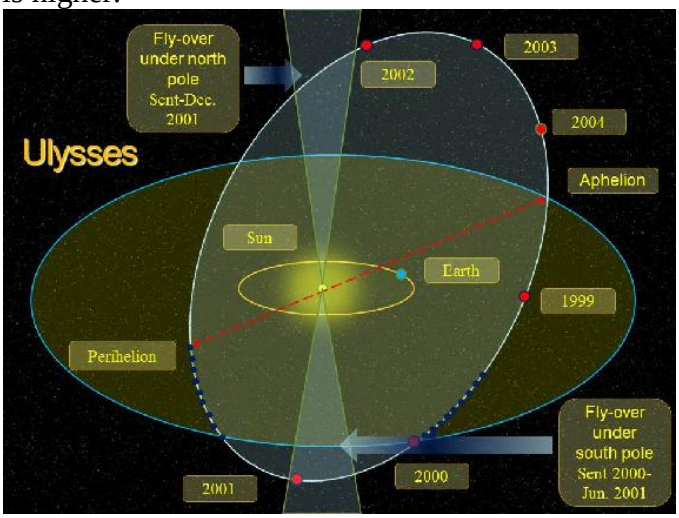

Fig. II-3-11. Spacecraft Ulysses' orbit.

[21]5Aleksey Pavlovich Ganskiy, (July the 8th (July the 20th) 1870, Nikolaevka village (Ganskoe) (Odessa region nowadays) Anan'jevskiy uezd, Kherson province. Died on the 29th of July (August the 11th) 1908, Simeiz)

Coronal holes (CH) are elongated areas of the corona with much decreased brightness. They are observed in X-rays on the solar disk. Density of corona is less in these areas. CH are the source of the intensified solar wind. CH remain within several revolutions of the Sun. It is possible that it is CH that condition known 27-day recurrence of many geophysical phenomena.

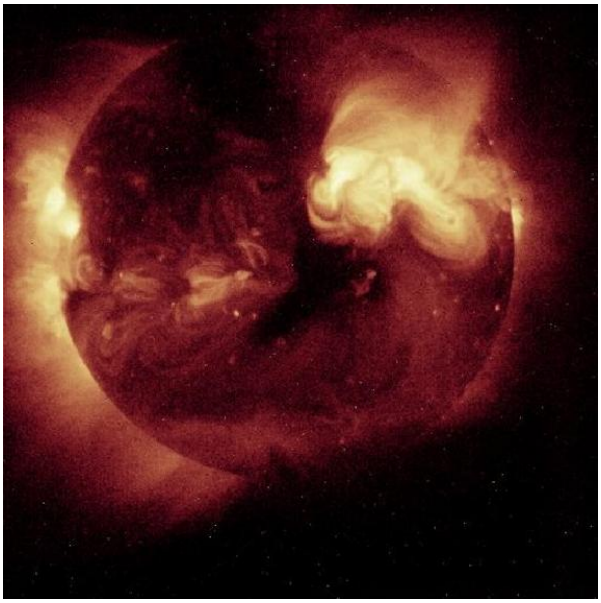

Fig. II-3-12 Coronal holes

Coronal holes are notable for absence of x-ray radiation due to heavy reduction of corona plasma density there. Coronal holes form radial "corridors" of intensified solar wind. Through CH accelerated flows of solar wind born by flashes spread into the space forming elongated areas in solar corona notable for the absence of x-ray radiation. .

2.2 Lecture 4. The Magnetic field of the Sun. Solar wind. Heliosphere

2.2.1 Differential rotation of the Sun

In 1912 D. Hale (USA) discovered a weak (approximately 1 Gauss) common magnetic field (MF) of the Sun. Babcock supposed that alike the terrestrial field it has a dipole character but is concentrated in outer layers with differential rotation (outer layers of the Sun rotate with the velocity changing with the latitude. See fig. II-4-1). According to Maxwell laws the movement of magnetic fields generates electric currents in a conductor (including plasma), and their magnetic effects according to electromagnetic induction laws block the movement caused them. As the result in a strong magnetic field plasma can move only along the magnetic lines of force. On the contrary if the plasma kinetic energy of movement is great it carries along weaker fields as it fields were trapped in it.

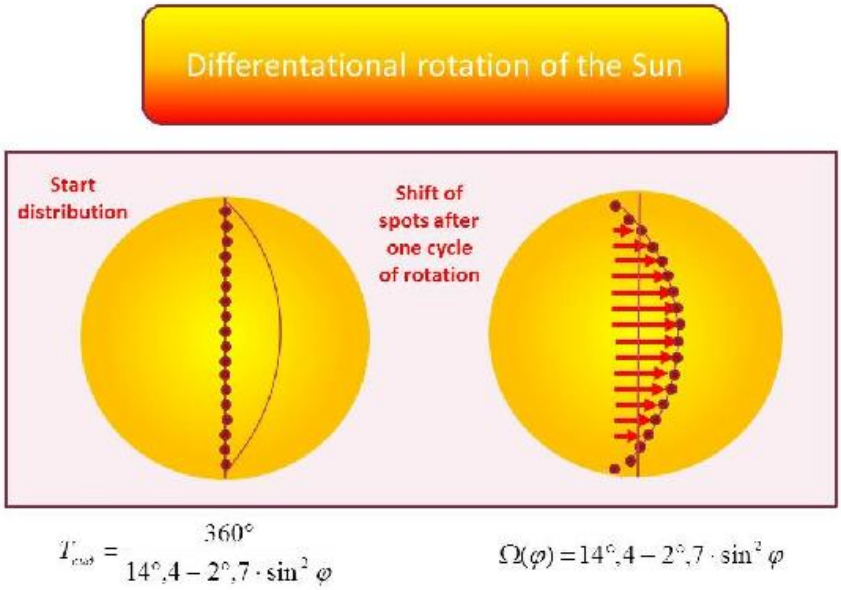

Fig. II-4-1. Differential rotation of the Sun. [22]

The dynamo effect is the intensification of the magnetic fields determined by some types of plasma movement. In qualitative explanation first it is supposed that the solar magnetic field contains poloidal (a) and toroidal (b) magnetic fields as components. In the first one the lines are directed along meridians like a dipole field and in the second one - along parallels like the field of the direct current. With the incoherent rotation when different layers have different angular velocity the trapped line of force of the poloidal magnetic field twists and some its parts go farther in comparison to the other parts due to freezing-in effect. According to electromagnetic induction laws faster rotation near the equator induces the additional magnetic field. As the result magnetic lines of force stretch around the rotation axis reinforcing the magnetic field due to deceleration of rotation (α-effect). Dynamo effect will be depicted in more details in lectures devoted to the magnetic field of the Earth

[22] http://www.kosmofizika.ru

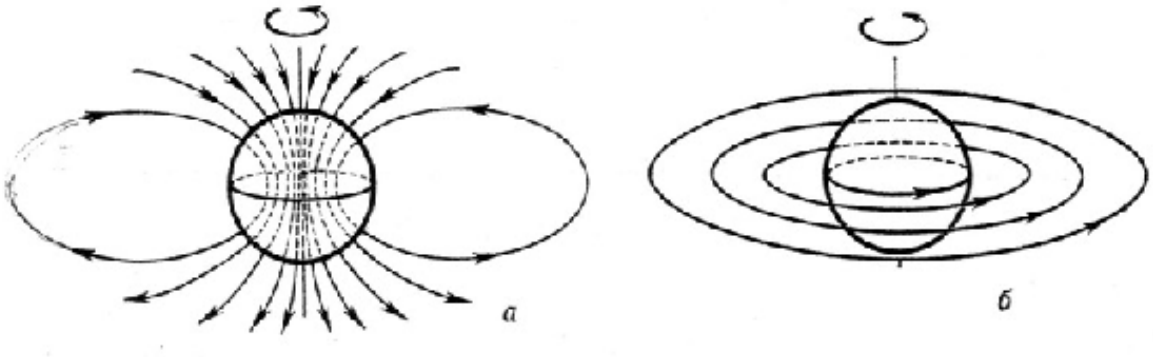

Fig. II-4-2 poloidal and toroidal components of the solar magnetic field. [23]

2.2.2 The solar corona and the solar wind

The solar wind

Parker's theory of solar wind is based on the following assumptions. The first one is that the solar wind is a hydrodynamic flow incipient in the solar corona due to its great temperature (thermal wind) and it is directed outward. Its speed is high enough to overcome the gravity. Therefore the first equation of the theory is Euler equation for radial gas flow in the gravitational field of the Sun:

$$u\frac{du}{dr} = -\frac{1}{\rho}\frac{dP}{dr} - \frac{GM_{\odot}}{r^2}. \qquad (2.1)$$

The second equation is also hydrodynamic equation representing mass conservation law having the following form in case of a radial stationary flow:

$$\rho r^2 u = \rho_0 r_0^2 u_0 = I = const. \qquad (2.2)$$

The latter equation of the Parker theory represents gas equation of state which can be written in different variants. In the simplest case it can be supposed that gas flows out of the corona without changing the temperature: $T = T_0 = const$ [7]. In this case we have the following form of the equation of state:

$$P = 2\frac{\rho}{m_p}kT, \qquad (2.3)$$

here m_p is the mass of wind particles i.e. protons.

Another assumption is adiabaticity of the flow which can be written in the following form:

$$P = K\rho^{\gamma}. \qquad (2.4)$$

In both cases the analysis leads to similar results so consider the simplest isothermal case. Substituting (2.1) and (2.2)) into (2.3) one obtains:

$$\frac{1}{u}\frac{du}{dr} + \frac{2kT}{m_p}\frac{1}{\rho}\frac{d\rho}{dr} + \frac{GM_{\odot}}{r^2} = 0,$$

or

$$\frac{1}{u}\frac{du}{dr}(u^2 - \frac{2kT}{m_p}) = \frac{4kT}{m_p}\frac{1}{r} - \frac{GM_{\odot}}{r^2} = \frac{1}{r^2}(\frac{4kT}{m_p}r - GM_{\odot}). \qquad (2.5)$$

This equation has an integral of motion in the following form:

[23] http://www.nmdb.eu/?q=node/288

$$\frac{1}{2}(u^2 - u_0^2) + 2\frac{kT}{m_p}(\ln\rho - \ln\rho_0) = \frac{GM_\odot}{r} - \frac{GM_\odot}{r_0}. \qquad (2.6)$$

Therefore the solutions with the given parameters of solar wind can be easily written. But it is more convenient to make qualitative analysis of this solution based on equation (2.5) .

Note that in the right part of the equation (2.5) there is only the radial distance from the center of the Sun. As it is seen the function equals to zero only at some critical distance r_c from the Sun which has the following expression :

$$r_c = \frac{GM_\odot m_p}{4kT}.$$

at this distance from the Sun determined only by the temperature T the left part of equation (2.5) must turn into zero. Therefore at this point the speed reaches either its minimal or maximal value and the condition is satisfied:

$$\left.\frac{du}{dr}\right|_{r=r_c} = 0,$$

or

$$u^2\big|_{r=r_c} = \frac{2kT}{m_p}.$$

In the second case we have:

$$u_c = \pm\sqrt{\frac{2kT}{m_p}},$$

which is also determined by the temperature. Therefore all possible curves $u = u(r)$ corresponding to the solutions of (2.6) divide into 4 classes.

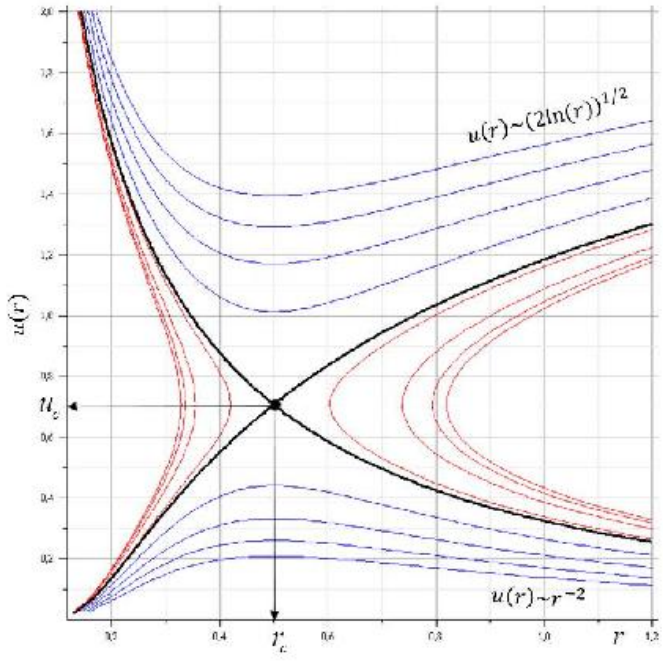

Fig. II-4-3 Integral curves for solutions of Parker's equations for solar wind in isothermal case.

These curves are represented in fig. II-4-3. For their parameterization the relation (2.6) was

represented in a form:

$$U^2 - \ln U = 2\ln R - \frac{A}{R} + B,$$

here $U = u/V_0$, $R = r/r_0$,

$$A = \frac{2GM_\odot}{r_0 V_0^2},\ B = \frac{u_0^2}{V_0^2} - A,\ V_0 = \frac{4kT}{m_p}.$$

Parameters u_0 and r_0 are the initial values at corona boundary. Curves in fig. II-4-3 are obtained for different A with fixed $B = 1$. In this case $R_c = 0.5$ and $U_c = 0.5$.

The blue curves in fig. II-4-3 lying below the critical point describe the flow with low speed near the solar surface and this flow decreases according to the law $u \sim r^{-2}$ at the distance from the Sun. Its speed increases only near the critical radius. The blue curves lying above the critical point describe the flow with high speed near the solar surface and slightly increasing with the distance according to the law $u \sim (2\ln r)^{1/2}$. The red curves to the right from the critical point describe flows flowing around the solar corona with high speed, the red curves to the left from the critical point describe flows which form in the Sun but return back again. This model has one imperfection that the obtained solutions describe the module of the solar wind speed and say nothing about its direction. As the result the blue curves can describe the flow directed either to the Sun or from it. Nowadays it is supposed that the magnetic field and its fluctuations play the major role in the formation of flow exactly from the Sun especially it is concerning to fast wind blowing from the coronal holes [13].

As it has turned out (see [8]) if the impossibility to determine the direction of wind with the help of the considered model of isothermal solar wind is not taken into account then this model describes the real situation relatively well (for outflowing wind) only in the area before the critical point. At farther distances an adiabatic model with $\gamma = 5/3$ fits better.

In the reality the solar wind represents hot plasma outflowing from the solar corona with the speed from little less than 300 km/s to more than 1000 km/s which can be observed during transient events. It is possible to single out two rates of standard solar wind: fast solar wind outflowing from coronal holes at up to 800 km/s and slow solar wind outflowing from other areas of corona (especially in big structures called coronal streamers well-known from photographs of eclipses) at up to 400 km/s. the wind mostly consists of charged particles: protons, electrons with a not big addition (5%) of ionized helium and some ions of heavy elements. All these elements can be found in images in fig. II-3-8 and II-3-11

Parameters of solar wind measured in the space near the Earth:

Parameter	Fast wind	Slow wind
Speed	500-800 km/s	250-400 km/s
Density	$3\cdot10^6$ m^{-3}	$10\cdot10^6$ m^{-3}
Protons temperature	$2\cdot10^5$ K	$4\cdot10^4$ K
Electrons temperature	$1.2\cdot10^5$ K	$1.5\cdot10^5$ K
Magnetic field	2-10 nT	2-10 nT

Table II-3. Parameters of solar wind.

Solar wind is inhomogeneous in space. The radial dependence is studied more detailed with the help of direct methods near the plane of the ecliptic at distances approximately from 0.3 a.u. to several tens a.u. The most distant spacecraft Pioneer 10, 11, Voyager 1,2 reached the distance of about 80-100 a.u. after thirty years of their flight. As it was measured by those spacecraft the density of protons n and their flux $n\cdot u$ decrease with the distance from the Sun under the law close to $\sim r^{-2}$. Solar wind speed weakly depends on distance. The temperature of protons beyond the Earth orbit is $T_p \sim r^{-0.52}$ according to the data from spacecraft "Pioneer-10" obtained during the flight from 1 to 12.2 a.u. in 1972-1977. The magnetic field weakens with the distance from the Sun in rough compliance with Parker model.

Parker spiral

A very important element of Parker Theory is that it is possible to describe how lines of force of solar magnetic field look like far from the Sun. The most important element of the theory of solar magnetic field given by Parker is the condition that the magnetic line of force is frozen into plasma. Under this condition the magnetic field is firmly tied to particles of plasma and it is transported by them. The condition of frozen lines is satisfied if the density of plasma kinetic energy $\rho u^2/2$ is more than the energy of magnetic field $B^2/8\pi$. This condition is satisfied for solar wind thanks to density high enough.

Examine the magnetic field in the equatorial plane of the Sun (in fact ecliptic). For the magnetic field in this plane the condition of absence of magnetic charges is satisfied:

$$\mathrm{div}B = 0.$$

In polar coordinates system this equation can be written as:

$$\frac{1}{r}\frac{\partial rB_r}{\partial r} + \frac{1}{r}\frac{\partial B_\varphi}{\partial \varphi} = 0.$$

And from here we obtain:

$$\frac{\partial rB_r}{\partial r} + \frac{\partial B_\varphi}{\partial \varphi} = 0.$$

That means that a function χ exists that:

$$rB_r = \frac{\partial \chi}{\partial \varphi},\ B_\varphi = -\frac{\partial \chi}{\partial r}.$$

Function χ is a function along the isolines of which the magnetic-field vector rB_r, B_φ is directed.

Magnetic field lines are tied to certain points of the solar surface and rotate together with them. As far as the magnetic field is tied to the Sun then from the observer's point of view, who is on the Sun, function χ must remain changeless. Therefore in such reference system the following condition must be satisfied:

$$\frac{d\chi}{dt} = 0.$$

Hence in the inertial reference system for the outer observer, who moves at rate $u = \dot{r}$ along the radial coordinate, we obtain:

$$\frac{d\chi}{dt} = \frac{\partial\chi}{\partial r}\frac{dr}{dt} + \frac{\partial\chi}{\partial\varphi}\frac{d\varphi}{dt} = 0.$$

Hence:

$$-B_\varphi \frac{dr}{dt} + rB_r \frac{d\varphi}{dt} = 0. \qquad (2.7)$$

This is the equation of transport trajectory for a constant in magnitude magnetic field from the point of view of an observer on the Sun. The magnetic field moves together with points of the surroundings and does not change either in magnitude or in sense. But from the observer on the Sun's point of view the sense of the field changes all the time. That means that from this observer's point of view the sense of magnetic field all the time coincide with the sense of the velocity of solar wind:

$$B = \alpha u,$$

Where α is some constant. But from this observer's point of view the solar wind has a radial component equal to u and linear velocity of rotation is equal to $r\Omega$, where Ω - angular velocity of the Sun on the equator. Hence:

$$B_r = \alpha u, \; B_\varphi = \alpha r\Omega.$$

Substituting these relations into (2.7) we get final equation for magnetic field line:

$$-r\Omega\frac{dr}{dt} + ru\frac{d\varphi}{dt} = 0.$$

And finally:

$$\frac{dr}{d\varphi} = \frac{u}{\Omega}.$$

Integrating this equation we obtain:

$$r = \frac{u}{\Omega}(\varphi - \varphi_0),$$

Where φ_0 - initial angle of spiral on the solar surface. This relation represents the equation of ***Archimedean spiral***. In application to magnetic field lines of the Sun this spiral is called ***Parker spiral***. Approximate appearance of Parker spiral lines of force is shown in fig. II-4-4. In each point of the spiral the magnetic field equals to a value both of magnitude and of sense which it would have on the surface of the Sun at the moment of separation from the surface together with the solar wind.

Calculating the motion of particles moving along the magnetic lines of force (solar cosmic rays (SCR)) it is necessary to calculate the length of Archimedean spiral. Its length equals to:

$$L = \int_0^\varphi k\sqrt{1+\varphi^2}\,d\varphi = \frac{k}{2}\left[\varphi\sqrt{1+\varphi^2} + \ln(\varphi + \sqrt{1+\varphi^2})\right]$$

This formula enables to calculate the time of the arrival of SCR to the Earth.

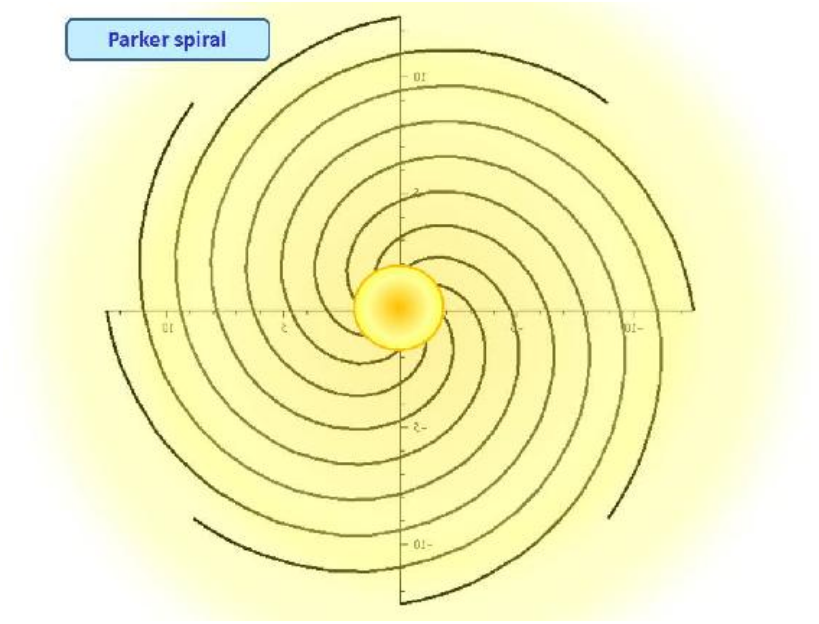

Fig. II-4-4. Parker spiral.

2.2.3 Sector structure of solar magnetic field

If moving along the solar equator the solar magnetic field changes in sense. It is directed towards the Sun in some areas and from the Sun in others. As the result solar wind carrying the magnetic lines away from the Sun forms a specific sector structure of solar magnetic field shown in fig. II-4-5.

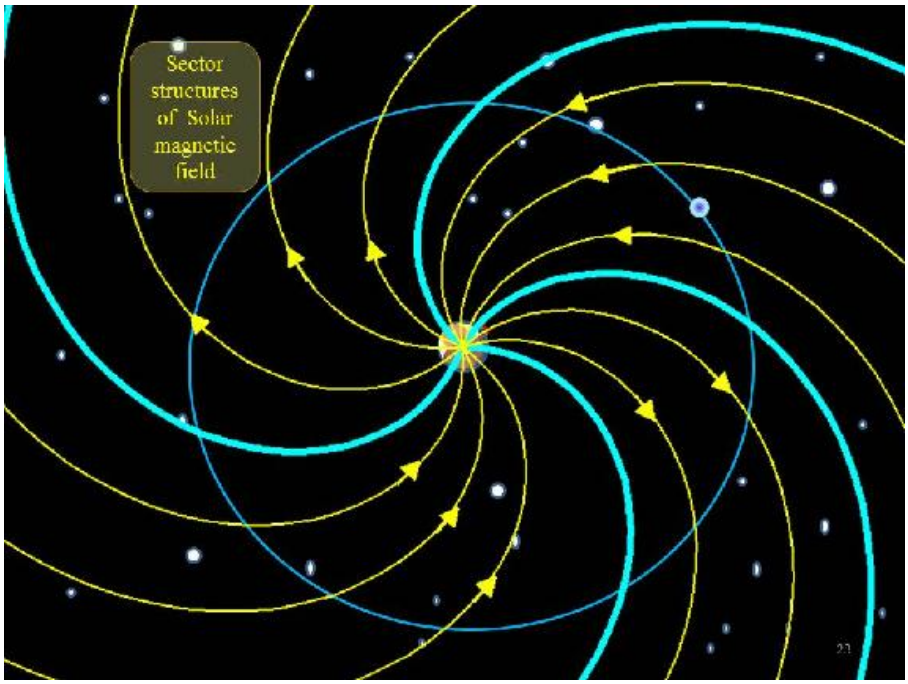

Fig. II-4-5. Sector structure of solar magnetic field.

Borders of sectors are represented in blue color in fig. II-4-5 and the magnetic lines of force

with the indication of the direction of the magnetic field intensity vector are represented in yellow color. The direction of magnetic lines of force rapidly reverses at the borders of a sector. From the placed on the Earth observer's point of view the sector structure rotates with the Sun at the same angular velocity equal to approximately one turn in 28 days in the same direction as the Earth motion along the orbit. Plasma moves at the same velocity on the solar equator. Therefore the borders of sectors permanently catch up with the Earth and when the sector passes the Earth it slightly disturbs the magnetosphere of the Earth.

2.2.4 Heliosphere

Heliosphere is a three-dimensional area around the Sun filled with solar wind and its components (inside) of the magnetic field. Supersonic solar wind collides with interstellar medium and forms an area where the velocity of solar wind drops. This transition area is called the heliosphere border. The jump of the velocity of the density in ***interstellar wind*** takes place at the shockwave border. ***Heliopause*** is an area where the solar wind velocity and interstellar wind velocity become equal.

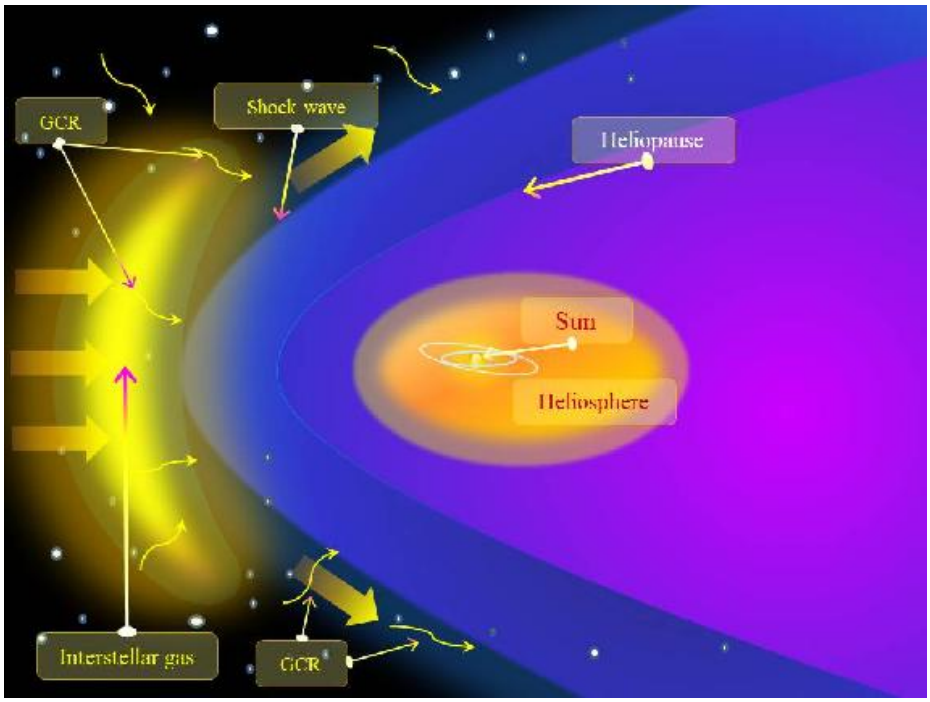

Fig. II-4-6 Structure of solar system surroundings interacting with galactic medium. [24].

The size of heliosphere is about 100 a.u. (1 a.u. is the distance between the Sun and the Earth - Astronomic unit $1.5 \cdot 10^8$ km)estimated on the basis of measures of neutron monitor of time variations of galactic cosmic rays (see further). This was directly observed by two spacecraft Voyager 1,2 when they crossed heliosphere in 2007 and 2008 (see fig. II-4-1).

Spacecraft have the possibility to measure directly all major physical parameters of the solar wind. The solar wind is not a quiet flow of gas: continuous oscillations of the magnetic field (Alfven waves) are generated by turbulent motion of gas on the Sun and then they move outwards. Discontinuities of the magnetic field and shock waves appear after the collision of fast and slow solar

[24] http://www.nasa.gov/centers/ames/images/content/72408main_ACD97-0036-1.jpg

wind (CIR) and eruptions in solar corona in the time of coronal mass ejection (CME) and solar flare. Coronal mass ejections spread over the solar system and can be measured near the Earth as the interplanetary corona mass ejection (ICMEs). Some of them are called magnetic clouds. When they are quite fast they cause a shock wave in front just like a plane flying faster than the speed of sound in the Earth atmosphere.

2.2.5 "Voyager 1" and "Voyager 2": The border for the Sun

Spacecraft launched in 1977 crossed the border of our solar system in the middle of 2005[25]. The outer border of the solar system lies beyond the Pluto orbit. At some certain distance from the Pluto orbit an area where the solar wind velocity drops sharply from supersonic speed to subsonic speed is placed. In this area called heliopause the density of interstellar material sharply decreases.

Voyagers discovered "anomalous cosmic rays", which decrease its velocity entering the heliopause and increase the velocity coming out of it. The data about anomalous cosmic rays received from Voyager solves many contradictions which have been met by astronomers for the last 30 years. Spacecraft Voyager 1 and Voyager 2 are the part of NASA mission targeted at the exploration of remote regions of solar system and interstellar medium. Both Voyagers are able to transmit scientific data with the help of their scientific tools set able to function until 2020 in accordance to the predictions of scientists. Their initial mission was the exploration of Jupiter and Saturn. But after the completion of this exploration it appeared that both spacecraft were still functioning and were in good condition. Moreover both Voyagers carry onboard the messages to undiscovered yet extraterrestrial civilizations. On board of both spacecraft there are 12-inch plates with terrestrial sounds and message and there is also the general information about Earthmen, our culture and life on our planet.

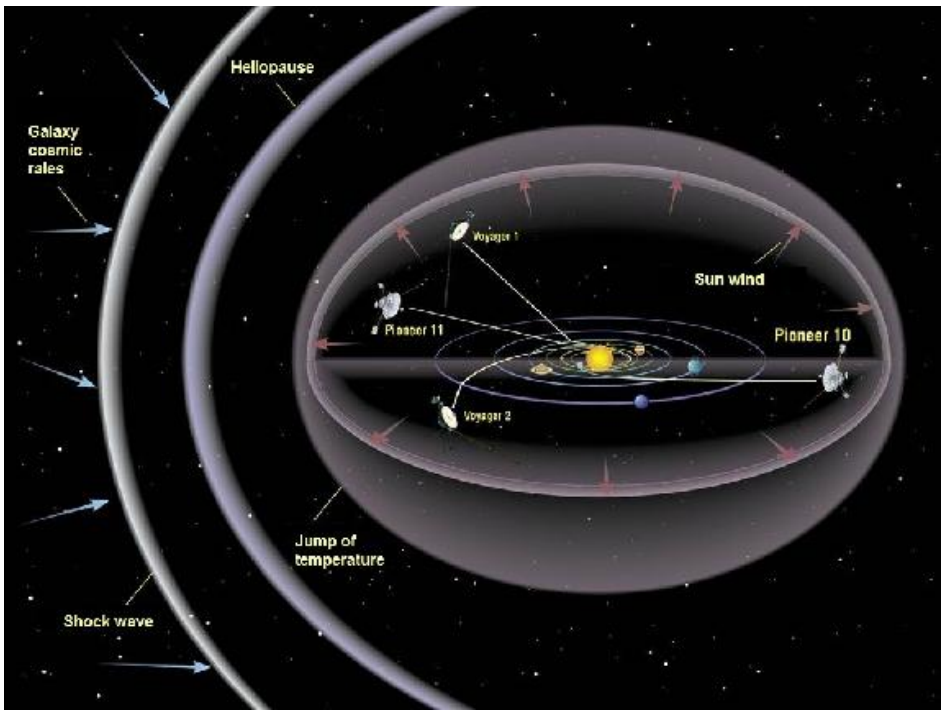

Fig. II-4-7. Heliosphere, heliopause, shockwave trajectories of spacecraft Pioneer 10, 11 and Voyager 1,2 [26]

[25] http://galspace.spb.ru/nature.file/geliosf.html

[26] http://dic.academic.ru/dic.nsf/ruwiki/863624,

2.3 Lecture 5. Solar activity and cosmic weather

2.3.1 Solar activity cycles

As it was established 200-300 years ago, the Sun changes with the time. Visually it looks like the appearance and disappearance of dark spots on its surface. Observation of these spots served as a departing point for monitoring the ***solar activity***. Nowadays the conditions of the Sun are estimated by a range of different indexes, the majority of them is shown in the Tab. II-5-1

Parameter	Symbols
Relative Wolf numbers	W
Areas of solar spots	S
Calcium flocculi area	K
Radiant flux 10.7	cm (2800 MHz) F10.7
Flare index	Numbers 1, 2, ...
Illuminance (Solar constant)	Q
Three directions averaged averaged	K-index
and three-hours interval	
variations of the geomagnetic field	
vector components for given observatory – a local	
three-hour index of the magnetic activity	
12 observatories averaged	K-index
Global (planetary) index	Kr
Variants are used	ar, Ar etc.
Hour index of magnetic storm power, storm-time-variation	Dst
Minute index, amplitude characteristic	AE
of polar geomagnetic disturbance	
and its components	AL, AU

Tab. II-5-1. Indexes of solar activity, used at present time.

When astronomers and physicists got the instrumentation precise enough and became able to measure the of solar energy at atmospheric boundary (see fig. II-3-1), it occurred that the total flux of energy from the Sun practically does not change in the course of time though we observe some changes on the surface of the solar (in the photosphere and the chromosphere) and in the condition of its corona. The diagram of solar "constant" change in the course of time - the total flux from the Sun in the period of 20 years, from 1978 to 2000.

As it is seen from this figure the value of solar constant changes in a part of percent. But these oscillations of the magnitude with the period of 11 years are clearly seen. Periodicity of solar activity variation was established in the XVII century when long and systematical enough ranges of data about number of observed spots on the Sun appeared.

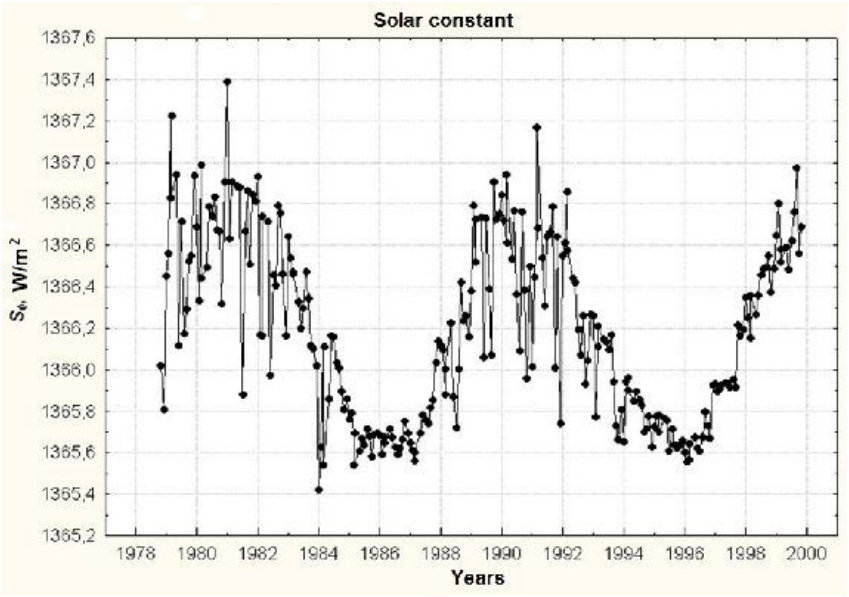

Fig. II-5-1 Changing of the solar constant.

2.3.2 Changes of the number of spots on the Sun. Wolf numbers sequence

Solar activity - is a sum of phenomena occurring periodically in the solar atmosphere. Effects of solar activity are closely associated with magnetic properties of plasma. Formation of active area starts with gradual growth of magnetic flux in some areas of photosphere. After this in corresponding areas of the chromosphere one can observe a growth of brightness in hydrogen and calcium lines. These areas are called floccules. Nearly in these areas in solar photosphere (a little bit deeper) the growth of brightness in white (visible) light can be observed - these are faculae. The growth of energy emitted in the area of facula or floccule is the consequence of the growth of the intensity of the magnetic field to several tens of Oersted. Then Sun spots are observed in the solar activity. They appear in 1-2 days after the appearance of a floccule in a form of small black dots - pores. Some of them disappear soon and just some single pores turn into large dark formations within 2-3 days. A typical sunspot has a size of some ten thousand kilometers and consists of the central dark part - shadow and fibrous semi shadow.

The most important peculiarity of sunspots is the presence of a strong magnetic field inside of them, reaching the magnitude of several thousands oersted in the area of the highest intensity of the magnetic field. In general sunspots represent a field tube coming out into the photosphere completely filling one or several cells of chromospheric network. The upper part of the tube broadens and lines of force diverge like ears in a sheaf. Therefore H lines take the direction close to horizontal around the shadow. The total pressure inside of the sunspot includes the pressure of the magnetic field and equalizes with the surrounding photosphere pressure therefore the gas pressure inside of the spot is less than in the photosphere. It looks like the magnetic field widens the spot from inside. In addition the magnetic field suppresses the convective motion of the gas transporting energy upward from the depth.

As a result the temperature in the area of the spot occurs to be about 1000 K less. The spot is like a cooled and locked by the magnetic field pit in the solar photosphere. Mostly spots appear in groups where two spots are distinguished. One is not big and it is placed to the west. Another one is little less and is situated to the east. Around and between them there usually are a number of small spots. Such group is called bipolar because both big spots have opposite polarity to the magnetic field. It is like they are tied by one and the same tube of magnetic lines which has emerged from under the

photosphere in a form of a giant loop and has left its ends somewhere in unobservable deep layers. The spot corresponding to the exit of magnetic field from the photosphere has northern polarity and the area where magnetic lines come back into the photosphere has southern polarity. The most powerful effect of the photosphere is flares.

Who has discovered spots on the Sun?

The first records about the observation of spots on the Sun refer to Ancient China and Antique Greece. A short table of major saved mentions about observations of spot on the Sun is given below.

- o Theophrastus from Athens 370-290 B.C.
- o China, chronicles (from 28 B.C. till 1638 A.D.).
- o Einhard "Vita Karoli Magni (Life of Charles the Great)" (about 807).
- o Ibn Rushd (1200 A.D.).
- o The first sunspots were sketched in 1128 in the Chronicon of John of Worcester [3]
- o Hypatian Codex (1365 and 1371).
- o Carrara (1450).
- o Telescopic observations 1610-1611: Goldschmidt, Galilei, Scheiner, T. Harriot.

Table II-5-2 Records about observation of spots on the Sun. [27]

It seems that Galilei was the first of explorers to confess the spots as a part of the solar structure. On the contrary Scheiner supposed spots to be planets passing in front of the Sun. Galilei's supposition allowed him to discover the period of rotation of the Sun and calculate this period. More than a ten years long polemic between Galilei and Scheiner was devoted to the priority of the discovery of spots and their nature. But it seems like the first observation and the first publication belongs to none of them [4].

Though sunspots have been observed since antique times their systematic observations refer just to the beginning of the XVII century. One of the first person who started to study sunspots systematically thanks to the first built telescope was Galilei. He did not just paid attentions to sunspots but he also found out that they move on the solar surface and in let him suppose the Sun rotating. This was the greatest achievement of that time.

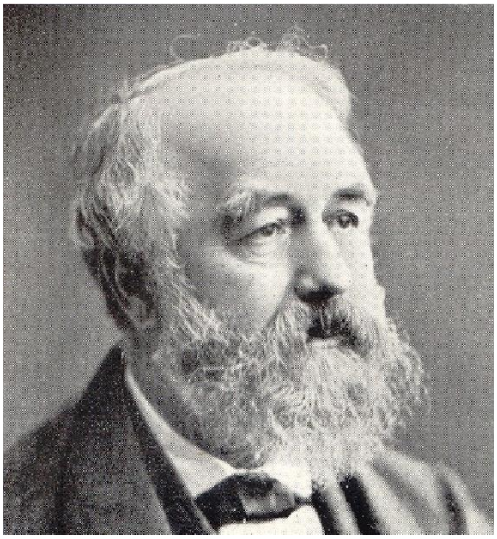

Fig. II-5-2 Rudolph Wolf.

[27] http://trv-science.ru/2009/06/09/solnechnye-pyatna-ot-galileya-do-nashix-dnej/ I. Usoskin. Sun spots: from Galileo to our days. Troitckiy variant 09 July 2009

The next important step in sunspots and solar activity study was taken by R. Wolf and Schwabe. R. Wolf offered a simple method for the calculation of "number of sunspots" which was supposed to be less dependent on instruments of observation and conditions of observation. This formula has the following form:

$$W = k(n+10g).$$

Here n is the number of observed separate spots, g is the number of observed groups of spots, k is a normalization coefficient with the help of which observations from different instruments and observers can be calibrated. Though observations of sunspots started practically at the beginning of the XVII century the consequence of Wolf number with the reliability high enough starts only from the year of 1749. Before this moment basing on the ground of observations carried out by different observers from the beginning and until the end of the XVII century Maunder established that there is an abrupt decrease of number of sunspots. This period is still called Maunder minimum. Another less long and less substantial than Maunder minimum period of decrease of sunspot number was registered in the XIX century. It is called Dalton minimum, by the name of a scientist who pointed out the existence of that minimum.

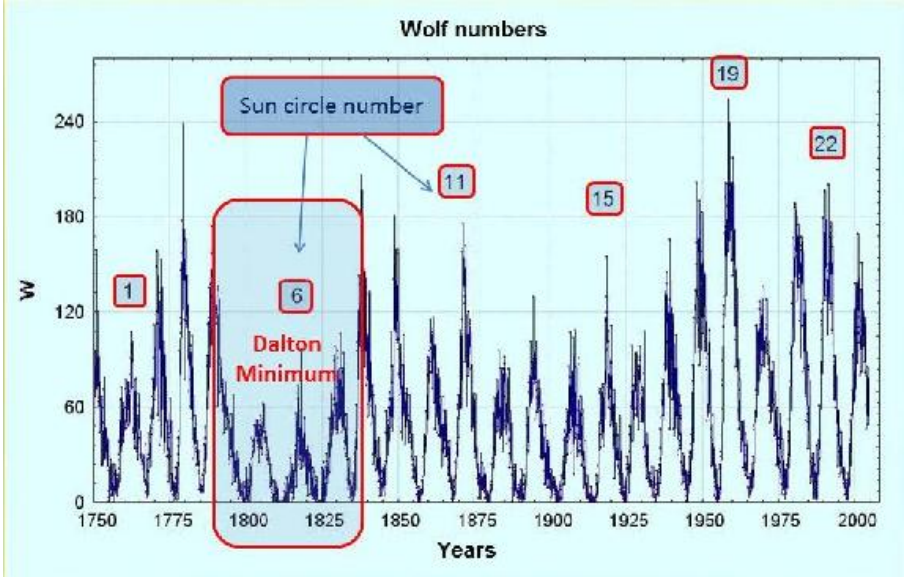

Fig. II-5-3 Consequence of Wolf numbers.

As Wolf and Schwabe have established the intervals between two adjacent minimums of solar activity vary from 8 to 14 years and the average is 11.1 years. This finding is called Schwabe-Wolf law. By the present time more precise data representing changing of Wolf number in the course of time is obtained. The existence of minima points at the fact that except the cyclic activity more complicated processes take place on the Sun which lead to the failure of cyclic activity mechanism. To all appearance such failures play a very important role in the work solar thermodynamic machine. In some degree it is seen from the Wolf number consequence shown in fig. II-5-3. More precise methods of analysis of temporal Wolf consequences allow to define explicitly the changeability in cyclic activity and to reveal other cycles except the 11-year one.

At the beginning of the cycle there are almost no spots. Then for 3-7 years their number grows up to the maximum value of W=50-200. After this W number decreases again to its minimum within 5-10 years. A 22-years cycle (Andersen cycle, 1939) physically is more reasonable with a glance at the alternation of the magnetic field polarity of spots in bipolar groups (Hale law) taking place in two adjacent cycles. Some data exists concerning longer cycles: 35-years cycle (Brukner cycle, 1890),

century-long cycle (80-100 years) and even longer. At the end of the XX century it appeared that quasi two-year period exists in solar activity, it is typical for a range of geophysical phenomena. In fig. II-5-4 components of Wolf numbers consequence obtained with the help of factor analysis are shown.

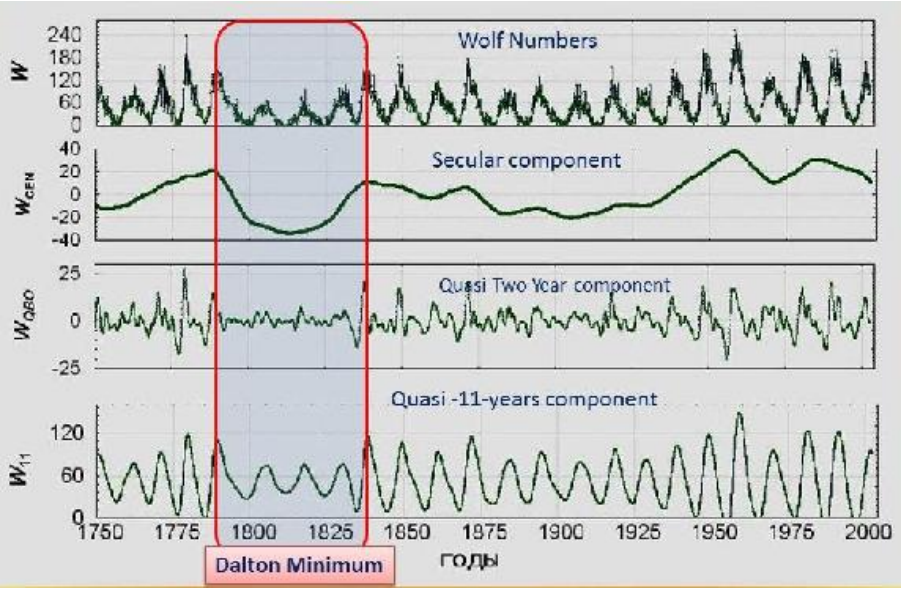

Fig. II-5-4 Expansion of Wolf numbers consequence in orthogonal modes. [28]

2.3.3 Changes of the global magnetic field in cycles. Mounder butterfly

Sunspots can be represented as a model of outlet of magnetic lines of force from the convective area into the chromosphere through the photosphere. This model is shown in fig. II-5-5.

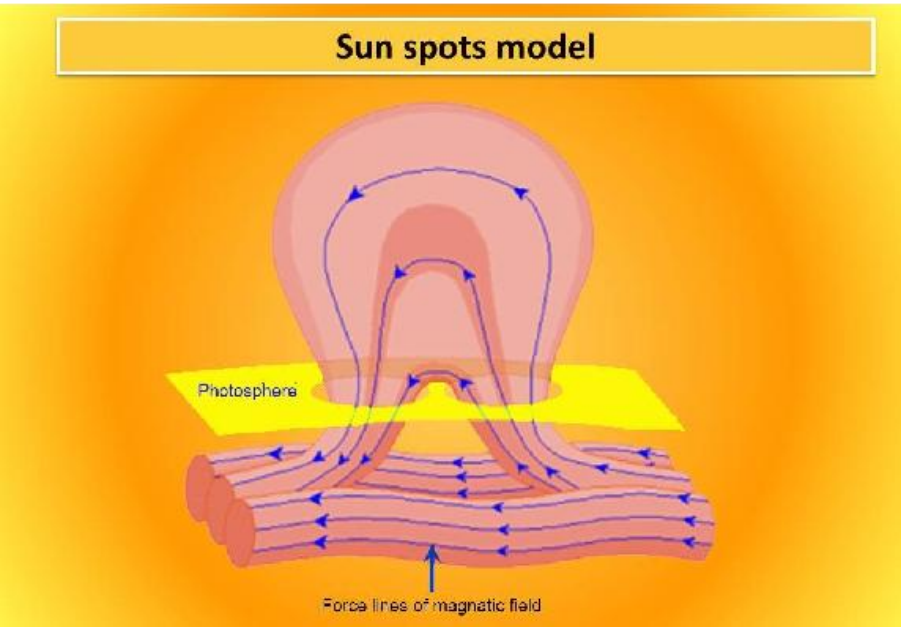

[28]The Earth life in Solar Atmospere. Ed. E.V.kanonovich. http://www.kosmofizika.ru/ucheba/sun_act.htm, http://www.tesis.lebedev.ru/sun_vocabulary.html

Fig. II-5-5. Model of magnetic field structure in sunspots.

Latitudinal dependence of sunspots formation area (Carrington 1858, Sperer 1881) in a form of Mounder "butterfly" diagram is shown in fig. II-5-6. At the beginning of a solar activity cycle spots appear at latitudes up to $\pm 30^{o}$, gradually approaching the equator, but avoiding the area of equator (Sperer law). Sunspot positions are plotted as vertical dashes and as a result sunspots formation areas remind butterfly wings:

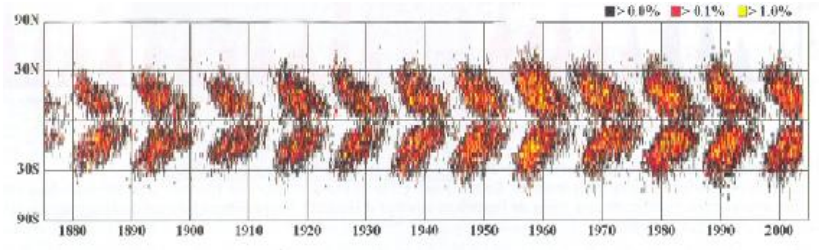

Fig. II-5-6 Mounder "Butterflies".

Solar activity is closely connected to solar magnetic field changes, what is reflected on Mounder diagram. A 22-year Andersen cycle detected in Wolf numbers consequence is connected to the fact that each 11 years magnetic poles of the Sun interchange so that the polarity of the global magnetic field of the Sun recovers each 22 years. But as it is seen from the Mounder diagram in fig. II-5-5 the change of polarity itself does not change the general behavior of sunspots which have direct relation to the magnetic field of the Sun but in a smaller scale.

Chapter 3. The Earth

3.1 Lecture 6. Gravitational field of the Earth and other planets

3.1.1 The gravitational field of point mass

The law of universal gravitation underlies in the Newton gravitational theory. According to this law two point masses with m_1 and m_2 placed at the distance r attract each other with the force:

$$\mathbf{F}_{12} = -G\frac{m_1 m_2 \mathbf{r}}{r^3}, \tag{3.1}$$

This force acts along the radius-vector $\mathbf{r}$ drawn from one point to another. A coefficient $G = 6.67 \cdot 10^{-11} m^3/kg \cdot s^2$ is called the gravitation constant. The gravitational force is a conservative or potential one. That means that the mechanical energy conservation law is satisfied for the particles moving under the effect of this force. The force can be written as a gradient of the potential energy U_{12} of the interaction between the two particles:

$$\mathbf{F}_{12} = -\nabla U_{12}.$$

Potential energy of a particle is numerically equal to the work needed to move away one of particles to the infinity and it can be written as:

$$U_{12} = -G\frac{m_1 m_2}{r}.$$

The gravitational interaction can be regarded as a field the source of which is each of the two particles. In this case the introduction of the terms of the field intensity and the field potential is useful. Let F_g be a force acting on a point mass m from side of other masses. Then by the gravitational field intensity the value numerically equal to the force F_g related to the mass of this body is understood:

$$g(r) = \frac{F_g(r)}{m}.$$

the dimension of this quantity corresponds to the acceleration of gravity of a point mass at the given point in space r affected by the external gravitational field.

Quantity $\phi(r) = U_g(r)/m$ equal to the ratio of potential energy U_g to mass of a body is called the gravitational potential at the given point in the space. Intensity and potential are linked to each other by a simple relation:

$$\mathbf{g} = -\nabla\phi,$$

or in a coordinate form:

$$g_x = -\frac{\partial\phi}{\partial x},\ g_y = -\frac{\partial\phi}{\partial y},\ g_z = -\frac{\partial\phi}{\partial z}.$$

From the Law of universal gravitation for the gravitational field of a point mass it (3.1) follows:

$$g = -\frac{GM}{r^2},\ \phi = -\frac{GM}{r}.$$

Here M is the mass of a point body generating the gravitational field and r is a distance from that point to the observer. As it is seen the intensity and the potential depend only on the mass creating the field and do not depend on the mass of a body put into the field.

The gravitational field has two important attributes. The first one is the principle of linear superposition and the second one is the absence of screening. The first attribute can be formulated in the following form. Suppose there are n material points with masses $m_1, m_2, \ldots, m_n$, their position is determined by a set of radius-vectors $r_1, r_2, \ldots, r_n$. Then gravitational field created by these material points at a point in the space with the radius-vector r_0 is characterized by intensity and potential which can be obtained in a form of a linear sum of separate intensities and potentials:

$$\mathbf{g} = \mathbf{g}_1 + \mathbf{g}_2 + \cdots \mathbf{g}_n = -G\frac{m_1(\mathbf{r}_1 - \mathbf{r}_0)}{|\mathbf{r}_1 - \mathbf{r}_0|^3} - \cdots - G\frac{m_n(\mathbf{r}_n - \mathbf{r}_0)}{|\mathbf{r}_n - \mathbf{r}_0|^3},$$

$$\phi = \phi_1 + \phi_2 + \cdots + \phi_n = -G\frac{m_1}{|\mathbf{r}_1 - \mathbf{r}_0|} - \cdots - G\frac{m_n}{|\mathbf{r}_n - \mathbf{r}_0|}$$

The second attribute means that the influence of one point over the other does not depend on the fact whether there are any other material bodies between them or not. As the alternative it can be shown that the electric field created by two types of charges (positive and negative) has an attribute of screening. It can be shown that the medium filled with particles with bound charges of different types will have an additional property - permittivity, which is characterized by the function of permittivity or permittivity tensor in more complicated cases. Self-gravitating medium does not have properties similar to the permittivity due to the absence of screening.

3.1.2 Gravitational field of material bodies. Poisson's equation

Now consider the gravitational field created by material bodies within continuous medium model. In this model each point in space with coordinates $r' = (x', y', z')$ can be considered as a material point having mass $dm(r') = \rho(r')dV'$, where $\rho(r')$ is mass density at the given point and dV' is unit volume of medium at the given point. Then at any point in space with coordinates $r = (x, y, z)$ the given element of medium creates the gravitational field with the following parameters:

$$d\mathbf{g} = -G\frac{(\mathbf{r}-\mathbf{r}')dm(\mathbf{r}')}{|\mathbf{r}-\mathbf{r}'|^3},\ d\phi = -G\frac{dm(\mathbf{r}')}{|\mathbf{r}-\mathbf{r}'|}.$$

Using the superposition principle we obtain that the integral field at the point r is characterized by the following quantities:

$$\mathbf{g}(\mathbf{r}) = G\int\frac{(\mathbf{r}-\mathbf{r}')\rho(\mathbf{r}')dV'}{|\mathbf{r}-\mathbf{r}'|^3}, \tag{3.2}$$

$$\phi(\mathbf{r}) = -G\int\frac{\rho(\mathbf{r}')dV'}{|\mathbf{r}-\mathbf{r}'|}. \tag{3.3}$$

These formulae enable to calculate characteristics of the gravitational field of any bodies. But for a number of calculations it is more convenient to use some properties of the gravitational field resulting from these formulae.

The most important property of these formulae is that function ϕ having a form (3.3) is the exact spatial solution of the linear partial differential equation called the Poisson's equation. In Cartesian coordinate system this equation has the following form:

$$\Delta\phi = 4\pi G\rho. \tag{3.4}$$

Here

$$\Delta = \frac{\partial^2}{\partial x^2} + \frac{\partial^2}{\partial y^2} + \frac{\partial^2}{\partial z^2}$$

is Laplace operator. In spherical coordinate system (r, ϕ, θ) Poisson's equation has a form of:

$$\frac{1}{r}\frac{\partial^2}{\partial r^2}(r\phi) + \frac{1}{r^2\sin^2\theta}\frac{\partial^2}{\partial\varphi^2}\phi + \frac{1}{r^2\sin\theta}\frac{\partial}{\partial\theta}\left(\sin\theta\frac{\partial}{\partial\theta}\right)\phi = 4\pi G\rho.$$

In some cases it is more convenient to obtain function ϕ solving the Poisson's equation than to do it using equations (3.2) and (3.3) directly. A situation can serve as the example when the density of mass of a body creating the gravitational field is a function of only one spheric coordinate r, i.e. mass distribution in space is spherically symmetrical. In this case $\rho = \rho(r),\ \phi = \phi(r)$ and Poisson's equation simplifies to the following form:

$$\frac{1}{r^2}\frac{\partial}{\partial r}r^2\frac{\partial}{\partial r^2}\phi \equiv \frac{1}{r}\frac{\partial^2}{\partial r^2}(r\phi) = 4\pi G\rho(r).$$

It is easier to integrate this equation than to use formula (3.3) .

3.1.3 The gravitational field of bodies with spherical symmetry

The field of spherically distributed masses has a number of additional properties. Integrating the latter equation we obtain:

$$\frac{\partial \phi}{\partial r} = \frac{4\pi G}{r^2}\int_0^r r^2 \rho(r) + g_0. \qquad (3.5)$$

Here g_0 - constant of integration. This value is usually chosen on the condition that intensity of the gravitational field away from the gravitating masses tends to zero. Therefore $g_0 = 0$ if density of mass of a planet or of any other body creating gravitational field is concentrated in some bounded area of space in such way that $\rho \to 0$ when $r \to \infty$. In this case the left integral:

$$m(r) = 4\pi\int_0^r r^2 \rho(r).$$

Is called the current mass as it represents mass of the matter enclosed inside of a sphere of radius r. The quantity in the right part of (3.5) is a radial component of gravitational field intensity but with the opposite sign at the distance r from the center of the spherical body. So this relation can be written in a form:

$$g(r) = -\frac{Gm(r)}{r^2}.$$

From this relation it follows that when the mass is distributed spherically the intensity of the field at distance r depends only on the mass of substance enclosed inside of a sphere with the same radius and does not depend on spherical distribution of the mass outside this sphere. For example, if a sphere-shaped body with the radius R creating gravitational field has the equal density ρ in every volume unit then intensity at distance r from the center will be:

$$g(r) = \begin{cases} -\frac{4\pi}{3}\rho G r, & r < R; \\ -\frac{4\pi}{3}\rho R^3 G r^{-2}, & r > R \end{cases}$$

respectively, potential will have the following form:

$$\phi(r) = \begin{cases} \frac{2\pi}{3}\rho G(r^2 - 3R^2), & r < R; \\ -\frac{4\pi}{3}\rho R^3 G r^{-1}, & r > R \end{cases}$$

in these formulae it is taken into account that $g(r)$ and ϕ are continuous and tend to 0 with $r \to \infty$.

3.1.4 Gravitational field of bodies of general form

In problems of satellite dynamics it is necessary to take into account nonsphericity of planet's form and mass distribution inside of it to predict positions of artificial Earth (and other planets) satellites with the adequate accuracy. In this case it is necessary to create such description of nonspherical bodies gravitational field which, on one hand, could be easily calculated on the basis of observations of satellites movement and, on the other hand, could be easily used for the description of their motion. To solve this problem a special instrument was created to represent the gravitational field of planets in a form of expansion in terms of special functions - spherical harmonics. Spherical harmonics $Y_{lm}(\theta,\phi)$ have the following general view:

$$Y_{lm}(\theta,\phi) = P_l^{|m|}(\cos\theta)e^{im\phi},\ l = 0,\ldots;\ m = -l,\ldots,l.$$

Here θ is polar angle in spherical coordinate system and φ is its azimuth angle. Functions

$P_l^{|m|}(\cos\theta)$ - associated Legendre polynomial which can be calculated in the following manner:

$$P_n^m(\xi) = (-1)^m (1-\xi^2)^{m/2} \frac{d^m}{d\xi^m} P_n(\xi),$$

where

$$P_n(\xi) = P_n^0(\xi) = \frac{1}{2^n n!} \frac{d^n}{d\xi^n} \left((\xi^2 - 1)^n\right)$$

are simple Legendre polynomials. These functions appear as coefficients of expansion of function $|r - r'|^{-1}$:

$$\frac{1}{|r-r'|} = \frac{1}{r\sqrt{1 - 2\frac{r'}{r}\cos\psi + \left(\frac{r'}{r}\right)^2}},$$

which enters into equation (3.3) for gravitational potential. In this equation ψ is angle between vectors r and r'. Taylor expansion of $|r - r'|^{-1}$ as power series of r'/r has the following form:

$$\frac{1}{|r-r'|} = \frac{1}{r} \sum_{n=0}^{\infty} \left(\frac{r'}{r}\right)^n P_n(\cos\psi). \qquad (3.6)$$

Angle ψ enters (3.6) and it is expressed by spherical angles θ and φ of coordinate system. To transform ((3.6) into a form including θ and φ let's use summation theorem of Legendre polynomials. According to this theorem we have:

$$P_n(\cos\psi) = P_n(\cos\theta) P_n(\cos\theta') + 2\sum_{m=1}^{n} \frac{(n-m)!}{(n+m)!} P_n^m(\cos\theta) P_n^m(\cos\theta') \cos m(\varphi - \varphi').$$

Here θ and φ - spherical angles of vector r directed to the point of observation and θ' and φ' - spherical angles of vector r' directed to the position of the current source.

Substituting the latter relation into equation (3.3) we obtain the following relation:

$$\phi = \frac{GM}{r}\left[1 + \sum_{n=1}^{\infty} J_n P_n(\cos\theta)\left(\frac{a}{r}\right)^n + \right. \qquad (3.7)$$

$$\left. + \sum_{n=1}^{\infty}\sum_{m=1}^{n} (C_n^m \cos m\varphi + S_n^m \sin m\varphi) P_n^m(\cos\theta)\left(\frac{a}{r}\right)^n\right]$$

In this relation coefficients J_n are called zonal harmonics amplitudes of the n-th order, C_n^n and S_n^n - amplitudes of sectorial harmonics (respective summands in (3.7) turn into 0 on the equator), and C_n^m and S_n^m - amplitudes of tesseral harmonics. These coefficients are linked with the distribution of density inside the body in the following manner:

$$J_n = \frac{1}{a^n M} \int_V \rho(r') P_n(\cos\theta')(r')^n dV',$$

$$C_n^m = 2\frac{(n-m)!}{(n+m)!} \frac{1}{a^n M} \int_V \rho(r') P_n^m(\cos\theta') \cos m\phi' (r')^n dV',$$

$$S_n^m = 2\frac{(n-m)!}{(n+m)!} \frac{1}{a^n M} \int_V \rho(r') P_n^m(\cos\theta') \sin m\phi' (r')^n dV'.$$

Here M - mass of the body, a - characteristic dimension, equatorial radius for example.

3.1.5 Gravitational field of planets

In case when a body has a shape of the sphere the gravitational field potential, as it is known, depends only on radial coordinate and conforms with Newtonian potential:

$$\phi(r) = \frac{GM}{r}.$$

If the body is slightly deformed the series (3.7) will contain negligible corrections for the Newtonian field. Planets and rotating single stars have axial symmetry i.e. $\rho = \rho(r,\theta)$. In this case sectorial and tesseral components of the gravitational field equal to zero: $C_n^m = S_n^m = 0$. As a result the series ((3.7) simplifies and takes the following form:

$$\phi = \frac{GM}{r}\left[1 + \sum_{n=2}^{\infty} J_n P_n(\cos\theta)\left(\frac{a}{r}\right)^n\right]. \qquad (3.8)$$

In case if there is an equatorial plane bilateral symmetry the odd components in series (3.8) disappear. The latter is true for single rotating stars. In this case series (3.8) can be written as:

$$\phi = \frac{GM}{r}\left[1 + \sum_{n=1}^{\infty} J_{2n} P_{2n}(\cos\theta)\left(\frac{a}{r}\right)^{2n}\right]. \qquad (3.9)$$

The analysis of data concerning the shape of planets obtained from the analysis of their natural (in case of their existence) or artificial satellites motion allows to make a conclusion that it is possible to use Newtonian approximation far away from planets to describe the dynamics of bodies with a high accuracy and near big planets and on their surface it is often possible to use the approximation containing only summand with $n = 2$:

$$\phi = \frac{GM}{r}\left[1 + J_2 \frac{3\cos^2\theta - 1}{2} \cdot \frac{a^2}{r^2}\right]. \qquad (3.10)$$

		$J_n \cdot 10^6$				
Planet	GM	n				
	m^3/c^2	2	3	4	5	6
Sun	$1.327 \cdot 10^{20}$	-	-	-	-	-
Mercury	$2.168 \cdot 10^{13}$	-	-	-	-	-
Venus	$3.249 \cdot 10^{14}$	-20	-	-	-	-
Earth	$3.987 \cdot 10^{14}$	-1082	2.54	1.58	0.22	-0.59
Moon	$4.903 \cdot 10^{12}$	-206	-37.7	33.3	-5.5	-
Mars	$4.298 \cdot 10^{13}$	-1995	29	-9.5	5	0.2
Jupiter	$1.267 \cdot 10^{17}$	-14750	-	580	-	5
Saturn	$3.793 \cdot 10^{16}$	-16670	-	1040	-	11
Uranus	$5.803 \cdot 10^{15}$	-12000	-	-	-	-
Neptune	$7.026 \cdot 10^{15}$	-3900	-	-	-	-

Tab. III-1. Data of zonal harmonics of solar system planets. [29]

3.1.6 The terrestrial gravitational field

Measurement of the Gravitational constant

The gravitational field parameters measurement starts with the measurement of the gravitational constant G. The first measurement of gravitational constant was realized by Henry Cavendish in 1798 with the help of torsion balance. Initially the experiment was offered by John Michell. He was designed the main part of the experimental installation - a torsion balance. But he died in 1793 having not realized the experiment. After his death Henry Cavendish got the installation. He modified it, realized experiments and described it in Philosophical Transactions in 1798

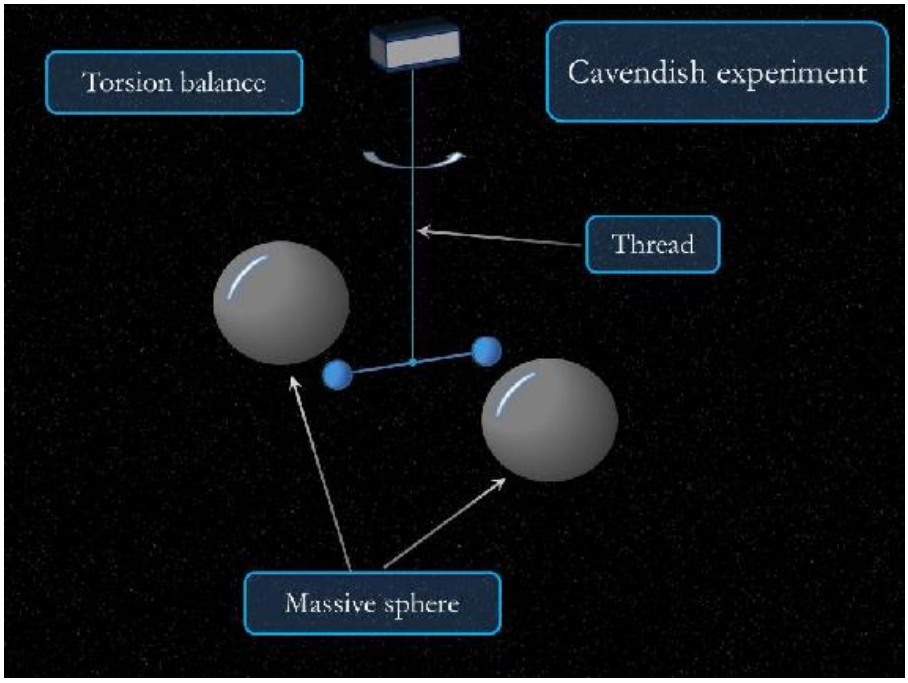

Fig. III-6-1. Method of gravitational constant measurement with the help of torsion balance.

Nowadays the gravitational constant can be measured in different ways and Cavendish's methods form the basis of some of them. But with the help of this method G can be measured accurate to 3 decimal places. Nowadays some attempts are made to compute G with the higher accuracy.

Measurement of the Terrestrial gravitational field and field of other planets

Measurement of gravitational field is very important for navigation tasks. On the other hand analyzing motion of bodies in the gravitational field it is possible to find the shape of a planet or a star and mass distribution inside of them. This task has been solved many times since the beginning of cosmic era. Nowadays the most accurate data is given by the ***satellite GOCE*** of European Space Agency. Since September of 2009 the spacecraft is at the height of 254.9 km above the surface - it is lower than any other satellite observing the planet. Its main task is to disclose gravitational anomalies and make a map of the terrestrial gravitational field with the accuracy to 1-2 centimeters.

[29] Table from: Y.V.Alexandrov. Introduction to planet physics. Kiev. ``Vischa Skola", 1982

Collected by the satellite information represents a great value in different sciences and especially in climate study because the gravity level influences the motion of oceanic streams which distribute heat over the planet (for more information about GOCE satellite see references: [30])

3.2 Lecture 7. Motion of spacecraft near the Earth

3.2.1 Motion of a point particle in the terrestrial gravitational field

Keplerian orbits

Newton's equations for a point particle with arbitrary mass in the gravitational field have the following form:

$$\frac{dv}{dt} = -\nabla\phi. \tag{3.11}$$

Here ϕ is gravitational potential of a field. Potential of the gravitational field of a spherically symmetrical body has the form of:

$$\phi = \frac{GM}{r}.$$

In such field angular momentum of a satellite is constant:

$$L = [r \times p] = const.$$

Thereby it is convenient to choose coordinate system so that the plane of satellite's motion is orthogonal to the constant vector L. Let's direct axis z along vector L. in this case $L = (0,0,L_z)$. Changing to polar coordinate system in orbit plane we obtain:

$$L_z = mr^2\dot{\phi} = const. \tag{3.12}$$

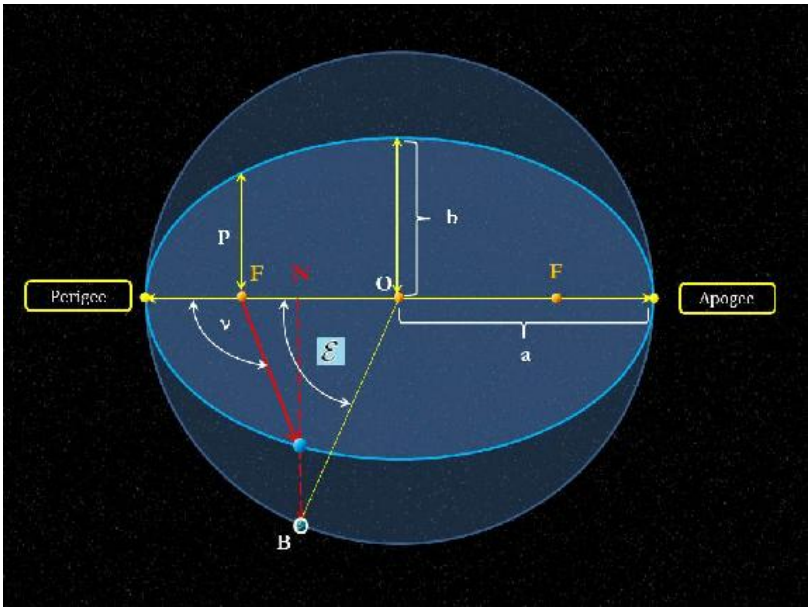

Fig. II-7-1. Elements of elliptic orbit

[30] http://elementy.ru/images/news/gravitational_anomalies_grace.jpg, http://elementy.ru/images/news/geoid_300.jpg

In chosen polar coordinates energy conservation law can be written like that:

$$E_0 = \frac{m}{2}(v_r^2 + r^2\dot{\phi}^2) - \frac{mMG}{r} = const. \qquad (3.13)$$

Here v_r - radial velocity of a satellite, E_0 is its total energy. With (3.12) taken into account this conservation law takes the form which contains only radial coordinate functions:

$$E_0 = \frac{m}{2}\left(\left[\frac{dr}{dt}\right]^2 + \frac{L_z^2}{m^2r^2}\right) - \frac{mMG}{r} = const. \qquad (3.14)$$

This conservation law form corresponds to one-dimensional radial movement of a particle in the potential gravitational field with the effective potential energy:

$$U_{eff} = \frac{L_z^2}{2mr^2} - \frac{mMG}{r},$$

which differ from potential energy of the initial problem by the presence of a summand corresponding to energy of orbital motion.

It is useful to transform (3.14) into the form of conservation law for harmonic oscillator to describe satellite's trajectory in examined gravitational field. It enables us to obtain series of relations based on this analogy to harmonic oscillator. Realizing sequentially substitution of variables $r(t) = r(\phi(t))$ and $\zeta(\phi) = r^{-1}(\phi)$ we obtain:

$$\frac{L_z^2}{2m}\left(\left[\frac{d\zeta}{d\phi}\right]^2 + \zeta^2\right) - mMG\zeta = E_0$$

And finally:

$$\left[\frac{d\zeta}{d\phi}\right]^2 + \left[\zeta - \frac{m^2MG}{L_z^2}\right]^2 = \frac{2mE_0}{L_z^2} + \left[\frac{m^2MG}{L_z^2}\right]^2 = const.$$

The obtained conservation law matches in a form with energy conservation law of a harmonic oscillator with unit mass, and equilibrium position and the position at a point with coordinate: $\zeta_0 = \frac{m^2MG}{L_z^2}$. With that angular variable ϕ plays the role of time. As far the law of harmonic oscillator motion is known beforehand we can write the solution for its effective coordinate ζ like:

$$\zeta = \frac{1}{r} = \frac{m^2MG}{L_z^2} + A\cos(\phi - \phi_0).$$

It is convenient to represent this solution in a form of ellipse canonical equation in polar coordinates:

$$r = \frac{p}{1 + e\cos\nu}, \qquad (3.15)$$

where p is focal parameter, e is eccentricity. Angle $\nu = \phi - \phi_0$ counted from perigee direction is called the true anomaly. Perigee is a point of an orbit with the minimal distance from the field center, and apogee is a point with maximum distance (if such point exists). All these parameters are shown in fig. I-1. On this figure angle E relative to the center of ellipse counted from perigee to line OB is called eccentric anomaly E.

Using the obtained solution it is possible to link ellipse canonical parameters to dynamic parameters of satellite movement - its total energy and angular momentum. Some simple considerations are needed for this. Radial velocity component is equal to zero in apogee and perigee. Therefore we find from energy conservation law:

$$E_0 = \frac{L_z^2}{2mr_{a,p}^2} - \frac{mMG}{r_{a,p}},$$

where r_a and r_p are distances from the field center (the Earth) in apogee and perigee respectively. Summing these two relations for r_a and r_p and taking into account the definition of semimajor axis a: $a = (r_a + r_p)/2$ we obtain the following equation for the total energy:

$$E_0 = -\frac{mGM}{2a}. \tag{3.16}$$

Hence we obtain a useful relation for squared absolute velocity of orbital movement:

$$V^2 = GM\left(\frac{2}{r} - \frac{1}{a}\right). \tag{3.17}$$

Now it is possible to obtain expressions for distances in apogee and perigee as functions of dynamic parameters of a satellite:

$$\frac{1}{r_{a,p}} = \frac{m^2MG}{L_z^2}\left(1 \pm \sqrt{1 + 2E_0\frac{L_z^2}{M^2m^3G^2}}\right).$$

On the other hand it follows from ellipse canonical equation (3.15) :

$$r_p = \frac{p}{1+e},\ r_a = \frac{p}{1-e}. \tag{3.18}$$

Hence we obtain expressions for impact parameter p and eccentricity e also as functions of dynamic parameters of satellite motion:

$$p = \frac{2r_pr_a}{r_p + r_a} = \frac{L_z^2}{m^2MG},\quad e = \frac{r_a - r_p}{r_a + r_p} = \sqrt{1 + 2E_0\frac{L_z^2}{M^2m^3G^2}}. \tag{3.19}$$

Kepler equation is used to describe the motion of a satellite on the orbit. The equation has the form of:

$$E - e\sin E = n(t - t_0) + M_0. \tag{3.20}$$

Here E is eccentric anomaly, $M = n(t - t_0) + M_0$ is called mean anomaly, and M_0 **is mean anomaly at epoch (t_0)**, $n = \sqrt{MGa^{-3}}$ is **mean motion**. The geometric sense of eccentric anomaly is clarified in fig. I-1. Eccentric anomaly is linked to natural anomaly (angle ν in fig. I-1) by formula:

$$\frac{\nu}{2} = \sqrt{\frac{1+e}{1-e}}\frac{E}{2} \tag{3.21}$$

True anomaly is defined from these two equations, corresponding to the definite moment of time t and therefore satellite position on the orbit is defined for example relative to perigee.

Position of the orbit in space

Obtained relations allow calculation of parameters of elliptic orbit of a satellite. But it is necessary to know not only parameters of ellipse but also the position of orbit in space in relation to geocentric coordinate system. These geometric parameters of orbit position in geocentric rectangular coordinate system for Earth satellites are introduced in the following way. Z -axis of this coordinate system coincides with the Earth axis of rotation with positive direction to the North Pole. This point is situated near the Pole star on the celestial sphere. X -axis directs from the Earth center to the vernal

equinox situated in the Golden Fish constellation of the modern epoch. Y -axis is perpendicular to the other two axes.

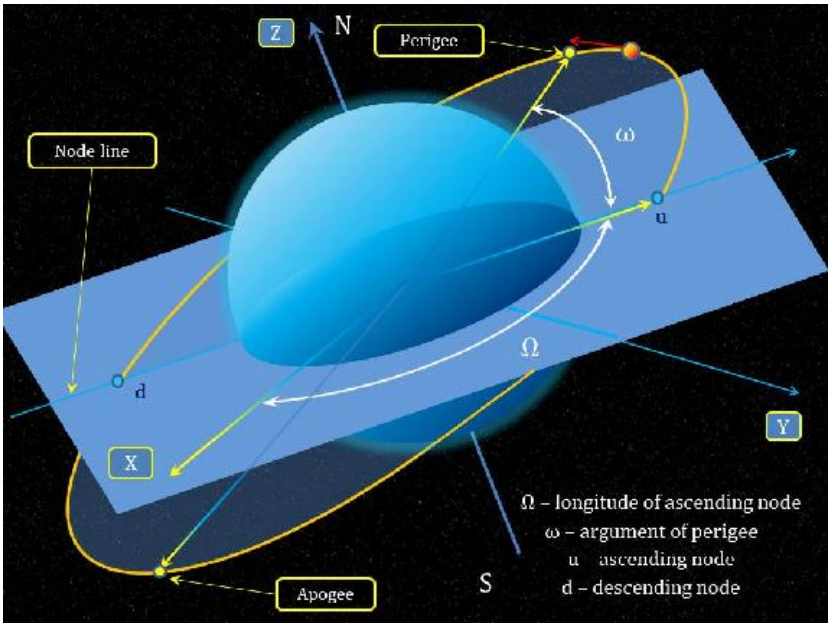

Fig. II-7-2. Position of the orbit in space.

The point where the orbit crosses the equatorial plane is called n**ode of orbit**. The point where a satellite passes from the southern hemisphere to the northern one is called **ascending node**. The point opposite to the Earth center is called **descending node**. Angle between the direction to the vernal equinox and ascending node, i.e. between the x -axis and ascending node, is called **longitude of ascending node** and is designated by Ω here. Angle in the plane of orbit counted from ascending node to perigee is called ascending node-perigee angle and is designated by ω. Angle between the plane of orbit and equatorial plane is called orbit inclination and is designated by i here. Orbit parameters also include focal parameter p and eccentricity e. These parameters are shown in fig. 2.

Cartesian coordinates of a satellite will have the following form in geocentric coordinate system:

$$x = r(\cos u \cos\Omega - \sin u \sin\Omega \cos i), \quad (3.22)$$

$$y = r(\cos u \sin\Omega + \sin u \cos\Omega \cos i), \quad (3.23)$$

$$z = r \sin u \sin i. \quad (3.24)$$

Here $u = \nu + \omega$. Details can be found in [14] [31]. The full set of formulae see in [15] (pages 171-180) [32].

Movement in spheroidal field. Model of precession

Slight difference between the real shape of planet and spherical form leads to the slow change of Keplerian orbit parameters in the course of time. A simple model of this evolution can be built basing on the analysis of the dynamics of satellite's angular momentum. As far as this model is equal in its parameters to rotating gyroscope precession we will call this model the model of precession though such terminology is not usually applicable to the dynamics of satellite orbit parameters.

[31] A.N. Matveev. Mechanics and the theory of relativity. M "Vysshaya shkola" 1986

[32] Handbook of celestial mechanics and astridynamics. Edited by Duboshin, M: "Nauka" 1971, 584

According to ((3.10) a good approximation for satellite potential energy in nonspherical gravitational field of the Earth is a function:

$$U = -\frac{GM_E m}{r}\left[1+\frac{J_2}{2}\left(3\frac{z^2}{r^2}-1\right)\cdot\frac{R_E^2}{r^2}\right], \tag{3.25}$$

where m is mass of satellite and the equation $\cos\theta = z/r$ was used. Newtonian equation of motion of a satellite in such field has the form of:

$$\frac{dp}{dt} = -\nabla U.$$

Multiplying the left part of this equation by radius vector $r = xe_x + ye_y + ze_z$, where e_x, e_e, e_z are unit vectors of Cartesian coordinates, we obtain equation for satellite angular momentum $L = [r \times p]$ in the following form:

$$\frac{dL}{dt} = -[r \times \nabla U]. \tag{3.26}$$

If the force acting on a satellite is central then moment of force in the right part of (3.26) is equal to zero. Indeed for the central force a condition is satisfied:

$$F = -\nabla U = Q(r)r,$$

is some scalar function of a radial coordinate r. for a spherical planet the gravitational field is central and moment of force equals to zero. This leads to the angular momentum conservation law. In case of nonsphericity of the Earth the gravitational field is not central and angular momentum is not conserved. Let's calculate momentum of force for potential energy (3.25) . Differentiating the potential energy equation (3.25) we obtain the following expression for the force acting on a satellite:

$$F = -\nabla U = Q(r,z)r + W(r)ze_z, \tag{3.27}$$

where

$$Q(r,z) = \frac{GM_E m}{r^3}\left[1+\frac{3J_2}{2}\left(5\frac{z^2}{r^2}-1\right)\cdot\frac{R_E^2}{r^2}\right],$$

$$W(r) = 3J_2\frac{GM_E m}{r^3}\frac{R_E^2}{r^2},$$

And vector e_z is a unit vector directed along axis z coinciding with Earth's axis of rotation. This implies that in such field momentum of force acting on a satellite equals to:

$$[r \times F] = W(r)z[r \times e_z].$$

Hence we find:

$$[r \times F] = W(r)z[(xe_x + ye_y + ze_z) \times e_z] = W(r)zx[e_x \times e_z] + W(r)zy[e_y \times e_z].$$

Taking into account that:

$$[e_x \times e_z] = -e_y,\ [e_y \times e_z] = e_x,$$

we finally obtain the following system of equations for angular momentum components:

$$\begin{aligned}
\frac{dL_x}{dt} &= W(r)zy,\\
\frac{dL_y}{dt} &= -W(r)zx,\\
\frac{dL_z}{dt} &= 0.
\end{aligned} \tag{3.28}$$

It is clear from this system that projection of angular momentum on the Earth axis of rotation is conserved: $L_z = const$.

Equation (3.28) together with the energy conservation law totally determines a satellite motion in the considered gravitational field. As far as the Earth has a slight deviation from the spherical shape (see Tab. III-1) it is possible to consider that there are no significant changes in orbit parameters within one revolution of a satellite. These deviations must appear only in a long enough period of time. So it is possible to suppose that law of orbital motion remains in the same form but orbit parameters become the time functions and slowly change in the course of time. That means that it is possible to use the same relations (3.22) to calculate satellite's Cartesian coordinates but we have to consider $\Omega = \Omega(t), \omega = \omega(t), i = i(t), \varepsilon = \varepsilon(t), a = a(t)$. Now it is possible to obtain from equations (3.28) and energy conservation law the whole totality of equations for these orbit parameters called osculating elements. But these calculations are too cumbersome so we will not produce them here. Here is just the derivation of an equation for secular variation of longitude of ascending node Ω in assumption that the orbit has small eccentricity i.e. it does not differ practically from circular.

Substituting expressions for coordinates x, y, z from (3.22) into the first two equations (3.28) we obtain as a result:

$$\frac{dL_x}{dt} = W(r)r^2 \sin i(\sin\Omega\sin(v+\omega)\cos(v+\omega) + \cos\Omega\sin^2(v+\omega)\cos i),$$

$$\frac{dL_y}{dt} = -W(r)r^2 \sin i(\cos\Omega\sin(v+\omega)\cos(v+\omega) - \sin\Omega\sin^2(v+\omega)\cos i).$$

Hence we obtain:

$$\frac{dL_x}{dt} = \frac{W(r)}{2}r^2 \sin i(\cos\Omega\cos i + \sin\Omega\sin 2(v+\omega) + -\cos\Omega\cos 2(v+\omega)\cos i),$$

$$\frac{dL_y}{dt} = -\frac{W(r)}{2}r^2 \sin i(-\sin\Omega\cos i + \cos\Omega\sin 2(v+\omega) + -\sin\Omega\cos 2(v+\omega)\cos i).$$

In these equations in the right part there are summands changing fast (for example within one revolution of a satellite around the Earth) and changing slowly. Fast changing are the summands containing true anomaly v changing from 0 to 2π within one revolution. Slow changing are summands without true anomaly. It follows from this analysis that expressions for angular momentum components can be similarly represented in a form of summands changing fast and slowly, i.e.:

$$L_x = L_x^{(0)}(t) + A(t)\sin(v+\omega) + B(t)\cos 2(v+\omega),\ L_y = L_y^{(0)}(t) + C(t)\sin(v+\omega) + D(t)\cos 2(v+\omega),$$

where functions L $L_x^{(0)}, L_y^{(0)}$ change slowly. Equations for these functions are obtained by substitution of the latter expressions for angular momentum into equations (3.29) and (3.30) and by equalization of slowly changing parts of the equation. As a result we obtain:

$$\frac{dL_x^{(0)}}{dt} = \frac{W(r)}{2}r^2 \sin i\cos\Omega\cos i, \qquad (3.29)$$

$$\frac{dL_y^{(0)}}{dt} = \frac{W(r)}{2}r^2 \sin i\sin\Omega\cos i. \qquad (3.30)$$

Slowly changing part of angular momentum projection on plane $x-y$ can be represented as following (see fig. I-3):

$$L_x^{(0)} = L_0 \sin\Omega\sin i,\ L_x^{(0)} = L_0 \cos\Omega\sin i,$$

where L_0 is absolute magnitude of angular momentum vector of slowly changing component. This vector is almost unchangeable, but vector L itself rotates around z-axis.

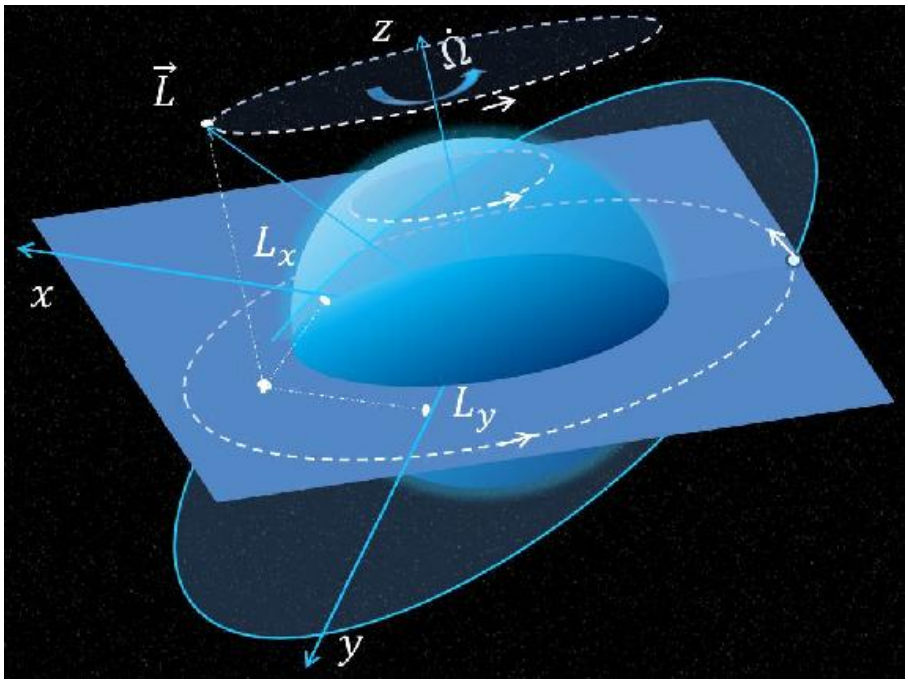

Fig. II-7-3. Rotation of orbit plane in space.

Substituting this relations into equations (3.29) and (3.30) and believing that inclination of an orbit does not change and longitude of ascending node changes we obtain the following equation for $\Omega(t)$:

$$\frac{d\Omega}{dt} = -\frac{W(r)}{2L_0} r^2 \cos i = -\frac{3J_2}{2L_0} \frac{GM_E m}{r} \frac{R_E^2}{r^2} \cos i.$$

Taking into account that for undisturbed motion along circular orbit

$$L_0 = mr^2 \sqrt{\frac{GM_E}{r}},$$

we finally obtain:

$$\frac{d\Omega}{dt} = \frac{3J_2}{2} \sqrt{\frac{GM_E}{r^3}} \frac{R_E^2}{r^2} \cos i.$$

Motion in the spheroidal field. Exact formulae

The more precise analysis considering possible deviation of an orbit from circular one shows that at a first approximation ascending node-perigee angle ω and mean anomaly M_0 also slowly change together with longitude of ascending node. Corresponding formulae for the rate of secular variation rate have the following form:

$$\frac{d\Omega}{dt} = \frac{3}{2} \sqrt{\frac{GM}{a^3}} J_2 \left(\frac{R_E}{p} \right)^2 \frac{\cos i}{(1-e^2)^2}, \tag{3.31}$$

$$\frac{d\omega}{dt} = \frac{3}{4} \sqrt{\frac{GM}{a^3}} J_2 \left(\frac{R_E}{p} \right)^2 \frac{(1-5\cos^2 i)}{(1-e^2)^2}, \tag{3.32}$$

$$\frac{dM_0}{dt} = \frac{3}{4}\sqrt{\frac{GM}{a^3}} J_2 \left(\frac{R_E}{p}\right)^2 \frac{(3\cos^2 i - 1)}{(1-e^2)^{3/2}}, \tag{3.33}$$

here $p = a(1-e^2)$ is orbit focal parameter. R_E is equatorial radius of the Earth, a - is semimajor axis. It is clear that for a circular orbit formula for Ω exactly coincides with the equation obtained earlier. These equations can be interpreted as a magnitude of orbit components changes in radian or angle measurement within some period of time, for example within on revolution of a satellite around the Earth. But as it will be shown further in real data parameters are usually given within twenty-four hours. Quantity $n = \sqrt{GMa^{-3}}$ is called mean motion and is given in NORAD data in a form of revolution number in twenty-four hours. Longitude of ascending node and ascending node-perigee angle is given in degree scale in NORAD data. In these units $\Delta\Omega$ and $\Delta\omega$ in twenty-four hours will be expressed in a following way:

$$\Delta\Omega_{day} = \frac{3}{2} 360 n J_2 \left(\frac{R_E}{p}\right)^2 \cos i, \tag{3.34}$$

$$\Delta\omega_{day} = \frac{3}{4} 360 n J_2 \left(\frac{R_E}{p}\right)^2 (1 - 5\cos^2 i), \tag{3.35}$$

$$\Delta M_{0day} = \frac{3}{4} 360 n J_2 \left(\frac{R_E}{p}\right)^2 (3\cos^2 i - 1) \tag{3.36}$$

Quantity $360n$ represents the total angular incursion on the true anomaly within twenty-four hours. Now we can easily estimate magnitude of changes of longitude of ascending node, ascending node-perigee angle and mean anomaly within twenty-four hours for some typical satellites. So for polar meteorological satellites of NOAA type $n \sim 14 rev/day$. $R_E/p \sim 1.2$, $i = 98^o$, $\cos i \sim -1.2^o$. Using value J_2 from Tab III-1 we obtain $\Delta\Omega_{day} \sim 1^o$, $\Delta\omega_{day} \sim 3^o$. .

Formulae (3.34) and (3.35) are taken from [16][33]. Formula (3.36) is taken from reference guide [15](page 438) [34] containing reference information concerning all parameters of satellite motion. There is a slight difference between formulae given in [16] and [15]. The difference is in absence and presence (respectively) of multiplier $(1-e^2)^{-2}$ for the first two formulae and multiplier $(1-e^2)^{-3/2}$ for mean anomaly. These multipliers practically do not differ from 1 for nearly circular orbits. Details of theory of satellite motion in spheroidal field of the Earth can be found in [15] [35].

3.2.2 Atmospheric resistance influence on satellite motion

This problem is targeted at the verification of a simple model of the effect of the force of molecular resistance form atmosphere side on satellites which move along relatively low and near-circular orbits. Suppose satellite with mass m and cross-sectional area σ is moving along an orbit and experiencing frontal resistance of the atmosphere. Designate the concentration of molecules of atmospheric gases by N. Then the satellite collides with $dN = NdV$ molecules enclosed in volume $dV = v\sigma dt$ within time dt, so $dN = Nv\sigma dt$ (see fig. 6).

[33] V.V.Beletckiy. Essay about celestial mechanics. M:``Nauka",1972, 320 p.

[34] Handbook of celestial mechanics and astridynamics. Edited by Duboshin, M: "Nauka" 1971, 584

[35] G.N. Duboshin. Celestial mechanics. Basic problems and methods. M.: Nauka, 1968, P.IV, Ch.XII, pp. 566-652

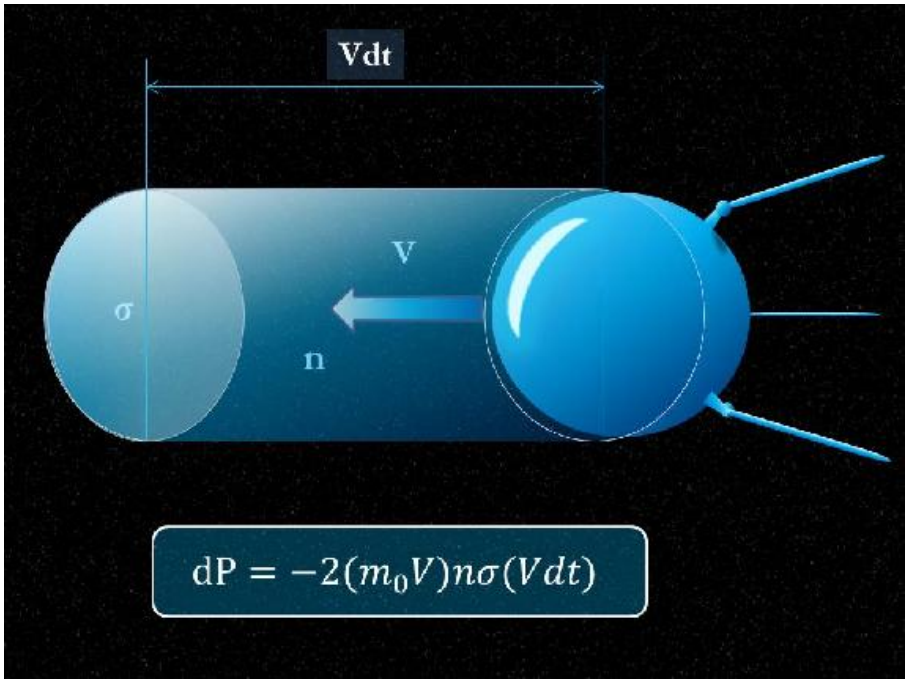

Fig. III-7-4 For molecular resistance force derivation.

Each impact is considered to be perfectly elastic. Then within time dt molecules give to the satellite momentum equal to $dp = 2m_0 v dN = 2v^2 m_0 \sigma N dt$. Here m_0 is mass of one molecule. Hence we obtain the resistance force experienced by a satellite:

$$\frac{dp}{dt} = F_d = -2v^2 \rho\sigma = -\gamma v^2,$$

where $\gamma = 2\rho\sigma$ is coefficient of friction, $\rho = m_0 N$ is density of the atmosphere.

Consider a satellite motion in the potential field of force under such friction force. Equation of motion of a satellite in Cartesian coordinate system has the following form:

$$m\frac{dv}{dt} = -\nabla U - F = -\nabla U - v v\gamma.$$

Then we multiply this equation scalarly by velocity of satellite's motion. After simple transformations we obtain:

$$\frac{d}{dt}\left[\frac{mv^2}{2} + U\right] = -\gamma v^3.$$

Hence total specific energy of a satellite $E_m = E_0/m$ changes according to the equation:

$$\frac{dE_m}{dt} = -\frac{\gamma}{m}v^3.$$

Now suppose a satellite to move along an orbit with small eccentricity $e << 1$, i.e. near-circular orbit. In this case radial component of satellite velocity is considerably less than the velocity of orbital motion $v_\phi = r\dot{\phi}$. So it is possible to consider:

$$v = \sqrt{v_r^2 + v_\phi^2} \simeq v_\phi = r\dot{\phi} = \frac{L}{rm} = \frac{L_m}{r},$$

where L - absolute magnitude of orbital angular momentum of a satellite, $L_m = L/m$ is specific

angular moment. Then we obtain the following relation:

$$\frac{r^3}{L_m^3}\frac{dE_m}{dt} = -\gamma m = const. \tag{3.37}$$

Taking into account (3.19) , relation (3.37) can be represented as the following:

$$-\frac{p^3}{(\mu p)^{3/2}}\frac{d}{dt}\left[\frac{(1-e^2)\mu}{p}\right] = -\gamma m$$

here $\mu = M_E G$. As far as it is supposed that satellites orbits examined in this task are close to circular (small eccentricity) then $r \sim p$.

In addition disturbing additions related to nonspherisity of the Earth are neglected in the formula for total energy due to their smallness. As a result the latter relation can be reduced to a form:

$$\rho = -\frac{m}{\sigma\sqrt{\mu}}\frac{d\sqrt{p}}{dt}. \tag{3.38}$$

Thus this formula allows us to estimate related change of atmospheric density at a satellite's orbit height. It is necessary to know cross-section and mass of a satellite to calculate absolute value of atmospheric density.

3.3 Lecture 8. The magnetic field of the Earth

Nowadays a presence of convective flows in the outer fluid metal (iron-nickel) core of the Earth is supposed to be the source of the magnetic field of the Earth. The general structure of the Earth is represented in fig. III-8-1. In the central part of the Earth, as it is supposed, there is a solid or nearly solid iron-nickel core. It is called the inner core. Due to high temperature complicated convective flows appear in the outer core creating electric current. As a result these currents are supposed to generate the magnetic field of the Earth.

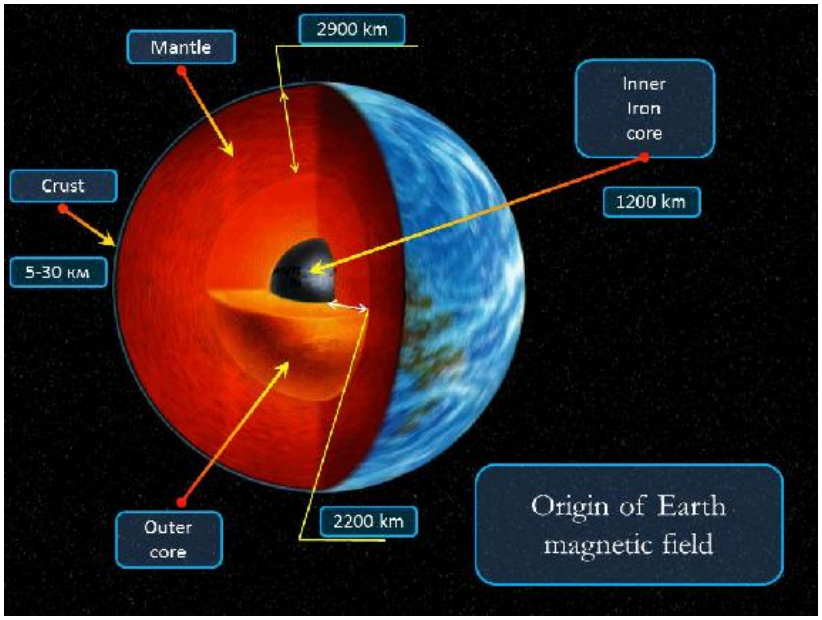

Fig. III-8-1. Structure of the Earth.

The structure of the terrestrial magnetic field is very complicated. It is well seen in fig. III-8-2, where lines of force of the terrestrial magnetic field are shown in different epochs. The complexity of the magnetic field is caused firstly by the fact that the process of magnetic field generation is possible only with complicated motion of convective flows in the outer core which change under the effect of the generated magnetic field. In addition the Earth is not homogenous. At the earlier stages of its formation a great number of asteroids, comets and planetoids fell on its surface creating irregularities in the distribution of matter and particularly in the magnetization of matter.

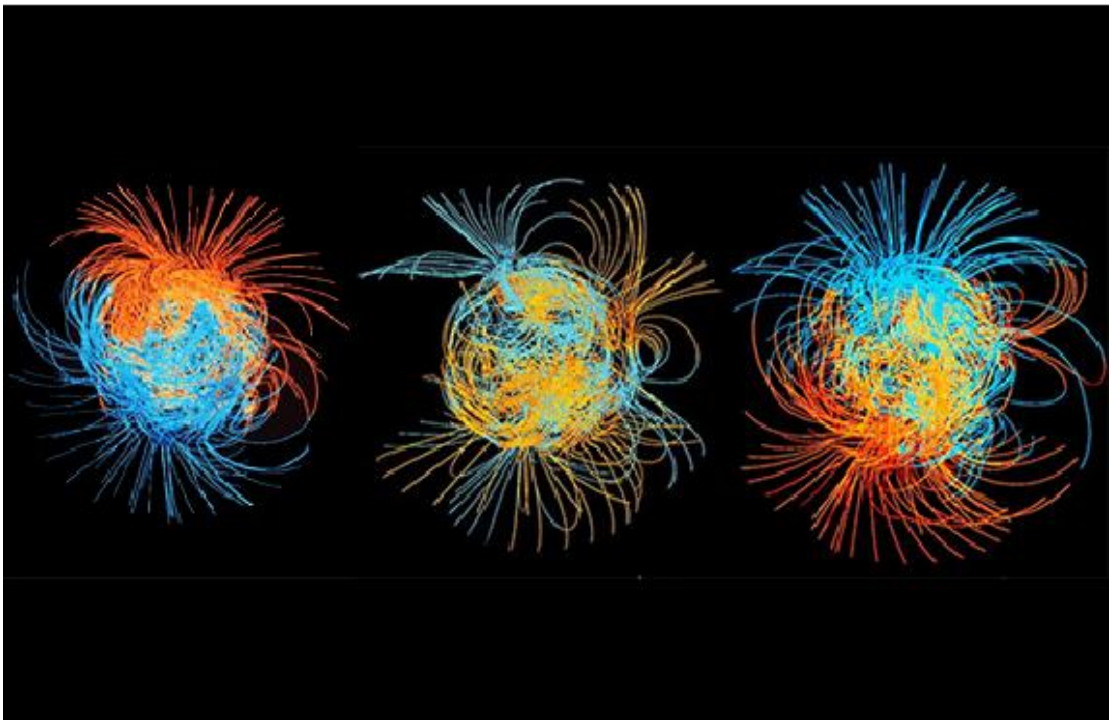

Fig. III-8-2. Lines of force of terrestrial magnetic field at different stages of its evolution. [36]

The major part of magnetic field intensity is dipole magnetic field. As far as by definition the northern pole of a magnetic needle points at the northern geographical pole the southern magnetic pole is situated near the northern geographical one and vice versa, there is the northern magnetic pole near the southern geographical pole, as it is shown in fig. III-8-3. It is sufficient to indicate magnitude and direction of magnetic moment to indicate the dipole moment. Magnetic moment direction is usually shown with the help of terrestrial magnetic poles position in geographical coordinates. This data will be presented further.

But the present position of the poles was not the same earlier. During the evolution of the Earth the magnetic field has changed its polarity and magnitude many times. Based on the examination of magnetization of igneous rocks which conserve the direction of magnetization vector at the moment of solidification it was established that exchange of terrestrial magnetic poles takes place not regularly and the magnetic field remains constant during the periods from hundreds thousands years to several million years long. Data of terrestrial magnetic field polarity for 55 million years is represented in fig. III-8-4.

[36] G. A. Glatzmaier and P.Olson. Probimg the Geodinamo. Scientific American Sp 15, 28 - 35 (2005)

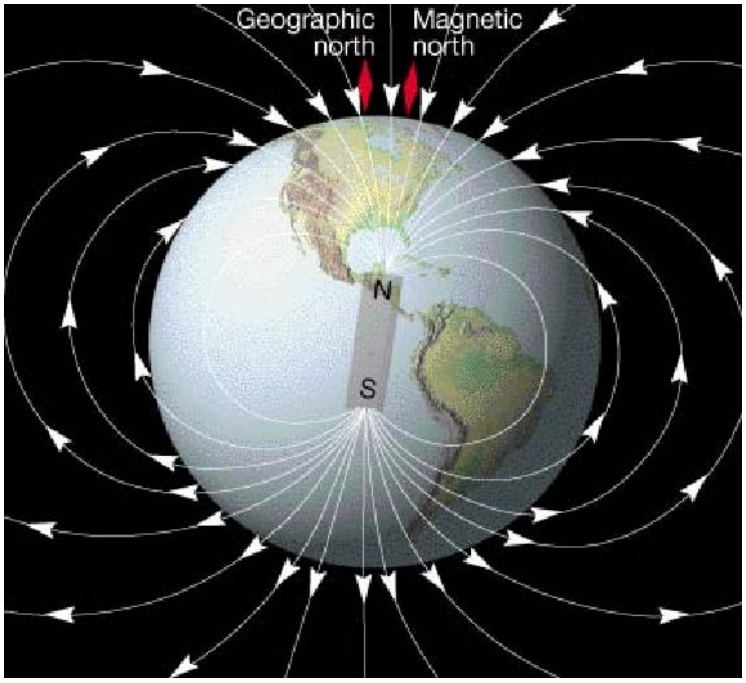

Fig. III-8-3 Terrestrial magnetic poles positioning.

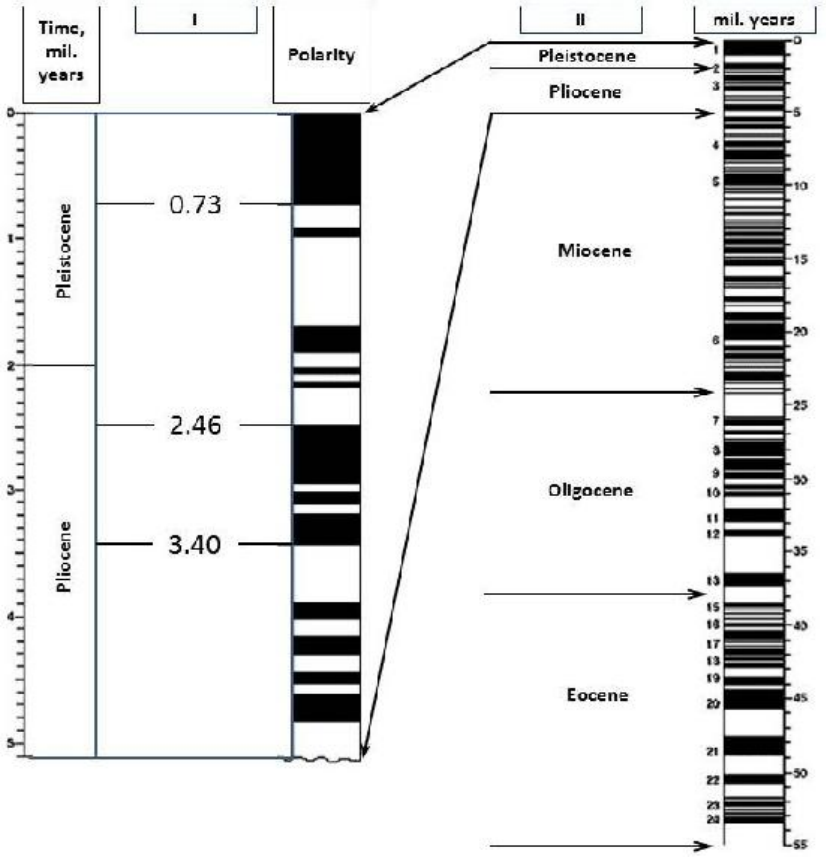

Fig. III-8-4. Inversion of the terrestrial magnetic field for the last 55 million years. Inversions of the last 5 million years with a higher resolution are shown at the insert separately. [37]

[37] http://www.ufo.obninsk.ru/images/5_9.gif

Complicacy of the magnetic field of the Earth increases during poles exchange. In all probability there can appear several poles of different polarity during the epoch of geomagnetic reversal. Such process is shown in fig. III-8-5.

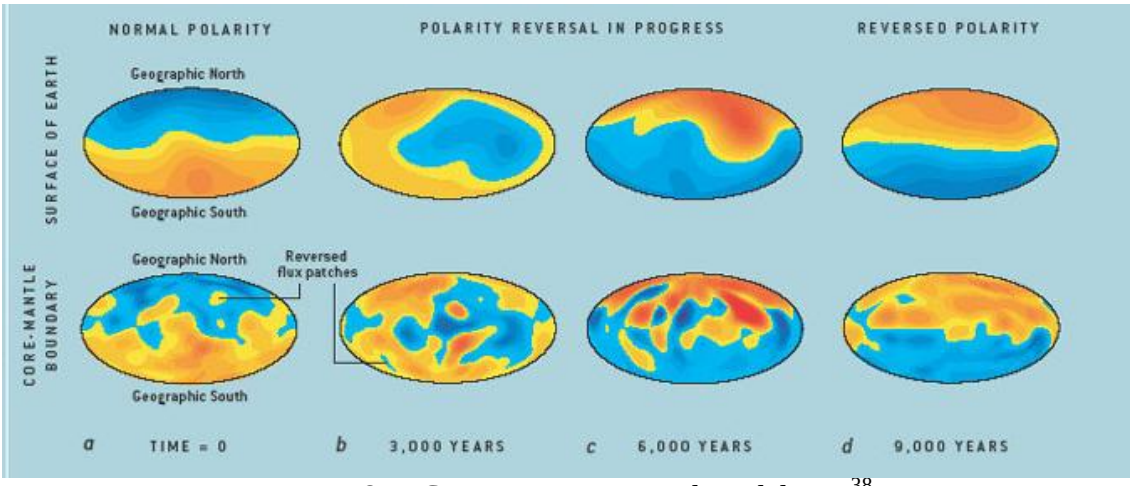

Fig. III-8-5. Geomagnetic reversal modeling. [38]

3.3.1 Dipole field

For many applied problems related to the near-Earth space exploration it is enough to know basic elements of geomagnetic field. Dipole component is that basic component.

Field intensity of a magnetic dipole can be represented as:

$$H = \frac{1}{r^5}\left(3(\mathcal{M}_E, r)r - \mathcal{M}_E r^2\right). \tag{3.39}$$

here $\mathcal{M}_E = \{M_1, M_2, M_3\}$ - dipole magnetic momentum of the Earth directed along the magnetic axis. This field is potential at any point except the origin of coordinates $r = 0$ where the source of that field is situated. Potential of this field can be written as:

$$\Phi_0 = \frac{(r, \mathcal{M}_E)}{r^3}, \tag{3.40}$$

And with this:

$$H = -\nabla\Phi_0, \quad \Delta\Phi_0 = 0$$

Dipole field lines of force are calculated basing on the solution of the equation:

$$\frac{dr}{ds} = H = \frac{1}{r^5}\left(3(\mathcal{M}_E, r)r - \mathcal{M}_E r^2\right). \tag{3.41}$$

In this equation s - is a parameter along the line of force. Equation of lines of force can be transformed into more simple presentation. Multiply (3.41) scalarly by r. As a result we obtain:

$$\frac{1}{2}\frac{dr^2}{ds} = \frac{2z}{r^3}\mathcal{M}_E.$$

here z is Cartesian coordinate along the dipole magnetic axis. Hence we find: Glatzmaier

[38] G. A. Glatzmaier and P.Olson. Probimg the Geodinamo. Scientific American Sp 15, 28 - 35 (2005)

$$\frac{dr}{ds} = \frac{2z}{r^3}\mathcal{M}_E. \qquad (3.42)$$

On the other hand component of equation (3.41) corresponding to axis z has the following form:

$$\frac{dz}{ds} = \frac{\mathcal{M}_E}{r^5}\left(3z^2 - r^2\right). \qquad (3.43)$$

Excluding parameter along trajectories from these equations we come to equation for dipole lines of force in the following form:

$$\frac{dz}{dr} = \frac{1}{2}\frac{\left(3z^2 - r^2\right)}{zr}.$$

This equation is universal and does not contain any parameters. Let's introduce new variables: $\xi = z^2$, $p = \ln r$. In these coordinates the equation takes a simple form:

$$\frac{d\xi}{dp} = 3\xi - e^{2p}.$$

Integrating that we obtain:

$$\xi = Ae^{3p} - e^{3p}\int e^{-3p}e^{2p}dp = Ae^{3p} + e^{-p}.$$

And returning to coordinates r, z we get:

$$z^2 = Ar^3 + r^2.$$

Changing from z to polar angle and setting $A = -L^{-1}$ we finally obtain:

$$r = L(1 - \cos^2(\theta)) = L\sin^2(\theta). \qquad (3.44)$$

Here θ - is polar angle. If we use latitude $\phi = \pi/2 - \theta$ instead of θ then equation of dipole lines of force takes the form:

$$r = L\cos^2(\phi). \qquad (3.45)$$

They are represented in fig. III-8-6.

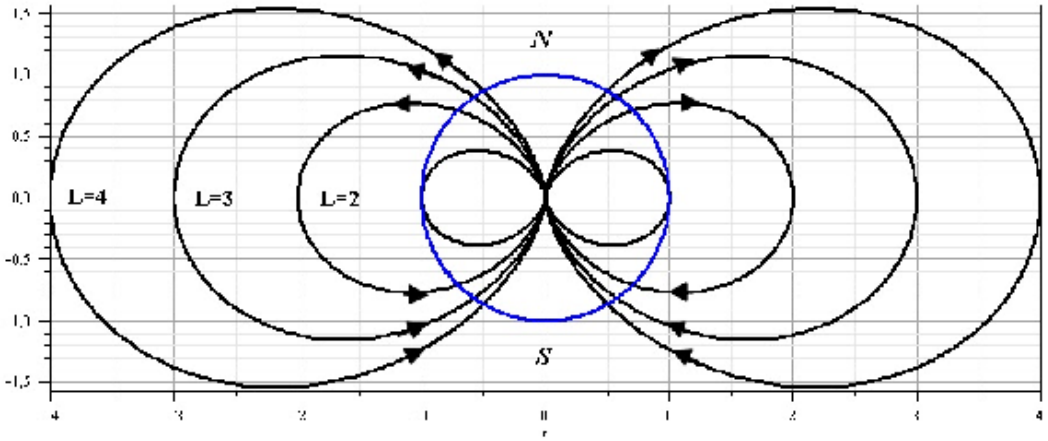

Fig. III-8-6. Dipole lines of force.

Parameter L is a distance from the dipole center to line of force stretched along the equator. Field intensity along the line of force as a function of polar angle θ and latitude ϕ will have the following:

$$H = \frac{\mathcal{M}_E}{L^3}\frac{\sqrt{3\cos^2(\theta)+1}}{\sin^6(\theta)} = \frac{\mathcal{M}_E}{L^3}\frac{\sqrt{3\sin^2(\phi)+1}}{\cos^6(\phi)}.$$

With that intensity on the equator for a given line of force with number L equals to:

$$H_{eq} = \frac{\mathcal{M}_E}{L^3}.$$

3.3.2 Shape of geomagnetic field

Maxwell's equations describing electromagnetic processes in the near-Earth space environment can be written in a general form like that:

$$\mathrm{div}D = 4\pi\rho_e, \quad \mathrm{div}B = 0,$$
$$\mathrm{rot}E = \frac{\partial B}{\partial t}, \quad \mathrm{rot}H = 4\pi j + \frac{\partial D}{\partial t},$$
$$D = \varepsilon E, \quad B = \mu H.$$

Here E, bD - intensity and induction of electric field, H, bB - intensity and induction of magnetic field, ε, μ - dielectric constant and magnetic permeability, j - current density, ρ_e - electric charge density. This set of equations considerably simplifies for description of geomagnetic field. As far as the basic terrestrial magnetic field does not change substantially for tens of years so when analyzing a component having a shape close to a dipole shape it is possible to neglect effects related to displacement current and eddy current created by variable fields. In addition planetary interior is electrically neutral so the charge density of a nucleus equals to zero: $\rho_e = 0$. As a result the set of equations takes the following form:

$$\mathrm{div}D = 0, \quad \mathrm{div}B = 0,$$
$$\mathrm{rot}E = 0, \quad \mathrm{rot}H = 4\pi j,$$
$$D = \varepsilon E, \quad B = \mu H.$$

Form of this equations shows that constant electric and magnetic fields of planets are not connected to each other. This allows separate examination of electric and magnetic components. For the near-Earth space the major role is played by the magnetic field stretching for the distance of several Earth radiuses while the electric field is concentrated only near the surface and it is considerable only at a height up to 50-100 km. That is why it is exactly the structure of the magnetic field that is to be examined.

The problem of the geomagnetic field examination can be divided into two parts. The first one is to describe the magnetic field near the terrestrial (or planetary) surface and in the near-Earth space environment. The second problem is to examine sources of that field supposed to be situated in the core of the Earth and its mantle and in the Sun if we talk about the near-Earth space and the interplanetary space.

Let's start with the description of the magnetic field near the terrestrial surface. Substantial current able to create magnetic field are absent in this area - both in the interior and in the space. So in this area $j = 0$. Thereby equation is true for magnetic field:

$$\mathrm{div}B = 0, \quad \mathrm{rot}H = 0.$$

So taking into account that the magnetic permeability is practically unchangeable in this area it is possible to suppose the magnetic field to be potential:

$$B = \nabla\Psi. \tag{3.46}$$

With that potential Ψ satisfies the Laplace equation:

$$\Delta\Psi = 0.$$

Therefore potential of magnetic field like potential of gravitational field can be expanded in spherical harmonics:

$$\Psi = R_E \sum_{n=1}^{\infty}\sum_{m=0}^{n} P_n^{|m|}(\cos\theta)\left[\left(\frac{R_E}{r}\right)^{n+1}(h_{nm}\sin(m\varphi)+g_{nm}\cos(m\varphi))+\right.$$

$$\left.+\left(\frac{R_E}{r}\right)^{-n}(p_{nm}\sin(m\varphi)+q_{nm}\cos(m\varphi))\right]. \qquad (3.47)$$

Here R_E is equatorial radius of the Earth. In this expression the first sum of powers r^{-n-1} relates to the magnetic field generated by flows inside the Earth, and the second one relates to the magnetic field generated by sources outside the Earth. As far as currents outside the Earth have nonstationary but practically random character they equal to zero upon average within a long enough period (approximately within one year). Part of the total sum remained after year averaging and decreasing while moving away from the Earth is called the ***principal field***. Corresponding coefficients h_{nm} and g_{nm} are called ***Gauss coefficients***.

In these sums summand with $n = 0$ is absent as $\mathrm{d}ivB = 0$ (there are no magnetic charges)

Component with $n = 1$ is a field of point dipole placed in the origin of coordinates with $r = 0$. Potential of a point dipole according to the previous chapter equals to:

$$\Psi_0 = \frac{(r, \mathcal{M}_E)}{r^3}$$

For spherical harmonics the following expressions are known:

$$P_1^{|0|} = \cos\theta, \;\; P_1^{|1|} = \sin\theta.$$

Therefore

$$z = rP_1^{|0|}, \;\; x = rP_1^{|1|}\cos(\varphi), \;\; y = rP_1^{|1|}\sin(\varphi).$$

Hence summands with $n = 1$ take the following:

$$\frac{R_E^3}{r^3}(g_{10}P_1^{|0|}z + P_1^{|1|}(xg_{11}+yh_{11})) = \frac{(r, \mathcal{M}_E)}{r^3} = \frac{x\mathcal{M}_E^x + y\mathcal{M}_E^y + z\mathcal{M}_E^z}{r^3}.$$

Therefore:

$$g_{11} = \frac{\mathcal{M}_E^x}{R_E^3}, \;\; h_{11} = \frac{\mathcal{M}_E^y}{R_E^3}, \;\; g_{10} = \frac{\mathcal{M}_E^z}{R_E^3}.$$

values of these Gauss coefficients for dipole and quadrupole components are given in Tab. III-2.

g_{10}	g_{11}	h_{11}	g_{20}	g_{21}	g_{22}	h_{21}	h_{22}
- 3057	-211	581	-127	296	164	-166	54

Table III-2. Gauss coefficients (by 1982) in $\grave{O}\cdot(10)^{-8}$. [39]

Values of dipole component for some solar system planets are shown in Tab. III-2 for comparison.

As far as dipole component of magnetic momentum is ten times more than quadrupole component the basic component of the terrestrial magnetic field is a dipole one. Magnitude of the magnetic field is calculated with the help of measured values of parameters g_{10}, g_{11}, h_{11}:

$$|\mathcal{M}_E| = R_E^{3/2}\sqrt{g_{10}^2 + g_{11}^2 + h_{11}^2} \simeq 8.1\cdot 10^{25} Gs\cdot cm^3,$$

[39] Table from book: Yu.V.Alexandrov. Introduction to planets physics. Kiev. ``Vischa shkola", 1982

and its direction is also calculated in geostationary coordinate system. Position of the Pole, i.e. point where vector of magnetic momentum crosses the surface of the Earth is determined by polar angle θ_0 and longitude λ_0:

$$\theta_0 = \frac{\sqrt{g_{11}^2 + h_{11}^2}}{g_{10}},\ \lambda_0 = \frac{h_{11}}{g_{11}}.$$

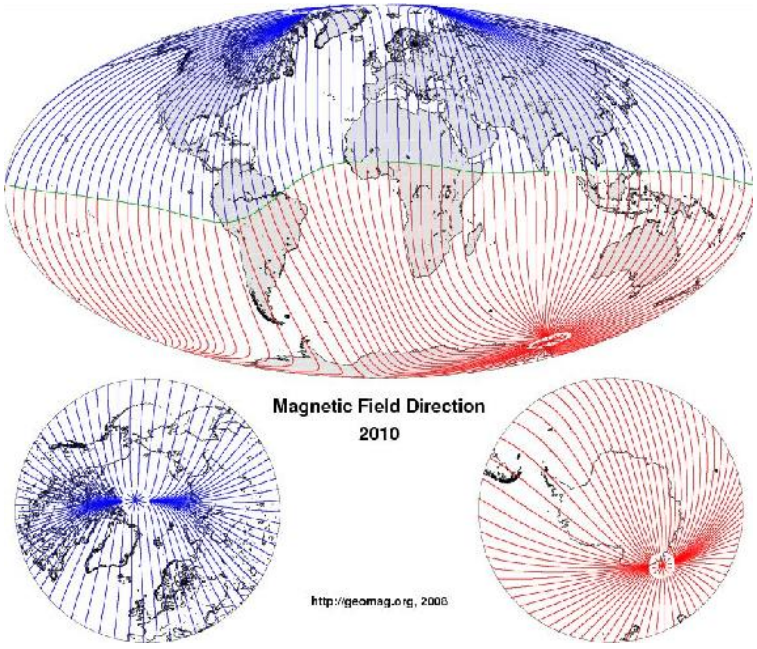

Fig. III-8-7. Magnetic lines of force in 2010.[40]

The more exact model is a model of dipole with displacement from the mass center of the Earth. Potential of such field has the following form:

$$\Psi_d = \frac{(r - r_0, \mathcal{M}_E)}{(r - r_0)^3}.$$

Numeral values of Gauss coefficients for this model are given in Tab. III-2. At the present time the absolute value of displacement vector of the center of dipole equals to approximately 340 km. position of the southern Pole is determined $\varphi_{0,s} = 75^o 36'$ NL, and $\lambda_{0,s} = 101^o$ WL (the north of Canada), and the Northen Pole is at $\varphi_{0,n} = 66^o 18'$ SL and $\lambda_{0,n} = 141^o$ EL (Antarctica)[41]

Representation of the magnetic field of the Earth as two or more dipoles is an improved but simple model. Thus for example it is possible to take into account so-called Brazilian magnetic anomaly.

A contemporary distribution of the geomagnetic field is represented in fig. III-8-7 and III-8-8.

[40] http://www.geomag.us/info/declination.html

[41] V.S.Murzin. Cosmic Ray Astrophysics. M:MSU,Logos, 2006

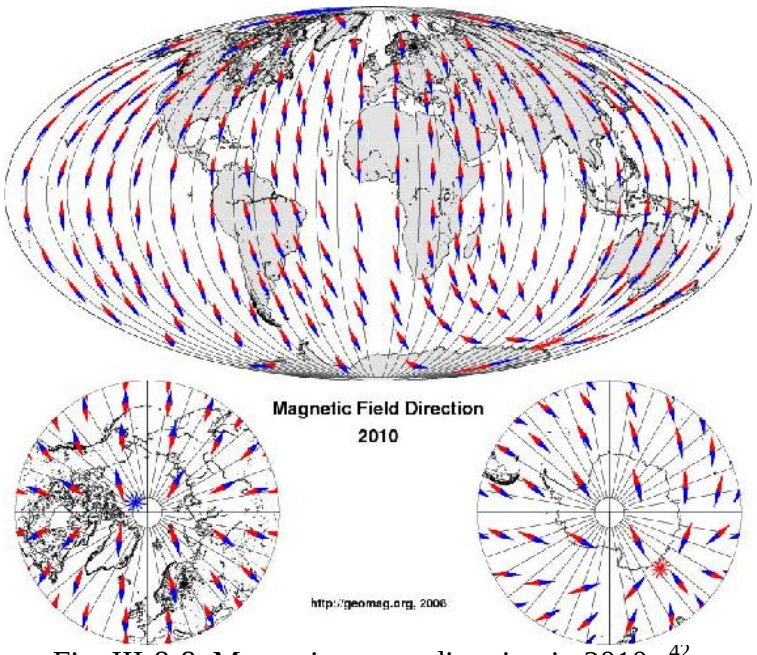

Fig. III-8-8. Magnetic vector direction in 2010. [42]

3.3.3 Units of the magnetic field measurement

Magnetic field intensity (H) (vector) has no name in honor of a famous physicist and is measured in (A/m). Magnetic field intensity in CGS is measured in ***Oersted*** (Oe). It is called in honor of Danish physicist Hans Christian Oersted (1777-1851).

1 Oersted equals to magnetic field intensity 1 cm from the infinite rectilinear conductor with extremely small cross-section conducting a current of 1 A. 1 oersted is related to Gauss. In vacuum, if the magnetizing field strength is 1 Oe, then the magnetic field density is 1 Gauss.

Gauss is the CGS unit of magnetic flux density. Called in honor of genius German mathematician, astronomer and physicist Johann Carl Friedrich Gaus (1777-1855).

Magnetic induction (B) in SI is measured in Tesla (T). The unit is called in honor of outstanding Serbian (American) physicist, engineer, inventor Nicola Tesla (1856-1943)

1 T = 10000 Gauss (CGS unit). $1 \cdot 10^9$ gamma (unit used in geophysics).

Maxwell — is a magnetic flux unit in CGS system. International abbreviation - Mw (do not confuse with megawatt - MW). The unit was introduced by the International Electrotechnical Commission in 1930. (before this unit was called line). The unit is called in honor of an outstanding English physicist James Clerk Maxwell (1831-1879). 1 Maxwell = 1 Gauss$\cdot$cm^2 = 10^{-8} 2 Weber.

In a uniform magnetic field with induction 1 gauss a magnetic flux of 1 Maxwell passes through a plane surface of 1 cm^2 area, placed perpendicularly to induction vector.

Weber (Wb) is magnetic flux unit in SI. By the definition, a change in flux of one Weber per second will induce an electromotive force of one volt (see Faradey's law). In other SI units weber can be represented as the following: $Wb=V \cdot s=kg \cdot m^2 \cdot s-2 \cdot A^{-1}$. The unit is called in honor of German physicist W.E.Weber (1804-1891).

[42] http://www.geomag.us/info/declination.html

3.3.4 Geomagnetic field source. Geomagnetic dynamo

Now let's examine a question of appearance of magnetic field of the Earth and the other planets. This question is still unsolved though there are some models explaining the generation of magnetic field. Such a model is a model called geomagnetic dynamo. As far as this model has a universal meaning for all problems related to the magnetic field generation we examine this model here. In order to create a simple model of ***hydromagnetic dynamo*** consider movement of material in the central parts of planets.

A mechanical model of magnetic dynamo

A simple model of a single-disk dynamo can be written in the following form. Suppose there is a conducting disk with a radius a rotating with a velocity ω. A magnetic field with induction B_0 is directed perpendicularly to the disk.

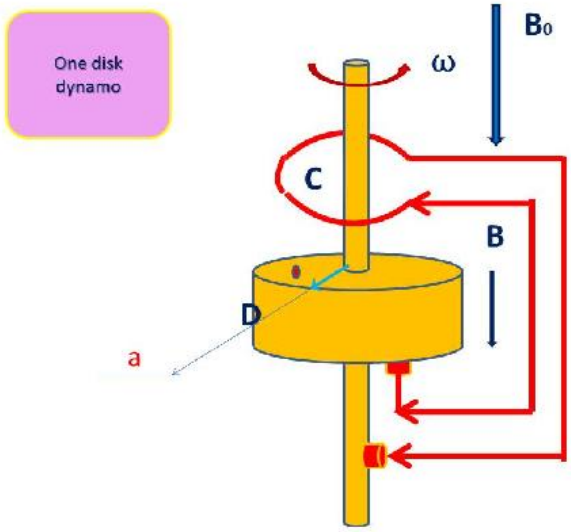

Fig. III-8-9. A single-disk dynamo model

Under rotation of the disk EMF appears at its ends. EMF appearing in a conductor when it moves rectilinearly in the magnetic field equals to:

$$E = B_0 L v,$$

where B is magnetic field induction, L - length of the conductor, v - velocity of the conductor motion. This formula is true for a part of the conductor with the length of Δr, situated at the distance r from the center of the disk. Velocity of this part equals to $v = \omega r$. Therefore EMF value at this part equals to:

$$\Delta E = B_0 \omega r \Delta r.$$

Summing all the parts along the disk we finally obtain:

$$E_0 = \int_0^a B_0 \omega r dr = \frac{1}{2} \omega a^2 B_0.$$

Now if we close the circuit between the axis of the disk and its edge current I will flow in the radial direction from the center of the disk to its edge. This current will produce an additional magnetic field

δb and it will lead to the additional EMF the value of which consists of two components. The first one is an additional EMF generated in the conductor when field increases by δb. It can be calculated by the same formula:

$$\delta E_1 = \frac{1}{2}\omega a^2 \delta b.$$

The second component is induction EMF equal to:

$$\delta E_2 = -\frac{d\Phi}{dt}.$$

Here Φ is a magnetic field flux through the contour area. Contour area is equal to the disk area so the magnetic field equals to $B = B_0 + \delta b$. Therefore:

$$\Phi = \pi a^2 (B_0 + \delta b).$$

$$\delta E_2 = -\pi a^2 \frac{d(B + \delta b)}{dt}.$$

Field magnitude can be calculated with the help of Kirchhoff laws. EMF created by disk rotation "drops" across the resistance of the contour ρ in the closed circuit. Therefore we find:

$$E_0 + \delta E_1 + \delta E_2 = I\rho.$$

Hence:

$$\frac{1}{2}\omega a^2 (B_0 + \delta b) - \pi a^2 \frac{d(B_0 + \delta b)}{dt} = I\rho.$$

The equation for the total field B has a form:

$$\frac{1}{2}\omega a^2 B - \pi a^2 \frac{dB}{dt} = I\rho.$$

For a thin disk current value can be calculated by the formula:

$$I = \frac{(B_0 + \delta b)a}{2\pi}.$$

Hence:

$$\pi a^2 \frac{dB}{dt} = B\left[\frac{1}{2}\omega a^2 - \frac{a}{2\pi}\rho\right].$$

or

$$\frac{dB}{dt} = \gamma B,$$

where

$$\gamma = \frac{1}{\pi^2 a^2}\left[\pi\omega a - \rho\right].$$

The field B will increase in the course of time if $\gamma > 0$ and it will decrease if $\gamma < 0$. Hence there a condition of appearance of the field can be written in a form:

$$\pi\omega a > \rho.$$

The sense of this equation is that if rotation velocity of the disk is high enough a self-maintained magnetic field will appear. The field cannot grow up to the infinity. At some stage saturation appears. This is hypothetically observed on planets.

But this model is too simplified. So a more complicated model of double-disk dynamo is used (see Fig. III-8-10). Saturation is already present in this model. This model behavior is similar to the behavior of real fields. But as it turns out it is very difficult to create such a mechanism realizing this

model in real processes.

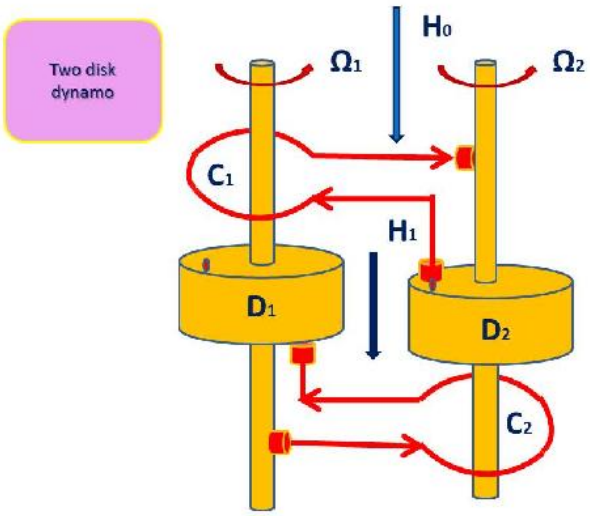

Fig. III-8-10 Double-disk dynamo model.

3.3.5 Magnetic fields of solar system planets

Planet	$H_{eqvator}, T \cdot 10^{-9}$	$\mathcal{M}_P, T \cdot m^3 \cdot 10^{-9}$	Angle θ_0, grad
Mercury	30	-	-
Venus	1		
Earth	3000	$8.2 \cdot 10^{15}$	11
Moon	2	$4 \cdot 10^{3}$	
Mars	6	$2.5 \cdot 10^{12}$	13-20
Jupiter	$4 \cdot 10^{5}$	$1.3 \cdot 10^{20}$	10

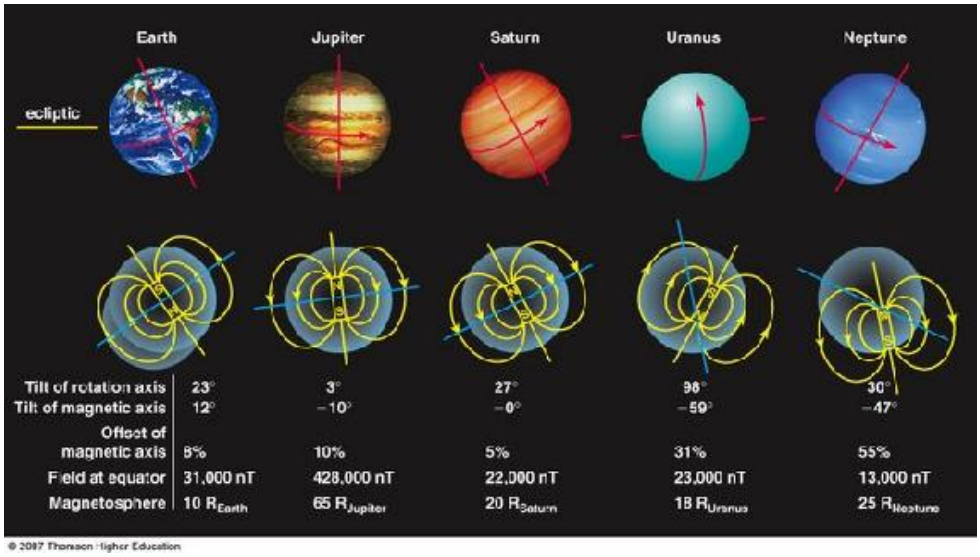

Fig. III-8-11. Characteristics of magnetic fields of solar system planets.

3.4 Lecture 9. Magnetosphere and solar wind interaction

3.4.1 Plane plasma front

As it was discussed in the chapter devoted to the Sun our star creates a dense flow of low-energy particles going away almost radially from it and which are not trapped into interplanetary magnetic field. This flow changes its speed from 100-200 km/s in a quiet time to 1000 km/s and more during powerful flares on the Sun. In case of a powerful flare an increased density plasma wave appear in solar wind. This wave runs against magnetosphere of the Earth deforming the shape of the magnetic dipole. Schematic image of such situation is given in a picture at the beginning of this chapter. The picture is taken from a site [43].

Taking into account oncoming a plane wave the shape of geomagnetic field can be calculated in quite simple problem where a wave of plasma can be considered as a semispace filled with perfectly conducting medium. This problem was solved in works [5]. In these works it was proved that an exact solution of a problem of a magnetic field facing a wave front has a form of a sum of fields of a dipole B_d and a mirror-image dipole B_d^- of the plasma front:

$$B = B_d + B_d^-,$$

The magnetic field equals exactly to zero behind the front in absolutely perfect medium because it is compensated by the inducted current. Current generating a compensation field of dipole behind the front in absolutely perfect medium is concentrated on the surface of the front and can be calculated with a common expression:

$$j = \frac{1}{2\pi}[n_s \times B_d], \tag{3.48}$$

where n_s - is a normal vector to the front surface. It follows from formula (3.48):

$$j_z = \frac{3Myz}{(x_0^2 + y^2 + z^2)^{5/2}}, \quad j_y = -\frac{2z^2 - x_0^2 - y^2}{(x_0^2 + y^2 + z^2)^{5/2}}.$$

Here z axis coincides with the dipole axis direction (vector $\mathcal{M}$). X -axis is directed perpendicularly to the plane of a plasma front and y -axis lies in a plane of magnetic equator parallel to the plane of front. Equation for lines of flow can be written in a form of:

$$\frac{dz}{dy} = \frac{j_z}{j_y} = -\frac{3Myz}{2z^2 - x_0^2 - y^2}.$$

Lines of flow are shown in fig. III-9-1.

A problem of calculation of current was solved in work [6].

Suppose plasma front to be parallel to dipole axis. Coordinate axis perpendicular to the front plane is denoted by x. Taking into account that a mirror-image of function $f(x)$ with the respect to a point with coordinates x_0 has a form $f^-(x) = f(2x_0 - x)$ it is possible to write for the total dipole field and the inducted field in medium behind the front:

[43] http://spacereal.ru/temnye-pyatna-na-solnce-i-24-solnechnyj-cikl/

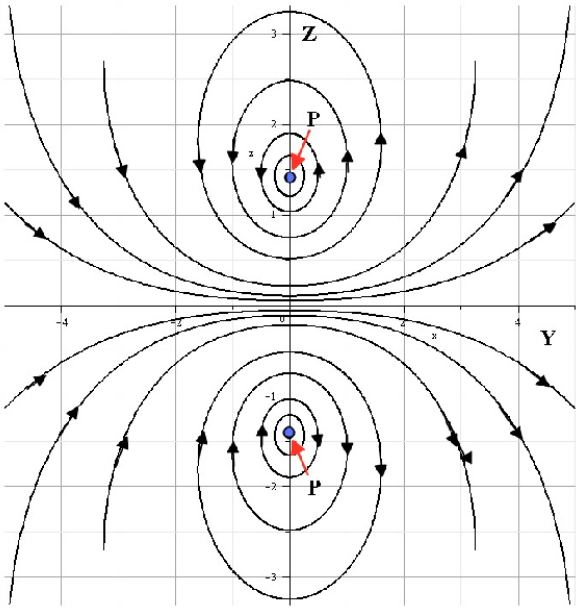

Fig. III-9-1. Force lines of current generating mirror-image dipole on Z-Y plane of plasma front.

$$B^x = B_d^x(x,y,z) - B_d^x(2x_0 - x, y, z) = 3\mathcal{M}z\left(\frac{x}{(x^2+y^2+z^2)^{5/2}} - \frac{2x_0 - x}{((2x_0-x)^2+y^2+z^2)^{5/2}}\right),$$

$$B_y = B_d^y(x,y,z) + B_d^y(2x_0 - x, y, z) = 3\mathcal{M}z\left(\frac{y}{(x^2+y^2+z^2)^{5/2}} + \frac{y}{((2x_0-x)^2+y^2+z^2)^{5/2}}\right),$$

$$B_z = B_d^z(x,y,z) + B_d^z(2x_0 - x, y, z) = \mathcal{M}\left(\frac{2z^2 - x^2 - y^2}{(x^2+y^2+z^2)^{5/2}} + \frac{2z^2 - (2x_0-x)^2 - y^2}{((2x_0-x)^2+y^2+z^2)^{5/2}}\right).$$

Components of the field perpendicular to the edge of plasma front are subtracted and parallel ones are added. In $z-x$ plane these equations can be rewritten in the following form:

$$B^x = 3\mathcal{M}\frac{zx}{(x^2+z^2)^{5/2}}\left(1 + (1-2x_0/x)Q(x,z)\right),$$

$$B_y = 3\mathcal{M}\frac{zy}{(x^2+z^2)^{5/2}}\left(1 + Q(x,z)\right),$$

$$B_z = \frac{1}{(x^2+z^2)^{5/2}}\mathcal{M}\left((2z^2 - x^2) + (2z^2 - (2x_0-x)^2)Q(x,z)\right). \qquad (3.49)$$

Here:

$$Q(x,z) = \frac{(x^2+z^2)^{5/2}}{((2x_0-x)^2+z^2)^{5/2}}.$$

The equation for lines of force of this field has the following form:

$$\frac{dz}{dx} = \frac{(2z^2 - x^2) + (2z^2 - (2x_0-x)^2)Q(x,z)}{zx(1 + (1-2x_0/x)Q(x,z))}$$

Numerical integration of this equation gives the following image of lines of force of a ``mutilated"

dipole:

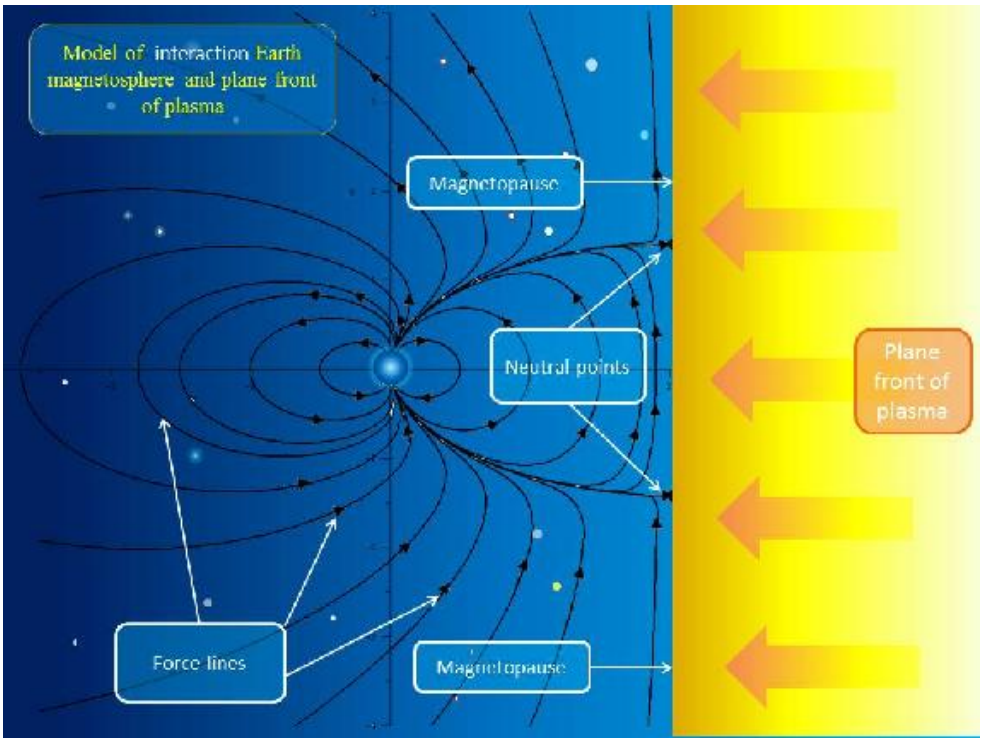

Fig. III-9-2. Dipole lines of force in the presence of a plane plasma front

Plasma front stops not reaching the Earth. The distance between the plasma front and the center of the Earth can be calculated on the assumption of a simple consideration given for the first time in the work [11] [44]. It was shown in this work that the plasma front stops under the conditions when the pressure created by the solar wind is equaled by the magnetic pressure. The pressure created by the solar wind can be calculated with the help of the following formula:

$$P_w = 2mnV^2, \qquad (3.50)$$

where m denotes mass of protons which form the major mass part of solar wind particles, n denotes the particles concentration in the solar wind, and V denotes solar wind velocity. Formula for solar wind pressure at the edge of the front can be obtained on the on the basis of supposition about perfectly elastic reflection of particles from this surface. When collision is perfectly elastic a momentum of a particle changes to the opposite so that momentum $\delta p_w = 2mV$ is given to the front within the time Δt a particle interacts with the front. Within this period of time $ndSVdt$ particles, enclosed in cylinder with length equal to Vdt, drop on the surface of the front dS. Then a total force applied to the surface dS by the oncoming flow equals to:

$$\Delta F = \frac{\delta p_w}{\Delta t} ndSV\Delta t = 2mV^2 ndS.$$

Therefore the solar wind pressure equals to $P_w = 2mnV^2$. As far as the reflection of particles from the front goes on thanks to interaction with the magnetic field it is this field that creates the force ΔF. At the same time the pressure on plasma of the magnetic field equals to the energy density of the magnetic field:

[44] Martyn D.F. The theory of magnetic storms and auroras. Nature, Lond. v. 167, 92-94 (1951)

$$P_B = \frac{B^2}{8\pi}. \qquad (3.51)$$

Thus equilibrium condition is denoted by the following relation:

$$P_B = P_w : \frac{B^2}{8\pi} = 2mnV^2.$$

In particularly, it follows from this relation that when the solar wind is ``calm`` with a velocity $V = 300$ km/s and particle concentration $n = 5$ cm^{-3} the magnitude of the magnetic field, where equilibrium is established, is about $B \simeq 60$ Gs. As far as at the edge of the front $B_d^2 = (B_d^-)^2$:

$$B^2 = 4B_d^2 = 4[(B_d^x)^2 + (B_d^y)^2]$$

At this point the dipole field must be approximately a half of the needed intensity. The other half is created by a mirror-image dipole field. So intensity of undistorted dipole field is equal to approximately 30 Gs at the point of equilibrium. This value corresponds to an equatorial distance equal to about 10 radiuses of the Earth $L \simeq 10$. On the other hand this equation shows that a model of the plane plasma front does not describe the real situation. Indeed the dipole energy decreases with the distance from the magnetic equator plane. So in currents placed at some distance from the plane of equator a solar wind pressure will be equalized by magnetic pressure at some other distance than the plane plasma theory gives. As a result the front becomes curved and mirror reflection condition must be figured out for a curved front which leads to a more complicated problem of a combined determination of mirror-image dipole magnetic field and a front where equilibrium $P_B = P_w$ to be established.

3.4.2 Magnetopause and the shape of shock wave surfaces

Having analyzed a simple formulation problem we are able to create a more exact solution of the problem being examined. The solution of a more common problem can be found within the following suppositions:

1) Particles of plasma experience a perfectly elastic collision at the edge of plasma front to be called a shock wave front.

2) Thickness of a layer where the current flows is infinitely small.

3) Electric currents are absent in magnetosphere itself.

On the assumption of the latter supposition equations for the magnetic field before the shock-wave front can be written. They have a standard form of magnetostatics without currents:

$$\mathrm{div}B = 0, \quad \mathrm{rot}B = 0. \qquad (3.52)$$

Hence the field B is still potential as before:

$$B = -\nabla\Phi.$$

Fig. III-9-3 illustrates calculation of the pressure exerted by solar wind particles on a curved front.

At point O, as it is shown, x axis coinciding with the initial direction of the solar wind makes an angle χ with a perpendicular to the shock-wave front. Upon perfectly elastic impact on a wave front it is only a normal component of particle's momentum that changes. As it is seen from the picture at the point O a change of the normal component of momentum equals to:

$$\Delta p_w = 2mV\cos(\chi)dS\Delta t.$$

As a result pressure exerted at this point equals to:

$$P_w = 2mnV^2\cos^2(\chi).$$

It follows from the equilibrium condition that at the edge a condition must be satisfied:

$$\frac{B^2}{8\pi} = \frac{(B^x)^2 + (B^z)^2}{8\pi} = 2mnV^2 \cos^2(\chi). \qquad (3.53)$$

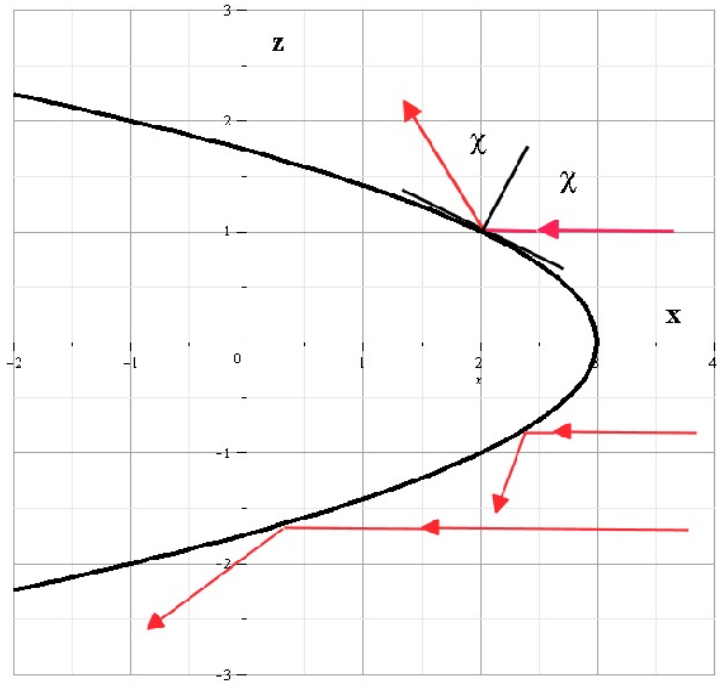

Fig. III-9-3. For the calculation of a pressure on the shock-wave surface

Hence:

$$B = 4V\sqrt{mn\pi}\cos\chi. \qquad (3.54)$$

This relation is practically a bounding solution for the set of equations.

Now it is possible to figure out the shape of the surface having calculated value B at the point of impact of the particle using $P_w = P_B$. Alike as in case of the plane plasma front the field tangent to the front surface equals to doubled magnitude of the corresponding component of the dipole field and the normal field becomes zero. According to fig. III-9-4 vector of a normal to the front is defined here by vector n_s with components: $n_s^x = \cos(\chi)$, $n_s^z = \sin(\chi)$. Hence we obtain a tangent component of a dipole field on the front surface:

$$B_s = B_d^x \sin(\chi) - B_d^z \cos(\chi).$$

As a result a relation for the front comes to the following equation for the angle χ:

$$(B_d^x \sin(\chi) - B_d^z \cos(\chi))^2 = \alpha \cos^2\chi, \qquad (3.55)$$

where $\alpha = 16V^2 mn\pi$. This equation is cubic relative to $\cos^2(\chi)$. Solving it we obtain:

$$\cos^2\chi = F(x,z).$$

where $F(x,z)$ is a positive root of equation (3.55). Since

$$\frac{dz}{ds} = \cos\chi, \quad \frac{dx}{ds} = -\sin\chi,$$

integral curve for the front can be found as the solution of equations:

$$\frac{dz}{dx} = \pm\sqrt{\frac{F(x,z)}{1-F(x,z)}}.\odot$$

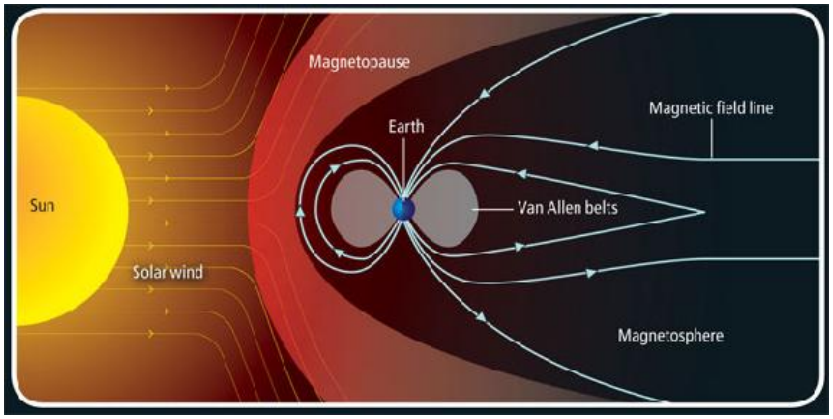

Fig. III-9-4. Basic elements of magnetosphere structure, connected to interaction with the solar wind.

The solution of this problem for the shape of magnetopause can be obtained with the help of simple mathematical tools - conformal transformations. This method was first offered in [12].

A given description of magnetosphere shape is much simplified. It is just qualitatively represents the processes leading to the formation of magnetosphere under the effect of a solar wind. With the help of modern computers taking into account more exact shape of the terrestrial magnetic field different from a dipole one more exact models of magnetosphere are being produced. It allows to model the dynamic of magnetosphere shape changes on changes of solar wind parameters. Such changes take place during flares on the Sun and on changes of a general solar activity. A schematic image of magnetosphere with all its structural components is given in fig. III-9-4.

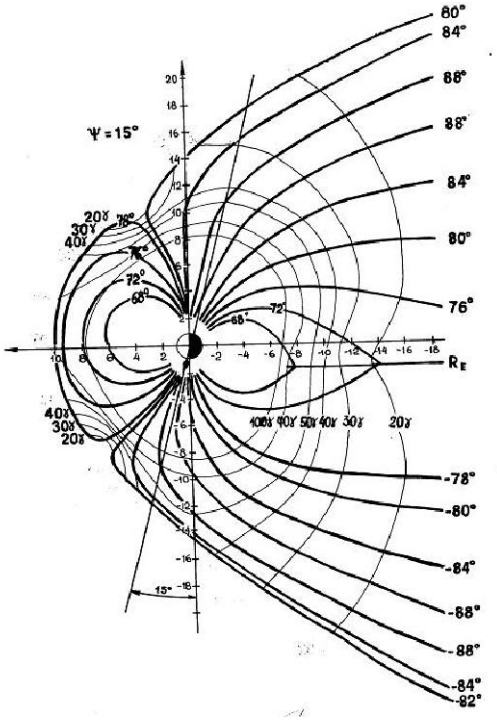

Fig. III-9-5. Magnetic lines of force and magnetopause

A distinctive feature of a real magnetosphere structure is a presence of a tail. Geomagnetic tail is a huge area filled with magnetic field stretched for a long distance from the Earth in the direction from the Sun. geomagnetic field is stretched by solar wind plasma. This area plays an important role in

formation of charged particles flows falling on the Earth surface in a form of aurora Polaris. It is the tail where particles of auroras Polaris are caught and transferred to the terrestrial poles where they are accelerated by electric fields appearing near the poles. Under these fields effect they obtain energy not allowing them to stay in the geomagnetic field longer.

All the other elements of the magnetosphere are similar to those obtained with the help of simple models. They are magnetopause, neutral points, radiation belts, shock-wave.

In fig. III-9-5 The shape of magnetosphere figured out with the help of more exact models is shown.

Chapter 4. Magnetosphere of the Earth

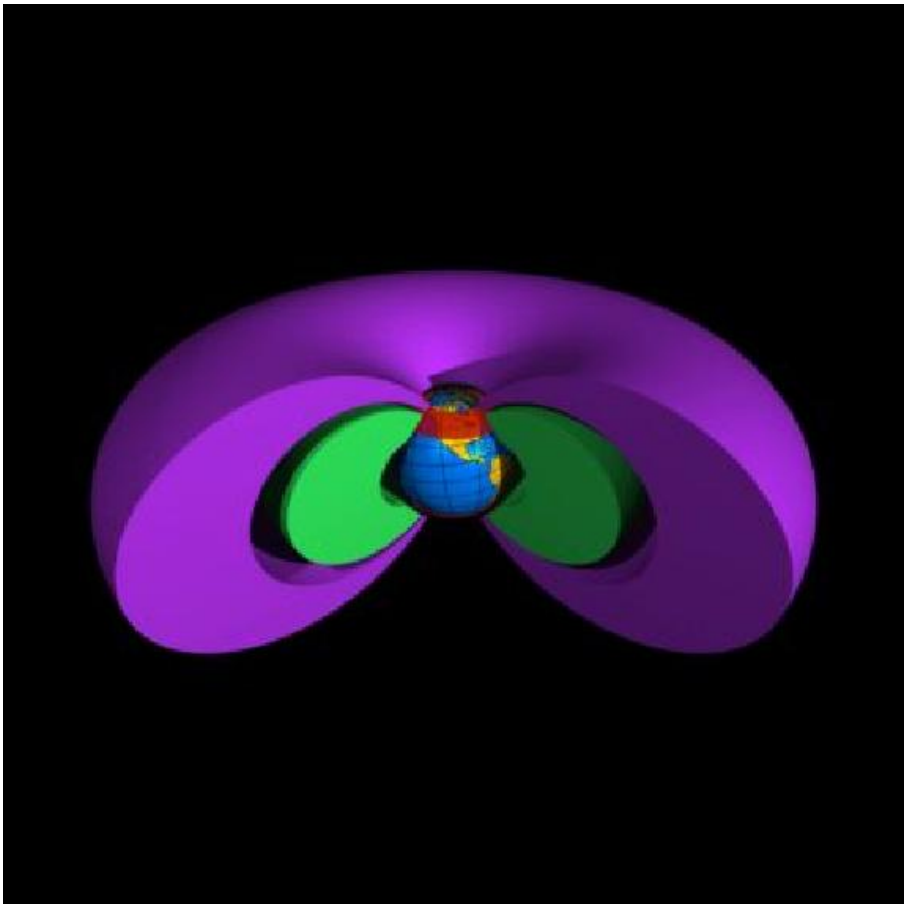

4.1 Lecture 10. Movement of particles in the magnetic field

4.1.1 Movement particles in a uniform field

Consider a problem of movement of a charged particle in a uniform magnetic field with intensity. Z -axis be directed along intensity vector H: $H = \{0,0,H\}$, q denotes the charge, m - denotes its mass. Then equation of motion takes the following form:

$$\frac{dv}{dt} = \frac{q}{mc}[v \times H]. \tag{4.1}$$

In a component form the equations to be written as the following:

$$\frac{dv_x}{dt} = \frac{q}{mc}(v_y H_z - v_z H_y) = \frac{q}{mc} v_y H, \tag{4.2}$$

$$\frac{dv_y}{dt} = -\frac{q}{mc}(v_x H_z - v_z H_x) = -\frac{q}{mc} v_x H, \tag{4.3}$$

$$\frac{dv_z}{dt} = \frac{q}{mc}(v_x H_y - v_y H_x) = 0. \qquad (4.4)$$

If a complex velocity $\hat{v} = v_x + iv_y$ is introduced the equations take the form of:

$$\frac{d\hat{v}}{dt} = i\frac{qH}{mc}\hat{v},\ \frac{dv_z}{dt} = 0.$$

Suppose a particle to have velocity $v_0 = \{v_\perp, 0, v_\parallel\}$ and the solution of these equations will be written as follows:

$$\hat{v} = v_\perp e^{i\Omega_L t},\ v_z = v_\parallel,$$

or

$$v_x(t) = v_\perp \cos\Omega_L t,\ v_y(t) = v_\perp \sin\Omega_L t,\ v_z = v_\parallel.$$

It is clear from the solution that a particle moves with a constant velocity $v_\parallel$ along z-axis and along perpendicular direction it performs a circular motion with frequency $\Omega_L = eH/mc$ called cyclotron frequency or Larmor frequency. Radius R of a circular orbit in the direction perpendicular to the field is calculated from a simple relation:

$$\frac{v_\perp^2}{R} = \frac{qH}{mc}v_\perp.$$

Hence an orbit radius of a circular movement of a particle to be calculated from the formula:

$$R = mc/v_\perp^2 qH = \frac{v_\perp}{\Omega_L}. \qquad (4.5)$$

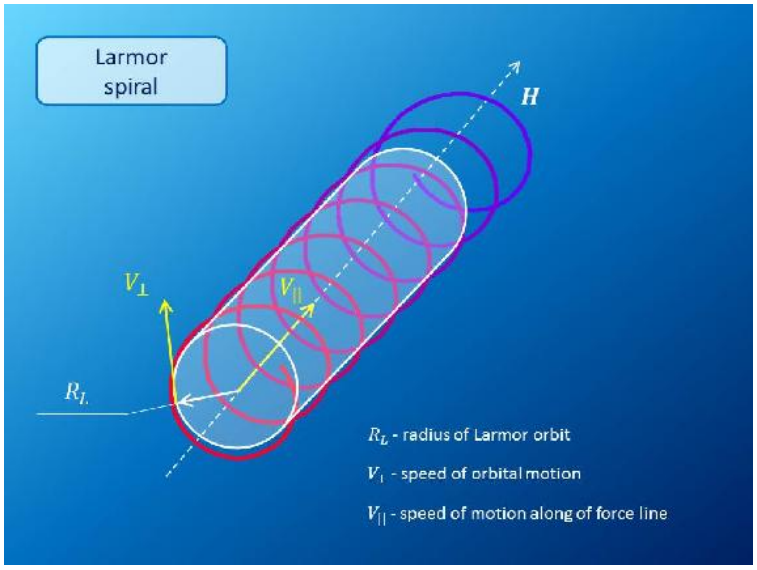

Fig. IV-10-1. Movement of a charged particle in the magnetic field

4.1.2 Drift motion of particles in a uniform magnetic field

Consider now the equation of movement of a charged particle in a magnetic field under the effect of a constant force $F = (F_x, F_y, 0)$ orthogonal to the direction of the field intensity. Instead of the equation (4.1) motion of a particle will obey the equation:

$$\frac{dv}{dt} = \frac{q}{mc}[v \times H] + \frac{1}{m}F. \qquad (4.6)$$

Equation for z-component will not change, but components x and y will take the following form:

$$\frac{dv_x}{dt} = \frac{q}{mc}v_y H + \frac{1}{m}F_x, \qquad (4.7)$$

$$\frac{dv_y}{dt} = -\frac{q}{mc}v_x H + \frac{1}{m}F_y. \qquad (4.8)$$

or in a complex form:

$$\frac{d\hat{v}}{dt} = i\frac{qH}{mc}\hat{v} + \frac{1}{m}\hat{F},$$

where $\hat{F} = F_x + iF_y$. Under the constancy of F the solution takes the following form:

$$\hat{v} = v_\perp e^{i\Omega_L t} + i\frac{c}{qH}\hat{F},\ v_z = v_\parallel,$$

Hence:

$$v_x = v_\perp \cos(\Omega_L t) - \frac{c}{qH}F_y,\quad v_y = v_\perp \sin(\Omega_L t) + \frac{c}{qH}F_x.$$

In vector form this solution can be represented in the following form:

$$v = v_\perp(t) + \frac{c}{qH^2}[F \times H].$$

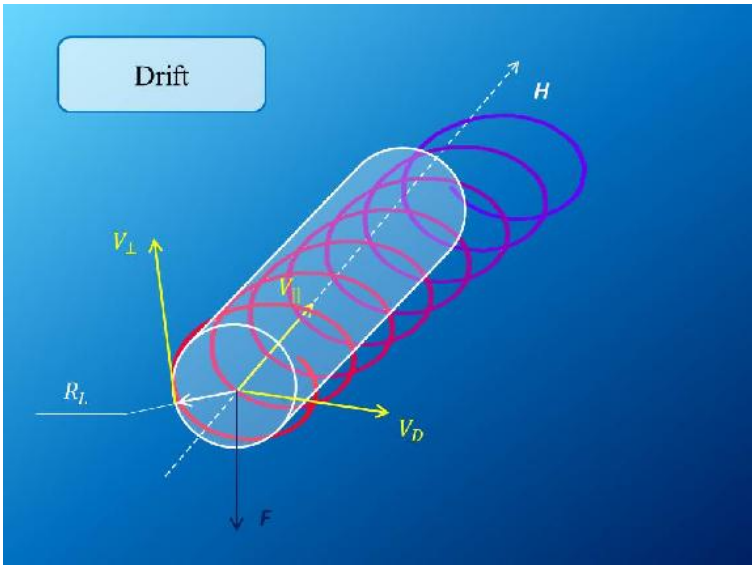

Fig. IV-10-2. Drift motion of a charged particle in a uniform magnetic field under the effect of force F

It is seen from the result that a rotary motion along the trajectory is accompanied by the motion with the constant velocity in the direction perpendicular to the field and to the additional force F acting on a particle. This motion with the speed

$$v_D = \frac{c}{qH^2}[F \times H],$$

is proportional to the force F is called drift motion and it plays a substantial role in plasma

dynamics.

4.1.3 Adiabatic invariants

It is adiabatic invariants that we have to deal with in the further description of the theoretical basis of charged particles motion in the magnetic field of the Earth. Invariant is a quantity remaining constant under any changes including displacement in time. Invariants of motion are mostly called integrals of motion. The word 'adiabatic invariant' means that the quantity remains constant under special conditions. Describe these conditions. As far as physical situations in which the theory of adiabatic invariant might be used in can considerably differ from each other it is useful to describe this theory in general solution.

It is the finiteness of motion that is the general condition which lies in the basis of the theory of adiabatic invariants. In finite motion there are one or several periods of time after which the system returns into the initial state (or a state close to the initial). It means that functions describing such systems are periodical (or quasi-periodical). Let T denote the period of such motion. Then the condition of slowness of change of λ parameter means that within the period T the system has time to go out of some state and to return back and parameter λ changes insignificantly, i.e.:

$$\left|\frac{d\lambda}{dt}\frac{T}{\lambda}\right| << 1.$$

Hence in the most general form we suppose that one of system's parameters slowly changes along the trajectory of motion while the system is moving. Let's denote this parameter as λ.

We are to study systems for which the energy conservation law is satisfied under the condition of the invariance of its parameters. Let the total energy be represented as a Hamiltonian function $H = H(p,q;\lambda)$. Here p represents the generalized momentum of a system, and q is the generalized coordinate. Equations of motion in Hamiltonian form can be written as:

$$\frac{dp}{dt} = -\frac{\partial H}{\partial q}, \quad \frac{dq}{dt} = \frac{\partial H}{\partial p}. \tag{4.9}$$

If

$$\dot{\lambda} = 0,$$

then

$$\frac{dH}{dt} = \frac{dp}{dt}\frac{\partial H}{\partial p} + \frac{dq}{dt}\frac{\partial H}{\partial q} = -\frac{\partial H}{\partial q}\frac{\partial H}{\partial p} + \frac{\partial H}{\partial p}\frac{\partial H}{\partial q} = 0.$$

That means the energy conservation law: $H(p,q,\lambda) = E(\lambda) = const$. Otherwise we have:

$$\frac{dH}{dt} = \frac{dp}{dt}\frac{\partial H}{\partial p} + \frac{dq}{dt}\frac{\partial H}{\partial q} + \frac{d\lambda}{dt}\frac{\partial H}{\partial \lambda} = \frac{d\lambda}{dt}\frac{\partial H}{\partial \lambda} \neq 0 \tag{4.10}$$

The energy is not conserved now. Let's average the latter relation on a period of finite motion of a system using the usual time averaging:

$$\overline{f} = \frac{1}{T}\int_0^T f(t)dt.$$

Then we obtain:

$$\overline{\frac{dH}{dt}} = \overline{\frac{dE(\lambda)}{dt}} = \frac{d\lambda}{dt}\overline{\frac{\partial H}{\partial \lambda}}.$$

As far as we consider parameter λ to change slowly it has no time to change within the time of averaging we take its derivative out of the sign of averaging. Using equations (4.9) we can substitute

time averaging by the path integral:

$$dt = \frac{dq}{\partial H/\partial p}.$$

therefore we can write:

$$T = \int_0^T dt = \oint \frac{dq}{\partial H/\partial p},$$

And also:

$$\overline{\frac{dE(\lambda)}{dt}} = \frac{d\lambda}{dt}\frac{1}{T}\oint \frac{\partial H}{\partial \lambda}\frac{dq}{\partial H/\partial p} = \frac{d\lambda}{dt}\frac{\oint \frac{\partial H}{\partial \lambda}\frac{dq}{\partial H/\partial p}}{\oint \frac{dq}{\partial H/\partial p}}. \qquad (4.11)$$

Here integral $\oint$ denotes the path integral of a system from some initial state to the restoration into that initial state. Averaging in the latter expression is to be done along the trajectory of a system under the condition $\lambda = const$. In his case $E = const$ in relation $H(p,q,\lambda) = E$. It is possible to express the momentum from this relation. It will be a function of q and parameter λ: $p = p(q;\lambda)$. So differentiating the relation $H(p,q,\lambda) = E = const$ with respect to λ we obtain:

$$\frac{\partial H}{\partial \lambda} + \frac{\partial p}{\partial \lambda}\frac{\partial H}{\partial p} = 0.$$

It allows us to transform the relation (4.11) :

$$\overline{\frac{dE(\lambda)}{dt}} = -\frac{d\lambda}{dt}\frac{\oint \frac{\partial p}{\partial \lambda}dq}{\oint \frac{\partial p}{\partial E}dq}.$$

Taking into account that $\dot{\lambda}$ and averaged quantities do not depend on time the latter relation can be written in the following form:

$$\oint\left(\frac{\partial p}{\partial E}\overline{\frac{dE(\lambda)}{dt}} + \frac{d\lambda}{dt}\frac{\partial p}{\partial \lambda}\right)dq = 0. \qquad (4.12)$$

Integrand of the latter relation represents the total time derivative of momentum p as a function along the trajectory without disturbances (i.e. $\lambda = const$). Therefore (4.12) takes finally the following form:

$$\oint \frac{dp}{dt}dq = \frac{d}{dt}\oint p dq = 0.$$

The latter means that the quantity

$$I = \oint p dq, \qquad (4.13)$$

is the integral of motion with slow changes of parameter λ and this quantity is to be called the adiabatic invariant.

Example. A harmonic oscillator is a simple example of usage of the adiabatic invariants theory. Consider a mathematical pendulum with length l in the terrestrial gravitational field. The frequency of small-amplitude oscillation of such a pendulum is calculated by the formula :

$$\omega_0 = \sqrt{\frac{g}{l}}.$$

The energy conservation law has a form of:

$$H = \frac{p^2}{2m} + \frac{m\omega_0^2 x^2}{2} = E = const. \qquad (4.14)$$

From this conservation law we obtain the expression for momentum:

$$p = \sqrt{2mE - m^2\omega_0^2 x^2}.$$

Let's consider the problem of calculation of oscillations characteristics change on the average under the condition that the length of pendulum rod changes slowly. Let's calculate and adiabatic invariant of such motion. According to (4.13) we have:

$$I = \oint \sqrt{2mE - m^2\omega_0^2 x^2}\, dx = m\omega_0 \oint \sqrt{A^2 - x^2}\, dx =$$

$$= -m\omega_0 A^2 \int_0^{2\pi} \sqrt{1 - \sin^2\varphi}\cos\varphi d\varphi = -m\omega_0 A^2 \int_0^{2\pi} \cos^2\varphi d\varphi = \pi m\omega_0 A^2.$$

Here $A = \sqrt{2E/(m\omega_0^2)}$ is a vibration amplitude and substitution $x = A\sin\varphi$ is used. Hence we finally find:

$$I = \pi m\omega_0 A^2 = \pi m\sqrt{\frac{g}{l(t)}}A^2(t) = const.$$

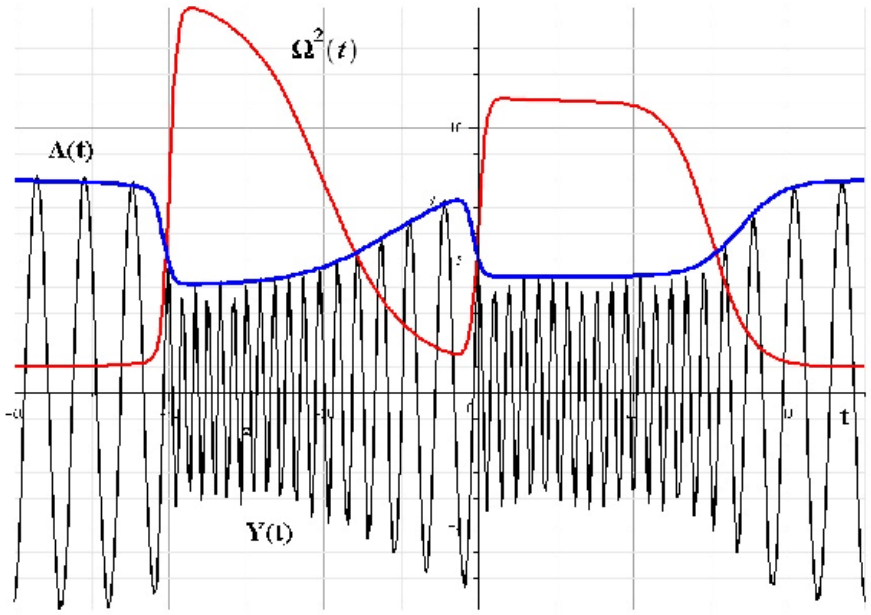

Fig. IV-10-3. Pendulum motion with the changing of its frequency.

Therefore vibration amplitude with slow change of length of pendulum rod will change according to the law:

$$A(t) = \sqrt{\frac{I}{\pi m}}\left(\frac{l(t)}{g}\right)^{1/4} = A(0)\left(\frac{l(t)}{l(0)}\right)^{1/4}.$$

A typical form of oscillation change on change of a harmonic oscillator frequency change is given in fig. IV-10-3.

4.2 Lecture 11. Motion of charged particles in the terrestrial magnetic field

4.2.1 Motion of particles in a non-uniform magnetic field. The first adiabatic invariant

As far as the terrestrial magnetic field is non-uniform the motion of particles appears to be more complicated. Reflection of a particle from an area with higher field intensity and different drift motion of a particle in the direction perpendicular to the field are the most important effects of a charged particle motion in a non-uniform field.

Suppose any external forces acting on the particle, except Lorentz force, are missing on the assumption of nonuniformity of the magnetic field intensity. Notice that the kinetic energy of the particle conserves in arbitrary magnetic field due to the fact that the Lorentz force does not work when the particle moves:

$$E_0 = E_\perp + E_\parallel = \frac{m}{2}(v_\perp^2 + v_\parallel^2) = const.$$

But now the orbital motion velocity $v_\perp$ of the particle and velocity along the direction of the magnetic field $v_\parallel$ will change slowly in the course of time. But the total energy of the particle conserves, i.e. it is invariant independent on the structure of the magnetic field.

Suppose the magnetic field to vary slowly in space and therefore so-called adiabatic invariants could be introduced in the theory. Here adiabatic invariants represent quantities slow varying with the magnetic field. If the field slowly varies it is possible to expect a particle motion to remind a motion in a uniform field, but with slowly varying characteristics. Among these characteristics there could be the ones which could be constant while there is a slow variation of the others. These constant characteristics are called adiabatic invariants. It is necessary to state exactly the slowness of the change of the field H when a particle moves in it in order to establish these adiabatic invariants. Indeed, when the field slowly varies the particle moves along the line of force with the speed $v_\parallel$ and along the circle of the radius R with the velocity $v_\perp$. from the particle's point of view the change of the magnetic field is related to how fast the field varies when the particle moves from one point in the space to the other within the characteristic period of time. It is clear that if the particle moves along the line of force very fast the field will also vary fast. The characteristic period of time for a particle in the magnetic field is the period $T = 2\pi/\Omega_L$ of its revolution on the orbit perpendicular to the line of force. In this case the slowness of change means that the field practically has not changed during the period of revolution, i.e :

$$\Delta H_T = T\frac{dH}{dt} << H. \qquad (4.15)$$

Suppose this condition to be satisfied. Exceprt it we should suppose that the field variation is also small in the direction perpendicular to the line of force.

With the slow change of the system parameters some physical quantities remain constant. These values are called adiabatic invariants. From the general theory of adiabatic invariants (e.g. see [62][45]) it follows that adiabatic invariant I is associated with the energy E of a finite motion of the particle in such a way that:

[45] L.D.Landau, E.M.Lifshitc. Mechanics. M.:Nauka, 1973

$$\frac{\partial E}{\partial I} = \omega,$$

where ω is the natural frequency of a finite motion which cannot be an adiabatic invariant and slowly changes in course of time. Thereby quantities I and ω are dynamically independent and it is possible to write:

$$E = \omega I. \tag{4.16}$$

This equation can be used to calculate adiabatic invariants.

If the particle moves in the weakly nonuniform magnetic field a part of the kinetic energy of orbital motion is the energy of the finite motion:

$$E_\perp = \frac{m}{2} v_\perp^2 = \frac{m}{2}\left(\frac{eH}{mc}\right)^2 R^2 = \frac{m}{2}\Omega_L^2 R^2. \tag{4.17}$$

Larmor frequency Ω_L is the natural frequency of the orbital motion. It follows from (4.17) that adiabatic invariant of the particle motion in the weakly non-uniform magnetic field is represented by the quantity:

$$I = \frac{E_\perp}{\Omega_L} = \frac{m v_\perp^2}{2\Omega_L} = \frac{m}{2}\Omega_L R^2.$$

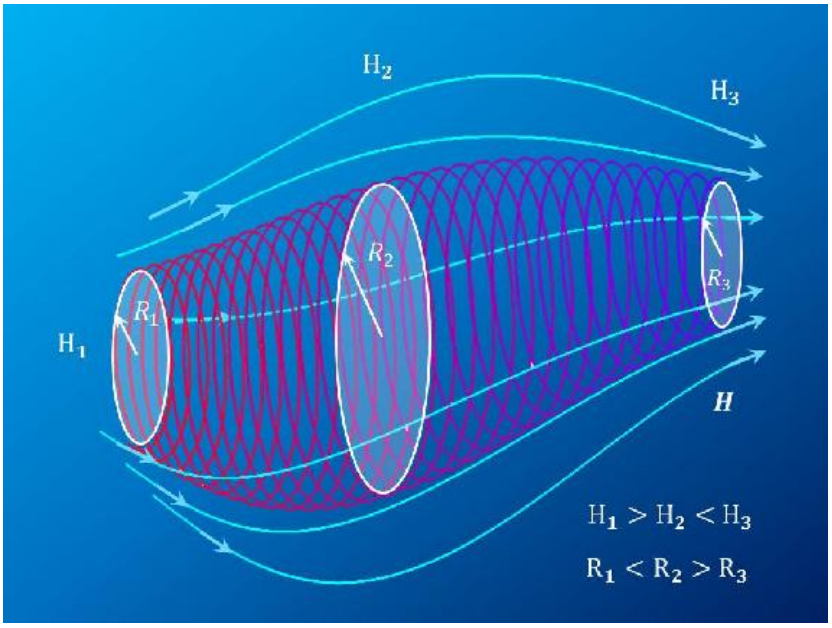

Fig. IV-11-1. A motion of the particle in a non-uniform magnetic field.

In other words the square of the speed and the kinetic energy of the orbital motion change proportionally to the frequency which linearly depends on the magnitude of the magnetic field:

$$E_\perp = I\frac{eH}{mc} = \mu H, \tag{4.18}$$

And it slowly changes with the field. A new adiabatic invariant μ is introduced instead of the invariant I in this equation. The new invariant coincides with the field in dimension:

$$\mu = \frac{e}{mc} I.$$

the square of the orbit radius changes in inverse proportion to the magnetic field (see fig. IV-11-1):

$$R^2 = \frac{2I}{m}\frac{1}{\Omega_L} = \frac{2Ic}{e}\frac{1}{H} = \frac{2\mu c^2 m}{e^2}\frac{1}{H}.$$

4.2.2 The energy conservation law in a nonuniform magnetic field. Magnetic traps and mirrors

Basing on the obtained relations it is possible to come to a very important conclusion. Suppose the total energy E_0 characterizes the motion of the particle in the magnetic field. Then we obtain:

$$E_{\|} + E_{\perp} = E_{\|} + \mu H = E_0.$$

This relation is equal to the mechanical energy conservation law in the potential field with a potential energy $U_{eff} = \mu H$. The energy U_{eff} is exactly equal to the energy of the particle with the magnetic moment μ in the magnetic field. Hence:

$$\frac{m}{2}v_{\|}^2 = E_0 - U = E_0 - \mu H > 0. \qquad (4.19)$$

therefore if the potential energy U_{eff} has a local minimum in the neighborhood of the point r_0 the particle in this case will oscillate between two walls of the potential well. With that the turning points (points where the velocity along the line of force turns into 0) should be found from the condition $\mu H(r) = E_0$. The systems where the capture of particles is realized with the help of the described principle are called adiabatic or magnetic traps.

It is useful to consider the example of such a system (fig. II-11-2) for the investigation of the probability of capture of particles in the magnetic trap.

Suppose the system to consist of two areas where the constant magnetic fields with magnitudes $H_1 < H_2$ are generated and these fields are directed along z-axis coinciding with the direction of the growth of the field.

Between these areas there is an area where the field increases slowly from H_1 to H_2. Let the particle be in the area with a smaller magnitude of the field H_1 and suppose the particle to move with the velocity $v_{\|}$ in the direction of the field with the greater magnitude H_2. With that the velocity of orbital motion is equal to $v_{\perp} = \sqrt{\Omega_1 R}$, Ω_1 - cyclotron frequency in area 1. In the area with field H_2 the velocities of the particles will be respectively $v'_{\|}$ and $v'_{\perp} = \sqrt{\Omega_2 R}$. The particle penetrates into area 2 if $v'_{\|} > 0$ in this area. From the relation:

$$v_{\|}^2 + \mu H_1 = v_{\|}'^2 + \mu H_2$$

it follows that only that particles will penetrate into the area with the field H_2 which have the velocity $v_{\|}$ along the field satisfying the inequality:

$$v_{\|}^2 > \mu(H_2 - H_1).$$

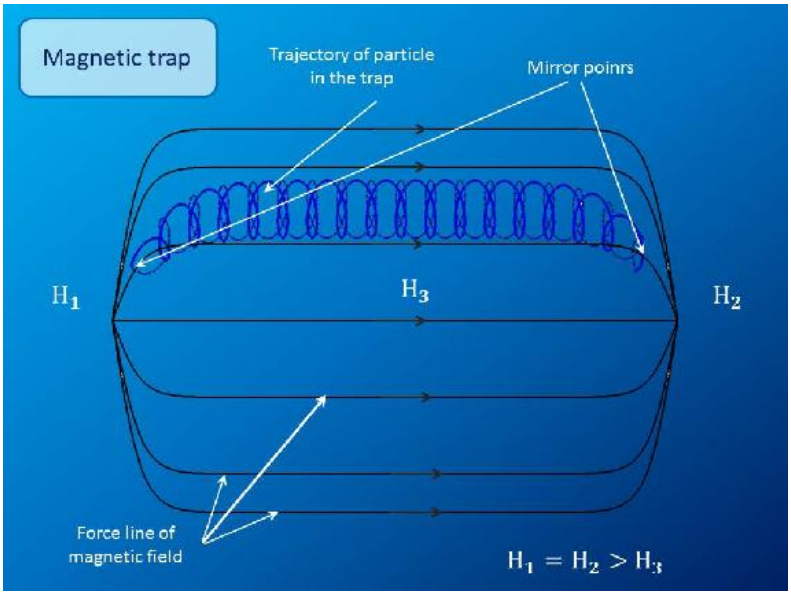

Fig. IV-11-2. A magnetic trap

This inequality can be written in a form of relation for the ratio of the orbital motion velocity and the velocity of the motion along the field:

$$v_{\|} > v_{\perp}\sqrt{1-H_2/H_1}. \qquad (4.20)$$

Particles for which the velocity $v_{\|}$ is less than the critical one:

$$v_{\|cr} = \sqrt{\frac{2\mu}{m}(H_2 - H_1)},$$

will be reflected from the area with higher intensity. Notice that only that particles are trapped which have a velocity component along the field less than some defined value (inequality (4.20))). But it is the slowness of the field variation during the motion of a particle that is related to a similar relation. So the escape of the particle from the trap is associated with the breakdown of motion adiabaticity.

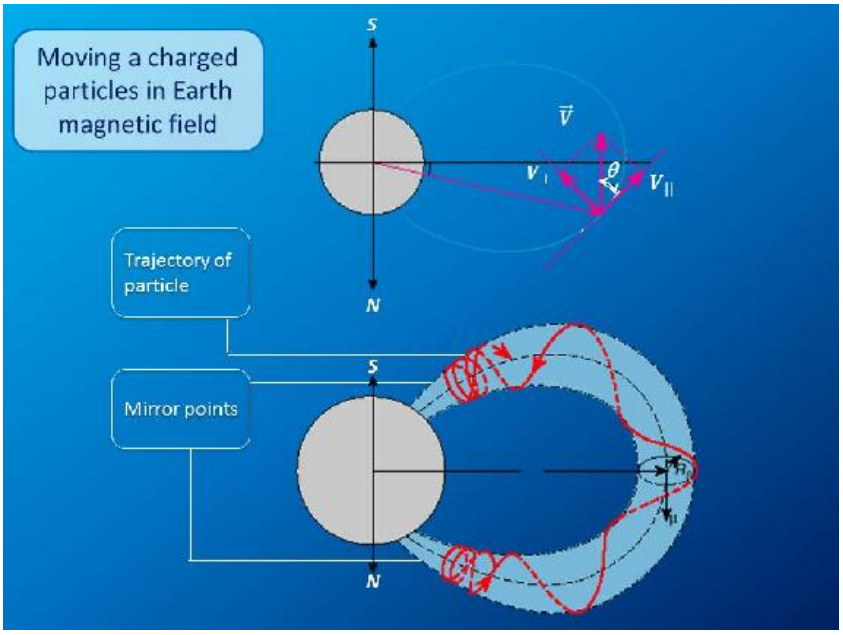

Fig. IV-11-3. Trajectories of particles in the terrestrial magnetic field

4.2.3 Zonal drift motion in the terrestrial magnetic field. The second adiabatic invariant

As far as the motion of charged particles along the magnetic field line represents a periodic process with quite a big frequency (characteristic period $T \simeq$) one more adiabatic invariant appear for such motion. In this case the kinetic energy of motion along the magnetic line of force is the energy of the finite motion, i.e. $E_{\parallel} = mv_{\parallel}^2/2$. slowly changing parameter of this motion is a slow magnetic field variation along the equator called zonal direction. Charged particles drift in this direction. To calculate adiabatic invariant explicitly in this case we make use of the general theory described in previous lectures.

Write the energy of the finite motion in the following form:

$$E_{\parallel} = \frac{m}{2} v_{\parallel}^2 = E_0 - \mu H.$$

Momentum respectively equals to:

$$p_{\parallel} = \sqrt{2m(E_0 - \mu H)}.$$

4.2.4 Distribution of particles in the trap

For the analysis of the situation of plasma confinement in the magnetic trap, especially concerning the description of the Earth radiation belts a question of the description of the distribution of particles in the trap is very important. The problem can be set like that: are the particles distributed uniformly or nonuniformly throughout the trap volume and in case of a nonuniform distribution in what part of the trap will the increased concentration of particles be observed.

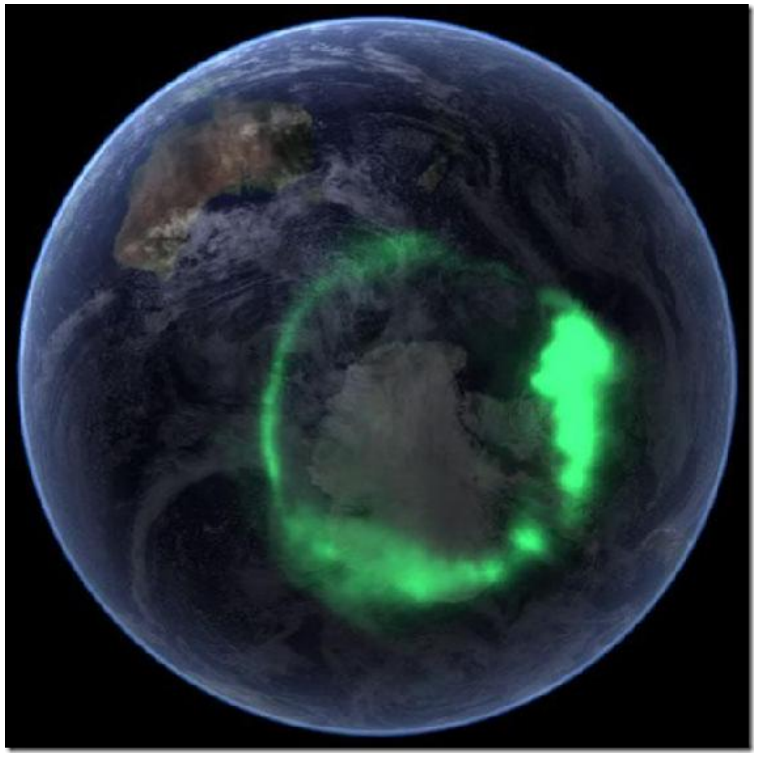

Fig. IV-11-4. The ring of auroras over the North Pole of the Earth.

To answer the question it is necessary to state it specifically. Particles captured by the trap move periodically from one turning point to the other. Therefore state the question like that: if glance (take photos, scan) at the inside area of the trap in a random manner, then where is each of the particles observed as often as not? A question stated like that has a simple answer. Suppose s to be a parameter along the line of force the particle moves along. Also suppose T to represent the period of motion from one turning point s_1 to the other s_2. According to (4.19) the period can be calculated in the following way:

$$T(E_0) = \int_{s_1}^{s_2} \frac{\sqrt{m}ds}{\sqrt{2E_0 - 2\mu H(s)}}.$$

Here s denotes the coordinate along the magnetic line of force determined as the integral curve of the equation:

$$\frac{dr}{ds} = H(r).$$

Then the probability of observation of the particle at a random point of the trap is proportional to the ratio of the observation time to the half-period of motion the particle inside the trap, i.e. if the observation time is dt the detection probability within this time equals to;

$$dp = \frac{2dt}{T}.$$

In order to calculate the probability density of the probability to detect the particle exactly at this point it is necessary to change from the particle observation time to the corresponding space interval where the particle may appear within the observation time. For this change of variable is needed:

$$dt = \frac{dt}{ds}ds = \frac{ds}{v_{\|}}.$$

As a result we obtain:

$$d(s) = \frac{\sqrt{2m}ds}{T\sqrt{E_0 - \mu H(s)}}.$$

Hence the detection probability for the particle equals to:

$$\rho(s) = \frac{\sqrt{2m}}{T\sqrt{E_0 - \mu H(s)}}. \qquad (4.21)$$

Fig. IV-11-5. Aurora Polaris over Norway.

It is clear that this probability density increases up to infinity near the turning points. Hence it follows that the particle should be observed as often as not near the turning points or in this case "magnetic traffic jams" of the trap. Equation (4.21) yields a partial answer to the stated question. It describes the distribution of particles along the particle's trajectory. It is necessary to have an idea of the number of particles along the given trajectory to describe the spatial distribution of particles. One should take into account the fact that there could be both the particles with the same total energy and the particles with different magnitudes of E_0. Suppose each line of force is numbered by two spatial parameters ξ and η and suppose the number of particles with the total energy within the interval dE_0 on the trajectory (ξ,η) to be equal to $n(\xi,\eta,E_0)dE_0$. Then the spatial density of particles at the point characterized by three parameters (s,ξ,η) takes the form:

$$\rho(s,\xi,\eta,E_0)=\frac{n(\xi,\eta,E_0)dE_0\sqrt{2m}}{T(E_0)\sqrt{E_0-\mu H(s)}}. \qquad (4.22)$$

4.2.5 Polar ovals and auroras Polaris

Particles coming from the Sun are captured by the magnetosphere of the Earth in its tail and are transported to the Poles. During the process of movement from the tail of the magnetosphere to the Poles particles accelerate and fall out in a form of aurora Polaris in the terrestrial atmosphere. It is the SSR but not the radiation belts particles that make the effect of aurora Polaris. The density of particles in radiation belts is too small to generate bright flashes in the polar areas.

The glow of aurora Polaris is caused by the collisions of charged particles with atoms of the atmosphere - mostly nitrogen and oxygen. Each atom gives its own chord. That is why aurora Polaris looks so colorful. The example of such glow is represented in fig. IV-11-5.

Chaper 5. Cosmic rays

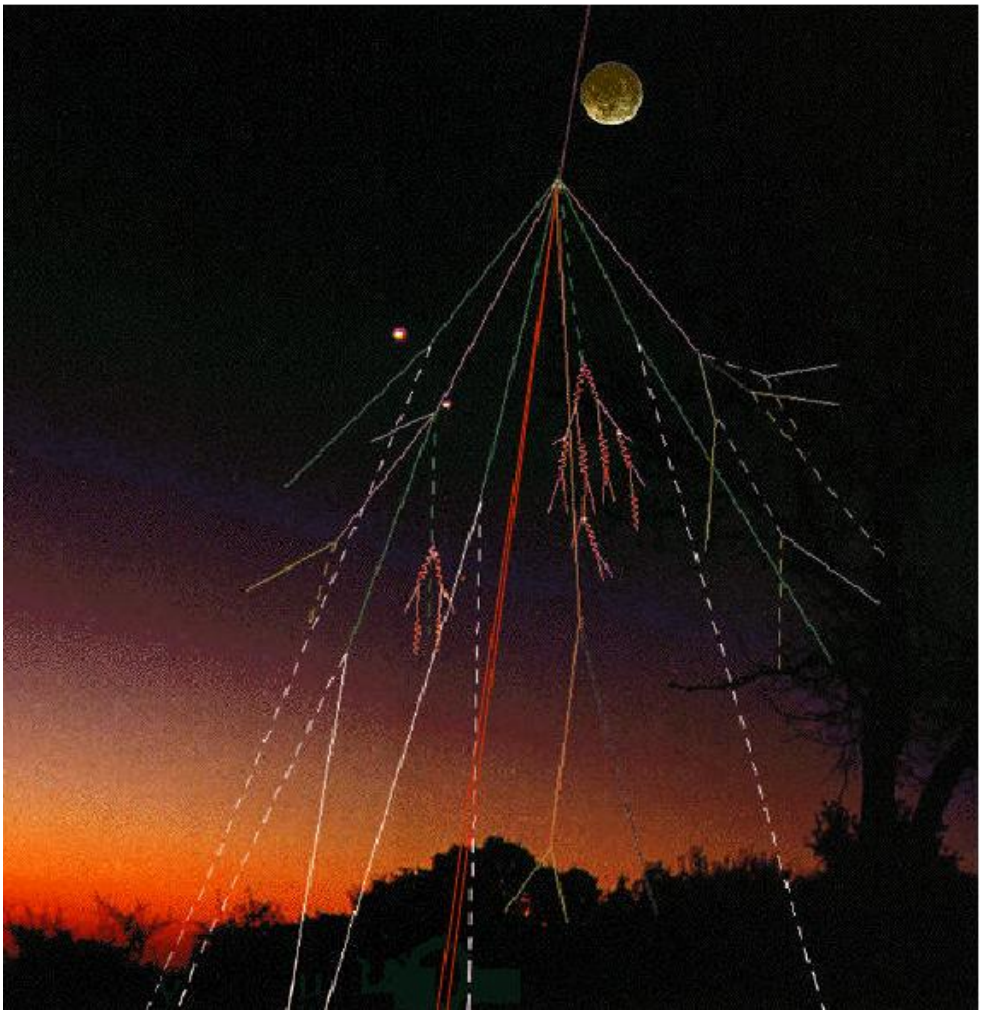

5.1 Lecture 12. Cosmic rays and the ways of observation

The end of the XIX - the beginning of the XX century is marked by new discoveries in microcosm area. After the discovery of x-rays and radioactivity charged particles coming from the space were detected. These particles were called ***cosmic rays*** (CR). The year of 1912 is considered to be the date of the discovery of cosmic rays. In that year an Austrian physicist V.F. Hess measured ionization rate in dependence on the height with the help of improved electroscope. For this purpose he used a balloon with the help of which he climbed to the height of more than 5 km. It occurred that the ionization first decreases with the growth of height but then it irrupts at a height of 3000-4000 m. It was the first proof that the ionizing radiation being weakly absorbed by the air and increasing with the height is generated by the CR falling on the atmosphere boundary from the space. The more exact results were obtained by Hess' opponent - W.Colchester who did not believe in cosmic origin of the cosmic rays. But having performed five flights on the balloon in 1912-1914 at the altitude up to 9300

m he confirmed and improved Hess' result.

CR represent nucleuses of different elements and therefore are the charged particles. Hydrogen and helium nucleuses are the most numerous in cosmic rays (85% and 15% respectively). The part of other elements of the periodic table does not exceed 5%. Electrons and positrons are a small part in cosmic rays (less than 1%).

Cosmic rays play an important role in processes going on in the Universe. Density of cosmic rays energy is 1 eV/cm^3 in our Galaxy. It is comparable to the energy density of interstellar gas and galactic magnetic field. It is possible to estimate the amount of matter X the cosmic rays passed through if we analyze the content of lithium, beryllium and bore elements in the cosmic rays which are generated as a result of nuclear interaction of the particles with atoms of interstellar medium. The quantity X is approximately equal to 5-10 g/cm^2. The time of roaming of cosmic rays (or their lifetime) in the space and the quantity X are connected by the relation $X \sim \rho c t$ where c denotes the speed of particles (it is usually supposed to be equal to the speed of light), ρ is an average density of the interstellar medium equal to 10-24 g/cm^3, t denotes the time of roaming of cosmic rays in this medium. Hence the cosmic rays lifetime is $3 \cdot 10^8$ years. It is determined by either the leaving the Galaxy and the halo or by their absorption due to inelastic interaction with the interstellar medium.

The major source of CR inside the Galaxy is supernova explosions. CR accelerate on shock-waves generated by these explosions. The maximum energy particles can get in such processes is $E_{max} \sim 10^{16}$ eV. In addition, a part of CR can accelerate to the same energy on shock-waves propagating in the interstellar space of the Galaxy. CR of even greater energy form in the Matagalaxy. One of their source could be cores of active galaxies. In Fig. V-12-1 there are energy spectra $J(E)$ for protons Í, helium nucleuses Íå, carbon C and iron Fe which are observed in the space. The quantity $J(E)$) represents the number of particles with the energy in the range from E to $E + \Delta E$ passing within unit time through the unit area in the unit of solid angle in the direction perpendicular to the surface. It is clear that the major part of CR is represented by protons and then helium nucleuses go. The part of the other elements is small.

By its origin CR could be divided in several groups.

1) ***CR of galactic origin (GCR)***. 1). The source of GCR is our Galaxy where the acceleration of particles to the energy $\sim 10^{18}$ eV. The spectra shown in fig. V-12-1 refer to GCR.

2) ***CR of matagalactic origin***, they have the greatest energy $E > 10^{18}$ eV and they are generated in other galaxies.

3) ***Solar CR (SCR)***, generated on the Sun during the Sun flares.

4) ***Anomalous CR (ACR)***, generated in the solar system on the periphery of heliomagnetosphere.

Cosmic rays of the smallest and the greatest energy differ in 10^{15} times. The only type of tools cannot help with the exploration of such great range of energy therefore different methods and tools are used to explore CR: devices mounted on satellites and spacecraft are used in the space, small balloons and high-altitude balloons are used in the atmosphere, on the ground there are ground based installations (some of them reach hundreds of square kilometers in size) placed either high in the mountains or deep underground or deep in the ocean where high energy particles penetrate. With their propagation in the interstellar space CR interact with interstellar gas and with atmospheric atoms when rays come to the Earth. Secondary particles are the result of these interactions: protons and neutrons, mesons, electrons, gamma-quanta, neutrino. The major types of detectors used for the CR exploration are photoemulsions and x-ray films, ionization chambers, gas-discharge counters, neutron counters, Cherenkov counters and scintillation counter, solid-state semiconductor detector, spark and drift chambers.

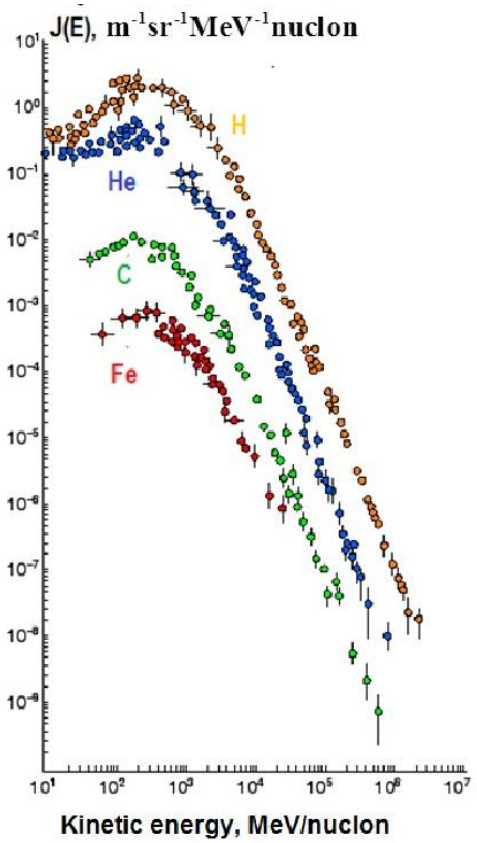

Fig. V-12-1. Differential spectra of galactic CR:
protons H, helium nucleuses He, Carbon C, iron Fe. [46]

5.1.1 Galactic cosmic rays

Cosmic rays coming from the far Space, galactic and matagalactic rays have a very great energy. It allows one to use them for exploration of nuclear reaction which cannot be reproduced in modern accelerators in laboratories. Ionization calorimeters are used to explore the interaction of high energy CR ($E \simeq 10^{15}$ eV) with the matter. These devices introduced by N.L.Grigoryev and collaborators consists of several rows of detectors - ionization chambers and scintillation counters with absorbent of iron or lead placed between them. In the upper part of the calorimeter there is a target made of a light matter - carbon or aluminium. A particle falling on the surface of the ionization calorimeter interacts with the nucleus of the target generating secondary particles. At first their number increases reaching some maximum magnitude and then gradually decreases with the further penetration into the body of the calorimeter. Detectors measure ionization under each layer of the absorbent. According to the curve of dependence of the ionization degree on the number of the layer it is possible to determine the energy of the particle got into the calorimeter. With the help of these instruments the primary CR spectrum in the range of energy from $\sim 10^{11}$ to $\sim 10^{14}$ eV was measured for the first time. CR in the range of energy $10^{11} < E < 3 \cdot 10^{15}$ eV have the galactic origin. Their energy spectrum can be described by the power law:

$$J(E) = J0 \cdot E^{-2,75}.$$

[46] http://www.astronet.ru/db/msg/1210273

To explore characteristics of nuclear interactions of very high energy CR one needs instruments with a great registration area since the flow of high-energy particles is too small. These instruments are called x-ray chambers. They have the area up to several hundreds of square meters and consist of layers of x-ray films interleaved with lead layers. As the result of interaction of CR with particles of the air mesons are generated. Then some of them breed in the lead putting spots on the x-ray film. The energy and the arrival direction of the interacting particle are detected on the analysis of quantity and size of spots, density of their darkening, their position in different layers.

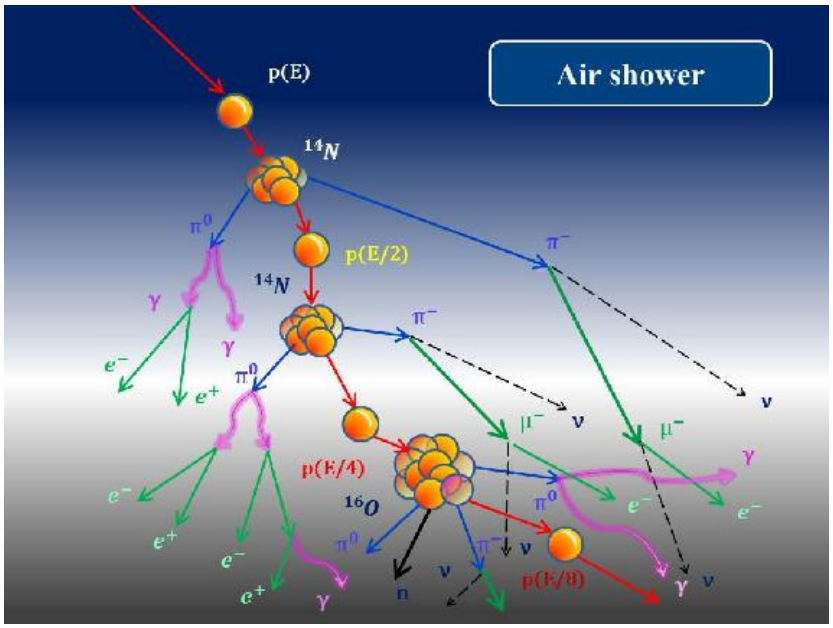

Fig. V-12-2. Formation of extensive air shower (EAS)

The characteristic of high-energy particles is their ability to produce a great amount of secondary particles, mostly protons and pions, as the result of interactions of a primary particle with nucleuses of atmospheric atoms. This feature is used for exploration of CR with the energy more 10^{14} eV. Having quite high energy protons and pions in their turn are radioactive particles and interact with nucleuses of the atmospheric atoms. Both charged ($\pi^{\pm}$) and neutral (π^0) pions are unstable particles with lifetime $t \sim 10^{-16}$ s for a neutral motionless π^0 and $t \sim 2.6 \cdot 10^{-8}$ s for a motionless $\pi^{\pm}$. Pions with relatively low energy have no time to interact with a nucleus of an atmospheric atom and may decay into γ-quanta and positive and negative muons ($\mu^{\pm}$), neutrino (ν) and antineutrino ($\tilde{\nu}$): $\pi^0 \to \gamma + \gamma$, $\pi^{\pm} \to \mu^{\pm} + \nu + \tilde{\nu}$. Muons are also unstable particles and with the lifetime of motionless muon $t \sim 2.2 \cdot 10^{-6}$ s and decay according to the scheme $\mu^{\pm} = e^{\pm} + \nu + \tilde{\nu}$. The scheme of shower formation is represented in fig. V-12-2.

Gamma-quanta and electrons (positrons) due to electromagnetic interaction with atmospheric atoms yield new gamma-quanta and electrons. Therefore cascade of particles forms in the atmosphere, it consists of protons, neutrons and pions (nuclear cascade), electrons (positrons) and γ-quanta (electromagnetic cascade see. Fig. V-12-3).

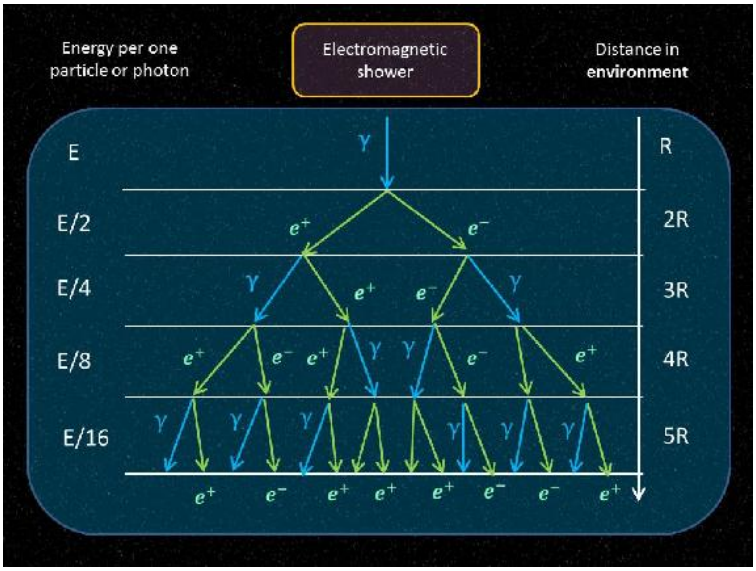

Fig. V-12-3. A simplified scheme of formation of electromagnetic avalanche in the medium. (electromagnetic cascade).

D.V.Skobelitsyn was the first one to observe showers at the end of 20s. Cascades in the atmosphere caused by high-energy particles and occupying vast areas got the name of extensive air showers. They were discovered by a French physicist P.Auge and his collaborators in 1938. A high-energy cosmic particle causes a shower with a great amount of secondary particles, for example, as a result of interactions with the atmospheric atoms near the surface of the Earth a particle with $E = 10^{16}$ generates 10 million secondary particles distributed across a vast area. Although the flux of high-energy CR falling on the terrestrial atmosphere boundary is extremely low extensive air showers occupy vast areas and could be registered with a high performance. For this purpose particle detectors are placed across the area of tens of square kilometers and only those events are registered when several detectors respond at once. An extensive air shower can be represented in a simplified form as a disk of particles moving in the atmosphere. In fig. V-12-2 it is shown how such disk of particles of an extensive air shower falls on the recording system detectors.

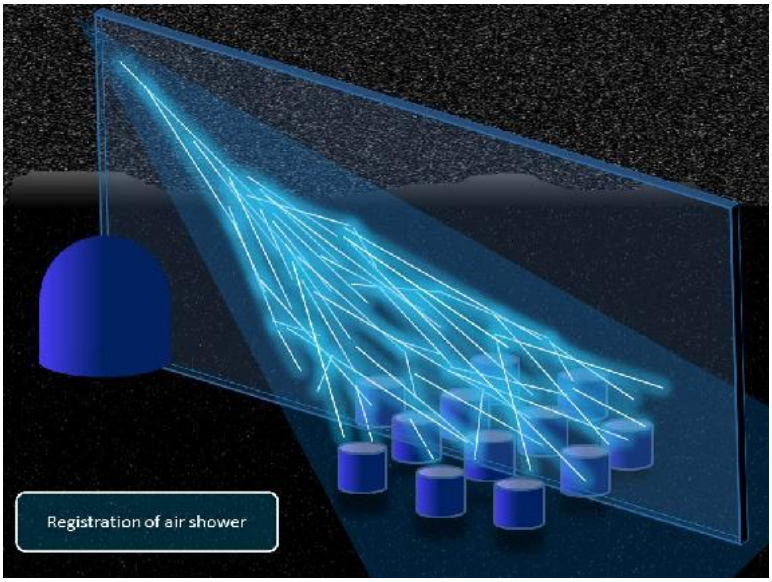

Fig. V-12-4. Registration of an extensive air shower (EAS)

Depending on the energy of the cosmic particle the disk size (diametrical size of a shower) can be from several tens of meters to a kilometer and its thickness (longitudinal size or front of a shower) can reach tens of centimeters. Particles in the shower move with the speed close to the speed of light. Quantity of particles considerably decreases with the distance from the center of the disk to its periphery. Diametrical size of an extensive air shower and the number of particles increases with the growth of the primary particle energy causing this shower. The biggest observed at the present time showers caused by particles with $E \simeq 10^{20}$ eV contain several billions of secondary particles. Measuring special distribution of particles in a shower with the help of many detectors it is possible to evaluate their total number and to evaluate the energy of the particle caused this shower. The flux of particles with energy $E \simeq 10^{20}$ eV is very low. For example the only particle with $E \sim 10^{19}$ drops on the surface of 1 m^2 in 1 million years. For the registration of such small flux it is necessary to have great areas covered with detectors to register enough events in reasonable time.

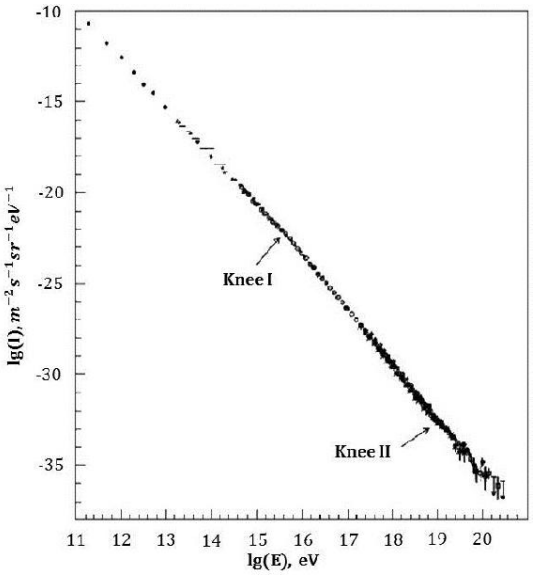

Fig. V-12-5. Galactic CR spectrum. [47]

Several particles with the energy more than 10^{20} eV (the maximum particle energy registered by the present time is $\sim 3 \cdot 10^{20}$ eV) were caught on huge installations registering extensive air showers. Do CR of even higher energies exist? In 1966 G.T.Zatsepin, V.A.Kuzmin and an American physicist K.Grazen supposed that the CR spectrum must be cut off due to high-energy particles interaction with the relict radiation of the Universe when the energy is $E > 3 \cdot 10^{19}$ eV. The registration of several events with the energy $E \cdot 10^{20}$ eV can be explained if suppose the source of particles be remoted at the distance not exceeding 50 Mpc (millions of parsecs). In this case there practically is not any interaction with photons of the relict radiation due to a small amount of photons on the way from the source to the observer. There are some peculiarities in the area of high energy. They are represented in fig. V-12-5.

1) CR spectrum has a knee at $E \sim 10^{15}$ (see fig. V-12-5). Inclination characteristic of CR spectrum is $\gamma \simeq 2.75$ before the knee, for greater energy spectrum becomes steeper, $\gamma \simeq 3.0$. this

[47] http://www.astronet.ru/db/msg/1210273

important feature of CR spectrum was found by S.N.Vernov and G.B.Christiansen when they examined extensive air showers. The observed knee of the spectrum with such high energy could be caused by the faster escape of CR from our Galaxy in comparison to the particles of lower energy and could be conditioned by the change of the source nature. The change of the chemical composition of the spectrum is also possible at the knee eV (see. Fig. V-12-5).

2) The spectrum of CR becomes steeper when the energy of particles is $E \simeq 10^{18}$ eV, $\gamma \simeq 3.3$ this energy range is shown in fig. V-12-5 as the "ankle". It is obviously caused by the fact that in this range CR are mostly of metagalactic origin and their spectrum has another inclination.

3) Spectrum of particles with $E > 10^{19}$ eV becomes more gradual, $\gamma = 3.3$. this effect is caused by the interaction of CR having the energy $E > 10^{19}$ eV with the relict photons, when CR lose part of their energy and pass into the low-energy area and this makes the spectrum of particles more gradual.

4) CR spectrum in the area of energy more than 10^{20} eV can be obtained only as the result of long-term observations when enough events with such an extreme energy are registered.

In order to increase considerably the number of events of extensive air showers caused by particles with $E > 10^{19}$ eV registration it is planned to build three giant installations with detectors placed across the area of more than 1000 km^2. With their help scientists hope to find the answer to the question concerning the CR spectrum in the area of ultrahigh energy and concerning the maximum possible energy of cosmic particles. Ultrahigh energy CR are captured in the Galaxy by its magnetic fields if the radius of curvature of a particle trajectory is much less than the galactic dimensions. Using the relation between the particle energy (E, eV), its trajectory radius r ($r \simeq 10^{22}$ - galactic radius) and the magnetic field intensity ($H \simeq 10^{-6}$ OE), $E = 300Hr$ one obtains maximum CR energy which could be captured in our Galaxy: E $E_{max} \simeq 10^{18}$ eV. It points to the fact that CR of higher energy could have metagalactic origin [48].

5.1.2 Solar cosmic rays

The Sun itself is also a source of cosmic rays (SCR). SCR - charged particles accelerated to energies many times exceeding thermal energy of the particles on its surface during the Sun flare processes. SCR were registered for the first time at the beginning of 1940s. They were registered with the help of ionization chambers - the ground-based installations registering high-energy muons. What is a SCR flare? Astronomers observing the Sun noticed that during the raise of the solar activity a bright glow suddenly appears in the optical spectrum in the active part of the Sun where a lot of sunspots are concentrated and where a complicated structure of photosphere magnetic fields is situated. Almost at the same time raise of the Sun radiation is observed and X-rays and gamma-radiation appear very often. They accompany ejection of coronal material in a form of a flow of charged particles. At present the energy of annihilation of solar magnetic field in the active area and the formation of neutral current layer are supposed to be the major source of Sun flare energy. Charged particles of SCR accelerated in the Sun flare are ejected into the interplanetary space and then spread across the space. Propagation of SCR is determined by the conditions established before the flare. If the conditions are still i.e. the solar wind speed does not differ much from the average and the magnetic field does not experience any considerable fluctuations, SCR will propagate according to the diffusion law and the diffusion along the lines of force will be determinative. If in the Sun flare a powerful shock-wave is generated particles are accelerated on the front of the wave with its

[48] http://astro.uchicago.edu/cosmus/projects/aires/iron200gev.gif

propagation in the Sun corona and in the interplanetary space. Most frequently SCR are observed on the Earth orbit when the magnetic line of force crossing the area of the flare passes through the Earth. A statistical analysis of the number of registered events of SCR with the energy more than several hundreds of megaelectronvolt points out that particles accelerated in flares on the western limb (edge) of the Sun are registered most frequently. Recently some proofs appeared proving that the acceleration of the particles can take place on the shock-wave front near the Sun. thus accelerated particles can be also registered far from the line linking the flare and the observer. Quite often SCR flares take place during Forbush decreases. The flow of particles accelerated on the Sun is very huge and represents a threat for everything alive. The terrestrial magnetic field and the atmosphere prevent the Earth from this awful radiation. But astronauts setting into a long-distance voyage, for example to Mars, need to have beforehand information about such events to take some preventive measures. A problem of establishing of the major regularities of SCR appearance and its forecasting is being solved by scientists from all over the world for tens of years. Unfortunately the question of a beforehand forecast of SCR and the determination of its characteristic on the terrestrial orbit is nowhere near the solution.

5.1.3 Cosmic rays in the Magnetosphere of the Earth

Before reaching the terrestrial surface CR have to pass through the terrestrial magnetic field (magnetosphere) and the atmosphere. The terrestrial magnetic field has a complicated structure. The inner area with the size of several Earth radiuses ($R_E = 6378$ km) has a dipole structure. On the faced to the Sun side of the Earth at the distance of $\sim 10R$ the solar wind interacts with the terrestrial magnetic field and a form a stationary shock wave. At this distance the solar wing flows around the terrestrial magnetic field breaking part of lines of force on the illuminated edge of the terrestrial magnetic field and transfers it to the night side of the Earth forming the tail of magnetosphere. The magnetotail consisting of broken lines of force stretches for a distance of several hundreds of Earth radiuses.

Cosmic rays getting into geo magnetic field move there in a complicated way as Lorentz force acts on each charged particle. Lorentz force is equal to $F = (q/c)[bv \times B]$ where q is a charge of a particle, c - the speed of light in vacuum, v - velocity of particles, B - magnetic induction. Knowing F one can determine the trajectory of the particle by the equation:

$$m(dv/dt) = (q/c)[v \times B],$$

where m is mass of a particle. As far as B depends on the coordinates of observation point in a complicated way the calculation of the charged particle trajectory in the geomagnetic field is unthinkable without the application of powerful computers and respective software and it became possible just at the present time.

The structure of magnetic field of the Earth. Areas of the charged particles capture (radiation belts) are shaded. At the beginning of our century the charged particles motion in the dipole field was considered by a Swedish scientist S.Stormer. in the magnetic field the motion of a particle is determined by its magnetic rigidity $\gamma = pc/Zq$, where p is the momentum of the particle, and Z is a charge number of the nucleus. Particles having the same rigidity γ will move similar in one and the same field. Calculations show that the particle gets into the given point of magnetosphere if its magnetic rigidity exceeds some minimum value called rigidity of geomagnetic cutoff γ_{min}. Particles having $\gamma < \gamma_{min}$ are not able to get into the given point at the given angle. Quantity γ is usually expressed in mega- of gigavolts: MV or GV. Particles with a very low magnitude of R penetrate into polar areas of geomagnetic field into areas of magnetic poles. But moving to the geomagnetic equator

the quantity γ_{min} increases considerably and reaches the value ~ 15 GV. Thus if one measures the cosmic ray flux moving from the pole to the equator its magnitude will decrease gradually as geomagnetic field prevent cosmic rays from penetration. This phenomenon got the name of latitudinal effect of cosmic rays. The discovery of the latitudinal effect of CR became the proof for the fact that CR are charged particles. The property of magnetosphere to transmit CR only with the rigidity more than γ_{min} is used to observe CR in different energy ranges. For this purpose CR are measured by standard devices (neutron monitors, cubic telescopes, radiosondes etc) in polar, middle and equatorial latitudes with different magnitudes γ_{min}.

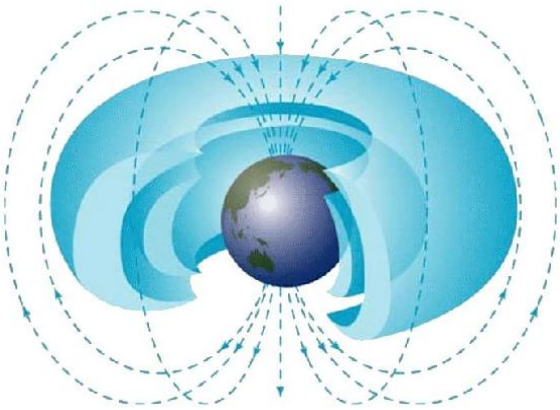

Fig. V-12-6. Model of the terrestrial radiation belts structure. [49]

Soon after the launch of the first satellites of the Earth in 1958 outer and inner radiation belts were discovered by the American Van Allen and the Soviet scientists S.N.Vernov and A.E.Chudakov. the radiation belts are the magnetic traps for charged particles. If the particle gets into such trap it is captured and lives there for quite a long time. That is why flows of charged particles in radiation belts are so huge in comparison to flows outside the radiation belts. The radiation belts are shown schematically in fig. V-12-6.

The inner radiation belt consists mostly of protons and it is situated at the distance of thousands of kilometers from the Earth surface if we measure the distance from the equatorial plane. The basic mechanism providing protons to the inner radiation belt is the mechanism of slow neutrons decay. Neutrons are generated when CR interact with the nucleuses of atmospheric elements. They are unstable particles with a lifetime equal to 10 minutes. Part of neutrons has enough speed to escape the atmosphere (the atmospheric boundary is at the height of about $\sim 30-35$ km), get into the area of a magnetic trap where the decay takes place: $n \to p + e^{-} + \tilde{\nu}$ Measures and calculations of neutron flows coming up from the atmosphere of the Earth show that this source is the basic provider of protons to the inner radiation field. The maximum of captured protons flow of the inner radiation belt (protons with $E > 35$ MeV) was recorded at the height of about $1.5R_E$. The inner radiation belt consists mostly of electrons with the energy from several hundreds of kiloelectronvolt to ~ 10 MeV. The electron flow in the outer radiation belt varies much during geomagnetic disturbance. The outer radiation belt is formed of particles ionized cover placed around the Earth and of solar wind electrons. During geomagnetic disturbances low-energy electrons are accelerated by magnetohydrodinamic waves (MHD-waves) propagating from the magnetosphere boundary to the Earth surface (more details concerning the nature and propagation of MHD-waves see in the article by M.I.Pudovkin

[49] http://www.astronet.ru/db/msg/1210273

"Solar wind" in this volume).

Magnetosphere on the day side and the night side is not symmetric so the areas of particles capture are also different. This difference is caused by the solar wind effect on the magnetosphere and mostly affects the outer areas. That is why a great asymmetry in the positions of the capture areas is observed for the outer radiation belt particles and it is much less for the inner belt particles. The role of CR in atmospheric phenomena attracts more attention in the recent time. Though the CR energy density is low in comparison to corresponding quantities of different atmospheric processes cosmic rays play a decisive role in some of them. CR are the main source of ions formation in the terrestrial atmosphere at the height of less than 30 km. the processes of condensation and water drops formation depend a lot on the density of ions. So during the Forbush decrease cloudiness and precipitation level decrease. After Sun flares and arrival of SCR on the Earth the quantity of clouds and precipitation level increase. Both changes in the first case and in the second case make a considerable part - not less than 10%. After the invasion of great flows of low-energy particles from Sun flares into the polar areas of the Earth the change of temperature in the upper layers of the atmosphere is observed. CR take an active part in the thunderstorm electricity generation. At the present time the influence of CR on the ozone concentration and other processes in the atmosphere is being studied.

As the result of the interaction with the nucleuses in the atmosphere the primary cosmic rays (mostly protons) generate a great amount of secondary particles - pions, protons, neutrons, muons, electrons, positrons and photons. Thus instead of one primary particle a great amount of secondary particles appear. They are divided into hadronic, muonic and electron-photon components. Such cascade covers a great area and it is called an extensive air shower. In one interaction act proton usually loses 50% of its energy and as the result mostly pions appear. Each following interaction of the primary particle adds new hadrons to the cascade. They fly mostly along the way of the primary particle making a hadronic core of the shower. Generated pions can interact with the nucleuses in the atmosphere or they can decay making muonic and electron-photon components of the shower. Hadronic component practically does not reach the surface of the Earth turning into muons, neutrino γ-quanta.

5.1.4 Cosmic rays interaction with the matter

Basic types of interactions:

1. ***Photoabsorption***. In this case photons moving in the medium interact with the electrons of atoms and make them to jump to the higher energy level. Particularly with the high energy of the colliding particle electron can be expelled from its orbit in the interacting atom. This process is called atomic ionization.

2. ***Compton scattering***. This interaction represents a free-electron scattering of γ-quanta. With that part of the γ-quant energy passes to the electron but γ-quant changes its direction.

3. ***Formation of electron-positron pairs.*** If the γ-quant energy exceeds the total rest mass of both electron and positron a formation of electron-positron pair is possible as the result of the collision of such γ-quant with the atom or nucleus. In this case electron and positron start to move in the medium and interact with other particles and γ-quanta.

The combination of all these processes leads to the formation of electromagnetic avalanches. The diagram of the avalanche is represented in fig. V-12-2 and V-12-3.

Some tools for the cosmic rays registration

Nowadays a great variety of tools used for registration of particles is created. But there are

based on the tools representing different variants of the simplest installations we are going to describe.

A. Gas-filled detector. Geiger-Muller counter.

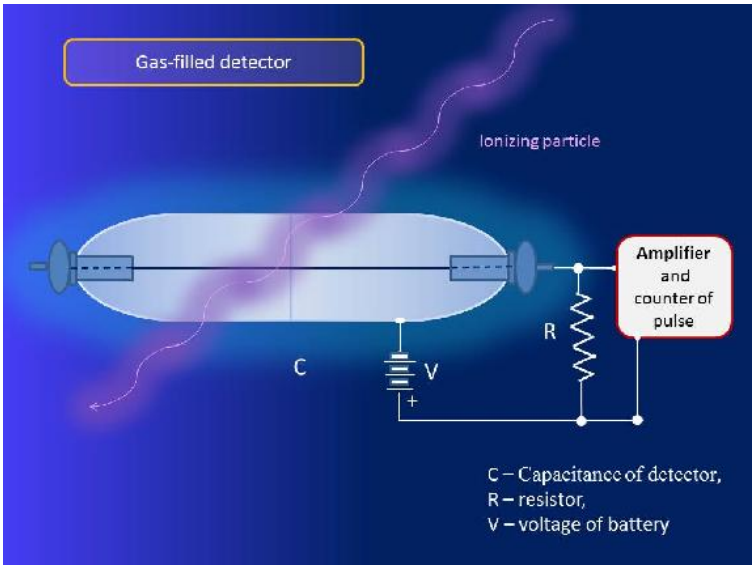

Fig. V-12-7. Gas-filled detector for the registration of cosmic rays.

volt-ampere characteristic of a gas-filled detector is represented in fig. V-12-8. The description of single parts of this characteristic is given below.

A- Voltage is such that part of electrons generated as the result of atomic ionization combine with the ions again. Such process is called recombination.

B- Voltage is high enough for almost all the electrons to reach the anode. Recombination process is insignificant.

C- Working area. electrons moving towards the anode gain the energy enough to ionize other atoms. As the result the current increases many times remaining proportional to the number of primary particles caused the ionization. Detectors working in this voltage range are called proportional detectors.

D- Voltage is so high that the number of secondary electrons is not longer proportional to the number of primary particles.

E- Voltage is so high that any particle able to ionize the atom generates a great current impulse. This rate is called saturation mode.

A gas-filled detector working in the saturation mode is called Geiger counter.

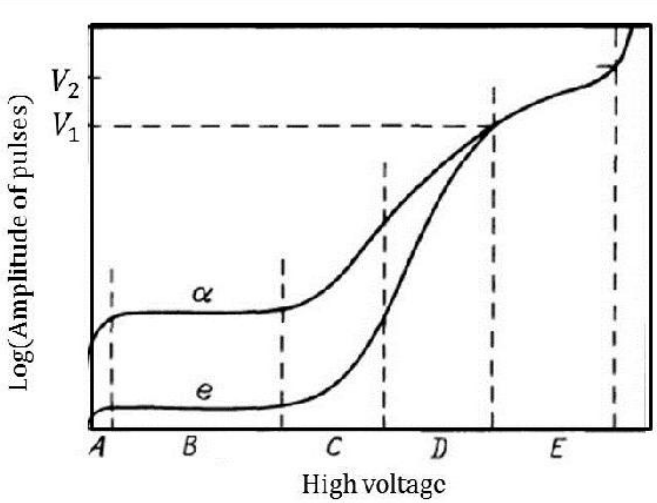

Fig. V-12-8. Volt-ampere characteristic of a gas-filled detector.

B. Semiconductor detector

Like in gases in solid bodies charged particles lead to the generation of secondary charged particles which could be collected with the help of electric fields and then the characteristics of the ionizing particle can be estimated. But unlike gases it is not electrons and ions that are generated under the effect of cosmic rays but electrons and holes are generated in solid bodies. There is one more distinction: much less energy is needed to generate one couple electron-hole than in gas. Therefore the accuracy of semiconductor registration devices is approximately 10 times more than of gas-filled ones. One more advantage of semiconductor devices is compactness and it allows to use them on spacecraft preferring them to gas-filled ones. The typical view of such instruments is represented in fig. V-12-9.

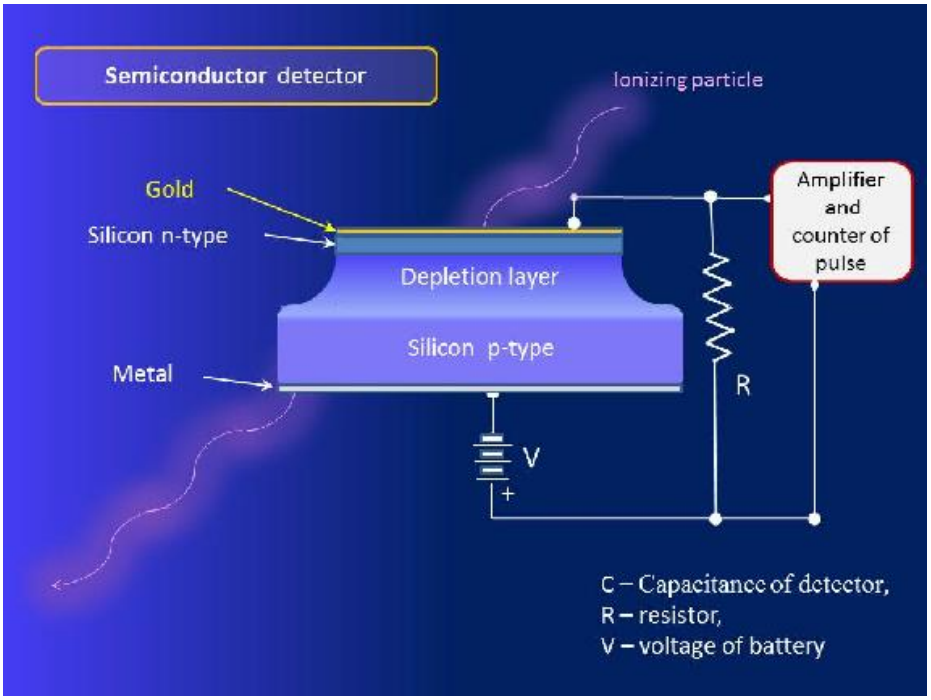

Fig. V-12-9. Semiconductor detector for cosmic rays registration.

C. Scintillation detector

Scintillation detector is one of the first instruments used for the charged particles registration. These instruments were used by Reserford during his famous experiment of alpha-particle scattering on a gold foil when the presence of positive nucleuses of gold atoms was demonstrated. As far as the efficiency coefficient of the conversion of the particle energy into light in scintillation crystals making the basis of an instrument is too low (about 5%), their efficiency depends on the possibility to intensify the light signal from these crystals. Nowadays such detectors are used in combination with photomultipliers. The general view of such detector is represented in fig. V-12-10.

If the light in detector is excited not due to collisions with the atoms of the medium but due to the fact that the charged particles speed could exceed the speed of light in the detector medium then such detector can also be referred to scintillation detectors. In this case so-called Cherenkov radiation or Vavilov-Cherenkov radiation appear. Such detectors are called Cherenkov detectors. Their general view is similar to scintillation detectors

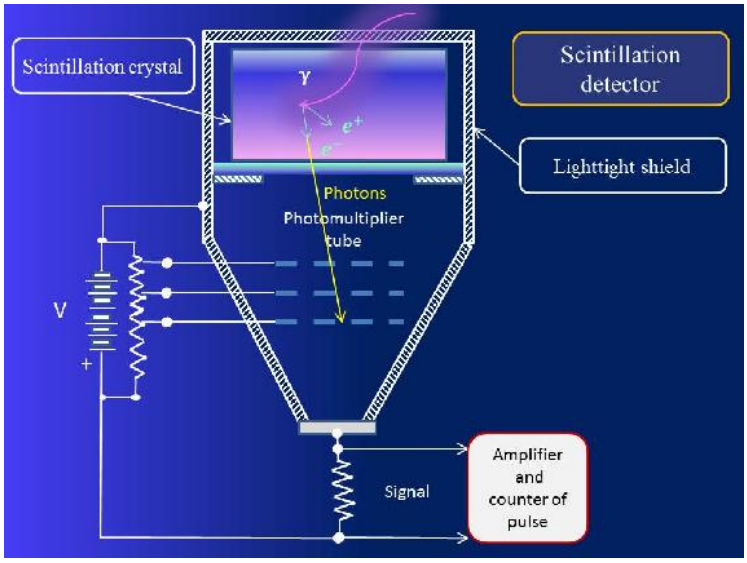

Fig. V-12-10. Scintillation detector for cosmic rays registration.

D. Telescope

Registration of cosmic rays and their arrival direction is based on the principle that cosmic rays pass through several different-type detectors sensible to different types of particles. Then the type of a particle is detected by the presence or absence of a signal from other detectors together with the signal of one detector. This task is realizable thanks to modern electronic circuits constructed in such way that the signal is not registered on output if the event has not got a needed attribute. Then the data from different detectors is memorized in the internal memory of the on-board computer and then the data is transmitted to the Earth. For the example in fig. V-12-11 there is a simplified scheme of γ -telescope installed on the satellite IMP-3. The telescope consists of four detectors $D_1 - D_4$. Only those particles are registered which call the signal from detectors $D_1 - D_3$ and do not call the signal from detector D_4. This scheme of registration is called D_4-detector anticoincidence scheme (see fig. V-12-11). This scheme determines the following properties of this telescope.

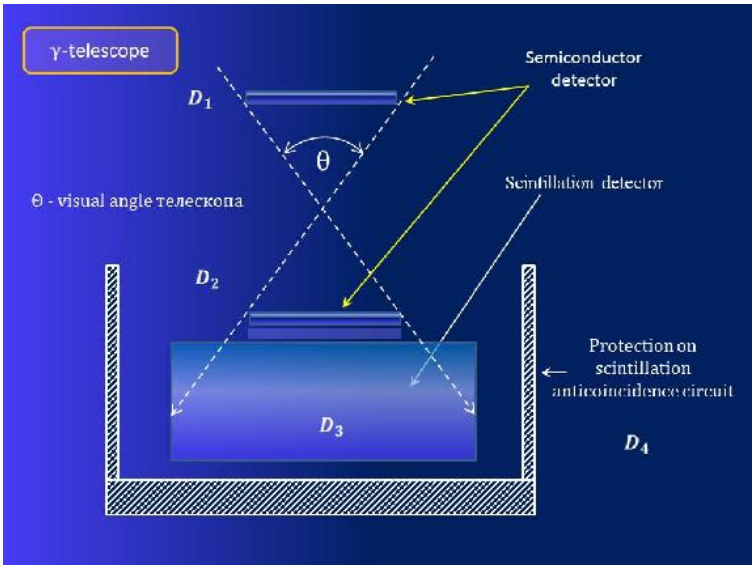

Fig. V-12-11 a simplified scheme of γ-telescope installed on the satellite I IMP-3.

The telescope pickup angle θ is determined by detectors D_1 and D_2. It means that only the particles coming in the boundaries of the cone shown in the figure can lead to the response of the system with the memorizing of the event. The telescope is sensible to the range of energy determined by the fact that particles must be energetic enough to get into D_3 passing through D_1 and D_2, but they must not be energetic so much to pass through D_3 and reach D_4. Properties of particles and their type are detected by the comparison of a signal from detector D_1 and the total signal from detectors $D_1 + D_2 + D_3$. The signal magnitude from D_1 determines the rate of energy loss in the detector for the track unit length, i.e. the quantity $\Delta E/\Delta x$. The total signal from all the detectors (except D_4) determines the total energy E of the particle. Comparing these two quantities one can define the type of this particle and other its properties. The graphic chart of

$$\frac{dE}{dx} = f(E)$$

is called the diagram of ionization loss.

5.1.5 Propagation of cosmic rays in the heliosphere

Cosmic rays penetrate into heliosphere interacting with the solar wind. Very energetic charged particles remain unchanged - they pass through the solar wind as if it does not exist. But cosmic rays with moderate energy, for example less than several GeV, experience its influence. But it is not collisions as far as the gas is too thin for the direct collisions of cosmic rays particles and solar wind particles. But the magnetic field variety makes the trajectory of moderate-energy cosmic rays diverted from a straight line very much.

One can realize that with the help of an elementary description of the charged particles propagation in the uniform magnetic field. When the magnetic field changes in time the particle meets very rapidly changing magnetic lines of force directed along the trajectory and therefore it has the direction of propagation changing all along. It tells that the particle is scattered on the magnetic irregularities of the field.

Galactic cosmic rays are scattered on the magnetic disturbances (irregularities) propagating with the solar wind. The quantity of such irregularities changes with the 11 year cycle of solar activity.

The cycle of solar activity must be clearly indicated by the number of sunspots (a green line). Within a long time the observations of worldwide network of neutron monitors have shown that the flux of galactic cosmic rays has the same change (a red line): when the number of sunspots is big the cosmic rays flux decreases and vice versa.

This is so-called solar modulation of galactic cosmic rays caused by the penetration of energetic particles into dynamic medium of the heliosphere. The magnetic field of the heliosphere varies (curves) a lot during the periods of high activity i.e. when the number of sunspots (and also flares and mass-ejections) is high. Turbulent interplanetary magnetic field diverts cosmic rays more efficiently than during the periods of low activity when the magnetic field is more stable. Great variation of the magnetic field leads not only to the decrease of cosmic rays but it also changes their energy spectrum (as the particles with lower energy have greater effect than very energetic particles) and their propagation direction (anisotropy).

The Sun also influences the propagation of cosmic rays at the expense of placement of active areas along its equator. It creates small variations of CR related to 27 days period of rotation of the Sun. In a long history of the existence of polar caps on the Earth cosmic rays have left their prints on polar ice. Analyzing these prints it is possible to track the variations of cosmic rays in periods of thousands and millions of years. By November 2010 we do not know if the minimum of activity is already in the past or it is ahead, though 14 years have already passed since the last minimum of the year 1996. Cosmic rays modulation proves that as far as their flux is higher at the present time than it was in previous minima of solar activity.

Like interplanetary coronal mass-ejections shock-waves propagating through the heliosphere and changing the configuration of the magnetic field also decrease the galactic cosmic rays flux. Decreases can reach the value of 20%. They are called Forbush-decreases by the name of the author of cosmic rays physics Scott Forbush. Decrease of cosmic rays flux is caused by scattering of cosmic rays by the shock-wave of a coronal ejection.

Chapter 6. Space Laboratories

6.1 Lecture 13. Exploration of near-Earth space with the help of spacecraft

6.1.1 Soviet and Russian spacecraft

For the first time meteorological observations from the space were carried out in the Soviet Union with the help of artificial Earth satellite ``Cosmos-144" (``Meteor-1") launched on 28 February 1967 from cosmodrome ``Plesetsk". Two months later an experimental system "Meteor" started to function as a part of satellites ``Cosmos-154" and ``Cosmos-156". Since 1969 meteorological satellites have the same names as the whole system - ``Meteor". A development of a low-orbit meteorological space system ``Meteor" was started. Later the satellites ``Meteor-2" and then ``Meteor-3" were joined to the system.

In their construction these satellites had two airtight modules. Instruments for meteorological observations were placed into the lower module (instrumental module) located in the lower part of a satellite. In the other one - energy equipment module - different auxiliary equipment was placed: radiotelemetric system, equipment of thermoregulation system, chemical piles of the electric system. Outside this module big plane solar panels (SP) were mounted. They open just after the separation of a satellite from rocket-carrier. Unlike SP usually inflexibly fixed on the frame of a satellite or automatic interplanetary station solar panels of "Meteors" were moving and they could turn in such way that the Sun could light up the sensitive elements of panels (of course it was impossible when a

satellite was in the shadow of the Earth). Such moving system and a great area of panels in combination with chemical buffering piles allowed supply of electric power to the system working in different rates for a number of months.

Axes of all registering equipment are directed along the longitudinal axis of a satellite. This axis is always directed to the center of the planet to provide the Earth surface observations of high quality. But it is not enough - a satellite should be stabilized along two axes. The initial damping after the separation from the carrier rocket and the orientation of satellite axes was realized with the help of micromotors of gas-jet system. During the further flight orientation and stabilization of a satellite was realized with the help of combined electric flywheel system in combination with torque magnetic drive using the terrestrial magnetic field. To control the axis orientation detectors of the Earth thermal radiation which can work independently on the position of a satellite on the dayside or on the night side.

``Meteors'' were launched from Plesetsk cosmodrome to polar near-circular orbits at the height of 950 km (``Meteor-2'') or 1200…1250 km (``Meteor-3'') with the help of carrier rocket ``Cyclone-3''.

Except the auxiliary systems the onboard equipment of ``Meteor-2'' there were: scanning television system for the transmitting of images of cloudiness with the mode of memorizing of the information in visible spectrum with the resolution of 1 km in the swath width of 2200…3100 km, infrared radiometer for the receipt of thermal images with the resolution of 0.8-1.5 km and actinometric equipment. Television and infrared images allow scientists to discover the peculiarities of the cloud fields' structure which are not available for the observation from the ground-based stations and they allow making conclusions concerning not only the position but also the evolution of corresponding meteorological objects and air masses. Actinometric equipment is designed to measure radiation flows going from the Earth. Usage of the space system ``Meteor'' helped to increase substantially the quality and immediacy of the prognostication of weather-forming processes over land and sea. More over a number of questions cannot be solved without the abilities given by the space system: almost 80% of the surface of our planet is still a ``blank spot'' for the ground-based stations.

Space craft ``Meteor-3''

Spacecraft ``Meteor-3'' was designed for the prompt round-the-clock gathering, transmission, processing, registration and distribution of the meteorological information and also of the radiation situation in the near-Earth space, condition of magnetosphere, and the ozone layer of the Earth. The spacecraft (SC) allowed reception of global and local images of cloudiness, the surface of the Earth, ice and snow covering and the data for determination of the temperature near the cloud top. Research equipment was installed on its unified platform 17F45. It was used for the measurement of the terrestrial spectral radiance in visible, infrared, ultraviolet and ultra-high frequency spectrum. It determined altitude profiles of temperature and humidity in the lower atmosphere, the general concentration of ozone and its vertical distribution and the conditions of the radiation situation along the flight trajectory of a SC. According to the flight program all gathered data was memorized in the onboard storage device and was transmitted to the main and regional centers collecting and processing the data.

The onboard information-measuring complex also included television equipment, equipment for snapshots in infrared spectrum, multi-channel infrared scanning spectroradiometer, equipment for radiation measurements, complex of spectrometric equipment of ozone probing, radio engineering equipment for collecting and processing the data from ground-based and sea-based data collecting platforms, transmitting equipment of radio lines and storage devices.

Spacecraft of ``Meteor-3'' series were designed in the Research Institute of electromechanics (NIIEM, Istra, Moscow region).

Spacecraft ``Meteor-3'' were launched to polar near-circular orbits at the altitude of 1200 km with the help of rocket-carrier ``Cyclon-3''. The first launch of "Meteor-3" N1 on the 27 of November 1984 ended up with an accident at the stage of flight of the third stage of the rocket-carrier and as the result the SC was set on the off-designed orbit. Spacecraft N1 and N2 were the transition ones form ``Meteor-2'' to "Meteor-3". Onboard SC ``Meteor-3'' N5 (15.08.91) as an additional pay-load the ozone mapper TOMS (USA) was installed. Experimental microsatellite ``TUBSAT'' and PRARE and SKARAB equipment were installed as an additional pay-load on the SC ``Meteor-3'' N7.

Microsatellite TUBSAT was designed at the technical university of Berlin (Germany) and in was intended for the test of the diminutive orientation system of promising spacecraft under the conditions of the space flight. The system uses solar and stellar detectors and electromechanical actuators. A retransmitter was installed onboard the satellite to support amateur radio communication. The mass of the satellite is 40 kg, dimensions: 380 x 380 x 490 mm. the speed of separation from the SC ``Meteor-3'' is 0.5 m/s.

The precision system of navigation measurement PRARE was designed by ``Keizer-Trade'' (Munich, Germany) and was intended to perform experiments on high-precision measurement of the distance and Doppler shift with the help of ground-based retransmitters. The principle of operation of PRARE system is based on the measurement of the group lag and phase change of the digital microwave carrier waves in the range S (2248 MHz) and X (8489 MHz). the equipment mass is 18.5 kg.

SKARAB equipment (another name: SRB Scanner of Radiation Balance) was designed by the Laboratories of the dynamic meteorology (Paliso, France) in collaboration with NPO ``Planeta'' (Dolgoprudny, Russia) and NIIEM (Istra, Russia) with the technical and financial support of the French Space Agency CNES. The German Space agency DARA also participated in the program. The agency provided the technical and financial support of the Laboratory for atmospheric research which was responsible for the on-ground solar calibration of the equipment. The SKARAB instrument was intended to collect information concerning the radiation balance conditions of the system ``The Earth - the atmosphere''. For this purpose the SKARAB equipment measured the density of outgoing radiation simultaneously in four spectra: two broad spectral bands permit to realize the measurement in solar and thermal areas of spectrum emitted and reflected by the Earth (the solar channel: 0.2 … 0.4 μm, the general channel: 0.2 … 50.5 μm). Two more narrow bands (visible channel 0.5 … 0.7 μm and window channel 10.5 … 12.5 μm) are fitted to determine cloudiness, one of them corresponds to the infrared atmospheric window and the other allows distinguishing between the visible region and the nearest infrared region of the solar spectrum. Measurements of the radiation balance carried out within a long period of time played an important role in understanding the phenomena responsible for the climate change and evolution on the Earth. The equipment mass is 40 kg.

Fig. VI-13-1. Meteor-M - apparatus of a new series of Russian meteorological satellites.

The general characteristics of SC of series Number of a SC 1, 2, 3, 5, 7, 4, 6 ``Meteor-3''

Mass of SC, kg	1750	2150	2250
Calculated parameters of the orbit:			
Inclination, grad	82.53	82.54	82.54
revolution period, minutes	110.29	109.38	109.46
Maximum altitude, km	1266.0	1222.5	1223.7
Minimum altitude, km	1229.0	1193.6	1187.3
Spacecraft dimensions, m:			
Length	6.5		
Diameter	2.4		
Width with spread solar batteries	12.7		
The orientation system			
Type	Active, triaxial flywheel motor, and correcting propulsion device with compressed gas		
Orientation accuracy	Not worse 20 angular minutes		
Television device			
Swath length of the television equipment, km	3100		
Resolution, km	0.8 x 1.5		
Accuracy of the position linkage of the received images, km	15		
Launch system			
Rocket-carrier type	``Cyclon-3''		
Duration of active existence	Not less than 2 years		

Coronas-I and Coronas-F

A complex international experiment ``Coronas-I``

A complex international experiment Coronas-I (Complex Orbital Near-Earth observations of solar activity IZMIRAN)[50] was carried out onboard the spacecraft AUOS-SM-KIIK designed especially for this purpose. Directing agency responsible for the realization of this scientific program was the Institute of Earth magnetism, ionosphere and radiowaves propagation of the Russian academy of science (IZMIRAN).

The project ``Coronas-I" developed within the program ``Intercosmos". Organizations, Scientists and specialists from Bulgaria, Germany, Poland, Czech Republic, Russia, Ukraine and Slovakia took part in the program. Later organizations, scientists and specialist from England, Brazil, the USA, France and Japan joined the program. Spacecraft Coronas-I was targeted at the research of physical processes taking place on the surface of the Sun and in its atmosphere and also at exploration of the solar interior. The major scientific tasks of the spacecraft were:

1. Clarification of the mechanism of the energy transport and its accumulation in the upper atmosphere of the Sun.
2. Basing on the complex study of a Sun flare to determine the mechanism of the emission of its energy and its location in the active area.
3. To determine parameters of flare plasma at different stages of its development with the help of spectrometric methods.
4. Observation of plasma ejection in spectral bands including radio band during Sun flares.
5. Detailed examination of particles acceleration mechanisms during flares.
6. Exploration of the solar interior with the help of helioseismology methods

There are two fundamental problems in the solar physics. The first one is connected to the interior structure of the Sun. Davis experiments were being realized for years. They concerned the exploration of the interior structure of the Sun with the help of solar neutrino registration and have shown that the existing scientific models represent incorrect idea of the interior structure of stars and particularly the Sun. it was necessary to find a new independent method of the exploration of the solar interior. It was a helioseismology method which enables to determine the temperature profile inside the Sun and rotation velocity by the natural period and to get information about magnetic fields and irregularities.

The second fundamental problem of the Coronas project was the study of the solar activity, its mechanisms and the influence on the near-Earth space. Nowadays more ecological problems connected to the technical activity of humans arise. But studying these problems and measures against them people often forget that the Earth, its atmosphere, ionosphere and magnetosphere are not the closed system and are the subject to the influence from outside and particularly from the Sun. For example the problem of the ozone layer should be studied with the solar activity influence on this layer taken onto account. It was impossible to study the Sun only with the help of ground-based instruments because the information obtained in the visual band is not enough to create the consistent representation of physical processes. Moreover cycling of the terrestrial atmosphere has the same frequency as that of the Sun. For the purpose of a detailed and systematic exploration of the Sun the equipment complex of the "CORONAS" project was composed in such way that it was able to cover as wide band of electromagnetic radiation as it was possible. .

Spacecraft AUOS-SM-KI-IK (``CORONAS") was designed in design department ``Yuzhnoe" by the name of M.K.Yangel and it was manufactured in the Yuzhny engineering plant

[50] http://plesetzk.ru/index.php

(Dnepropetrovsk, the Ukraine). It was a unified platform (base SC AUOS-SM) consisting of a complex of supporting onboard systems and construction elements and representing the basis for the creation of specialized SC by the equipping the unified platform with special onboard complex according to the purpose of the spacecraft.

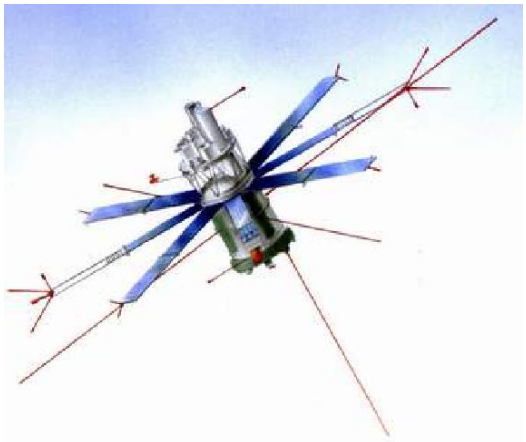

Fig. VI-13-2 Space observatory CORONAS-I

Scientific equipment of the ``CORONAS'' project included:

1. Equipment for registration of X-ray and gamma radiation of the Sun. among them there was x-ray telescope-coronograph TEREK (reception of the image of the Sun in soft x-ray band and visible band), HELICON equipment (complex exploration of the solar flare activity in x-ray and gamma-rays with a high temporal and energetic resolution), x-ray spectrometer IRIS (exploration of x-ray precursors of flares in soft x-ray band and of temporal structure of hard x-ray radiation in the impulsive phase of a flare), x-ray spectropolarimeter RES-K (exploration of the solar corona), DIOGENESS equipment (Diagnostics of the energetic conditions of solar flares - a complex diagnostics of the energy ejection and dispersion process and the determination of the main parameters of flare plasma), amplitude-time analyser of spectrum ABC (examination of characteristics of hard x-ray and gamma flows from the solar flares)..

2. Complex of equipment for the registration of ultraviolet radiation from the Sun. it is included in the ultraviolet radiometer SUFR-Sp-K (measurement of the solar radiation intensity in the far-ultraviolet band). And there is also vacuum ultraviolet spectrometer VUSS (measurement of the spectral characteristics of the ionized area of the solar radiation)..

3. Solar photometer DIFOS for the high accuracy exploration of global variation of the intensity of solar radiation (solution of helioseismology problems).

4. Solar radiospectrometer SORS (exploration of mechanisms of solar radiation generation in a range from 30 KHz - 20 KHz)..

5. Cosmic rays spectrometer SKL (exploration of cosmic rays bursts and phenomena caused by them).

6. Three-component magnetometer IMAP-5 (registration of the terrestrial magnetic field in a wide dynamic range).

7. SSNI - the system of gathering and transmission of scientific information to the Earth.

The following reception centers were used to receive the information from the spacecraft: Neusterlitz (Germany), Tarusa (Space research institute of the Russian academy of science), Troitsk (IZMIRAN), Medvezh'i lakes (OKB MEI). The transmission of commands for the DIOGENESS equipment was carried out from the station Pansk Ves (Czech Republic).

A unified supporting onboard complex included command-program-trajectory radio line, power supply system (solar and chemical batteries), experimental solar powerplant. System of thermal rate supply, in-flight orientation and stabilization system of the spacecraft, bars for installation of antennae and scientific equipment.

The basic information about the spacecraft ``CORONAS-I".

satellite revolution period, minutes Maximum altitude, km Minimum altitude, km Spacecraft dimensions Length Diameter in compacted form Width with spread solar batteries The orientation system

Mass of SC, kg	2298.2
Spacecraft dimensions, m	
Length	5.0
Diameter	2.3
Width with spread solar batteries	12.8
The orientation system	
Type	Active, triaxial flywheel motor, and correcting propulsion device with compressed gas
Orientation devices	triaxial flywheel motor, and correcting propulsion device with compressed gas
Orientation accuracy, angular minutes	10
Active lifetime	more 1 year
Orbit	polar, near-circular
Calculated parameters of the orbit:	
inclination	82.485o
revolution period, minutes	94.755
Maximum altitude, km	539.8
Minimum altitude, km	498.5
Launch system	
Rocket-carrier type	11K68 (``Ciclon-3")
Launching mass of the rocket-carrier with the spacecraft, ton	184.3

CORONAS-F

Targeted at the exploration of the Sun and solar-terrestrial relations a russian-ukranian satellite CORONAS-F[51] was launched on the 31st of July 2001 and completed its program and ended up its existence as the result of the natural evolution of the orbit on the 6th of December 2005.

The satellite was launched to the near-Earth orbit at the altitude of about 500 km with the inclination of 83 degrees.

A scientific complex of the satellite included 15 tools so the satellite represented a space solar observatory working in the independent mode and controlled from the Earth. Devices of the satellite

[51] http://www.federalspace.ru/main.php?id=171

observed the Sun in the whole spectrum range - from the visual band to the gamma band. And that enables to carry out the complex analysis of the solar phenomena and solar-terrestrial relations basing on the collected information.

The most significant equipment among the scientific tools of the satellite was an x-ray equipment complex designed by the Institute of Physics of Russian academy of science in cooperation with a range of scientific organizations and universities it was targeted at the exploration of the space-time structure of the solar activity phenomena, heating mechanism of the solar corona, Sun flares and ejections

,

Fig. VI-13-3 the satellite CORONAS-F on the orbit

Since the maximum of the solar cycle in 2001 equipment of the satellite CORONAS-F have registered the most powerful flares on the Sun and their influence on the near-Earth space.

Multichannel spectrophotometer DIFOS registered eigenmodes of the global variation of the Sun in a wide range of radio waves, its dynamics was studied and new experimental data concerning the effects of these variations in the observed radiation was obtained, a considerable growth of the global variations amplitude was established in the ultraviolet radiation.

Multichannel solar x-ray telescope was one of the most unique scientific devices in the space in the Russian cosmonautics history. A great program of the solar exploration was performed with its help

In October-November 2003 the most powerful for the latest years active events on the Sun were registered: ejections of the coronal matter with the speed up to 2000 km/s and associated phenomena (dimming, coronal holes, coronal waves), localization of numerous active phenomena was carried out and their morphology was explored. Repetition of ejections from the same magnetic configurations on the Sun were observed, the configurations had time to restore their magnetic field and luminosity within the time between the events.

A new class of phenomena was discovered in the solar corona in a resonance line Mg XII

(8.42a) on the basis of the observations from the unique spectroheliograph RES-K. The phenomena represented rapid dynamic plasma formations with the temperature up to 20 mln. degrees while the temperature of the solar corona is just about 1-2 million degrees. The image and the dynamics of such high-temperature formations were obtained for the first time. These formations have different form: ``hot clouds'', ``spiders'', ``loops'', propagating wave fronts, consequently igniting magnetic arches. The observation of these phenomena disclosed one of the mechanisms of the solar corona heating as the result of the magnetic energy emission in magnetic configurations and its transformation into plasma energy .

A relation was established between hot plasma formations in the corona and mass ejections from the solar atmosphere observed by the coronograph onboard the European satellite SOHO. These jets cause magnetic storms on the Earth.

The observations with the help of x-ray telescope in a coronograph mode let for the first time obtain the data concerning the solar corona dynamics at the distance up to 3 solar radiuses. Mass ejections and eruptive prominences were observed in this area which is very important for the understanding of the nature of many phenomena but which cannot be observed with the help of other tools.

CORONAS-F satellite's instruments with a high temporal and spectral resolution in a wide energy range (from visual to gamma) obtained a great amount of new information about different physical processes into flares.

These are temporal, spectral, polarization and energy characteristics of the flare radiation, spectra of accelerated particles, gamma lines etc.

Linear polarization of hard x-ray radiation from the solar flares was measured for the first time, which is the direct proof for not only the existence of the beams of charged particles but it is also the confirmation of the fact that these particles are accelerated by the impulsive electrical field and not by any stochastic mechanism.

Gamma lines are registered into flares and the content of different elements and their isotopes was determined by these lines. In gamma spectrum of flares a line of capture of neutrons born into flares was observed and annihilation line of electrons and positrons was also observed.

Registration of high-energy gamma radiation and of neutron flows from powerful flares in October 2003 was carried out and the primary spectrum of protons accelerated inside a flare and the moment of their escape from the solar corona were established.

A spectroscopic diagnostic was carried out of the flare plasma and atomic processes: an absolute x-ray shift of x-ray spectrum lines in solar flares were defined; absolute content of K (Potassium), and Cl (chlorine) in the solar corona was measured, spectral lines of astrophysical (solar) plasma ions with big quantum numbers n were discovered, which give the opportunities for a new method of thermal diagnostics of the coronal plasma; new spectral lines were discovered and identified, hundreds of spectra of helium (He)-similar ions of Ca XIX, Si XV and Si III were measured.

Performing the measurements of solar cosmic rays along the orbit CORONAS-F satellite explored the radiation situation of the near-Earth space and the dynamics the magnetosphere and the radiation belts of the Earth during periods of solar activity. On the basis of these measurements geomagnetic storms and penetration of the energetic solar particles inside the terrestrial magnetosphere were examined.

A continuous range of data on the flows of energetic solar particles were obtained by the solar cosmic rays complex of the CORONAS-F satellite, and the data for energy higher than 300 KeV is unique because there are no more other measurements by the present time

During strong magnetic storms the phenomena of the magnetosphere deformation, movement of the radiation belts into the magnetosphere and related to this penetration of energetic solar particles

were registered. A new phenomenon was discovered which represents the disappearance of the outer radiation belt of electrons in the main phase of the magnetic storm on the condition of energy higher than 1,5 MeV.

Together with the known particle precipitation in the ionosphere from the magnetosphere in the Polar areas and in the vicinity of the Brazilian anomaly some quasi stationary equatorial precipitation was discovered, and obviously their origin is related to the peculiarities of this thin structure if the terrestrial magnetic field in these regions of the Earth. This precipitation is characterized by the substantial growth of the radiation background (about 20-30) and it can last up to 8 days.

With the help of solar x-ray telescope the examination with the height resolution improved by 100 times of the upper terrestrial atmosphere was carried out. The examination concerned the ability of the atmosphere to absorb the hard x-ray radiation. The dependence of the atmospheric density and composition on the solar activity level was established at the height up to 500 km and the content of the molecular nitrogen and atomic oxygen was determined.

For the purpose of the observation in ultraviolet band with the help of radiometer SUFR and spectrophotometer VUSS a new method of the definition of content of molecular oxygen - the basic component of the atmosphere - was developed.

All these observations make the experimental basis for the design of the contemporary model of the terrestrial atmosphere.

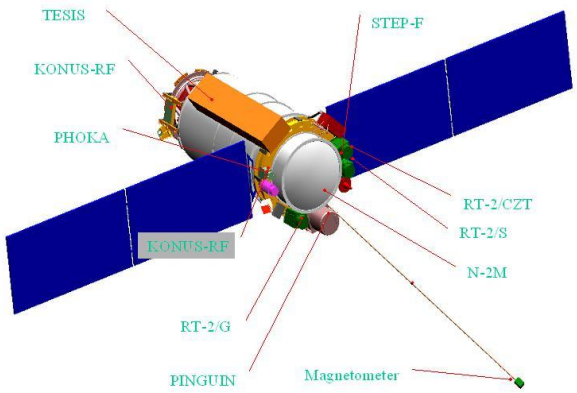

Fig. VI-13-4. CORONAS PHOTON - the latest apparatus of this series.

With the help of gamma-spectrometer HELICON on the 27th of December 2004 a rare phenomena was registered - the reflection of the gamma burst of a neutron star by the Moon, which allowed the estimation of the explosion energy of that neutron star. It was about 1044 erg and considerably exceeded the power of the visible radiation of all 100 billion stars of our Galaxy. This was the first observation of the reflection of the cosmic gamma-burst by a celestial body in the world, or, in other words, the first localization of the celestial body with the help of the natural superpowerful impulse of gamma-radiation.

RESOURCE and RESOURCE-DK

Spacecraft ``Resource-F''

The information about the presence of natural resources and their conditions on the land and in the World Ocean is very important for the existence and the evolution of the mankind on the Earth. Having the global coverage and the immediacy the space system became a very effective tool for the

exploration of natural resources of the Earth.

The first step in the exploration of the Earth from the space was space photography of the surface which was performed on the 9th and on the 25th of March 1961 during the flights of the Fourth and the Fifth spacecraft-satellites. Further it became an integral part of the scientific and national programs both for manned spacecraft and automatic satellites of the ``Cosmos'' series.

For the purpose of planned exploration of natural resources of the Earth and the control of environmental conditions a space system ``Resource'' [52] was designed which included three subsystems: ``Resource-O'', ``Resource-F'' and ``Ocean-O''. Satellites of the ``Resource-F'' and ``Ocean-O'' subsystems were launched from the Plesetsk cosmodrome.

Satellites ``Resource-F'' were launched with the help of the rocket-carrier ``Soyuz-U'' to elliptic polar orbits with the apogee altitude 250-275 km, and the perigee altitude 190-200 km. the first launch of the ``Resource'' took place on the 5th of September 1979. After the orbital injection a working orbit was formed with the help of onboard correction system. Its parameters were chosen under the condition of the ensuring of global coverage of the Earth surface by photo equipment span with the necessary cross overlay. The complex of the scientific equipment of the satellite ``Resource-F1'' included three wide-frame topographic tools ``KATE-200'' which allowed production of synchronized images of the terrestrial surface with the resolution of 15 … 20 meters, and two long-focal wide-frame instruments KFA-1000 for a specrozonal survey with the resolution of 6 .. 8 meters. With the help of star photo camera photographing of the stars was realized in purpose of the coordinate fix of the spacecraft axes in the space during photographing the surface of the Earth.

``Resource-F1'' was able to stay on the orbit up to 25 days and part of time it was in stand-by mode (11 days). The usage of stand-by mode allowed either repeated photographing of the given areas of the surface or taking photographs of the needed area during the second pass if it was not possible during the first pass due to unfavorable weather conditions. The made photographs were sent to the Earth by a landing module.

The spacecraft ``Resource-F2'' made synchronized multiareal and multispectral (or colored) photographing of the surface with the high resolution. Unlike ``Resource-F1'' solar batteries were used here which allowed the prolongation of the satellite's lifetime to 30 days. In addition, instead of equipment KATE-200 and KFA-1000 a high quality multispectral photo camera MK-4 was installed which realized photographing in four of six possible bands of spectrum. With the help of MK-4 multispectral images were obtained with the resolution 5 .. 8 meters and spectral zonal images with the resolution 8 .. 12 meters. The satellite's equipment allowed multispectral photographing together with spectral zonal and colored photographing. Prolonged active flight time of ``Resource-F2'' allowed to realize double or triple coverage of the surface without a standby mode. Images made by ``Resources'' are used for mapping of the surface in scale to 1:200000 (Resource-F1) and 1:50000 (Resource-F2``). Blank spots were erased from maps of the Pamirs and the Tien Shan, the maps of Chukchi peninsula, Novaya Zemlya, Kuril islands, deserts of the Central Asia, polar regions of Antarctica were improved and detailed.

Ocean

Spacecraft ``Ocean-O1''

The automatic specialized spacecraft of the ``Ocean-O1'' [53] series (NEM national economical activity marine) were designed by the design department ``Yuzhnoe'' (Dnepropetrovsk, The Ukraine) and were targeted at oceanographic explorations from the space and ice patrol in polar areas

[52] http://plesetzk.ru/index.php

[53] http://plesetzk.ru/index.php

independently on the weather conditions, seasons and parts of the day in order to increase the safety of navigation and the choice of optimal routs of the vessel navigation along the Northern seaway to prolong the navigation season to year-round long.

The experiment was realized with the help of two spacecraft - NH-1 and NH-2 (Ocean-E) designed on the basis of the spacecraft of AUOS-Z type. The first of these satellites was launched to the polar orbit on the 12th of October 1979 (``Cosmos-1076''). During the experiment an adjustment of principles and the general methodology of collecting of oceanographic information with the help of space tools and its utilization for the benefits of science and the national economical activities were realized

Spacecraft NH were supplied with a centimeter polarization radiometer RADON, the infrared spectrometer 174K1, photometer-block of chromaticity BC, equipment of subscriber call ABA and of the collection of the information BUKAZ-KA, and the controlling block of the research equipment. On the spacecraft NM-2 an additional radiolocation scattering meter (scatterometer) was mounted.

In the ``Ocean-E'' experiment network two satellites were launched on which the principles and methods of collection and utilization of the oceanographic information were adjusted. Particularly means of collection and transmission of regular information about the ice situation in polar regions were adjusted.

Structurally the spacecraft NHM consists of hermetic enclosure with frames for installation of research equipment, four panels where detectors of research equipment are placed, two blocks of panels of solar batteries fixed on a special rotating crossbar and the outer frame with a gravitational stabilizer.

The research equipment of the SC NHM included a complex of radiophysical equipment RFA, radio-television complex RTVC, UNF-spectrometer and the system Condor for collection of information from buoy-based station and its transmission to information acquisition centers. Radiotelevision complex using multichannel scanning devices of a low resolution MSU-M carried out memorizing, storage, transformation and transmission of video information received in visible and infrared spectrum concerning the cloud covering and underlying surface.

The basic difference of NHM from NH except the changed research equipment was in changed composition and placement of some serving equipment in order to clear the volume inside the hermetic enclosure to install the research equipment and in improvement of the damping, orientation and stabilization system in purpose to increase its accuracy characteristics (a new gravitational stabilizer was introduced with the mass 12 kg the length of the retractable beam was increased to 17 m).Multichannel scanning devices with intermediate resolution MSU-S were installed on the SC ``Ocean-OE'' N2.

Basic characteristics ``Ocean-O1''

Spacecraft dimensions compact form, m	
Length	4.99
Diameter	2.4
Spacecraft dimensions in work state, m	
Length	21.52
Width with spread solar batteries	4.92
Width along panel of devices	7.70
Width along antenna	12.0
The orientation system	
Type	Active, triaxial, magneto-gravitational
Orientation devices	triaxial flywheel motor, and correcting propulsion device, hygroscope, extention rod
Power supply	

Power supply	Solar and chemical batteries
Orbit parameters	
Orbit	polar, near-circular
inclination, grad	82.5
revolution period, minutes	98
Height,km	650
Mass, kg	≤ 2000 (505 kg mass devices)
Launch system	
Rocket-carrier type	11K68 (``Ciclon-3'')
Launching mass of the rocket-carrier with the spacecraft, ton	183.9

Musson

Spacecraft ``Musson'' http://plesetzk.ru/index.php

Space geodesic complex (SGC) "Musson" had a mission of creation of a united geodesic coordinate system of higher accuracy on the whole terrestrial surface, the further improvement of parameters of the shape of the Earth, its gravitational field and refinement of geodesic relation between the continents and islands of the Earth. Spacecraft Musson were designed and produced in the scientific production association of the applied mechanics, Krasnoyarsk-26 (Zheleznogorsk nowadays). In January 1981 the attempt to launch the SC "Musson" was not successful - due to an accident at the stage of injection the satellite was not injected on the orbit and burnt down in dense layers of the atmosphere together with the rocket carrier. The further launches were successful - on the 30th of September the first satellite "Musson" was injected on the orbit (Cosmos 1312). The total number of spacecraft of this series injected on the orbit is 13. The spacecraft Musson is the basic element of (SGC). To solve the problem of creation of a worldwide geodesic network methods of orbital and space triangulation are used. For this purpose the Doppler system of measurement of a radial component of the speed, retransmitter of a slant distance measurement system, corner reflectors for a ground-based laser equipment of the distance measurement and the light signaling system were mounted onboard the spacecraft. The light signaling system enabled to produce the series of flashes which were photographed by the ground-based photoastronomic devices on the background of the sky. SC "Musson" N24 had radiotechnical complex "Elicon" targeted at navigational guiding of valuable cargos. The refinement of the terrestrial gravitational field was carried out with the help of a high accuracy altimeter which realizes measurement of the altitude in relation to the ocean and it also realizes the primary processing of results of that measurement with the following transmission to the Earth. Further the satellite altimetry was processes together with the results of the ground-based gravimetric survey

Simultaneously with the measurement the delivery of the work program of KGK (the observation program) was realized with the help of onboard storage devices. SC "Musson" consisted of a hermetic enclosure where special and service equipment and systems were mounted with the help of equipment frames. With the help of thermoregulation system specified climatic and temperature conditions were maintained which were necessary for a normal functioning of the equipment. The hermetic enclosure was mounted inside the frame and on its outer surface a phototransformer and eight panels of solar batteries were mounted. The surface of the frame was used as a radiator of the thermoregulation system. In the upper part of the enclosure there was a beam where mechanisms of a gravitational device and other orientation systems were installed. The spacecraft was attached to the

rocket carrier with the help of connector of the detachment system and a shock-absorbing framework preserving the satellite against the vibration affect. Orientation and stabilization of the spacecraft after the launch and the maintenance of its continuous orientation of the longitudinal axis to the Earth center was provided by the combined system of orientation, stabilization and position control. This system included a magneto-gravitational orientation system which performed angular motion stabilization along the longitudinal axis. The system also included a megnetogravitational orientation system which stabilized angular motion along longitudinal axis, a flywheel stabilizing the SC in relation to SC heading, a system of the antennae platform orientation to the center of the Earth and a position controlling system of the SC

Basic characteristics ``Musson''

Spacecraft dimensions compact form, m	
Length	5.84
Diameter	2.36
Spacecraft dimensions in work state, m	
Length	17.77
Width with spread solar batteries	7.50
The orientation system	
Type	Active, triaxial, magneto-gravitational with self-regulating antenna orientation
Orientation devices	hygroscope, extention rod
Power supply	
Power supply	Solar and chemical batteries
Orbit parameters	
Orbit	polar, near-circular
inclination, grad	73.6 and 82.6
revolution period, minutes	116
Height,km	1500
Mass, kg	$\leq$1530 (working condition)
Launch system	
Rocket-carrier type	11K68 (``Ciclon-3'')
Launching mass of the rocket-carrier with the spacecraft, ton	183.5

6.1.2 Foreign satellites

METEOSAT

The series of meteorological satellites designed by the European space agency (ESA) in purpose of its utilization in the international program of the global atmospheric processes exploration the satellite carries out the photographing of the terrestrial surface in near and far infrared bands. The first satellite of the Meteosat series was launched in 1977 and it went down in the history as ``The first Earth observation mission of the ESA". Later five more spacecraft were launched and the last was launched in 1997. Being on the geostationary orbit at the height of 36 thousand kilometers from the terrestrial surface Meteosat satellites provide a continuous flow of the data concerning the weather conditions in Europe and Africa.

In 2010 Meteosat -6, -7, -8 and -9 are in use.
Meteosat -8, -9's mission will end up in 2021.
Meteosat-8 The launch date - 28th of august 2002, orbit type: geosrationary.
Meteosat 9 the launch date: 21st of December 2005. Orbit type: geostationary .

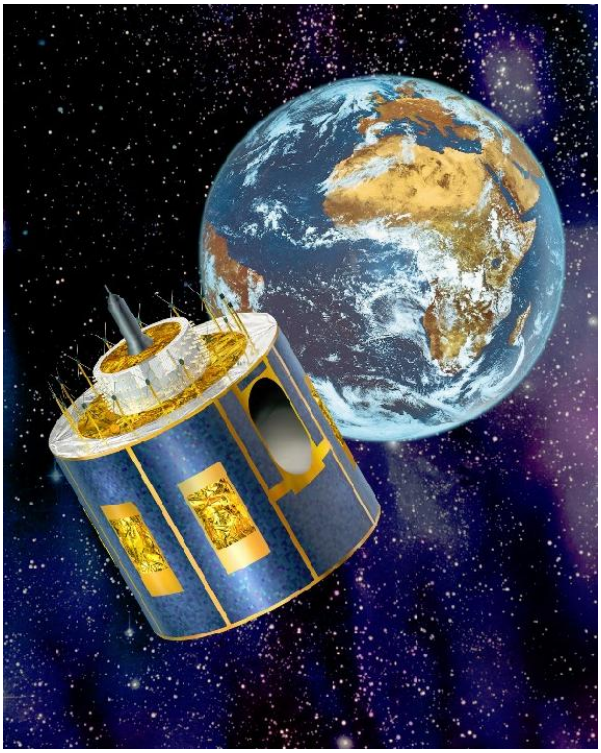

Fig. VI-13-5 European geostationary meteorological satellites Meteosat

POES

Satellites of NOAA series (National Oceanic and Atmosphere Administration, USA) fly at the height of about 800 km since the beginning of 70s (it is considered that the first satellite of this series was the one TIROS-M launched on the 23rd of January 1970). The NOAA series satellites have two complexes of instruments installed: AVHRR (Advanced Very High Resolution Radiometer) and the equipment for vertical sounding of the atmosphere. The major volume of information is the data from scanning radiometer of AVHRR. The sounder TOVS (Tiros Operational Vertical sounder) serves for the vertical sounding of the atmosphere. The sounder is a three-component system including:

1) A four-channel Unit of Microwave sounding MSU: observation of cloudy regions;

2) A three-channel Unit of Stratosphere Sounding SSU: measurement of the atmospheric temperature;

3) A 20-channel infrared sounder of high resolution HIRS/2: the definition of the vertical temperature profile of the atmosphere and the content of water vapour.

The data of the polar-orbital satellites NOAA is used for long-term weather forecasts, monitoring of the atmosphere and weather phenomena and also to provide the safety of flights (including the detection of clouds of volcanic dust) and the safety of water transport (monitoring and forecasting of the icing conditions). The data received by the satellites is memorized in the onboard storage device and then it is transmitted to the information collecting centers. At the present moment in VRCPOD the receiving of the information is being carried out from five satellites of NOAA series.

They are NOAA-15, NOAA-16, NOAA-17, NOAA-18, NOAA-19.

Fig. VI-13-6. Meteorological satellites of NOAA series (USA)

Spheres of the information application:

a) The detection of huge industrial ejections and monitoring of their further spreading.
b) Detection of huge discharges of pollutants into water.
c) Detection and estimation of the scale of catastrophic floods.
d) Monitoring of vast regions to detect dangerous sources of contamination.
e) Monitoring of dust storms.

Meteorology:

a) Determination of the vertical temperature and humidity profile of the atmosphere.
b) Operative forecast of areas of strong cyclogenesis.
c) Visual imaging of the weather conditions and the creation of meteorological maps.
d) Estimation of the conditions and control of the snow covering dynamics

Agriculture and forestry:

a) Control of appearance and spread of forest and steppe fires.

Oceanology and hydrology:

a) Estimation of icing conditions;
b) Operative tracking of spring flood areas.

Characteristics of NOAA-15

basic dimension, m	4.2 , 1.88 (diameter)
Solar battery dimension, m	2.73 , 6.14
Mass, (on orbit), kg	2231.7 (756.7 fuel)
Rocket-carrier	Lockheed Martin Titan II
Launch date	May 13, 1998 Vandenburg Air Force Base, CA
Orbit	Solar-synchronous
Height, km	833
Revolution period, min	101.2
Inclination, grad	98.7

GOES

Geostationary satellites of the environmental observations (GOES) turn around the Earth along geosynchronous orbit with the speed respective to the Earth rotation speed. It allows them to observe one and the same point on the terrestrial surface. Being at the altitude of 35800 km (22 300 miles) above the Earth the satellites GOES-8 and GOES-9 provide the information about the surface conditions and the environmental conditions every 30 minutes. Satellites GOES are launched to the geostationary orbit from the space launching site on the Cape Canaveral. At the moment satellites of the following series are used:

GOES-11 (L) Launch: 07:07 03.05.2000
GOES-12 (M) Launch: 07:23 23.07.2001
GOES-13 (N) Launch: 22:11 24.05.2006
GOES-14 (O) Launch: 22:51 27.06.2009
GOES-15 (P) Launch: 23:57 04.03.2010 (test operations)

Satellites GOES having been launched by NASA since 1975. Nowadays the USA maintain functioning of satellites GOES-10 and GOES-12 (GOES-9 functions partially and is used by the Japanese Meteorological Agency instead of their own satellite). GOES-11 is on the orbit as a replacement satellite for GOES-12 or GOES-10 in case of their breakdown. On the 24th of May 2006 satellite GOES-13 was launched and now it undergoes tests and will be conserved.

GOES-10 and GOES-12

Fig. VI-13-7. Meteorological geostationary satellites GOES (USA)

Each of these satellites observers almost one third of the surface of the Earth: one of them watches the Northern and the Southern America and almost the whole Atlantic Ocean, the other one watches the rest part of the Northern America and the Pacific Ocean. The basic instruments of the GOES onboard observation are Imager and Sounder equipment. Imager is a multichannel instrument registering solar radiation reflected by the atmosphere and the surface. Sounder collects the information for the determination of the vertical profiles of the temperature and humidity (water vapor) and the temperature at the cloud level and ozone distribution. The satellite GOES-N (improved GOES) with the dimensions 4.2x4.6x6.2 and the all-up-weight 3300 kg is designed to work on a geostationary orbit at 35600 km. onboard the satellite, produced on the basis of the BSS-601 platform, one panel of solar batteries with gallium-arsenide is installed and it is designed for the generation of 2.3 kW (2 kW by the end of its exploitation). It was launched with the help of the rocket carrier Delta

IV produced by Boeing.

By the present time the last satellite GOES was launched on the 4th of March 2010 at 18:57 from the pad SLC-37B of the US Air Force site "Cape Canaveral" The parameters of the satellites after the detachment (calculated parameters are in brackets)

Orbit parameter (in brackets - calculation):

Inclination, grad	12.01(12)
Height in peregee, km	6638(6623)
Height in apogee, km	35215(35177)
Revolution period, min	747.8

6.1.3 Space solar observatories

SOHO

SOHO[54] satellite is a specialized satellite designed to obtain images of the Sun.

The general characteristics:

Dimensions, m	4.3 x 2.7 x 3.7
Width with solar batteries, m	9.5
General mass at the launch, kg	1850
Speed data translation ,Kb/s	200
Speed data translation from board memory, Kb/s	40

Satellite SOHO was launched on the 2nd of December 1995 (08:08 UTS) with the help of the rocket carrier Atlas II-AS (AC-121) from the launching site on the cape Canaveral. It was injected on the geostationary orbit near the liberation point between the Earth and the Sun and moves together with the Earth around the Sun slowly rotating around the first Lagrange Point (L1) where the combined gravitational force of the Sun and the Earth holds the satellite on the radius the Earth-the Sun. the First Lagrange point is 1.5 million kilometers from the Earth (about four Moon radiuses) in the direction to the Sun. at this point SOHO carries out a continuous observation of the Sun. All previous observatories were on orbits around the Earth and the observations interrupted periodically when they entered the Earth shadow.

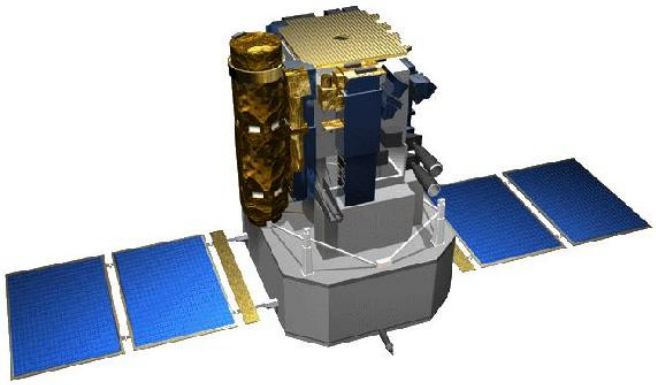

Fig. VI-13-8 Solar observatory SOHO (NASA, ESA)

[54] http://infox.ru/science/universe/2008/11/12/sunspots_print.phtml

ACE

On the 25th of august 1997 at 14:39:53 GMT (10:39:53 EDT) a rocket carrier ``Delta-2" (variant 7920-8) with an American research SC ACE was launched from the launch pad LC-17A of the US Air Force station ``Cape Canaveral".

According to the message of the NASA operative control Center of Space flights by the name of Goddard the spacecraft ACE received the international registration designation 1997-045A. it also received the number 24912 in the US Space Headquarters catalogue.

The development of the spacecraft was financed by NASA in the program ``Explorer" and with that the customer of the project was the Program of the Sun-Earth relations which is the department of the NASA Space science headquarters. The total cost of the SC was 111 mln. It was the last spacecraft of the ``Explorer" family designed to be launched with the help of rocket carrier ``Delta"

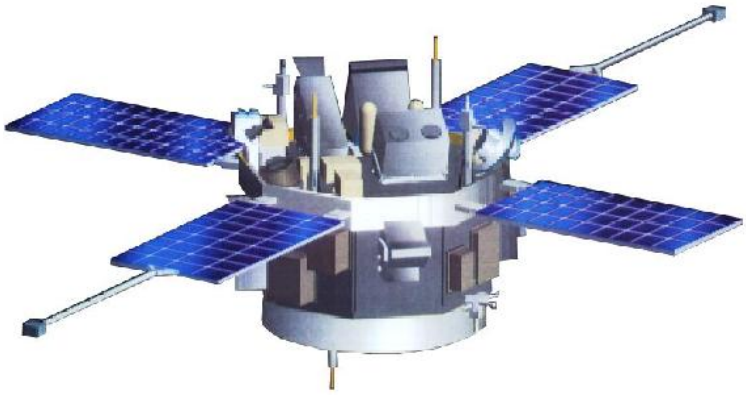

Fig. VI-13-9 The solar observatory ACE (NASA, ESA)

The satellite is targeted at registration and exploration of low energy solar cosmic rays and high-energy galactic CR with the speed up to 1500 km/s. the equipment of ACE allows the precise definition of isotope and element content of some types of space matter: solar corona matter, interplanetary gas medium, more rarefied local interstellar matter and matter from remote parts of the Galaxy. The mission determined the name - ACE - Advanced Composition Explorer).

The basic systems and equipment installed on ACE.

* Communication Subsystem: Primary Mission, S-band, DSN;
* Communication Subsystem: NOAA - S-band @ NOAA Receiving Stations, TBD
* Total Onboard Data Storage in Two Solid State Recorders -- 2 Gigabits
* Primary Mission Downlink Rates: 78 & 6.9 kbps and 434 bps
* NOAA Real Time Solar Wind Mission: 434 bps

The frame of the SC ACE is 1.6 m in diameter and 1 m in a height, four solar batteries and the bar of magnetometer mounted on the two of them are not included. The weight of the spacecraft is 785 kg including 189 kg of fuel. Solar batteries supply the power 500 W. The spacecraft is stabilized by the rotation (5 turns per min) around the axis close to the direction the Sun-the Earth. The most part of equipment is placed on the "solar" part of the satellite.

STEREO

STEREO - Solar TErrestrial RElations Observatory - is a NASA mission devoted to the exploration of solar activity. Two similar spacecraft were launched on the 26th of October 2006. The system is designed so that one of satellites overtakes the Earth and the other lags behind. It allows realization of stereoscopic exploration of the Sun and study in details the phenomena of coronal mass ejections. As for the 22nd of January 24 comets were discovered by STEREO satellites.

Fig. VI-13-10. STEREO spacecraft

Satellites are equipped with instruments designed by scientists from the University of Minnesota in collaboration with a group of the Paris Observatory.

Characteristics of the spacecraft

Dimension, m	1,14x1,22(6,47 (with spread batteries x2,03)
Mass, kg	620
Power , W	475
Speed data translation, Kb/s	720

SDO

Solar dynamics observatory (SDO) is a space observatory of NASA for the exploration of the Sun and it is designed for a 5 years-long functioning. It was launched on the 11th of February 2010 within the program ``Living with a star'', LWS. The LWS program is targeted at the development of scientific knowledge needed for the solution of solar-terrestrial relations aspects which directly influence the life and the society. The target of SDO is the understanding of the solar influence on the Earth and the near-Earth space by the exploration of the solar atmosphere within a small temporal and spatial scale and in many wave lengths simultaneously.

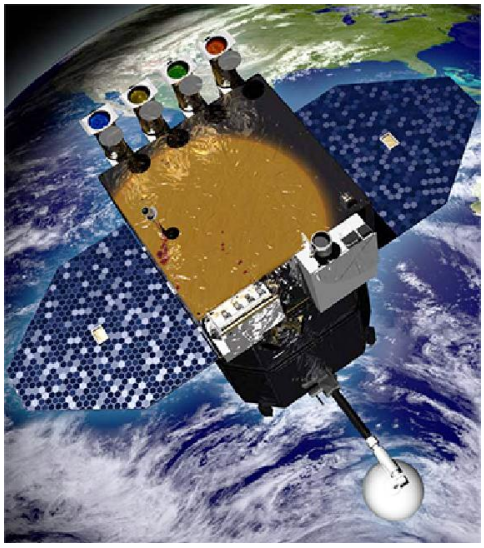

Fig. VI-13-11. A new solar observatory SDO.

The key characteristics

Type of orbit	Geo-synchronous
Height, km	36000
Revolution period, hour	24
Data launch	11 February 2010 15:23:00 UTC
Spaceport	``Canaveral''
Rocket-carrier	Atlas-5
Mission time, years	5
Launch mass, kg	3100
Payload, kg	270
Fuel, kg	1400

Hinode

Hinode (Japanese ``Sunrise'', before the launch - Solar-b) is a Japanese scientific satellite for the research in the sphere of solar physics. The satellite was launched on the 23rd of September at 06:36:30 (22nd of September at 21:36:30 UTC) in 2006 from the launch site Utinoura with the help of the rocket carrier M-V. the basic mission of the satellite is to realize very precise measurements of small variations of solar magnetic field intensity and with that the research program includes:

study of the dynamics of the solar magnetic fields;

study of the solar luminosity variations;

study of the solar wind energetic;

exploration of the processes generating ultraviolet and x-ray radiation;

Hinode has only three basic scientific tools:

SOT (Solar optical telescope) - solar optical telescope targeted at the measurement of intensity of the magnetic field in the photosphere;

XRT (X-ray telescope) - X-ray telescope for the exploration of the solar corona;

EIS (Extreme-Ultraviolet Imaging Spectrometer) Ultraviolet spectrometer designed to measure the speed of particles ejected by the Sun and to measure the temperature and density of the solar plasma.

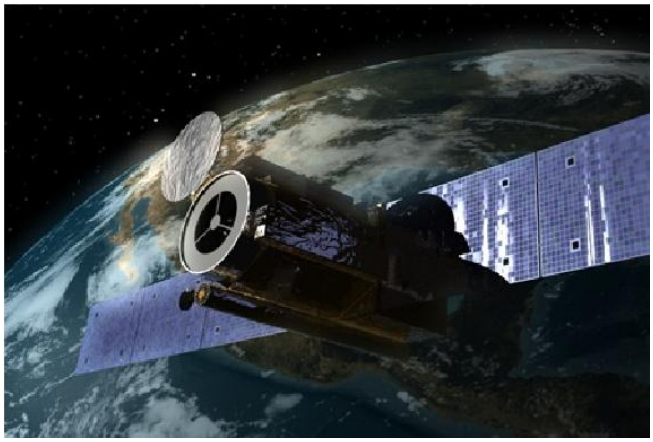

Fig. VI-13-12Space observatory Hinode (Japan)

The key characteristics

Type of orbit	Solar-synchronous
Height, km	682x689
Revolution period, min	98,5
Mass, kg	900

Ulysses

Ulysses is a spacecraft coproduced by ESA and NASA designed for the exploration of the Sun and the exploration of Jupiter as an additional mission. The spacecraft was launched in October 1990 (It was planned for 1986 but it was delayed due to the crash of Challenger). At all the spacecraft worked for 17 years which was four times more that it was designed for. Officially the mission of the spacecraft was finished on the 1st of July 2008 due to lack of generated energy to maintain the orientation of the spacecraft. Ulysses is the first spacecraft exploring the Sun not only from the ecliptic plane (the equatorial plane) but also from the Poles. It enables to create a more precise model of the near-Sun space.

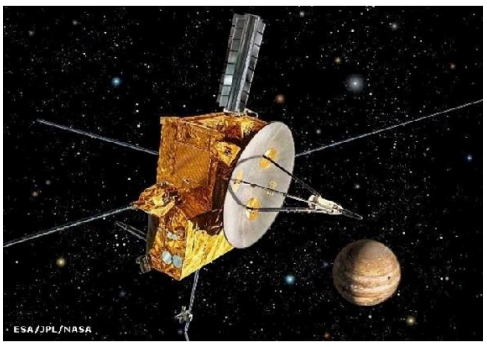

Fig. VI-13-13. Space observatory Ulyssses.

The key characteristics

Dimensions, m	3.2x3.3x2.1
Power, Wt	to 285
Speed of data translation, b/s	to 1024
Mass, kg	370 (55 scientific devises)

Chapter 7. The satellite data and its processing

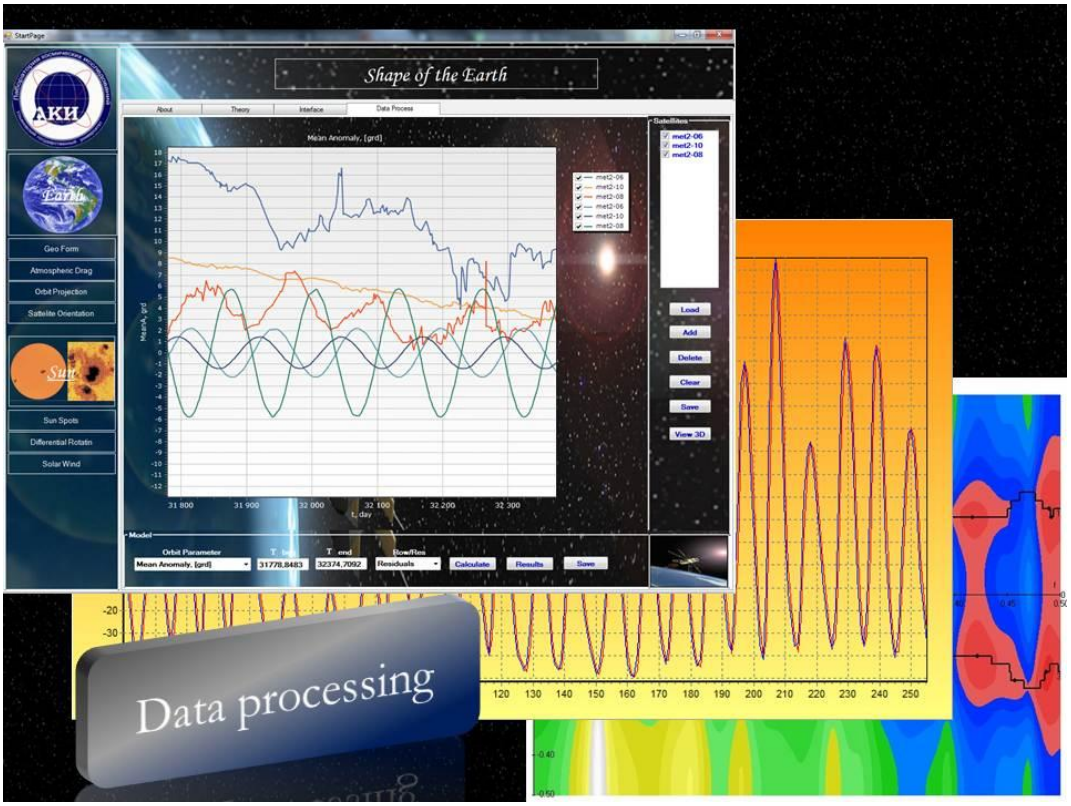

7.1 Lecture 14. Methods of the processing of cosmophysical data

One of the basic elements of the exploration of the space is the processing of the data incoming from spacecraft. This data in a form of measurements made by some devices onboard a spacecraft and in a form of telemetric data about the conditions of the satellites and the surrounding medium makes the primary information where the scientific information is to be extracted. As a rule scientific measurements onboard the spacecraft are represented in a form of numeric codes which have its own meaning and importance for each device. These codes should be transformed in a form of a real data. Moreover, this date needs to be tied to a specific moment of time and to a specific position of a satellite. After the numerical codes are transformed into scientific data they must be interpreted from the point of view of models representing the scientific content of the received data. In the purpose of analysis of the scientific data a great number of mathematical programs and algorithms are developed and with the help of them the relation of the data to some mathematical models can be established. And with that a quantity of information has grown so much that in order to process all this information it is necessary to develop new methods increasing the speed of analysis and increasing the quantity of the information processed simultaneously. As far as the models related to the observed phenomena also change and become more complicated it is necessary to create new algorithms and programs in

this area. In this lecture the basic methods of the experimental data analysis are to be described. These methods are used in processing of the satellite data and they are also needed for the lab works of this course.

7.1.1 The method of least squares

An empirical model most frequently used in the analysis of data is the model in which some parameters, called independent, are related to some parameters, called dependent, with the help of functions of a given form. With that the problem is to calculate unknown parameters of the given function and prove the existence of such dependence. Such problems can be solved with the help of different variants of the method of least squares.

Suppose there is a model of the examined process in the general form:

$$y(t) = \sum_{s=1}^{M} A_s f_s(t) + \delta(t), \tag{7.1}$$

where A_s are the parameters of the model, $f_s(t)$ - strictly given functions of time, $\delta(t)$ - random deviations of the process $y(t)$ from the model. Suppose it is necessary to find out the model (7.1) which should describe a set of measured quantities of the process $y(t)$ at any moment of time $t_i, i = 1,\ldots,N$ in the best way. Denote measured quantities of the process as y_i and δ_i denotes the deviations $\delta(t_i)$ at moments t_i with that it is supposed that deviations δ_i are independent random quantities with zero mean and the same variance. That means the following conditions are true:

$$< \delta_i >= 0;\ < \delta_i \delta_j >= 0,\ i \neq j;\ < \delta_i^2 >= \sigma^2. \tag{7.2}$$

Here brackets <> mean statistical average (mathematical expectation) of the corresponding quantities.

The general principle of the method of least squares is that as the best model a model (7.1) should be chosen parameters of which $A_s^{(0)}$ satisfy the condition that the function:

$$\sigma^2(A_1,\ldots,A_M) = \frac{1}{N-1}\sum_{i=1}^{N}\left[y_i - \sum_{s=1}^{M} A_s f_s(t_i) \right]^2 = \sigma^2$$

reaches minimum with $A_s = A_s^{(0)}$. This problem can be reduced to the solution of a set of linear equations in the following common form:

$$\frac{\partial \sigma^2(A_1,\ldots,A_M)}{\partial A_s} = 0,\ A_s = 0,\ldots,M. \tag{7.3}$$

Calculating derivatives we obtain:

$$\frac{\partial \sigma^2}{\partial A_k} = -2\sum_{i=1}^{N}(y_i - \sum_{s=1}^{M} A_s f_s(t_i)) f_k(t_i) = 0,\ k = 1,\ldots,M.$$

This set of equations can be written as:

$$\sum_{j=1}^{M}[\sum_{i=1}^{N} f_k(t_i) f_j(t_i)] A_j = \sum_{i=1}^{N} f_k(t_i) y_i,\ k = 1,\ldots,M,$$

Or in matrix form:

$$QA = F, \tag{7.4}$$

where $A = (A_1, A_2, \ldots, A_M)$, matrix Q and vector F have the following elements:

$$Q_{kj} = \sum_{i=1}^{N} f_k(t_i) f_j(t_i),\quad F_k = \sum_{i=1}^{N} y_i f_k(t_i).$$

The solution of (7.4) can be written as:

$$A = Q^{-1}F.$$

Or in component form this relation looks like:

$$A_j = \sum_{k=1}^{M} R_{jk} \left(\sum_{i=1}^{N} y_i f_k(i) \right), \quad j = 1, \ldots, M, \tag{7.5}$$

here R_{ik} - are matrix elements of matrix $R = Q^{-1}$, inverse to Q.

Calculate error of the regression parameters estimation. To do that, introduce the following determinations and designations. Denote true coefficients of regression as $A_k^{(0)}$ supposing the considered model to take place in reality. Coefficients A_k obtained as the result of calculations and satisfying relations (7.5) are to be called estimations of true regression coefficients. Substitute expressions for y_i from (7.1) into (7.5) supposing true regression coefficients $A_k^{(0)}$ to be in that expressions. As the result we obtain:

$$A_j = \sum_{k=1}^{M} R_{jk} \left(\sum_{i=1}^{N} \left(\sum_{s=1}^{M} A_s^{(0)} f_s(t_i) + \delta_i \right) f_k(t_i) \right), \quad j = 1, \ldots, M,$$

Transforming this relation we obtain:

$$A_j = \sum_{k=1}^{M} \sum_{s=1}^{M} R_{jk} Q_{ks} A_s^{(0)} + \sum_{i=1}^{N} \delta_i \sum_{k=1}^{M} R_{jk} f_k(t_i), \quad j = 1, \ldots, M,$$

As far as matrixes Q and R are reverse to each other, i.e.:

$$\sum_{k=1}^{M} \sum_{s=1}^{M} R_{jk} Q_{ks} = \delta_{js},$$

where $\delta_{kk} = 1, k = 1, \ldots, M$ and $\delta_{ks} = 0, k \neq s$, we finally obtain:

$$A_j = A_j^{(0)} + \sum_{i=1}^{N} \delta_i \sum_{k=1}^{M} R_{jk} f_k(t_i), \quad j = 1, \ldots, M. \tag{7.6}$$

According to the condition (7.2) we find:

$$< A_j >= A_j^{(0)}.$$

The latter condition means that the estimation of A_j is **not displaced**. Therefore:

$$\sigma_{A_j}^2 = < (A_j - A_j^{(0)})^2 >= \sigma^2 R_{jj}.$$

These equations can be used for calculations in general case but it is more useful to consider specific models which are mentioned in this cosmophysical practical work.

7.1.2 Linear regression

Estimation of regression coefficients

In the majority of laboratory works it is necessary to use the method of least squares to estimate inclination of the time dependence of different orbital parameters and parameters of satellites motion. This is the simplest variant of the model (7.1) .

Suppose the physical parameter y to depend on any other parameter t (for example the time) in the following way:

$$y(t) = At + B + \delta(t),$$

where A and B are the parameters of the model. Following the general instruction we obtain:

$$\frac{\partial\sigma^2(A,B)}{\partial A} = -2\sum_{i=1}^{N}(y_i - At_i - B)t_i = 0, \tag{7.7}$$

$$\frac{\partial\sigma^2(A,B)}{\partial B} = -2\sum_{i=1}^{N}(y_i - At_i - B) = 0. \tag{7.8}$$

Introduce the following designations:

$$\overline{Y} = \frac{1}{N}\sum_{i=1}^{N} y_i,\ \overline{T} = \frac{1}{N}\sum_{i=1}^{N} t_i,$$

$$\sigma_T^2 = \frac{1}{N}\sum_{i=1}^{N} t_i^2,\ C_{YT} = \frac{1}{N}\sum_{i=1}^{N} y_i t_i.$$

Then equations (7.7) and (7.8) can be written as:

$$\sigma_T^2 A + \overline{T}B = C_{YT},$$

$$\overline{T}A + B = \overline{Y}.$$

Solving the set of two linear algebraic equations we find:

$$A = \frac{C_{YT} - \overline{Y}\,\overline{T}}{\sigma_T^2 - \overline{T}^2},$$

$$B = \overline{Y} - A\overline{T}.$$

Such values of the model parameters are accepted as the best ones according to the method of least squares. With the help of such calculations the estimation of variation speed of the ascending node, perigee argument and the speed of decrease of total energy is realized in problems of this practical work.

Calculation of the error of linear regression coefficients estimation

To calculate the error of estimation of A and B coefficients represent their solution as:

$$A = \frac{1}{\sigma_T^2 - \overline{T}^2}\frac{1}{N}\sum_{i=1}^{N} y_i t_i,$$

$$B = \frac{1}{N}\sum_{i=1}^{N} y_i - A\overline{T}.$$

Denote as A_0 and B_0 the true values of model coefficients which unlike A and B are to be called estimations A_0 and B_0. The relation between A_0, B_0 and A, B can be obtained if we substitute y_i by values from the model taking into account random deviates $\delta_i = \delta(t_i)$ in the expression for A and B. As the result we obtain:

$$A = A_0 + \frac{1}{\sigma_T^2 - \overline{T}^2}\frac{1}{N}\sum_{i=1}^{N}\delta_i t_i,$$

$$B = B_0 + \frac{1}{N}\sum_{i=1}^{N}\delta_i$$

It is supposed that:

$$\overline{\delta} = \frac{1}{N}\sum_{i=1}^{N}\delta_i = 0, \sigma^2 = \frac{1}{N-1}\sum_{i=1}^{N}\delta_i^2,$$

And correlations between δ_i and δ_j with $i \neq j$ are equal to 0, i.e.:

$$< \delta_i \delta_j >= 0.$$

In this case it is possible to calculate the average and variance of the estimates A and B. Calculations yield the following:

$$< A >= A_0, \; < B >= B_0, \tag{7.9}$$

$$\sigma_A^2 = D_A = \frac{\sigma^2}{N(\sigma_T^2 - \overline{T}^2)}, \; \sigma_B^2 = D_B = \frac{\sigma^2}{N}. \tag{7.10}$$

Quantities σ_A and σ_B are the errors of the calculation of linear regression coefficients.

7.1.3 Square regression

In a similar way it is possible to make the estimation of square regression parameters. The square regression model has the following form:

$$y(t) = At^2 + Bt + C + \delta(t).$$

Equations (7.3) in this case look like:

$$AT_4 + BT_3 + CT_2 = Y_2,$$
$$AT_3 + BT_2 + CT_1 = Y_1,$$
$$C = Y_0 - AT_2 - BT_1.$$

Excluding C we come to:

$$M_1 A + M_0 B = F_1, \; M_0 A + M_2 B = F_2, \tag{7.11}$$

where

$$M_1 = T_4 - T_2^2, \; M_2 = T_2 - T_1^2, \; M_0 = T_3 - T_1 T_2,$$
$$F_1 = Y_2 - T_2 Y_0, \; F_2 = Y_1 - T_1 Y_0,$$

And quantities T_m and Y_n are determined as:

$$T_m = \frac{1}{N}\sum_{i=1}^{N} t_i^m, \; m = 1,2,3,4, \; Y_n = \frac{1}{N}\sum_{i=1}^{N} y_i t_i^n, \; n = 0,1,2.$$

The solution of relations (7.11) has the following form:

$$A = \frac{M_2 F_1 - M_0 F_2}{M_1 M_2 - M_0^2}, \; B = \frac{-M_0 F_1 + M_1 F_2}{M_1 M_2 - M_0^2}. \tag{7.12}$$

Parameter C can be found from the relation $C = Y_0 - AT_2 - BT_1$.

This model can be used to estimate the deviation of the longitude of ascending node from secular motion.

7.1.4 Model of a harmonic process

In applied problems of analysis of different physical and other processes it is often necessary to single out harmonic processes and estimate their basic parameters. A model of one-dimension harmonic process $y(t)$ with the natural frequency ω has the following form:

$$y(t) = A\cos\omega t + B\sin\omega t + C + \delta(t). \tag{7.13}$$

According to the general principle of the method of least squares the condition of minimum of function σ has the form:

$$\frac{\partial \sigma^2}{\partial A} = A(1 - C_2) - S_2 B + 2S_1 C - 2S_y = 0,$$

$$\frac{\partial \sigma^2}{\partial B} = B(1+C_2) - S_2 A + 2C_1 C - 2S_y = 0,$$
$$\frac{\partial \sigma^2}{\partial C} = C + AS_1 + BC_1 - \bar{Y} = 0,$$

where

$$C_2 = \frac{1}{N}\sum_{i=1}^{N} \cos 2\omega t_i,\ S_2 = \frac{1}{N}\sum_{i=1}^{N} \sin 2\omega t_i,$$
$$C_1 = \frac{1}{N}\sum_{i=1}^{N} \cos \omega t_i,\ S_1 = \frac{1}{N}\sum_{i=1}^{N} \sin \omega t_i,$$
$$\bar{Y} = \frac{1}{N}\sum_{i=1}^{N} y_i,\ S_y = \frac{1}{N}\sum_{i=1}^{N} y_i \sin \omega t_i,\ C_y = \frac{1}{N}\sum_{i=1}^{N} y_i \cos \omega t_i.$$

After the exclusion of C the equations for harmonic's amplitudes A and B take again the form of equations (7.11) where coefficients should be calculated from:

$$M_1 = 1 - C_2 - 2S_1^2,\ M_2 = 1 + C_2 - 2C_1^2,$$
$$M_0 = -S_2 - 2C_1 S_1,$$
$$F_1 = 2[S_y - S_1 \bar{Y}],\ F_2 = 2[C_y - C_1 \bar{Y}].$$

The solution of (7.11) will have the same form (7.12) . Parameter C should be calculated as:

$$C = -AS_1 - BC_1 - \bar{Y}.$$

The total amplitude of a harmonic and the estimation of the initial phase have the following form:

$$A_0 = \sqrt{A^2 + B^2},\ \phi = \frac{B}{A}.$$

This model can be used to estimate parameters of secular motion, perigee argument and mean anomaly estimation.

7.1.5 Calculation of measurement error of complicated parameters

One of the targets of this practical work is the problem of errors calculation of quantities which are the functions of quantities measured directly in the experiment. Such quantities are to be called complicated. In problems concerning the measurement of parameter J_2, parameters measured directly in the experiment are the parameters of orbital motion of a satellite: perigee argument, longitude of ascending node etc. Parameter J_2 is a function of these parameters.

Suppose a measured parameter p to be some function of directly measured quantities X_i, $i = 1, \ldots, L$, i.e.:

$$p = P(X_1, X_2, \ldots, X_L).$$

Then suppose these directly measured quantities X_i to be characterized by the estimation of mean values $\overline{X_i}$ and the total statistical and instrument inaccuracy equal to σ_i, i.e. σ_i^2 is a variance of scattering generated by uncontrolled outer reasons and inaccuracy of an instrument. Then as a p parameter estimation a value is chosen:

$$\bar{p} = P(\bar{X}_1, \bar{X}_2, \ldots, \bar{X}_L),$$

In case of independence of random variances of single quantities X_i the absolute error of p parameter measurement is determined by:

$$\sigma_p = \sqrt{\left|\frac{\partial P}{\partial X_1}\right|^2 \cdot \sigma_1^2 + \left|\frac{\partial P}{\partial X_2}\right|^2 \cdot \sigma_2^2 + \cdots + \left|\frac{\partial P}{\partial X_L}\right|^2 \cdot \sigma_L^2}\Bigg|_{X_1=\bar{X}_1,\, X_2=\bar{X}_2,\ldots,X_L=\bar{X}_L}. \qquad (7.14)$$

Relative error is calculated from:

$$\frac{\sigma_p}{\bar{p}} = \sqrt{\left|\frac{\partial \ln P}{\partial X_1}\right|^2 \cdot \sigma_1^2 + \left|\frac{\partial \ln P}{\partial X_2}\right|^2 \cdot \sigma_2^2 + \cdots + \left|\frac{\partial \ln P}{\partial X_L}\right|^2 \cdot \sigma_L^2}\Bigg|_{X_1=\bar{X}_1,\, X_2=\bar{X}_2,\ldots,X_L=\bar{X}_L}.$$

Calculation of measurement errors for J_2 parameter

As the example let's consider the calculation of measurement error for parameter J_2 by the data on longitude of ascending node. The corresponding equation for the estimation of J_2 is:

$$\frac{d\Omega}{dt} = \frac{3}{2}\sqrt{\frac{GM}{a^3}} J_2 \left(\frac{R_E}{p}\right)^2 \frac{\cos i}{(1-e^2)^2}. \qquad (7.15)$$

Notice that directly measured parameters are included: i - inclination, p - focal parameter, n - mean motion and the inclination of the linear regression curve R_{anl}. The Earth radius is supposed to be a constant value measured with a perfect accuracy. The same is about the eccentricity e which is supposed to be zero. That refers to a circular orbit. Notice that in the considered approximation quantities i, p, n are supposed to be constant. But analysis of the data shows that within a period of time when parameters of linear regression are estimated all these parameters evolve considerably especially if rather long periods of time are considered. So in this approximation these variations of parameters must be considered as random (unpredictable) ones and to estimate parameter J_2 by the relation (7.15) the average values of the given period of time should be taken. For small orbit eccentricities $e \sim 0$, which are examined in this practical work, quantities p and n are dependent and are connected by the relation:

$$p = \left(\frac{GM}{n^2}\right)^{1/3}.$$

So to calculate the error of J_2 only n and i variance should be substituted into (7.14)). (7.15) also includes parameter R_{anl} of the linear regression of a curve of the longitude of ascending node secular variation. To estimate its error it is necessary to use (7.10) for the estimation of A parameter of the linear regression.

As the result we obtain the following relation for the estimation of the relative error of J_2:

$$\frac{\sigma_{J_2}}{\bar{J}_2} = \sqrt{\frac{\sigma_{R_{anl}}^2}{R_{anl}^2} + \frac{49}{9}\frac{\sigma_n^2}{n^2} + \frac{\sigma_i^2 \sin^2 i}{\cos^4 i}}. \qquad (7.16)$$

It follows that i variations can lead to considerable errors in measurement of J_2 for satellites on near-polar orbits when $\cos i << 1$.

For perigee argument error can be calculated as:

$$\frac{\sigma_{J_2}}{\bar{J}_2} = \sqrt{\frac{\sigma_{R_{anl}}^2}{R_{anl}^2} + \frac{49}{9}\frac{\sigma_n^2}{n^2} + 25\frac{\sigma_i^2 \cos^2 i \sin^2 i}{(1-5\cos^2 i)^4}}, \qquad (7.17)$$

And for a mean anomaly:

$$\frac{\sigma_{J_2}}{\bar{J}_2} = \sqrt{\frac{\sigma^2_{R_{anl}}}{R^2_{anl}} + \frac{49}{9}\frac{\sigma_n^2}{n^2} + 9\frac{\sigma_i^2 \cos^2 i \sin^2 i}{(1-3\cos^2 i)^4}}, \tag{7.18}$$

Here σ_i and σ_n are the errors of inclination and mean motion including statistical variance of measurement of these quantities, $\sigma_{R_{anl}}$, $\sigma_{R_{arp}}$, $\sigma_{R_{aan}}$ - errors of the method of linear regression for corresponding parameters.

7.1.6 Time series filtration

Time series filtration is understood as a linear transformation allowing change of Fourier spectrum of this series deleting a part of harmonic components. Suppose there is a discrete time series of measurements $u_0, u_1, u_2, \ldots, u_N$ of a parameter $u(t)$ taken in equal periods of time Δt:

$$u_k = u(t_k), \;\; t_k = k\Delta t, \;\; k = 0,1,2,\ldots,N.$$

In this case the linear smoothing (low frequency transmission band) filtration is understood as the transformation:

$$U_k = \sum_{j=-P}^{P} W_j u_{k-j}, \;\; k = P,\ldots,N-P. \tag{7.19}$$

Here real not negative numbers $W_j \geq 0, \;\; j = -P,\ldots,P$ are called filter coefficients and integer number P is called half-width of the filter window. Numbers W_j must satisfy normalizing conditions:

$$\sum_{j=-P}^{P} W_j = 1,$$

And symmetry conditions:

$$W_j = W_{-j}, \; j = -P,\ldots,P.$$

Except smoothing and low-frequency filtration a high-frequency filtration is also used. It allows to delete trends and band filtration. High-frequency filtration is a linear transformation including the transformation (7.19) and the consequent subtraction of the obtained series from the initial:

$$V_k = u_k - U_k, \;\; k = -P,\ldots,P. \tag{7.20}$$

Here numbers U_k are determined by (7.19) . Band filtration represents the application of sequential transformations of low-frequency filtration with a window half-width P and high-frequency filtration with a window half-width $Q > P$. in case of high-frequency filtration the obtained series contains frequency components higher than some characteristic cut-off frequency of a filter and in case of band filtration - in some limited band of frequencies.

Using filters it is necessary to take into account that their usage is connected with the decrease of the initial series length by the value of the window width $2P$. It is clear from the determinations of their linear transformations. It is very important when using high-frequency filters, which have a big window half-width that leads to a considerable decrease of the initial series length and as the result to the loss of accuracy and the reliability of statistical estimation based on them.

Depending on the choice of filter coefficients W_k there are a lot of different types of smoothing filters which determine quantity of different ways of blanking of high-frequency components of the incoming signal spectrum. We examine only three of them. Other types are described in different books devoted to data processing. [24, 25]). Notice that for the purpose of problem 3 there is no difference which filter to apply. Choice of the window half-width plays an

important role for the obtaining quite reliable focal parameter derivative values. Choice of the half-width is realized during the work with the certain time series.

Rectangular filter

Rectangular filter is determined by the choice of coefficients according to the following rule:

$$W_k = w_0,\ k = -P,\ldots,P. \qquad (7.21)$$

Basing on the normalizing condition we obtain that the number w_0 must be related to the window half-width as:

$$w_0 = \frac{1}{2P+1}.$$

Curves of filter weight factor are shown in Tab. 2.1 (a,b,c).

Cosine filter (Tukie)

Cosine filter is specified by the relation

$$W_k = \frac{1}{2P}\left(1+\cos\left(\frac{\pi k}{P}\right)\right),\ k = -P,\ldots,P. \qquad (7.22)$$

Triangular filter:

Triangular filter is specified by the relation:

$$W_k = \frac{1}{P^2}(2P-|k-P|),\ k = -P,\ldots,P. \qquad (7.23)$$

Appreciations

The author thanks professor I.V.Belokonov for the idea of this course creation, associate professor A.V.Kramlikh for the help in organization of studies. The author also thanks students and undergraduates of Samara State Aerospace University Efim Ustyugov, Dmitri Stolyarov, Denis Avaryaskin and Zafar Gimranov for the interactive and creative study of this course, help in determination of misprints and for creation of additional tests for the revision of knowledge.

The author thanks I. Mitchenko for assistance in translation of this lections.

References

[1] Solar-terrestrial phisics. Ed. V.A. Kuznetzov. M.: Nauka, 2009

[2] A.N. Tomilin. Sky of Earth. M: ``Detskaya literatura", 1974

[23] V.S. Murzin. Cosmik ray astrophysics. M.: Logos, 2006. 486 p.

[4] SOLAR CYCLE VARIATIONS OF LARGE SCALE FLOWS IN THE SUN Sarbani Basu, H. M. Antia. //arXiv:[astro-ph] 0001294v1

[5] Chapmen S., Ferraro V.C. A new theory of magnetic storms. Terr. Magn. atmos. Elect., **36**, 77-97,171-186 (1931)

[6] Maxwell J.C. A treatise on electricity and magnetism. Cambridge Univ. Press (1843)

[7] Akasofu S.I., Chapmen S. Solar-terrestrial physics. M.: Mir, V.1,2, 1974.

[8] I.S. Veselovskiy. Solar wind and heliospheric magnetic field. In Space model. V.1. Ed. Yu.I. Logachev. M.: KDU, 2007.

[9] P. Charbonneau, Living Rev. Solar Phys., 7, (2010), 3 http://www.livingreviews.org/lrsp-2010-3

[10] Chapmen, Ferraro JGR, v. 36, 77, (1931)

[11] Martyn D.F. The theory of magnetic storms and auroras. Nature, Lond. v. 167, 92-94 (1951)

[12] Zhigulev, V.N., Romashevskiy, E.A., 1959, DAN 127, 1001

[13] Veselovskiy I.S. Why solar wind blasen? ``Moden space investigations". Kostroma, 25-30 okt. 2010

[14] A.N.Matveev. Mecheniks and Special Relativistic theory. M.: Vyshaya shkola, 1986.

[15] Handbook of celestial mechanics and astridynamics. Edited by Duboshin, M: "Nauka" 1971, 584

[16] V.V.Belrtckiy. Essay about celestial mechanics. M:``Nauka",1972, 320 p.

[17] V.F. Sokurov. Cosmic ray physics: Cosmic radiation. Rostov-na-Donu: Feniks, 2005

[18] M.S. Longair. High energy astrophysics. Cambridge University Press, 1981.

[19] Physics encyclopedia vocabulary. M.: Sov. encyclopedia, 1983.

[20] V.L. Hynzburg. Cosmic ray near the Earth and into Univers. M.: Nauka, 1967. 95 p.

[21] V.L. Hynzburg. About physics and astrophysics. M.: Pub Quantuma, 1995. 512 p.

[22] V.L. Hynzburg, S.I. Syrovatskiy. Origin of cosmic ray. M.: Pub. AS SSSR, 1963.

[23] V.S. Murzin. Introduction to cosmic ray physics. M.: MSU, 1988. 316 p.

[24] Jenkins G., Watts D. Spectral analysis and its application. M.: Mir, 1972. V.1-2.

[25] Box D., Jenkins G. Analysis of time series. M.: Mir, 1974.

[26] Zatcepin G.T. // Proceedings of AS of SSSR . 1949. V. 67. P. 993.

[27] Smith G., Smith E. Solar flash. M.: Mir. 1966.

[28] Brey R., Louhed R. Sun spots. M.: Mir. 1967.

[29] HundHauzen A. Spreding of corona and solar wind. M.: Mir. 1976.

[30] Bravo S., Cruz-Abeyro J.A.L., Rojas D. The spatial relationship between active regions and coronal holes and the occurence of intense geomagnetic storms throughout the solar activity cycle // Ann. Geophys. 1997. V. 16. P. 49.

[31] McAlister A.H., Knipp D.J. Identification of solar drivers: The November 3 - - 4, 1993 geomagnetic storm // J. Geophys. Res. 1998. V. 221. P. 10326.

[32] Webb D.F., McIntosh P.S., Nolte J.T., Solodyna C.V. Evidence linking coronal transients to the evolution of coronal holes // Solar Phys. 1978. V. 58. P. 389.

[33] Gosling J.T. The solar flare myth // J. Geophys. Res. 1993. V. 98. P. 18937.

[34] R. Devis. Half a century with neutrino.// UFN, 2004, V. 174, N 4, pp. 408-417

[35] Gershtein S.S. Puzzel of solar neutrino.
http://www.pereplet.ru/nauka/Soros/pdf/9708_079.pdf

[36] Hundhausen A.J. Sizes and locations of coronal mass ejections - SMM observations from 1980 and 1984 - - 1989 // J. Geophys. Res. 1993. V. 98. P. 13177.

[37] Dryer M. Comments on the origins of coronal mass ejection // Solar Phys. 1996. V. 169. P. 421.

[38] Harrison R.A. The nature of solar flares associated with coronal mass ejection // Astron. Astrophys. 1995. V. 304. P. 585. 15.

[39] Harrison R.A. Coronal magnetic storms: a new perspective on flares and the 'Solar flare myth' debate // Solar Phys. 1996. V. 166. P. 441.

[40] Maksimov V.P., Nefedyev V.P. The observation of a 'negative burst' with high spatial resolution // Solar Phys. 1991. V. 136. P. 335.

[41] Maksimov V.P., Nefedyev V.P. Some possibilities of microwave diagnostics of eruptive prominences // Ann. Geophys. 1992. V. 10. P. 354.

[42] Dere K.R., Brueckner G.E., Howard R. et al. EIT and LASCO observations of the initiation of a coronal mass ejection // Solar Phys. 1997. V. 175. P. 601.

[43] Svestka Z. On 'The solar flare myth' postulated by Gosling // Solar Phys. 1995. V. 160. P. 53 - - 56.

[44] Svestka Z., Cliver E.W. History and basic characteristics of eruptive flares // Eruptive Solar Flares. Proceed. IAU Coll. 133 / Eds Z.Svestka et al. NY: Springer-Verlag. 1992. P. 1 - 24.

[45] Joselyn J.A., McIntosh P.S. Disappearing solar filaments - a useful predictor of geomagnetic activity // J. Geophys. Res. 1981. V. 86. P. 4555.

[46] Wang H. Space weather: scientific forecasting // COSPAR Colloquium: Solar-Terrestrial Magnetic Activity and Space Environment. Bejing, China. 2001. P. 55.

[47] Pick M. Coronal mass ejections from the corona to the interplanetary medium // Ibid. P. 67.

[48] Maximov V.P., kaleynykh A.V. // SAKS-2001: Proceedings international scienc-practical conference / Ed. G.N. Polyakov. Krasnoyarsk. 2001. P. 37.

[49] Maximov V.P., Ermakova L.V. // Astronom. jornal. 1985. V. 62. p. 558.

[50] Maximov V.P., Ermakova L.V. // Astronom. jornal. 1987. V. 64. p. 841.

[51] Maximov V.P., Prokopiev A.A. // Astronom. jornal. 1993. V. 70. p. 1099

[52] G.I. Marchuk. Methods of computational mathemetics. M.: Nauka, 1977.

[53] http://nmp.nasa.gov/st5/SCIENCE/magnetosphere2.html

[54] http://blog.2012pro.com/wp-content/uploads/2012_Magnetic_field_Solar_Cycle.jpg

[55] http://www.geophys.washington.edu/People/Students/eharnett/mars/mars.html

[56] http://mgs-mager.gsfc.nasa.gov/

[57] http://movelife.ru/article/picture?page=0000040

[58] http://ligaspace.my1.ru/picc/moon_17.gif

[59] http://www.metatechcorp.com/aps/SuperStormAnimation.html -

[60] http://radbelts.gsfc.nasa.gov/outreach/RadMovies.html

[61] Gary A. Glatzmaier and Peter Olson. Scientific American Sp 15, 28 - 35 (2005) doi:10.1038/scientificamerican0705-28sp

[62] L.D.Landau, E.M.Lifshitc. Mechanics. M.:Nauka, 1973

Contents